

Moving Towards an Improved Liquefaction Hazard Framework: Lessons Resulting From the
2010-2011 Canterbury, New Zealand, Earthquake Sequence

Brett W. Maurer

Dissertation submitted to the faculty of the Virginia Polytechnic Institute and State
University in partial fulfillment of the requirements for the degree of

Doctor of Philosophy
In
Civil Engineering

Russell A. Green, Chair
Martin C. Chapman
Roberto T. Leon
Adrian Rodriguez-Marek

9 September 2016
Blacksburg, VA

Keywords: earthquake, New Zealand, soil liquefaction, hazard assessment

Moving Towards an Improved Liquefaction Hazard Framework: Lessons Resulting From the 2010-2011 Canterbury, New Zealand, Earthquake Sequence

Brett W. Maurer

ABSTRACT (Academic)

The 2010-2011 Canterbury, New Zealand, Earthquake Sequence (CES) resulted in a liquefaction dataset of unprecedented size and quality, presenting a truly unique opportunity to assess and improve the efficacy of liquefaction-analytics in the field. Towards this end, the study presented herein develops and analyzes a database of 10,000 high-quality liquefaction case histories resulting from the CES. The objectives of these analyses are varied, but underlying each is the desire to more accurately assess liquefaction hazard for civil infrastructure (i.e., to predict both the occurrence and damage-potential of soil liquefaction). Major contributions from this work include, but are not limited to: (1) the Liquefaction Potential Index (LPI), the state-of-practice framework for assessing liquefaction hazard, is shown to produce erroneous predictions for a significant percentage of the assessed case histories; (2) the cause of poor predictions is rigorously investigated and specific shortcomings of the LPI framework are identified; (3) based on the limitations identified, and using insights from historical data, a revised liquefaction hazard framework is developed; and (4) the revised framework is shown to assess liquefaction hazard more efficiently relative to both LPI and a competing alternative framework newly proposed in the literature. Ultimately, significant room for improvement remains with respect to accurate assessment of liquefaction hazard. The findings presented in this dissertation thus form the basis for future development of a further-improved framework. Moreover, a methodology is proposed by which improvements can be measured in a standardized and objective manner.

Moving Towards an Improved Liquefaction Hazard Framework: Lessons Resulting From the 2010-2011 Canterbury, New Zealand, Earthquake Sequence

Brett W. Maurer

ABSTRACT (General Public)

Soil liquefaction is a common cause of ground failure during earthquakes and is directly responsible for tremendous damage to civil infrastructure. Manifestations of liquefaction include the occurrence of sand blows and lateral spread failures, settlement and tilting of structures, cracking of pavements, and failure of buried lifelines due to flotation or differential settlements, among others. These effects were vividly displayed during the 2010-2011 Canterbury, New Zealand, Earthquake Sequence (CES), which resulted in a liquefaction dataset of unprecedented size and quality, presenting a truly unique opportunity to advance the science of liquefaction hazard. Towards this end, the study presented herein develops and analyzes a database of 10,000 high-quality liquefaction case histories resulting from the CES. The objectives of these analyses are varied, but underlying each is the desire to more accurately assess liquefaction hazard for civil infrastructure (i.e., to predict both the occurrence and damage-potential of soil liquefaction). Major contributions from this work include, but are not limited to: (1) the Liquefaction Potential Index (LPI), the state-of-practice framework for assessing liquefaction hazard, is shown to produce erroneous predictions for a significant percentage of the assessed case histories; (2) the cause of poor predictions is rigorously investigated and specific shortcomings of the LPI framework are identified; (3) based on the limitations identified, and using insights from historical data, a revised liquefaction hazard framework is developed; and (4) the revised framework is shown to assess liquefaction hazard more efficiently relative to both LPI and a competing alternative framework newly proposed in the literature. Ultimately, significant room for improvement remains with respect to accurate assessment of liquefaction hazard. The findings presented in this dissertation thus form the basis for future development of a further-improved framework.

TABLE OF CONTENTS

TABLE OF CONTENTS	iv
LIST OF FIGURES	viii
LIST OF TABLES	xii
PREFACE	Error! Bookmark not defined.
Chapter 1: Introduction	1
1.1 Motivation.....	1
1.2 Contributions	2
1.3 Dissertation Structure and Contents.....	3
Chapter 2: Evaluation of the Liquefaction Potential Index (LPI) for Assessing Liquefaction Hazard in Christchurch, New Zealand	7
2.1 Abstract.....	8
2.2 Introduction.....	8
2.3 Data and Methodology.....	11
2.3.1 CPT Soundings	11
2.3.2 Liquefaction Evaluation and Liquefaction Potential Index (LPI).....	12
2.3.3 Estimation of a_{max} (PGA)	13
2.3.4 Liquefaction Severity.....	15
2.4 Results and Discussion	16
2.4.1 Prediction of Liquefaction Occurrence	16
2.4.2 Prediction of Liquefaction Severity	17
2.4.3 Spatial Analysis of LPI Performance.....	18
2.5 Conclusions.....	21
2.6 Acknowledgements.....	22
References.....	22
2.7 Electronic Supplement.....	38
Chapter 3: Assessment of CPT-Based Methods for Liquefaction Evaluation in a Liquefaction Potential Index (LPI) Framework	45
3.1 Abstract.....	46
3.2 Introduction.....	46
3.3 Data and Methodology.....	48
3.3.1 CPT Soundings	48
3.3.3 Liquefaction Severity.....	48
3.3.4 Estimation of a_{max} (PGA)	49
3.3.5 Estimation of ground water table (GWT) depth	49
3.3.6 Liquefaction Evaluation and LPI.....	49

3.4 Overview of ROC Analyses.....	50
3.5 Results and Discussion	51
3.5.1 Prediction of Liquefaction Occurrence	51
3.5.2 Prediction of Liquefaction Severity	53
3.5.3 Comparative Performance in an Applied Framework	54
3.6 Summary and Conclusions	56
3.7 Acknowledgements.....	57
References.....	58
3.8 Electronic Supplement.....	71
Chapter 4: Fines-Content Effects on Liquefaction Hazard Assessment for Infrastructure during the 2010-2011 Canterbury, New Zealand, Earthquake Sequence.....	76
4.1 Abstract.....	77
4.2 Introduction.....	77
4.2 Data and Methodology.....	80
4.2.1 CPT Soundings	81
4.2.2 Liquefaction Severity.....	82
4.2.3 Estimation of a_{max} (PGA).....	82
4.2.4 Estimation of ground water table (GWT) depth	82
4.2.5 Liquefaction Evaluation and LPI.....	83
4.3 Overview of Receiver-Operating-Characteristic (ROC) Analyses	83
4.4 Results and Discussion	84
4.5 Summary and Conclusions	89
4.6 Acknowledgements.....	90
References.....	91
Chapter 5: Moving Towards an Improved Index for Assessing Liquefaction Hazard: Lessons from Historical Data	107
5.1 Abstract.....	108
5.2 Introduction.....	108
5.3 Derivation of LPI_{ISH}	110
5.3.1 Assumptions.....	110
5.3.2 Functional Form.....	110
5.3.3 Determining Constants.....	111
5.4 Final Form.....	113
5.3 Evaluation of LPI_{ISH}	114
5.4 Conclusions.....	116
5.5 Acknowledgements.....	117
References.....	117

Chapter 6: Investigating the Influence of Post-Liquefaction Strain Potential on the Accuracy of Liquefaction Severity Number (LSN) Hazard Assessments	130
6.1 Abstract.....	131
6.2 Introduction.....	131
6.2.1 Estimating Post-Liquefaction Volumetric-Strain (ϵ_v).....	132
6.3 Data and Methodology.....	134
6.3.1 CPT Soundings	134
6.3.2 Liquefaction Severity.....	135
6.3.3 Estimation of Peak Ground Acceleration (PGA).....	135
6.3.4 Estimation of Ground Water Table (GWT) Depth	135
6.3.5 Liquefaction Evaluation and LSN	135
6.3.6 Receiver Operating Characteristic (ROC) Analyses.....	136
6.4 Results and Discussion	137
6.5 Conclusions.....	138
6.6 Acknowledgements.....	138
References.....	138
Chapter 7: Deterministic and Probabilistic Correlations for Predicting Liquefaction Susceptibility and Fines Content: A Study of the Cone Penetration Test in Christchurch, New Zealand	147
7.1 Abstract.....	148
7.2 Introduction.....	148
7.3 Background: Role of I_c Correlations in CPT-Based Liquefaction Hazard Assessment.....	150
7.4 Field and Laboratory Testing.....	152
7.5 Predicting Liquefaction Susceptibility from I_c	152
7.5.1 Deterministic Correlations	152
7.5.2 Probabilistic Correlations.....	155
7.6 Predicting FC from I_c	156
7.6.1 Deterministic and Probabilistic Correlations	156
7.7 Conclusions.....	159
7.8 Acknowledgements.....	160
References.....	160
Chapter 8: Liquefaction Hazard Assessment Considering Misprediction Economies: A Study of 4 Hazard Frameworks and 10,000 Global Case Histories.....	175
8.1 Abstract.....	176
8.2 Introduction.....	176
8.3 Overview of Liquefaction Hazard Frameworks.....	178
8.3.1 Liquefaction Potential Index (LPI)	178
8.3.2 Modified Liquefaction Potential Index (LPI_{ISH})	178

8.3.3 One Dimensional Post-Liquefaction Reconsolidation Settlement (1DS)	179
8.3.4 Liquefaction Severity Number (LSN).....	180
8.4 Data and Methodology.....	181
8.4.1 Canterbury Earthquake Sequence (CES) Dataset	181
8.4.2 Global Dataset.....	183
8.4.3 Liquefaction Triggering and Hazard Assessment.....	184
8.5 Receiver Operating Characteristic (ROC) Analyses.....	184
8.6 Results and Discussion	187
8.6.1 Demonstration ROC Curves	187
8.6.2 Optimal Decision Thresholds & Hazard Frameworks for Various Misprediction Costs ..	188
8.6.3 Using ROC Analyses to Inform Hazard Assessment and Mitigation Strategies	191
8.6.4 Evaluating Overall Model Performance	192
8.7 Conclusions.....	193
References.....	195
8.8 Electronic Supplement.....	210
Chapter 9: Conclusions	228

LIST OF FIGURES

Figure 2.1	Liquefaction severity observations following the (a) Darfield and (b) Christchurch earthquakes.....	29
Figure 2.2	Histograms and cumulative probabilities of LPI values for CPT soundings at sites with and without liquefaction manifestations in the Darfield and Christchurch earthquakes: (a) all soundings; (b) sounding depths ≥ 20 m.....	30
Figure 2.3	Probability of liquefaction manifestation.	31
Figure 2.4	Correlation between LPI and severity of liquefaction manifestation in the Darfield and Christchurch earthquakes: (a) all soundings; (b) sounding depths ≥ 20 m.	32
Figure 2.5	Probability of moderate or severe liquefaction (sand blows).	33
Figure 2.6	Computed LPI values for the (a) Darfield and (b) Christchurch earthquakes.	34
Figure 2.7	Prediction errors for the (a) Darfield and (b) Christchurch earthquakes.	35
Figure 2.8	Correlation between liquefaction prediction error and uncertainty of conditional PGA....	36
Figure 2.9	Correlation between liquefaction prediction error and average soil behavior type index in the (a) strata predicted to have liquefied and (b) crust and/or interspaced strata predicted not to have liquefied.	37
Figure 2.10	(S1) Depth of CPT soundings.....	40
Figure 2.11	(S2) Surficial (10 m) Soil Type inferred from CPT data.....	41
Figure 2.12	(S3) Representative observations of four liquefaction severity classes: (a) marginal liquefaction; (b) moderate liquefaction; (c) severe liquefaction; (d) severe lateral spreading (After CGD, 2012b).....	42
Figure 2.13	(S4) (a) Change in liquefaction severity prediction error from the Darfield earthquake to the Christchurch earthquake; (b) prediction error for Darfield earthquake vs. prediction error for Christchurch earthquake.	44
Figure 3.1	Correlations between I_c and apparent FC: Christchurch-specific correlation (Robinson et al., 2013) and generic correlation (Robertson & Wride, 1998).....	62
Figure 3.2	ROC analyses: (a) Frequency distributions of No Surficial Liquefaction Manifestation and Surficial Liquefaction Manifestations as a function of LPI, with four different threshold LPI values shown; and (b) Corresponding ROC curve.	63
Figure 3.3	Illustration of how a ROC curve is used to assess the efficiency of a diagnostic test. The optimum operating point (OOP) indicates the threshold value for which the misprediction rate is minimized, as described in text.	64
Figure 3.4	ROC analysis of LPI model performance in predicting the occurrence of surficial liquefaction manifestation. The optimum threshold LPI values (i.e., OOPs) for each LEP are highlighted in the inset figure.....	65
Figure 3.5	Probability of liquefaction manifestation.	66
Figure 3.6	Probability of moderate or severe liquefaction manifestation.	67
Figure 3.7	Distribution of LPI prediction errors, computed from the LPI hazard-scales defined by the (a) <i>Iwasaki criterion</i> ; and (b) LEP-specific calibrations given in Table 2.	68
Figure 3.8	Comparison of LPI model prediction errors at each investigation site, as computed by (a) R&W98 vs. MEA06; (b) R&W98 vs. I&B08 ² ; and (c) MEA06 vs. I&B08 ²	69
Figure 3.9	LEP/LPI model comparisons at site with inconsistent errors in the Darfield earthquake: (a) stress reduction coefficient, r_d ; (b) $CSR_{M7.5}$; and (c) LPI.	70
Figure 3.10	(S1) LPI prediction errors for the 4/9/2010 Darfield earthquake, using the calibrated (a) R&W98; (b) MEA06; (c) I&B08 ¹ ; and (d) I&B08 ² LPI models. The classification scheme is detailed in Table S1, where “U-P” indicates under-predictions of manifestation severity	

	(i.e., severity was more than predicted), and “O-P” indicates over-predictions of manifestation severity (i.e., severity was less than predicted).	72
Figure 3.11	(S2) LPI prediction errors for the 22/2/2011 Christchurch earthquake, using the calibrated (a) R&W98; (b) MEA06; (c) I&B08 ¹ ; and (d) I&B08 ² LPI models. The classification scheme is detailed in Table S1, where “U-P” indicates under-predictions of manifestation severity (i.e., severity was more than predicted), and “O-P” indicates over-predictions of manifestation severity (i.e., severity was less than predicted).	73
Figure 3.12	(S3) Representative observations of four liquefaction severity classes: (a) marginal liquefaction; (b) moderate liquefaction; (c) severe liquefaction; (d) severe lateral spreading.	75
Figure 4.1	Representative observations of (a) marginal manifestation; (b) moderate manifestation; and (c) severe manifestation of liquefaction at the ground surface (after Green et al., 2014).	98
Figure 4.2	Correlations between I_c and apparent FC: Christchurch-specific correlation (Robinson et al., 2013) and generic correlation (Robertson & Wride, 1998).	99
Figure 4.3	ROC analyses: (a) Frequency distributions of No Surficial Liquefaction Manifestation and Surficial Liquefaction Manifestations as a function of LPI, with four different threshold LPI values shown; and (b) Corresponding ROC cur.....	100
Figure 4.4	Illustration on how a ROC curve is used to assess the efficiency of a diagnostic test. The optimum operating point (OOP) indicates the threshold value for which the misprediction rate is minimized, as described in text.	101
Figure 4.5	ROC analysis of LPI model performance in predicting the occurrence of surficial liquefaction manifestation (using I_c -cutoff value of 2.6). The optimum threshold LPI values (i.e., OOPs) for each LEP are highlighted in the inset figure.	102
Figure 4.6	Area under ROC curve (AUC) vs. soil-behavior-type index (I_c) cutoff used in the LPI framework, considering (a) all manifestations of liquefaction, ranging from marginal to severe; and (b) manifestations of liquefaction more likely to damage infrastructure, ranging from moderate to severe. Increasing AUC indicates better model performance.	103
Figure 4.7	Map of study area showing locations of investigation sites, parsed by I_{c10} , the soil-behavior-type index (I_c) averaged over the uppermost 10 m of each site profile.....	104
Figure 4.8	Area under ROC curve (AUC) vs. soil-behavior-type index (I_c) cutoff used in the LPI framework, considering all manifestations of liquefaction, ranging from marginal to severe, for cases with (a) $I_{c10} < 2.05$; and (b) $I_{c10} \geq 2.05$	105
Figure 4.9	Area under ROC curve (AUC) vs. soil-behavior-type index (I_c) cutoff used in the LPI framework, considering manifestations of liquefaction more likely to damage infrastructure, ranging from moderate to severe, for cases with (a) $I_{c10} < 2.05$; and (b) $I_{c10} \geq 2.05$	106
Figure 5.1	Liquefaction severity prediction errors for the (a) M_w 7.1 Darfield and (b) M_w 6.2 Christchurch New Zealand earthquakes. After Maurer et al. (2014).	121
Figure 5.2	a) Conditions of subsurface soil stratification discriminating between occurrence and non-occurrence of ground rupturing due to liquefaction (200 gal PGA); (b) Boundary curves proposed for identification of liquefaction-induced damage. After Ishihara (1985).	122
Figure 5.3	(a) Illustration of assumption #3, stated in the text, and used in the derivation of LPI_{ISH} . It can be seen that H_1 and H_2 are related via m , the slope unique to each boundary curve; (b) Assumed boundary curve slopes (m) used in the derivation of LPI_{ISH}	123
Figure 5.4	Comparison of depth weighting functions used in the LPI and LPI_{ISH} procedures.	124

Figure 5.5	CPT data at site LEN-37 following the 1989 Loma Prieta earthquake. Site Len-37 had no surficial manifestations of liquefaction.	125
Figure 5.6	CPT data at site SF-5 following the 1999 Kocaeli earthquake. Surficial manifestations of liquefaction were present at site SF-5.	126
Figure 5.7	CPT data at site AVD-49 following the 2010 Darfield earthquake. Site AVD-49 had no surficial manifestations of liquefaction.	127
Figure 5.8	CPT data at site WYN-5a following the 1994 Northridge earthquake. Surficial manifestations of liquefaction were present at site WYN-5a.	128
Figure 5.9	Histograms and cumulative probabilities of (a) LPI and (b) LPI _{ISH} values for CPT soundings at sites with and without surficial liquefaction manifestation.	129
Figure 6.1	(a) Curves for estimating post-liquefaction volumetric-strain (ϵ_v) as a function of the factor of safety against liquefaction (FS_{liq}) and initial relative density (D_r) (after Ishihara and Yoshimine 1992); (b) curves derived from (a) for estimating ϵ_v as a function of FS_{liq} and equivalent clean sand normalized CPT tip resistance (q_{c1Ncs}), as proposed by Zhang et al. (2002) utilizing Equation (2), with curves added for this study (after Zhang et al. 2002).	142
Figure 6.2	Correlations relating equivalent clean sand normalized CPT tip resistance (q_{c1Ncs}) to relative density (D_r).	143
Figure 6.3	Curves derived from Figure 1a for estimating post-liquefaction volumetric-strain (ϵ_v) as a function of the factor of safety against liquefaction (FS_{liq}) and equivalent clean sand normalized CPT tip resistance (q_{c1Ncs}), herein developed utilizing Equation (3) with $C = 0.9$: (a) in the style of Zhang et al. (2002); and (b) using approximate, continuous solutions proposed by Yoshimine et al. (2006).	144
Figure 6.4	ROC analyses: (a) frequency distributions of liquefaction manifestation and no liquefaction manifestation as a function of LSN; (b) corresponding ROC curve, and illustration of how a ROC curve is used to assess the efficiency of a diagnostic test. The optimum operating point (OOP) indicates the LSN decision threshold for which the rate of misprediction is minimized.	145
Figure 6.5	(a) ROC analyses of six LSN variants in predicting liquefaction likely to cause damage; (b) magnified view of optimal-performance area, wherein optimal LSN thresholds are identified for S1 through S5.	146
Figure 7.1	Liquefaction susceptibility criteria proposed by (a) Polito (2001) [P01]; (b) Seed et al. (2003) [SEA03]; (c) Bray and Sancio (2006) [B&S06]; and (d) Boulanger and Idriss (2006) [B&I06].	166
Figure 7.2	Example FC (a) and I_c (b) profiles from a site in Christchurch; 300 mm intervals over which I_c statistics were recorded, each corresponding to a soil sampling location, are shown in (b).	167
Figure 7.3	ROC analyses: (a) frequency distributions of soils susceptible and unsusceptible to liquefaction as a function of measured I_c , with four different threshold I_c values shown; (b) corresponding ROC curve, and illustration of how a ROC curve is used to assess the efficiency of a diagnostic test. The optimum decision threshold is that for which the rate of misprediction is minimized.	168
Figure 7.4	Frequency distributions of samples classified by liquefaction-susceptibility criteria based on Atterberg limits, plotted as a function of measured I_c : (a) Polito (2001); (b) Seed et al. (2003); (c) Bray and Sancio (2006); and (d) Boulanger and Idriss (2006). Classifications in (a) – (d) are as defined in the text. Optimal I_c thresholds for identifying liquefaction-susceptible soils are also identified in (a) – (d).	169

Figure 7.5	ROC analysis of I_c index performance in segregating soils susceptible to liquefaction from soils unsusceptible to liquefaction, as defined by the Polito (2001) [P01], Seed et al. (2003) [SEA03], Bray and Sancio (2006) [B&S06], and Boulanger and Idriss (2006) [B&I06] criteria. Optimum I_c thresholds are identified for each criteria in the inset figure.	170
Figure 7.6	The probability of liquefaction susceptibility as a function of measured I_c . Susceptibility is as defined by the Polito (2001) [P01], Seed et al. (2003) [SEA03], Bray and Sancio (2006) [B&S06], and Boulanger and Idriss (2006) [B&I06] criteria. The range of deterministic I_c thresholds commonly used in practice is also highlighted.	171
Figure 7.7	(a) Christchurch-specific $I_c - FC$ data and proposed correlation (Eq 7); (b) Comparison with the Robertson and Wride (1998) and Boulanger and Idriss (2014) generic $I_c - FC$ correlations.	172
Figure 7.8	Soil behavior type index, I_c , vs. fines content, FC , color-coded by unified soil classification system (USCS) characterization.	173
Figure 7.9	Locations of samples classified as: (a) clean sands to silty sands; (b) ML or OL variants; (c) CL-ML variants; (d) CL variants; and (e) MH or OH variants. The soil behavior type index computed from CPT data and averaged over the uppermost 10 m, I_{c10} , is mapped in (f) using inverse-distance-weighting interpolation between CPT locations. Black dots represent all soil sampling locations in (a-e) and all CPT locations in (f).	174
Figure 8.1	ROC analyses: (a) frequency distributions of liquefaction manifestation and no liquefaction manifestation as a function of LSN ; (b) corresponding ROC curve, and illustration of how a ROC curve is used to assess the performance of a diagnostic test. The optimum LSN decision threshold is that for which the misprediction cost is minimized.	203
Figure 8.2	ROC analyses demonstrating that: (a) classifiers with equivalent AUC (i.e., equivalent overall efficiency) can perform very differently in specific regions of ROC space; (b) classifiers with higher AUC can, in specific regions of ROC space, perform worse than classifiers with lower AUC	204
Figure 8.3	ROC analysis of LPI , LPI_{ISH} , LSN , and IDS performance in predicting the occurrence of surficial liquefaction manifestations, wherein the I&B08 procedure was used. Optimal decision thresholds for the scenario $CR = 1$ are highlighted for each liquefaction hazard framework in the inset figure.	205
Figure 8.4	Optimal decision threshold vs. CR , as determined from analyses of the CES and global datasets using the I&B08 and B&I14 liquefaction triggering procedures within the frameworks of: (a) LPI ; (b) LPI_{ISH} ; (c) LSN ; and (d) IDS	206
Figure 8.5	Optimal liquefaction hazard framework as a function of CR , as determined from ROC analyses of the: (a) Sept 2010 M_w 7.1 Darfield Earthquake; (b) Feb 2011 M_w 6.2 Christchurch Earthquake; (c) Feb 2016 M_w 5.7 Christchurch Earthquake; (d) CES dataset (i.e., a, b, and c combined); and (e) global dataset.	207
Figure 8.6	AUC values computed from ROC analyses of the CES and global datasets using the (a) I&B08 and (b) B&I14 liquefaction triggering procedures within the LPI , LPI_{ISH} , LSN , and IDS liquefaction hazard frameworks. AUC is a popular measure of overall prediction efficiency.	208
Figure 8.7	AUC computed from ROC analyses of the CES dataset vs. global dataset using the I&B08 and B&I14 procedures within the LPI , LPI_{ISH} , LSN and IDS liquefaction hazard frameworks. Figure 7 is an alternative visualization of data presented in Figure 6.	209

LIST OF TABLES

Table 2.1 LPI values used to assess prediction accuracy.....	28
Table 2.2 LPI prediction error classifications.....	28
Table 2.3 (S1) Liquefaction severity classification criteria	39
Table 3.1 Liquefaction severity classification criteria (after Green et al., 2014).....	61
Table 3.2 Summary of Receiver Operator Characteristic (ROC) analyses ^a	61
Table 3.3 (S1) LPI prediction error classifications.....	74
Table 4.1 Liquefaction severity classification criteria (after Green et al., 2014).....	97
Table 4.2 Summary of ROC Analyses to Investigate Performance in High-FC Soils: Part A	97
Table 4.3 Summary of ROC Analyses to Investigate Performance in High-FC Soils: Part B	97
Table 6.1 Summary of ε_v estimation methods to be assessed in the LSN framework.	141
Table 7.1 Criteria-specific coefficients for use in Eq 2.	165
Table 7.2 Summary of ROC analyses to investigate I_c -based soil classification.....	165
Table 8.1 Summary of Liquefaction Case Histories Analyzed in this Study.....	201
Table 8.2 Criteria for Classifying the Severity of Liquefaction Manifestation.	202
Table 8.3 (S1) Global Dataset of Liquefaction Case Histories.....	210

Chapter 1: Introduction

1.1 Motivation

Liquefaction is a common cause of ground failure during earthquakes and is directly responsible for tremendous damage to civil infrastructure. Manifestations of liquefaction include the occurrence of sand blows and lateral spread failures, settlement and tilting of structures, cracking of pavements, and failure of buried lifelines due to flotation or differential settlements, among others. These effects were vividly displayed during the 2010-2011 Canterbury, New Zealand, Earthquake Sequence (CES), which caused widespread, severe, and recurrent liquefaction throughout the city of Christchurch. The CES includes the $M_w 7.1$, 4 September 2010 Darfield, $M_w 6.2$, 22 February 2011 Christchurch, and $M_w 5.7$, 14 February 2016 Christchurch earthquakes, as well as 11 other $M_w \geq 5.0$ events epicentrally located within 20 km of central Christchurch. In the 22 February 2011 Christchurch earthquake, nearly half of developed land was affected by liquefaction, with the thickness of vented sediments on the ground surface exceeding 0.5 m at some sites, making it one of the most pervasive and severe liquefaction events on record.

As the CES illustrates, there is a critical need to predict the occurrence and severity of soil liquefaction. Whitman (1971), and Seed and Idriss (1971), first developed the “simplified” liquefaction triggering procedure to compute the factor of safety against liquefaction (FS_{liq}) at a given depth in the soil profile. While this procedure predicts liquefaction triggering at a specific depth, it does not predict the severity of liquefaction manifested at the ground surface, which more directly correlates to damage potential to infrastructure. To fill this gap, Iwasaki et al. (1978) proposed the liquefaction potential index (LPI) to better characterize the damage potential of liquefaction, where LPI is computed as:

$$LPI = \int_0^{20 \text{ m}} F \cdot w(z) dz \quad (1)$$

where $F = 1 - FS_{liq}$ for $FS_{liq} \leq 1$ and $F = 0$ for $FS_{liq} > 1$; $w(z)$ is a depth weighting function given by $w(z) = 10 - 0.5z$; and z is depth in meters below the ground surface. LPI has since become the state-of-practice framework for assessing liquefaction hazard and has been used in countless seismic regions around the world. While widely used, opportunities to evaluate the performance of LPI in the field are rare (this is true of liquefaction-related methodologies in general). Owed in part to the expense of performing in-situ geotechnical testing, and to limited ground motion recordings in the effected areas, only 200 to 300 liquefaction case histories have resulted from all earthquakes combined prior to the CES. Thus, nearly all empirical procedures for evaluating liquefaction related phenomena are based on a relatively small number of well-documented cases.

Importantly, in addition to displaying the damage-potential of liquefaction on a massive scale, the CES also provides the chance to develop a liquefaction dataset of unprecedented size and quality. Ground motions from these events were recorded by a dense network of strong motion stations (e.g., Bradley & Cubrinovski, 2011), and due to the pervasiveness of liquefaction, the New Zealand Earthquake Commission funded an extensive geotechnical reconnaissance and characterization program. The combination of densely recorded ground motions, well-documented liquefaction response, and detailed subsurface characterization comprises the high-quality data needed to develop liquefaction case histories. The work presented in this dissertation is thus motivated by the truly unique opportunity resulting from the CES to assess and improve the efficacy of liquefaction-analytics.

1.2 Contributions

Given the critical need to predict the occurrence and severity of earthquake-induced soil liquefaction, this research makes the following succinctly summarized contributions:

1. The development of a truly unparalleled dataset comprised of ~10,000 high-quality liquefaction case histories resulting from the CES. An additional 265 case histories resulting from 20 other global earthquakes are also compiled from the literature. With respect to the latter dataset, many of these case histories did not previously exist in an accessible, easily analyzed format and/or have never before been used to study liquefaction-damage potential. Collectively, these datasets provide a truly unique opportunity to improve our understanding of liquefaction hazard.
2. A rigorous and unprecedented field assessment of LPI, which while used in practice worldwide, is shown to perform poorly at many sites. Pertinent investigations include: (a) performance comparisons of the Robertson and Wride (1998), Moss et al. (2006), Idriss and Boulanger (2008), and Boulanger and Idriss (2014) liquefaction triggering procedures, operating within the LPI framework, for assessing liquefaction hazard; (b) proposal of site-specific optimum decision thresholds for assessing and mitigating liquefaction hazard; and (c) analyses to determine the cause of erroneous liquefaction hazard assessments, resulting in the recognition that existing methodologies perform particularly poorly at sites where soils with high fines-content are present, specifically when such soils “cap” the soil profile or are interbedded among liquefiable deposits. Collectively, these investigations illuminate the need for a more reliable liquefaction hazard index and identify specific shortcomings of existing methodologies.
3. The development of new liquefaction hazard framework, termed LPI_{ISH} , which accounts for the influence of the non-liquefied capping layer on the surface manifestation of liquefaction. The

predictive capability of LPI_{ISH} is compared to both LPI and a competing alternative framework newly proposed in the literature (i.e., LSN). LPI_{ISH} is shown to provide the most efficient assessments of liquefaction hazard, both for the CES, and for the dataset of global case histories.

4. Ultimately, significant room for improvement still exists with respect to accurate assessment of liquefaction hazard. The findings presented in this dissertation form the basis for developing a further-improved liquefaction hazard framework. Moreover, a methodology is proposed by which improvements can be measured in a standardized and objective manner.

1.3 Dissertation Structure and Contents

The chapters of this dissertation consist of a series of manuscripts that combine to make the contributions outlined previously. The manuscripts describe various aspects of liquefaction hazard assessment investigated using an unprecedented dataset resulting from the 2010-2011 Canterbury, New Zealand, earthquake sequence. The papers that comprise this dissertation may each be read as a stand-alone document. In this regard, each chapter contains a review of pertinent literature, an overview of data and methodology, and a list of references cited within. Consequently, some information is presented multiple times. As an example, receiver operating characteristic (ROC) analyses are used throughout the dissertation to analyze the performance of liquefaction hazard frameworks (in addition to other types of data). Many chapters therefore contain a summary of the ROC methodology. In this case and others, the reader may wish to skim repetitive sections once familiar with the methodology. Chapters are assembled in chronological order, progressing from preliminary assessments based on relatively limited data, to evaluations using 10,000 liquefaction case histories and robust analysis techniques. In the following, a brief overview of the content of each chapter is provided, with particular emphasis on establishing the motivation for undertaking each study. Notably, the circumstances under which this dissertation was developed are unique in that the data available to the author consistently increased (both in type and quantity) during the years following the Canterbury earthquake sequence. Accordingly, each manuscript is placed in the context of the available data, and of other important research developments.

In Chapter 2, the performance of LPI for predicting the occurrence and severity of surficial liquefaction manifestation is evaluated using approximately 2,350 liquefaction case histories resulting from the CES, wherein the Robertson and Wride (1998) liquefaction triggering procedure is used within the LPI framework. These case histories were developed from cone penetration test soundings performed in the 18 months following the 4 September $M_w7.1$ Darfield earthquake. This study thus represents a “rapid” and preliminary investigation of the performance of liquefaction hazard assessment in Christchurch.

While the assessed dataset is small relative to that developed at the conclusion of this dissertation (Chapter 8), it contains significantly more case histories than had been collected from all previous earthquakes combined. As such, this initial evaluation provides unprecedented insights into liquefaction hazard assessment. Of greatest interest, it is shown that while LPI is generally effective, hazard assessments are highly erroneous for large portions of Christchurch.

In Chapter 3, a significantly larger dataset of approximately 7,000 case histories is developed, to include the use of robust, event-specific ground water models. Moreover, three competing liquefaction triggering procedures are evaluated within the LPI framework: Robertson and Wride (1998); Moss et al. (2006); and Idriss and Boulanger (2008). In practice, there is considerable debate as to which of these procedures should be used to predict liquefaction triggering. Accordingly, the influence of the adopted triggering procedure on the accuracy of derivative LPI hazard assessments is investigated. Moreover, this investigation introduces and utilizes the ROC methodology, which provides a standardized and objective assessment of diagnostic-model performance. Consistent with Chapter 2, it is shown that LPI performs poorly at a significant percentage of locations assessed, regardless of which triggering procedure is used within the LPI framework.

In Chapter 4, “fines-content effects” on liquefaction hazard are investigated. A major conclusion of Chapters 2 and 3 is that LPI hazard assessments appear to be significantly less efficient (i.e., inaccurate) at sites where soils with high fines-content are present. Accordingly, several possible explanations are investigated in Chapter 4. Through these analyses, it is hypothesized that non-liquefiable, high fines-content soils are likely to inhibit liquefaction manifestation by affecting pore pressure development and redistribution, resulting in over-predictions of hazard. It is thus recognized that liquefaction hazard frameworks should consider not only the behavior of liquefiable soils, but also the influence of non-liquefiable soils that “cap” the soil profile or are interbedded among liquefiable deposits.

In Chapter 5, a new liquefaction hazard framework, termed LPI_{ISH} , is derived from the H_1 - H_2 chart proposed by Ishihara (1985). The proposed framework considers the influence of the non-liquefied capping layer on the manifestation of liquefaction, which while shown to be significant, is not accounted for by LPI. LPI_{ISH} is evaluated using select liquefaction case histories and is found to be consonant with observed surface effects, demonstrating improvement over LPI in mitigating false-positive predictions.

Coinciding with the development of LPI_{ISH} , an alternative to LPI was also proposed by a group of practitioners and academics from New Zealand and the United States. The proposed Liquefaction Severity Number (LSN) considers the influence of post-liquefaction volumetric strain potential (ϵ_v) on liquefaction hazard. LSN thus recognizes that soils of different density have different consequences

once liquefaction is triggered. However, many different techniques exist for estimating ε_v , each of which could lead to different computed LSN values, and by corollary, different assessments of liquefaction hazard. Accordingly, Chapter 6 investigates the influence of six techniques for estimating ε_v on the accuracy of LSN assessments. It is shown that a control model in which ε_v was removed performed best, suggesting that ε_v either provides no statistically distinguishable benefits in terms of prediction accuracy, or is accounted for by LSN in such a way that is not optimal.

In Chapter 7, deterministic and probabilistic correlations are developed for predicting (a) soil fines-content; and (b) whether soil is *susceptible* to liquefaction. While each of these predictions is a required input in the LPI, LPI_{ISH}, and LSN hazard frameworks, the use of generic correlations developed from global data could be inaccurate on local scales. The development of Christchurch-specific correlations could thus lead to a better understanding of observed liquefaction phenomena. The findings presented in Chapter 7 represent an extensive case study of CPT-based soil characterization and are particularly pertinent to ongoing research using data from Christchurch. However, the approach used to develop deterministic and probabilistic correlations is not limited to parts of New Zealand, but rather, can be applied worldwide.

In Chapter 8, nearly 10,000 liquefaction case histories, to include 265 cases compiled from 20 global earthquakes, are used to assess and compare the performance of LPI, LPI_{ISH}, and LSN using a methodology considering the consequences, or economies, of misprediction, to which the performance of hazard assessment is intimately linked. It is shown that optimal decision thresholds are inherently tied to underlying economic assumptions, since the threshold that is “optimal” for one project, or one category of land-use, may be inappropriate for others. The decision thresholds proposed in Chapter 8 can be used to inform strategies for assessing and/or mitigating liquefaction hazards. Additionally, for the assessed dataset, LPI_{ISH} was the most efficient of the assessed frameworks. However, it is also shown that significant room for improvement remains, forming the basis for the future development of a further-improved liquefaction hazard framework.

References

- Boulanger, R.W. and Idriss, I.M. (2014). "CPT and SPT based liquefaction triggering procedures." *Report No. UCD/CGM.-14/01*, Center for Geotech. Modelling, Department of Civil and Environmental Engineering, UC Davis, CA, USA.
- Bradley, B.A. and Cubrinovski, M., (2011). "Near-source Strong Ground Motions Observed in the 22 February 2011 Christchurch Earthquake." *Seismological Research Letters*, 82: 853-865.
- Idriss, I.M. and Boulanger, R.W. (2008). "Soil liquefaction during earthquakes." Monograph MNO-12, Earthquake Engineering Research Institute, Oakland, CA, 261 pp.
- Ishihara, K. (1985). "Stability of natural deposits during earthquakes." *Proceedings of the 11th International Conference on Soil Mechanics and Foundation Engineering*, San Francisco, CA, USA, 1, 321-376.
- Moss, R.E.S, Seed, R.B., Kayen, R.E., Stewart, J.P., Der Kiureghian, A., and Cetin, K.O. (2006). "CPT-based probabilistic and deterministic assessment of in situ seismic soil liquefaction potential." *Journal of Geotechnical and Geoenvironmental Engineering*, ASCE, 132(8):1032-1051.
- Robertson, P.K. and Wride, C.E. (1998). "Evaluating cyclic liquefaction potential using cone penetration test." *Canadian Geotechnical Journal* 35(3): 442-459.
- Seed, H.B. and Idriss, I.M. (1971). "Simplified procedure for evaluating soil liquefaction potential." *Journal of the Soil Mechanics and Foundation Division*, ASCE, 97(9): 1249-1273.
- Whitman, R.V. (1971). "Resistance of soil to liquefaction and settlement." *Soils and Foundations*, 11(4): 59-68.

Chapter 2: Evaluation of the Liquefaction Potential Index (LPI) for Assessing Liquefaction Hazard in Christchurch, New Zealand

Brett W. Maurer¹, Russell A. Green², Misko Cubrinovski³, Brendon A. Bradley⁴

¹ Graduate Research Assistant, Dept. of Civil and Environmental Engineering, Virginia Tech, Blacksburg, Virginia 24061, U.S.A.

² Professor, Dept. of Civil and Environmental Engineering, Virginia Tech, Blacksburg, Virginia 24061, U.S.A.

³ Professor, Dept. of Civil and Natural Resources Engineering, University of Canterbury, Private Bag 4800, Christchurch, New Zealand

⁴ Professor, Dept. of Civil and Natural Resources Engineering, University of Canterbury, Private Bag 4800, Christchurch, New Zealand

2.1 Abstract

While liquefaction potential index (LPI) has been used to characterize liquefaction hazards worldwide, calibration of LPI to observed liquefaction severity is limited, and the efficacy of the LPI framework and accuracy of derivative liquefaction hazard maps are thus uncertain. Herein, utilizing CPT soundings from nearly 1200 sites, in conjunction with field observations following the Darfield and Christchurch, New Zealand earthquakes, this study evaluates the performance of LPI in predicting the occurrence and severity of surficial liquefaction manifestations. It was found that LPI is generally effective in predicting moderate-to-severe liquefaction manifestations, but its utility diminishes for predicting less severe manifestations. Additionally, it was found that LPI should be used with caution in locations susceptible to lateral spreading, as LPI may inconsistently predict its occurrence. A relationship between over-predictions of liquefaction severity and profiles having soils with high inferred fines-content was also investigated. It was determined that the LPI procedure might be improved if it accounted for the characteristics of soils in the crust and interbedded non-liquefiable layers, as well as the characteristics of the soils predicted to liquefy. Further research is needed in this regard. Finally, it was found that for the in-situ conditions in Christchurch, the computed LPI values were relatively sensitive to estimates of ground water depth because of the proximity of liquefiable strata to the ground surface.

2.2 Introduction

The objective of the study presented herein is to assess the liquefaction potential index (LPI) for predicting the severity of the manifestation of soil liquefaction using data from the 2010-2011 Canterbury (New Zealand) Earthquake Sequence (CES). Liquefaction is a common cause of ground failure during earthquakes and is directly responsible for tremendous damage to civil infrastructure. Manifestations of liquefaction include the occurrence of sand blows and lateral spread failures, settlement and tilting of structures, cracking of pavements, and failure of buried lifelines due to flotation or differential settlements, among others. These effects were vividly displayed during the 2010-2011 CES, which caused widespread, severe, and recurrent liquefaction throughout the city of Christchurch. The CES includes the M_w 7.1, 4 September 2010 Darfield and M_w 6.2, 22 February 2011 Christchurch earthquakes, as well as eleven other $M_w \geq 5.0$ events epicentrally located within 20 km of central Christchurch (GeoNet, 2012). In the 22 February 2011 Christchurch earthquake, nearly half of developed land was affected by liquefaction, with the thickness of vented sediments on the ground surface exceeding 0.5 m at some sites, making it one of the most pervasive and severe liquefaction events on record (e.g., Cubrinovski and Green, 2010; Cubrinovski et al., 2011b; Orense et al., 2011).

As the CES illustrates, there is a critical need to predict the occurrence and severity of soil liquefaction for engineering design, hazard mapping, urban planning, and regulatory purposes. Whitman (1971), and Seed and Idriss (1971), first developed the “simplified” liquefaction evaluation procedure to

compute the factor of safety against liquefaction (FS) at a given depth in the soil profile. While the simplified procedure predicts liquefaction triggering at a specific depth, it does not predict the severity of liquefaction manifestation at the ground surface, which more directly correlates to damage potential due to liquefaction. To fill this gap, Iwasaki et al. (1978) proposed the liquefaction potential index (LPI) to better characterize the damage potential of liquefaction, where LPI is computed as:

$$\text{LPI} = \int_0^{20 \text{ m}} F \cdot w(z) dz \quad (1)$$

In Equation (1), $F = 1 - \text{FS}$ for $\text{FS} \leq 1$ and $F = 0$ for $\text{FS} > 1$, where FS is obtained from a simplified liquefaction evaluation procedure, and $w(z)$ is a depth weighting function given by $w(z) = 10 - 0.5z$, where z = depth in meters below the ground surface. Thus, it is assumed that the severity of liquefaction manifestation is proportional to the thickness of a liquefied layer; the amount by which FS is less than 1.0; and the proximity of the layer to the ground surface. It can be shown that the depth weighting function allots maximum contributions to LPI from the 1st, 2nd, 3rd, and 4th 5-meter depth increments of 43.75%, 31.25%, 18.75%, and 6.25%, respectively. Given this definition, LPI can range from 0 for a site with no liquefaction potential to a maximum of 100 for a site where FS is zero over the entire 20 m depth. Using SPT data from 45 liquefaction sites in Japan, Iwasaki et al. (1978) found that 80% of the sites had $\text{LPI} > 5$, while 50% had $\text{LPI} > 15$. Based on this data, it was proposed that severe liquefaction should be expected for sites where $\text{LPI} > 15$ but should not be expected for sites where $\text{LPI} < 5$. This criterion for liquefaction manifestation, defined by two threshold values of LPI, is subsequently referred to herein as the *Iwasaki criterion*.

Since its inception, LPI has been used to develop liquefaction hazard maps for seismic regions around the world (e.g., Sonmez, 2003; Papathanassiou et al., 2005; Baise et al., 2006; Holzer et al., 2006ab; Lenz and Baise, 2007; Hayati and Andrus, 2008; Yalcin et al., 2008; Chung and Rogers, 2011; Dixit et al., 2012, among others), including probabilistic liquefaction hazard maps (e.g., Cramer et al., 2008) derived from geologic maps using liquefaction probability curves specific to each geologic unit (e.g., Holzer et al., 2011). However, while researchers and practitioners have used LPI to characterize liquefaction hazards, a thorough evaluation of the LPI framework and calibration of LPI to observed liquefaction severity, or to specific ground-surface manifestations, is relatively limited and the applicability of the original Iwasaki criterion is thus highly uncertain. Toprak and Holzer (2003) computed LPI for historic liquefaction sites in California (USA) using the Robertson and Wride (1998) CPT-based liquefaction evaluation procedure to determine FS. They found that while the median LPI values generally matched the originally proposed threshold values for minor and severe liquefaction (i.e., 5 and 15, respectively), the manifestation and severity of liquefaction was not accurately predicted for some sites. The lower and upper LPI quartiles were 3 and 10 for sand blows, and 5 and 17 for lateral

spreads, respectively. Toprak and Holzer suggested these findings were consistent with the Iwasaki criterion, a conclusion subsequently supported by a study of liquefaction sites following the 2003 San Simeon (USA) earthquake (Holzer et al., 2005). Conversely, Lee et al. (2003) used the Robertson and Wride (1998) method to evaluate 72 CPTs at sites with field observations during the M_w 7.6, 1999 Chi-Chi (Taiwan) earthquake and found the Iwasaki criterion to be a poor predictor of liquefaction occurrence. It was found that 85% of the non-liquefied sites had an $LPI > 5$ while 30% of the non-liquefied sites had an $LPI > 15$. Based on these results, Lee et al. suggested the original threshold values proposed by Iwasaki et al. (1978) be changed to 13 and 21, respectively, such that liquefaction risk is high for sites with $LPI > 21$ and low for sites with $LPI < 13$. Similarly, Papathanassiou (2008) used the Youd et al. (2001) SPT procedure to compute LPI from 79 SPT borings performed following the Chi Chi, 1999 Kocaeli (Turkey), and 2003 Lefkada (Greece) earthquakes. The median LPI values for cases of “high” liquefaction severity, “medium” liquefaction severity, and “no failure” were 38, 24, and 14, respectively. Accordingly, Papathanassiou suggested using threshold LPI values of 19 and 32 as opposed to 5 and 15 per the Iwasaki criterion.

To account for uncertainty in LPI predictions, some researchers (e.g., Sonmez and Gokceoglu, 2005; Juang et al., 2008; Jha and Suzuki, 2009) have extended the LPI framework to give hazard assessments that are probabilistic, rather than deterministic. While these models allow practitioners to compute the probability of liquefaction manifestation, this approach does not supplant the need for an expanded LPI case-history database, consistency in how threshold LPI values are determined and how LPI values are computed to assess liquefaction hazard, and/or further fundamental studies of the LPI framework. As evident from the preceding discussion, existing calibrations of LPI to observed liquefaction severity are limited, are based on generally modest datasets, and give a wide range of suggested LPI threshold values for low and high severity of liquefaction manifestation, ranging from 5 and 15, to 19 and 32, respectively. The applicability of the Iwasaki criterion and the Iwasaki et al. (1978) LPI framework is thus uncertain, and consequently, so too are the accuracies of derivative liquefaction hazard maps for regions around the world.

Thus, the present study aims to evaluate both the Iwasaki criterion and the Iwasaki et al. (1978) LPI framework following an approach similar to that used by Toprak and Holzer (2003). Towards this end, the Robertson and Wride (1998) CPT-based liquefaction evaluation procedure (also refer to Youd et al. (2001)) is used in conjunction with a large, high-quality dataset from the 2010-2011 CES. Facilitated by ground motion records from a dense network of strong-motion stations, extensive soil characterization data, and detailed documentation of severity of liquefaction manifestations, the Canterbury earthquakes present a truly unique opportunity to rigorously evaluate the Iwasaki criterion and the Iwasaki et al. (1978) LPI framework for assessing risk to the built environment from

liquefaction. Towards this end, CPT soundings from nearly 1200 sites, each with observations of liquefaction severity during the Darfield and Christchurch earthquakes, are analyzed.

In the following, brief overviews of the geology of the Canterbury plains and the 2010-2011 CES are given. This is followed by a description of the geotechnical site characterization program that was initiated following the start of the 2010-2011 earthquake sequence and how LPI was computed for the study presented herein. The results of the LPI analyses are then discussed, with observations on the efficacy of the Iwasaki et al. (1978) LPI criterion and framework for assessing the liquefaction hazard of Christchurch and surrounding areas.

2.3 Data and Methodology

The study area of roughly 200 km² generally encompasses the extent of liquefaction in Christchurch and its environs during the CES. Located on the Pacific coast and amongst the Heathcote, Avon, and Waimakariri Rivers, much of Christchurch and surrounding areas have shallow water tables and surficial geology consisting of loose, non/low-plasticity, Holocene alluvial deposits (Brown et al., 1995), resulting in very high liquefaction susceptibilities. In both the M_w7.1 Darfield and M_w6.2 Christchurch earthquakes, widespread liquefaction occurred in Christchurch and the town of Kaiapoi to the north, causing extensive damage to residential and commercial buildings and other civil infrastructure. Overviews of liquefaction and related damage during the Darfield and Christchurch earthquakes is given by Cubrinovski and Green (2010), Cubrinovski et al. (2011a; 2011b), Green et al. (2011a) and Orense et al. (2011), among others. To assist in assessing insurance claims resulting from liquefaction damage and to aid in rebuilding Christchurch, the New Zealand Earthquake Commission (EQC) launched an intensive geotechnical characterization program following the Darfield earthquake (Murahidy et al., 2012). Much of the data used in this study is a product of that effort.

2.3.1 CPT Soundings

In the 18 months following the Darfield earthquake, 1495 CPT soundings were performed in the study area (see Figure 1), with 467 exceeding a depth of 20 m. As shown in Eq. (1), LPI requires integration over 20 m depth. However, computing LPI from soundings that do not meet this requirement does not necessarily result in an underestimation of the liquefaction hazard. If the local subsurface geology is well-characterized, it may be known that dense, non-liquefiable soils are typically found at a particular depth and unlikely to be underlain by looser liquefiable deposits that contribute to LPI. Specific to the Canterbury plains and this study, termination depths of CPT soundings were geo-spatially analyzed, and ones having anomalously shallow termination depths were removed from this study. For the

remaining soundings, however, the termination depths were reasonably assumed to define the maximum depths of liquefiable strata.

As sea level rose during the late Pleistocene and Holocene, estuarine, beach, and coastal swamp deposits prograded westward across present-day Christchurch until sea level reached a highstand ~6,500 years before present, with the coastline located 1-2 km west of the present-day central business district (CBD) (Brown et al., 1995). Since then, alluvial deposition has resulted in progradation of the coast to its present location (Brown et al., 1995). Collectively, the deposits resulting from coastline transgression and progradation are known as the Christchurch formation, and overlay Pleistocene gravels, i.e., the Riccarton Gravel formation. The thickness of the Christchurch formation is greatest (~40 m) beneath the present-day coastline and attenuates westwardly, terminating at the location of the mid-Holocene highstand, beyond which the Springston formation dominates the surface geology (alluvial gravels, sands, and silts) (Begg and Jones, 2012). Thus, where the Springston formation dominates (and in some areas of the Christchurch formation), gravelly soils result in CPT termination at shallow depth. In such cases, there still exists a possibility of deeper soils that contribute to LPI, but in general, the vertical extents of liquefiable soils tend to be greatest near the coast and diminish west of the CBD.

The locations and termination depths of CPT soundings are shown in Figure S1. It can be seen that the depth trends generally agree with the known geologic profile such that termination depths diminish from east to west. In addition, termination depths are correlated with the surficial soil types (inferred from CPT data), shown in Figure S2. For this study, it was assumed that the depths of soundings generally define the limits of the Christchurch formation, and consequently, the limits of liquefiable soils. However, the CPT database was first parsed using an Anselin Local Morans I analysis (Anselin, 1995) to identify sounding depths statistically less than the spatial average (i.e., soundings which may have been terminated before reaching the Riccarton Gravel formation). Using this analysis, which computes spatial means and variances to identify outliers, 322 soundings were removed from the study, leaving a total of 1173 soundings. In consideration of the Iwasaki et al. (1978) LPI framework and the assumptions made herein, some of the results presented in this study are given for both the complete CPT database (1173) referred to as “all,” and separately, the portion of soundings exceeding 20 m depth (467). Of the soundings that do not exceed 20 m, 191 terminate at 15-20 m depth, 237 terminate at 10-15 m depth, 203 terminate at 5-10 m depth, and 75 terminate at a depth less than 5 m.

2.3.2 Liquefaction Evaluation and Liquefaction Potential Index (LPI)

Factors of safety against liquefaction were computed using the CPT-based liquefaction evaluation procedure proposed by Robertson and Wride (1998). Although other CPT procedures have been

proposed (e.g., Moss et al., 2006; Idriss and Boulanger, 2006), several of the more extensive LPI studies that were performed previously (e.g., Toprak and Holzer, 2003; Lee et al., 2003, Holzer et al., 2005) used the Robertson and Wride (1998) procedure to compute the factors of safety against liquefaction in conjunction with LPI. Therefore, antecedent to calibrating LPI models based on newly developed liquefaction evaluation procedures, use of a reasonably consistent framework for assessing the Iwasaki criterion and for comparing to results from previous LPI studies is prudent. In a future study, the authors plan to evaluate other CPT-based liquefaction procedures in the LPI framework to assess their influence on the accuracy of hazard assessments.

To compute the total and effective vertical stresses as a function of depth, soil unit weights were estimated from CPT data using the method proposed by Robertson and Cabal (2010). Additionally, ground water table (GWT) depths were inferred from CPT pore pressure (u) measurements, but occasionally calibrated to published GWT maps (CGD, 2012a) or interpolated from nearby CPTs when obvious measurement errors existed (2.5% of CPTs). The effect of GWT depth estimation on LPI is discussed later in this paper. The soil behavior type index, I_c , developed by Robertson and Wride (1998), was used to identify non-liquefiable soils, where soils with $I_c > 2.6$ were considered to be too plastic to liquefy. Factors of safety were computed at either 1- or 2-cm depth intervals, corresponding to the measurement rate of CPT soundings. LPI was then computed with the Iwasaki et al. (1978) method, given by Eq. (1).

2.3.3 Estimation of a_{max} (PGA)

To evaluate the factor of safety against liquefaction, both the soil's resistance to liquefaction and the demand imposed on the soil by the earthquake need to be estimated. For the simplified approach used herein, the amplitude of cyclic loading is proportional to the PGA at the ground surface and the duration is related to the earthquake magnitude. Accordingly, the PGAs at CPT sites need to be estimated for both the Darfield and Christchurch earthquakes. The Canterbury earthquake sequence was recorded by a dense array of more than 20 near-source strong motion stations (Bradley and Cubrinovski, 2011; Bradley, 2012a), and consequently, PGAs can be estimated with a good level of accuracy. As outlined below, and similar to the approach outlined in Bradley (2013) and used by Green et al. (2011b, 2013), the PGAs recorded at the strong motion stations (GeoNet, 2012) were used to compute the conditional PGA distribution at the exact location of CPT soundings. The PGA at a strong motion station i can be expressed as:

$$\ln(\text{PGA}_i) = \overline{\ln\text{PGA}_l}(\text{Site, Rup}) + \eta + \varepsilon_i, \quad (2)$$

where $\ln(\text{PGA}_i)$ is the natural logarithm of the observed PGA at station i ; $\overline{\ln\text{PGA}_i}(\text{Site}, \text{Rup})$ is the median value of the natural logarithm of PGA at the same station predicted by an empirical ground motion prediction equation (GMPE), which is a function of the site and earthquake rupture; η is the inter-event residual; and ε_i is the intra-event residual. Based on Eq. (2), empirical GMPEs provide the (unconditional) distribution of PGA shaking as:

$$\ln(\text{PGA}_i) \sim N(\ln \overline{\text{PGA}_i}, \sigma_\eta^2 + \sigma_\varepsilon^2), \quad (3)$$

where $X \sim N(\mu_X, \sigma_X^2)$ is shorthand notation for X having a normal distribution with mean, μ_X , and variance, σ_X^2 . By definition, all recorded PGAs from a single earthquake have the same inter-event residual, η . On the other hand, the intra-event residual, ε_i , varies from site to site, but is correlated spatially among various locations due to similarities of path and site effects. Accordingly, PGAs at strong motion stations can be used to compute a conditional distribution of PGAs at the CPT sounding locations. First, the empirical GMPE proposed by Bradley (2010; 2013b) was used to compute the unconditional distribution of PGAs at the strong motion stations. A mixed-effects regression was then used to determine the inter-event residual, η , and the intra-event residuals, ε_i 's, for each strong motion station (Abrahamson and Youngs 1992; Pinheiro et al. 2008). Second, the covariance matrix of intra-event residuals was computed by accounting for the spatial correlation between all of the strong motion stations and a test site of interest. The joint distribution of intra-event residuals at a test site of interest and the strong motion stations is given as:

$$\begin{bmatrix} \varepsilon^{\text{site}} \\ \varepsilon^{\text{SMstation}} \end{bmatrix} = N\left(\begin{bmatrix} 0 \\ 0 \end{bmatrix}, \begin{bmatrix} \sigma_{\varepsilon^{\text{site}}}^2 & \Sigma_{12} \\ \Sigma_{21} & \Sigma_{22} \end{bmatrix}\right), \quad (4)$$

where $X \sim N(\boldsymbol{\mu}_X, \boldsymbol{\Sigma})$ is shorthand notation for X having a multivariate normal distribution with mean $\boldsymbol{\mu}_X$ and covariance matrix $\boldsymbol{\Sigma}$ (i.e., same as above, but in vector form, with bold denoting vectors or matrices); and $\sigma_{\varepsilon^{\text{site}}}^2$ is the variance in the intra-event residual at the site of interest. In Eq. (4), the covariance matrix has been expressed in a partitioned fashion to elucidate the subsequent computation of the conditional distribution of $\varepsilon^{\text{site}}$. The individual elements of the covariance matrix were computed from:

$$\Sigma(i, j) = \rho_{i,j} \sigma_{\varepsilon_i} \sigma_{\varepsilon_j}, \quad (5)$$

where $\rho_{i,j}$ is the spatial correlation of intra-event residuals between the two locations i and j , and σ_{ε_i} and σ_{ε_j} are the standard deviations of the intra-event residual at locations i and j . Based on the joint

distribution of intra-event residuals given by Equation 4, the conditional distribution of $\varepsilon^{\text{site}}$ was computed from Johnson et al. (2007):

$$\begin{aligned} [\varepsilon^{\text{site}} | \varepsilon^{\text{SMstation}}] &= N(\Sigma_{12} \cdot \Sigma_{22}^{-1} \cdot \varepsilon^{\text{SMstation}}, \sigma_{\varepsilon^{\text{site}}}^2 - \Sigma_{12} \cdot \Sigma_{22}^{-1} \cdot \Sigma_{21}) \\ &= N(\mu_{\varepsilon^{\text{site}} | \varepsilon^{\text{SMstation}}}, \sigma_{\varepsilon^{\text{site}} | \varepsilon^{\text{SMstation}}}^2) \end{aligned} \quad (6)$$

Using the conditional distribution of the intra-event residual at a test site of interest given by Eq. (6) and substituting into Eq. (3), the conditional distribution of the PGA_i was computed from:

$$[\ln \text{PGA}_{\text{site}} | \ln \text{PGA}_{\text{SMstation}}] = N(\ln \overline{\text{PGA}}_{\text{site}} + \eta + \mu_{\varepsilon^{\text{site}} | \varepsilon^{\text{SMstation}}}, \sigma_{\varepsilon^{\text{site}} | \varepsilon^{\text{SMstation}}}^2) \quad (7)$$

Thus, in cases where the CPT sounding was located far from any strong motion station, the conditional distribution was similar to the unconditional distribution, and for a sounding located very close to a strong motion station the conditional distribution approached the value observed at the strong motion station. To estimate the PGAs at the CPT sounding locations, the unconditional PGAs were estimated using the empirical GMPE proposed by Bradley (2010, 2013b) and the conditional PGAs were estimated following the approach outlined above wherein the spatial correlation model of Goda and Hong (2008) was used.

2.3.4 Liquefaction Severity

Observations of liquefaction and the severity of manifestations were made by the authors for each of the CPT sounding locations following both the Darfield and Christchurch earthquakes. This was accomplished by ground reconnaissance and using high-resolution aerial and satellite imagery (CGD, 2012b) performed in the days immediately following each of the earthquakes, and required hundreds of hours to complete. In addition, lateral spreading observations and measurements from the Canterbury Geotechnical Database (CGD, 2012c) were utilized. CPT sites were assigned one of six damage classifications: no liquefaction, marginal liquefaction, moderate liquefaction, severe liquefaction, lateral spreading, and severe lateral spreading. The criteria for each classification are given in Table S1. Aerial images that are representative of four liquefaction severity classes are shown in Figure S3. It should be noted that the classifications describe the predominant damage mechanism and manifestation of liquefaction. For example, some “severe liquefaction” sites also had minor lateral spreading, and likewise, many “lateral spreading” sites also had some amount of liquefaction ejecta present. The distributions of liquefaction severity observations following the Darfield and Christchurch earthquakes are shown in Figure 1a and Figure 1b, respectively, and reflect the combined effects of liquefaction susceptibility (loose soil with high water table) and the intensity of shaking.

2.4 Results and Discussion

2.4.1 Prediction of Liquefaction Occurrence

The cumulative distribution functions (CDFs) of LPI values for soundings at sites with and without liquefaction manifestations are shown for all soundings and for soundings with depth ≥ 20 m in Figure 2a and Figure 2b, respectively. For brevity, these sites are subsequently referred to as *liquefied* and *non-liquefied* sites. The CDFs indicate that while LPI does not precisely segregate liquefied and non-liquefied sites, liquefaction observations are generally associated with higher LPI values, whereas sites without liquefaction manifestations are generally associated with lower LPI values. For all data (Figure 2a), the CDFs indicate that 76% of liquefied sites have $LPI > 5$ and 34% have $LPI > 15$. In addition, 59% of sites without liquefaction observations have $LPI < 5$. Recall that in the Iwasaki et al. (1978) database, 80% and 50% of liquefied sites were found to have LPI values greater than 5 and 15, respectively, while 70% of non-liquefied sites had LPI less than 5. Thus, while the mean LPI value for liquefied sites (11) is lower in this study than in Iwasaki et al. (1978), the CDFs are relatively similar for both studies around an LPI value of 5. Still, it is worth restating that if the lower threshold (5) of the Iwasaki criterion is used to predict liquefaction manifestations, 24% of liquefied sites are misclassified, while 41% of non-liquefied sites are misclassified. Similar findings result from the analysis of soundings with depth ≥ 20 m. For example, it can be seen in Figure 2b that if a threshold LPI value of 5 is used, 15% of liquefied sites and 38% of non-liquefied sites are misclassified.

To assess the importance of GWT depth estimation, LPI values were computed at each site applying a ± 0.5 m change in GWT depths. The resulting variation in CDFs of LPI values is shown in Figure 2. It can be seen that a ± 0.5 m change in GWT depth induces considerable variation to the CDFs for both liquefied and non-liquefied sites. For example, considering all soundings (Figure 2a), the percentage of liquefied sites with $LPI < 5$ ranges from 16-31%, while the portion of non-liquefied sites with $LPI > 5$ ranges from 34-51%. In Christchurch, loose sandy soils are commonly found at shallow depths, often at depths near that of the GWT. Consequently, raising the GWT often increases the vertical extent of the profile that is susceptible to liquefaction. Because shallower soils are more heavily weighted in computing LPI, and because raising the GWT increases the cyclic stress ratio (CSR) throughout the profile via the ratio of total and effective vertical stress term, and thus reduces FS, the computed LPI values in Christchurch are relatively sensitive to GWT depth estimations. Corresponding to the ± 0.5 m adjustment to the original GWT depth estimate, the average LPI values from all sites for the Darfield and Christchurch earthquakes change from 5.6 to 8.8 and from 10.5 to 14.2, respectively, with a change in LPI exceeding 6.7 for 10% of sites in the Christchurch earthquake. Given that such a change could alter the assessment of liquefaction hazard, crude estimates of ground water depth should be avoided (for additional study of the influence of the GWT on LPI, see Chung and Rogers, 2011).

The CDFs shown in Figure 2 suggest that threshold values of LPI could be useful for preliminary assessments of liquefaction hazard. However, given the considerable overlap in LPI values between sites with and without surficial manifestations of liquefaction, use of LPI in a risk-based liquefaction assessment might be of greater value. As proposed by Toprak and Holzer (2003), the probabilities of surficial liquefaction manifestations were computed herein as the fraction of sites having liquefaction manifestations in a particular LPI bin (e.g., $0 \leq \text{LPI} < 1$, $1 \leq \text{LPI} < 2$, etc.). The resulting probabilities are plotted in Figure 3 as functions of the central LPI values for the corresponding bins. Although methodologies differ, the findings of Iwasaki et al. (1978), Lee et al. (2003), Toprak and Holzer (2003), and Papathanassiou (2008) are shown for comparison. For some studies, the number of sites in a particular LPI bin may be too few (e.g., 1 or 2) to give reliable results. Based on the results of this study, a suggested range of probabilities is shown in Figure 3, created from regression through the $\pm 1\sigma$ confidence intervals. The lower and upper probability-bounds are given by $P = (3\text{E-}05)\text{LPI}^3 - (0.0025)\text{LPI}^2 + (0.0756)\text{LPI} + 0.0879$ and $P = (3\text{E-}05)\text{LPI}^3 - (0.0027)\text{LPI}^2 + (0.0746)\text{LPI} + 0.2977$, respectively. Using this range, the probability of the manifestation of liquefaction at sites with LPI values of 5, 10, and 15 ranges from 0.40 - 0.60, 0.62 - 0.80, and 0.76 - 0.91, respectively. While acceptable levels of risk may vary between locations, predicting liquefaction hazards using a threshold LPI value of 5 could be too high given that the probability of manifestations is approximately 45% for $3 \leq \text{LPI} < 5$. Further, if modifications to the Iwasaki criterion proposed by others (e.g., LPI threshold for liquefaction of 19: Papathanassiou, 2008) are applied to the present study, the resulting hazard assessments would be very inappropriate (i.e., the probability of the manifestation of liquefaction for $14 \leq \text{LPI} < 19$ is ~85%). This illustrates the importance of having consistency in how threshold LPI values are determined and how the LPI values are computed to assess liquefaction hazard.

2.4.2 Prediction of Liquefaction Severity

While predicting the occurrence of liquefaction is an important component of hazard analysis, the severity of liquefaction is of greater consequence to society and the built environment. Thus, LPI would be of greater value if it can be correlated to the severity of liquefaction manifestations, as originally intended by Iwasaki et al. (1978). The distributions of LPI values for each liquefaction severity classification are shown in Figure 4. The severity of liquefaction manifestation generally increases with increasing LPI such that the median LPI values for marginal, moderate, and severe liquefaction, considering all soundings (Figure 4a), are 8.4, 13.1, and 21.0, respectively. While marginal liquefaction is of concern, damage to infrastructure (e.g., settlement and tilting of structures, cracking of pavements, failure of lifelines) is more likely a consequence of moderate or severe liquefaction. As shown in Figure 4a, 75% of sites with moderate liquefaction have LPI values greater than 7.4, while 75% of sites with severe liquefaction have LPI values greater than 15.0. However, it can also be seen that lateral spreading

was observed at sites having a wide range of LPI values. While marginal liquefaction and lateral spreading have similar LPI distributions, lateral spreading is a potentially very damaging manifestation of liquefaction and its effects on the built environment are decidedly different. As such, the damage potential of lateral spreading may not be well-estimated by LPI, and it is therefore treated separately in the subsequent analysis. To compute the likelihood of damaging liquefaction due to sand blows, the probability of moderate or severe liquefaction as a function of LPI is computed (Figure 5) using the methodology previously discussed, where marginal liquefaction is considered non-damaging. Based on the suggested range for soils in Christchurch, defined in Figure 5, the probability of damaging liquefaction at sites with LPI values of 5, 10, and 15 ranges from 0.05 - 0.19, 0.14 - 0.34, and 0.26 - 0.52, respectively. Based on these results, the Iwasaki criterion is more applicable for assessing the damage potential, rather than occurrence of liquefaction.

Lateral spreading is treated separately in this study because it is a unique form of liquefaction manifestation associated with large lateral permanent ground displacements, and there are separate criteria for assessing its severity (e.g., Youd et al., 2002). These criteria include the ground slope, the height of the nearest free-face (e.g., river bank), and the lateral distance between the free-face and spreading crack. Consequently, while site profiles with thin liquefiable layers may have low LPI values, these sites may be susceptible to lateral spreading if located near rivers or on sloping ground. As such, it is not surprising that 25% of sites with lateral spreading have LPI values less than 4.5 (Figure 4). This illustrates that while LPI is a useful tool for large-scale hazard assessments, it does not eliminate the need for site-specific analyses or consideration of the influence of local conditions on the manifestation of liquefaction.

2.4.3 Spatial Analysis of LPI Performance

While the Iwasaki et al. (1978) framework and threshold LPI values have been shown to be useful in a general sense (i.e., for general trends in terms of median values of LPI), the occurrence or severity of liquefaction was inaccurately predicted for a non-trivial percentage of sites. To evaluate LPI performance spatially, computed LPI values are mapped in Figure 6. To quantify the accuracy of LPI predictions, a prediction error (E) was computed using the LPI values assigned to each damage classification, shown in Table 1, such that $E = \text{LPI} - (\text{min or max})$ of relevant range. For example, if the computed LPI is 15 for a site with marginal liquefaction, $E = 15 - 8 = 7$ (where 8 is the maximum of the range of LPI values for marginal liquefaction), whereas if the computed LPI is 6 for a site with moderate liquefaction, $E = 6 - 8 = -2$ (where 8 is the minimum of the range of LPI values for moderate liquefaction). As such, positive errors indicate over-predictions of liquefaction severity, and conversely, negative errors indicate under-predictions. Errors were then assigned one of nine classifications, shown

in Table 2, based on the magnitude of the error. In light of the additional criteria for assessing lateral spreads, and because the Iwasaki criterion may be more applicable to sand blows, lateral spreading was assigned a wide range of expected LPI values, independent of spreading displacement. The prediction errors for the Darfield and Christchurch earthquakes are mapped in Figure 7a and Figure 7b, respectively. It can be seen that using the LPI criteria shown in Table 1, LPI accurately predicts liquefaction severity in both earthquakes for much of the study area. In particular, prediction errors ranged from moderate under-predictions to moderate over-predictions throughout the majority of the eastern and northern suburbs and the Kaiapoi area. However, it can also be seen that in both earthquakes, liquefaction severity was moderately-to-excessively over-predicted in many of the southern and southwestern areas of the city. Since the majority of over-predictions are confined to a particular area, there is likely a common underlying cause.

Possible causes of the generally poor LPI predictions in these areas of the city were investigated as follows:

- (1) As previously discussed, CPT soundings along the western margins of the city tend to terminate at shallow depths, but based on knowledge of local geology and a statistical outlier analysis, many of these soundings were included in the present study. Since using these shallow soundings could only result in low LPI estimations, and thus under-predictions of liquefaction severity, their inclusion cannot be the source of error.
- (2) The sensitivity of LPI to GWT depth at sites with moderate-to-excessive over-predictions of liquefaction severity was compared to the overall average. Applying a ± 0.5 m adjustment relative to the estimated GWT depth, the corresponding change in average LPI for these sites was 4.1 and 4.6 for the Darfield and Christchurch earthquakes, respectively. Compared to the average change in LPI resulting from GWT adjustment for all sites, these variations represent the 70th and 67th percentiles for the respective earthquakes. Thus, the sensitivity of LPI to GWT depth is above average at sites with moderate-to-excessive over-predictions of liquefaction. However, this is expected since profiles with the highest LPI have shallow liquefiable soils and are therefore most sensitive to GWT changes. In addition, equally high LPI values were computed for sites in the eastern suburbs and in Kaiapoi, but predictions of liquefaction severity were generally good in those areas. Further, considering that “severe” and “excessive” over-predictions correspond to respective minimum errors of 10 and 15 LPI units, a 1.0 m error in GWT depth estimation will still not resolve these over-predictions. Accordingly, the prediction errors are unlikely a result of widespread GWT depth estimation errors or GWT fluctuation.
- (3) The uncertainty of conditional PGAs (σ_{PGA}) increases with increasing distance from seismic recording stations. Correspondingly, the uncertainty of the FS estimates, and hence LPI values, increase with σ_{PGA} . However, as shown in Figure 8, there is no correlation between over-

predictions ($E > 5$) and σ_{PGA} . The conditional PGA estimates in the area of interest are strongly influenced by strong motion recordings at Cashmere High School (CMHS). As compared to the Bradley (2010, 2013b) GMPE, the PGAs recorded at CMHS during the Darfield and Christchurch earthquakes were as predicted ($R = 0.06$) and less than predicted ($R = -0.29$), respectively, where R is the total residual (i.e., $R = \ln(PGA_{\text{recorded}}/PGA_{\text{predicted}})$). Since the recorded PGAs for these earthquakes are not greater than expected, it is unlikely that strong-motion instrument errors or bias are the cause of liquefaction severity over-predictions in this area.

- (4) To compute the demand imposed on the soil with the simplified procedure used herein, the duration of cyclic loading is related to the earthquake magnitude via the magnitude scaling factor (MSF). It is assumed that the CES events are accurately represented by the MSF inherent to the simplified procedure, but an inconsistency could result in poor predictions. While the authors are working to address this issue, no existing LPI study has considered the accuracy of the MSF and a mechanical framework to assess this has yet to be established.
- (5) A trend was identified between prediction error and soil type, wherein liquefaction severity is often over-predicted at sites with high inferred silt and clay fractions (i.e., inferred from I_c). This trend could be the result of conservatism in the Robertson and Wride (1998) fines correction factor, such that FS is underestimated for soils with high fines-content. Alternatively, the plasticity of soils capping liquefied layers might affect the severity of liquefaction manifested at the ground surface. Since plastic soils are generally more resistant to piping and hydraulic fracture, these soils might affect water flow and pore pressure development/dissipation among liquefied strata within the profile, and between liquefied strata and the ground surface. This would diminish the cumulative effects inherent in the LPI framework and limit the severity of surficial liquefaction manifestations. To investigate each of these hypotheses, the average soil behavior type index (I_c) was computed for strata predicted to liquefy and for the crust and/or interspaced strata predicted not to liquefy. Since the upper 10 m contribute up to 75% of the computed LPI, these averages were limited to 10 m depth. The correlation between prediction error and average I_c in the strata predicted to liquefy is shown in Figure 9a. If over-predictions are the result of conservatism in the liquefaction evaluation procedure, due to the fines correction factor and/or the I_c limit for liquefiable soils, there should be a shift toward larger prediction errors at high I_c values. However, it can be seen that no such trend exists.

The correlation between prediction error and average I_c in the strata predicted not to liquefy is shown in Figure 9b. It can be seen that for inferred sands and silty sands ($I_c \leq 2.2$) the number of over- and under-predictions is approximately equal, but that as I_c increases, there is a noticeable shift toward over-predictions. This suggests that the plasticity of the crust and/or interbedded non-liquefied soils has an effect on the severity of surficial liquefaction manifestation, and inherent

limitations in the Iwasaki et al. (1978) LPI framework to account for the influence of these layers could be the cause of the over-predictions. This hypothesis is supported by Ozutsumi et al. (2002), who found the presence of interbedded or overlying cohesive layers to be a primary factor for reducing liquefaction-induced deformations in river dikes. This hypothesis might also explain the high threshold LPI values proposed by Lee et al. (2003) and Papathanassiou (2008), who analyzed soils with high fines-content. Consequently, the depth weighting function might be improved by accounting for both the geometric and physical characteristics of non-liquefied strata. At present, it assumes a simple linear form and does not account for soil characteristics, other than soils having a $FS \geq 1$ not contributing to the computed LPI value. Further research is needed to explore in detail and elucidate these findings.

Finally, a discussion of trends in the prediction errors for the Darfield earthquake versus the Christchurch earthquake is presented in the Electronic Supplement to this paper. In summary, the intensity of the ground motions generally does not influence the type of prediction error (i.e., over-prediction versus under-prediction), but rather, only influences the magnitude of the error. This is the case for all but 10 of the 1176 cases analyzed.

2.5 Conclusions

Utilizing CPT soundings from nearly 1200 sites where the severity of liquefaction manifestation was well-documented during the Darfield and Christchurch earthquakes, this study evaluated the efficacy of the Iwasaki et al. (1978) LPI criterion and framework to assess liquefaction hazards. For the study area, the Iwasaki criterion was found to be more effective for assessing the damage potential, rather than the occurrence of liquefaction; the Iwasaki criterion was found to be less effective for predicting marginal manifestations of liquefaction. In addition, this criterion should be used with considerable caution in locations susceptible to lateral spreading, as it was found that LPI predicts lateral spreading less consistently than it predicts damaging sand blows, and particularly because lateral spreading is possible at very low LPI values. Accordingly, one may argue that LPI is not appropriate for evaluation of lateral spreading potential. More extensive analyses of lateral spreading based on observations from the CES are ongoing at the University of Canterbury (e.g., Cubrinovski et al., 2012).

Since LPI did not clearly segregate liquefied and non-liquefied sites, LPI is better used to assess the probability of damaging liquefaction than simply using threshold LPI values to predict the occurrence of liquefaction. A range of probabilities was proposed herein for soils in Christchurch, with the probability of damaging liquefaction ranging from 5% to 19% for an LPI value of 5, but this does not consider the potential for lateral spreading. Lastly, a trend was identified between over-predictions of liquefaction severity and soils with inferred elevated silt or clay fractions. The effect of plastic soils

limiting propagation of liquefied soil to the ground surface was identified as a likely contributor to this trend. This hypothesis could also explain disparities in the existing literature. As such, the LPI model might be improved by accounting for the characteristics of soils in both layers predicted to liquefy and the crust and/or interbedded layers predicted not to liquefy, but further research is needed to better understand and quantify these effects.

Finally, this study evaluated LPI with the Robertson and Wride (1998) liquefaction evaluation procedure. Computation of LPI based on other liquefaction evaluation procedures should be individually calibrated to liquefaction severity observations. The authors are presently evaluating the influence of the selected liquefaction evaluation procedure used within the LPI framework on the accuracy of hazard assessments.

2.6 Acknowledgements

The study presented herein is based upon work supported by the National Science Foundation under Grant No. OISE 1209494, CMMI 1030564, and CMMI 1306261. The third and fourth authors would like to acknowledge the continuous financial support provided by the Earthquake Commission (EQC) and Natural Hazards Research Platform (NHRP), New Zealand, of the research and investigations related to the 2010-2011 Canterbury earthquakes. The authors also acknowledge the New Zealand GeoNet project and its sponsors EQC, GNS Science and LINZ for providing the earthquake occurrence data and the Canterbury Geotechnical Database and its sponsor EQC for providing the CPT soundings, lateral spread observations, and aerial imagery used in this study. However, any opinions, findings, and conclusions or recommendations expressed in this paper are those of the authors and do not necessarily reflect the views of the National Science Foundation, EQC, NHRP, or LINZ.

References

- Abrahamson, N.A. and R.R. Youngs (1992). "A stable algorithm for regression analyses using the random effects model." *Bulletin of the Seismological Society of America* 82 (1), 505–510.
- Andrus, R.D. and Stokoe II, K.H. (1997). "Liquefaction resistance based on shear wave velocity." Proc. of the NCEER workshop on Evaluation of Liquefaction Resistance of Soils. In: Youd, T.L. and Idriss, I.M., (Eds.), Technical Report NCEER-97-0022, State Univ. of New York at Buffalo, NY, pp. 89-128.
- Anselin, L. (1995). "Local Indicators of Spatial Association—LISA." *Geographical Analysis* 27(2): 93–115.

- Baise, L.G., Higgins, R.B., and Brankman, C.M. (2006). "Liquefaction hazard mapping-statistical and spatial characterization of susceptible units." *Journal of Geotechnical and Geoenvironmental Engineering*, ASCE, 132 (6): 705-715.
- Begg, J. and Jones, K. (2012). "20,000 years of time in Christchurch." [presentation] New Zealand Geotechnical Society, Canterbury Branch, 28 June 2012.
- Bradley, B.A. (2010). *NZ-specific Pseudo-spectral Acceleration Ground Motion Prediction Equations Based on Foreign Models*. Department of Civil and Natural Resources Engineering, University of Canterbury, Christchurch, New Zealand, 324 pp.
- Bradley, B.A. (2012a). "Strong ground motion characteristics observed in the 4 September 2010 Darfield, New Zealand earthquake." *Soil Dynamics and Earthquake Engineering*, 42: 32-46.
- Bradley, B.A. (2012b). "Ground motions observed in the Darfield and Christchurch earthquakes and the importance of local site response effects." *New Zealand Journal of Geology and Geophysics*, 55: 279-286.
- Bradley, B.A. (2013a). "Site-specific and spatially distributed estimation of ground motion intensity in the 2010-2011 Canterbury earthquakes." *Soil Dynamics and Earthquake Engineering*, (in review)
- Bradley, B.A. (2013b). "A New Zealand-specific pseudo-spectral acceleration ground-motion prediction equation for active shallow crustal earthquakes based on foreign models." *Bulletin of the Seismological Society of America*, 103(3), 1801-1822..
- Bradley, B.A. and Cubrinovski, M., (2011). "Near-source Strong Ground Motions Observed in the 22 February 2011 Christchurch Earthquake." *Seismological Research Letters*, 82: 853-865.
- Brown, L.J., Beetham, R.D., Paterson, B.R., and Weeber, J.H. (1995). "Geology of Christchurch, New Zealand." *Environmental and Engineering Geoscience*, 1: 427-488.
- CDG - Canterbury Geotechnical Database (2012a) "Groundwater surface elevations", Map Layer CGD0800 - 16 Aug 2012, retrieved [12/12] from <https://canterburygeotechnicaldatabase.projectorbit.com>
- CDG - Canterbury Geotechnical Database (2012b) "Aerial Photography", Map Layer CGD0100 - 1 June 2012, retrieved [12/12] from <https://canterburygeotechnicaldatabase.projectorbit.com>
- CDG - Canterbury Geotechnical Database (2012c) "Observed Ground Crack Locations", Map Layer CGD0400 - 23 July 2012, retrieved [12/12] from <https://canterburygeotechnicaldatabase.projectorbit.com>
- Cetin, K.O., Seed, R.B., Der Kiureghian, A., Tokimatsu, K., Harder, L.F., Kayen, R.E., and Moss, R.E.S. (2004). "Standard Penetration Test-Based Probabilistic and Deterministic Assessment of Seismic Soil Liquefaction Potential." *Journal of Geotechnical and Geoenvironmental Engineering*, ASCE, 130(12): 1314-1340.

- Chung, J. and Rogers, J., (2011). “Simplified method for spatial evaluation of liquefaction potential in the St. Louis Area.” *Journal of Geotechnical and Geoenvironmental Engineering*, ASCE, 137(5): 505-515.
- Cramer, C.H., Rix, G.J., and Tucker, K. (2008). “Probabilistic liquefaction hazard maps for Memphis, Tennessee.” *Seismological Research Letters*, 79(3): 416-423.
- Cubrinovski, M. and Green, R.A. (eds.) (2010). “Geotechnical Reconnaissance of the 2010 Darfield (Canterbury) Earthquake”, (contributing authors in alphabetical order: J. Allen, S. Ashford, E. Bowman, B. Bradley, B. Cox, M. Cubrinovski, R. Green, T. Hutchinson, E. Kavazanjian, R. Orense, M. Pender, M. Quigley, and L. Wotherspoon), *Bulletin of the New Zealand Society for Earthquake Engineering*, 43(4): 243-320.
- Cubrinovski, M., Bray, J.D., Taylor, M., Giorgini, S., Bradley, B., Wotherspoon, L., and Zupan J. (2011a). “Soil liquefaction effects in the central business district during the February 2011 Christchurch earthquake.” *Seismological Research Letters*, 82(6): 893-904.
- Cubrinovski, M., Bradley, B., Wotherspoon, L., Green, R., Bray, J., Woods, C., Pender, M., Allen, J., Bradshaw, A., Rix, G., Taylor, M., Robinson, K., Henderson, D., Giorgini, S., Ma, K., Winkley, A., Zupan, J., O’Rourke, T., DePascale, G., and Wells, D. (2011b). “Geotechnical aspects of the 22 February 2011 Christchurch earthquake.” *Bulletin of the New Zealand Society for Earthquake Engineering*, 43(4): 205-226.
- Cubrinovski, M., Robinson, K., Taylor, M., Hughes, M.M., and Orense, R. (2012). “Lateral spreading and its impacts in urban areas in the 2010-2011 Christchurch earthquakes.” *New Zealand Journal of Geology and Geophysics*, 55(3): 255-269.
- Dixit, J., Dewaikar, D.M., and Jangrid, J.S. (2012). “Assessment of liquefaction potential index for Mumbai City.” *Natural Hazards and Earth Science Systems*, 12: 2759–2768.
- Goda, K. and H. P. Hong (2008). “Spatial correlation of peak ground motions and response spectra.” *Bulletin of the Seismological Society of America* 98 (1), 354–465.
- Green, R.A., Allen, A., Wotherspoon, L., Cubrinovski, M., Bradley, B., Bradshaw, A., Cox, B., and Algie, T. (2011a). “Performance of levees (stopbanks) during the 4 September M_w 7.1 Darfield and 22 February 2011 M_w 6.2 Christchurch, New Zealand, earthquakes.” *Seismological Research Letters*, 82(6): 939-949.
- Green, R.A., Cubrinovski, M., Cox, B., Wood, C., Wotherspoon, L., Bradley, B., and Maurer, B. (2013). “Select Liquefaction Case Histories from the 2010-2011 Canterbury Earthquake Sequence.” *Earthquake Spectra*, (in review).
- Green, R.A., Wood, C., Cox, B., Cubrinovski, M., Wotherspoon, L., Bradley, B., Algie, T., Allen, J., Bradshaw, A., and Rix, G. (2011b). “Use of DCP and SASW Tests to Evaluate Liquefaction Potential: Predictions vs. Observations During the Recent New Zealand Earthquakes.” *Seismological Research Letters*, 82(6): 927-938.

- Hayati, H. and Andrus, R.D. (2008). "Liquefaction potential map of Charleston, South Carolina based on the 1986 earthquake." *Journal of Geotechnical and Geoenvironmental Engineering*, ASCE, 134 (6): 815-828.
- Holzer, T.L., Noce, T.E., Bennett, M.J., Tinsley III, J.C., and Rosenburg, L.I. (2005). "Liquefaction at Oceano, California, during the 2003 San Simeon earthquake." *Bulletin of the Seismological Society of America*, 95(6): 2396-2411.
- Holzer, T.L., Bennett, M.J., Noce, T.E., Padovani, A.C., and Tinsley III, J.C. (2006a). "Liquefaction hazard mapping with LPI in the greater Oakland, California, area." *Earthquake Spectra*, 22(3): 693-708.
- Holzer, T.L., Blair, J.L., Noce, T.E., and Bennett, M.J. (2006b). "Predicted liquefaction of east bay fills during a repeat of the 1906 San Francisco earthquake." *Earthquake Spectra*, 22(S2), S261-277.
- Holzer, T.L., Noce, T.E., and Bennett, M.J. (2011). "Liquefaction probability curves for surficial geologic units." *Environmental and Engineering Geoscience*, 17(1): 1-21.
- Idriss, I.M. and Boulanger, R.W. (2006). "Semi-empirical procedures for evaluating liquefaction potential during earthquakes." *Soil Dynamics and Earthquake Engineering*, 26: 115-130.
- Ishihara, K. (1985). "Stability of natural deposits during earthquakes." *Proceedings of the 11th International Conference on Soil Mechanics and Foundation Engineering*, San Francisco, CA, USA, Aug. 1985, A.A. Balkema, Rotterdam, 1: 321-376.
- Iwasaki, T., Tatsuoka, F., Tokida, K., and Yasuda, S. (1978). "A practical method for assessing soil liquefaction potential based on case studies at various sites in Japan." *Proceedings of the 2nd International Conference on Microzonation*, Nov 26-Dec 1, San Francisco, CA, USA.
- Johnson, R. A., and D. W. Wichern (2007). *Applied Multivariate Statistical Analysis*. Upper Saddle River, NJ: Pearson Prentice-Hall.
- Juang, C.H., Yuan, H., Lee, D.H., and Lin, P.S. (2003). "A simplified CPT-based method for evaluating liquefaction potential of soils." *Journal of Geotechnical and Geoenvironmental Engineering*, ASCE, 129(1): 66-80.
- Lee, D.H., Ku, C.S., and Yuan, H. (2003). "A study of liquefaction risk potential at Yuanlin, Taiwan." *Engineering Geology*, 71: 97-117.
- Lenz, A. and Baise, L.G. (2007). "Spatial variability of liquefaction potential in regional mapping using CPT and SPT data." *Soil Dynamics and Earthquake Engineering*, 27: 690-702.
- Moss, R.E.S, Seed, R.B., Kayen, R.E., Stewart, J.P., Der Kiureghian, A., and Cetin, K.O. (2006). "CPT-based probabilistic and deterministic assessment of in situ seismic soil liquefaction potential." *Journal of Geotechnical and Geoenvironmental Engineering*, ASCE, 132(8):1032-1051.
- Murahidy, K.M., Soutar, C.M., Phillips, R.A., and Fairclough, A. (2012). "Post earthquake recovery - Development of a geotechnical database for Christchurch central city." *15th World Conference on Earthquake Engineering*, Lisbon, Portugal. p. 10.

- Orense, R.P., Kiyota, T., Yamada, S., Cubrinovski, M., Hosono, Y., Okamura, M., and Yasuda, S. (2011). "Comparison of liquefaction features observed during the 2010 and 2011 Canterbury earthquakes." *Seismological Research Letters*, 82(6): 905-918.
- Ozutsumi, O., Sawada, S., Iai, S., Takeshima, Y., Sugiyama, W., and Shimazu, T. (2002). "Effective stress analyses of liquefaction-induced deformation in river dikes." *Soil Dynamics and Earthquake Engineering*, 22: 1075-1082.
- Papathanassiou, G. (2008). "LPI-Based Approach for Calibrating the Severity of Liquefaction-Induced Failures and for Assessing the Probability of Liquefaction Surface Evidence." *Engineering Geology*, 96: 94-104.
- Papathanassiou, G., Pavlides, S., and Ganas, A. (2005). "The 2003 Lefkada earthquake: field observation and preliminary microzonation map based on liquefaction potential index for the town of Lefkada." *Engineering Geology*, 82: 12-31.
- Pinheiro, J., Bates, D.M., DebRoy, S., Sarkar, D., and the R Core Team (2008). *nlme: Linear and Nonlinear Mixed Effects Models*. R package version 3.1, 89 pp.
- Robertson, P.K. and Cabal, K.L. (2010). "Estimating soil unit weight from CPT." *2nd International Symposium on Cone Penetration Testing*, Huntington Beach, CA, USA, May 2010, Paper # 2-40.
- Robertson, P.K. and Wride, C.E. (1998). "Evaluating cyclic liquefaction potential using cone penetration test." *Canadian Geotechnical Journal* 35(3): 442-459.
- Seed, H.B. and DeAlba, P. (1986). "Use of the SPT and CPT tests for evaluating the liquefaction resistance of sands," *Use of In-situ Tests in Geotechnical Engineering*, ASCE Geotechnical Special Publication, 6: 281-302.
- Seed, H.B. and Idriss, I.M. (1971). "Simplified procedure for evaluating soil liquefaction potential." *Journal of the Soil Mechanics and Foundation Division*, ASCE, 97(9): 1249-1273.
- Seed, H.B., Tokimatsu, K., Handler, L.F., and Chung, R.M. (1985). "Influence of SPT procedures in soil liquefaction resistance evaluations." *Journal of the Geotechnical Engineering Division*, ASCE, 111(2): 1425-1445.
- Sonmez, H. and Gokceoglu, C. (2005). "A liquefaction severity index suggested for engineering practice." *Environmental Geology*, 48(1): 81-91.
- Stark, T.D. and Olson, S.M. (1995). "Liquefaction Resistance Using CPT and Field Case Histories." *Journal of Geotechnical Engineering*, ASCE, 121(12): 856-869.
- Toprak, S. and Holzer, T. (2003). "Liquefaction potential index: field assessment." *Journal of Geotechnical and Geoenvironmental Engineering*, ASCE, 129(4): 315-322.
- Whitman, R.V. (1971). "Resistance of soil to liquefaction and settlement." *Soils and Foundations*, 11(4): 59-68.
- Yalcin, A., Gokceoglu, C., and Sonmez, H. (2008). "Liquefaction severity map for Aksaray city center." *Natural Hazards and Earth Science Systems*, 8: 641-649.

- Youd, T.L., Idriss, I.M., Andrus, R.D., Arango, I., Castro, G., Christian, J.T., Dobry, R., Finn, W.D.L., Harder, L.F., Hynes, M.E., Ishihara, K., Koester, J.P., Liao, S.S.C., Marcuson III, W.F., Martin, G.R., Mitchell, J.K., Moriwaki, Y., Power, M.S., Robertson, P.K., Seed, R.B., and Stokoe II, K.H. (2001). "Liquefaction Resistance of Soils: Summary Report from the 1996 NCEER and 1998 NCEER/NSF Workshops on Evaluation of Liquefaction Resistance of Soils." *Journal of Geotechnical and Geoenvironmental Engineering*, 127(4): 297-313.
- Youd, T.L., Hansen, C.M., and Bartlett, S.F. (2002). "Revised multilinear regression equations for prediction of lateral spread displacement." *Journal of Geotechnical and Geoenvironmental Engineering*, ASCE, 128(12): 1007-1017.

Tables

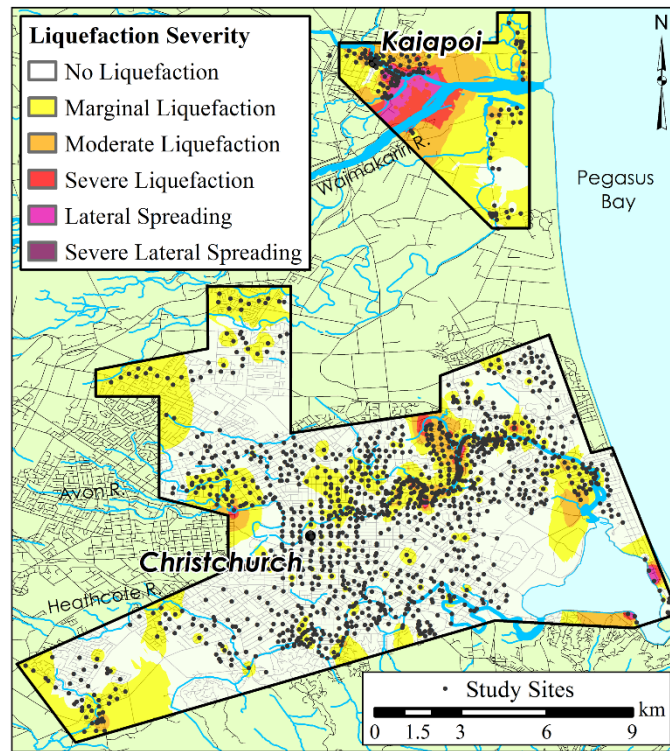
Table 2.1 LPI values used to assess prediction accuracy

Damage Classification	Expected LPI Range
No Liquefaction	$LPI < 4$
Marginal Liquefaction	$4 \leq LPI < 8$
Moderate Liquefaction	$8 \leq LPI < 15$
Severe Liquefaction	$LPI \geq 15$
Lateral Spreading	$LPI \geq 4$
Severe Lateral Spreading	$LPI \geq 4$

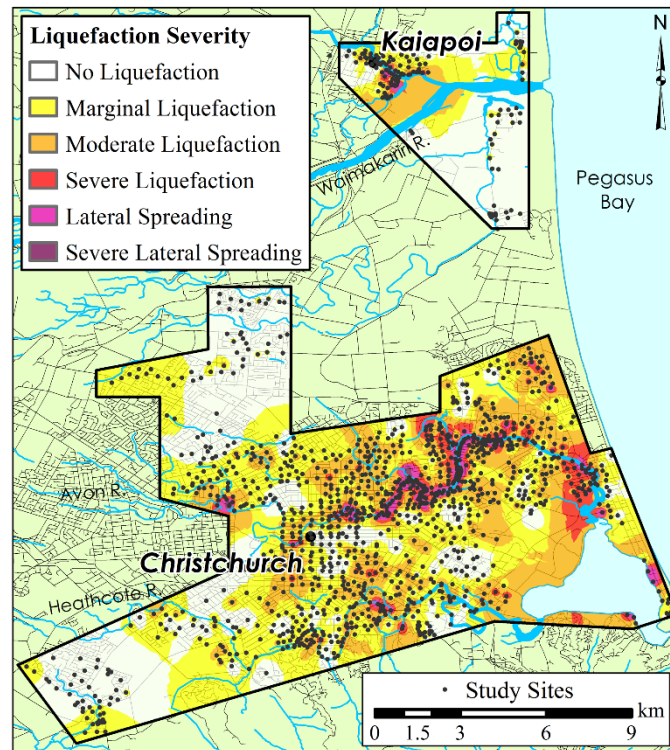
Table 2.2 LPI prediction error classifications

Error (E) Classification	E (LPI units)
Excessive Underprediction	$E < -15$
Severe to Excessive Underprediction	$-15 \leq E < -10$
Moderate to Severe Underprediction	$-10 \leq E < -5$
Slight to Moderate Underprediction	$-5 \leq E < -1$
Accurate Prediction	$-1 \leq E \leq 1$
Slight to Moderate Overprediction	$1 < E \leq 5$
Moderate to Severe Overprediction	$5 < E \leq 10$
Severe to Excessive Overprediction	$10 < E \leq 15$
Excessive Overprediction	$E > 15$

Figures



(a)



(b)

Figure 2.1 Liquefaction severity observations following the (a) Darfield and (b) Christchurch earthquakes.

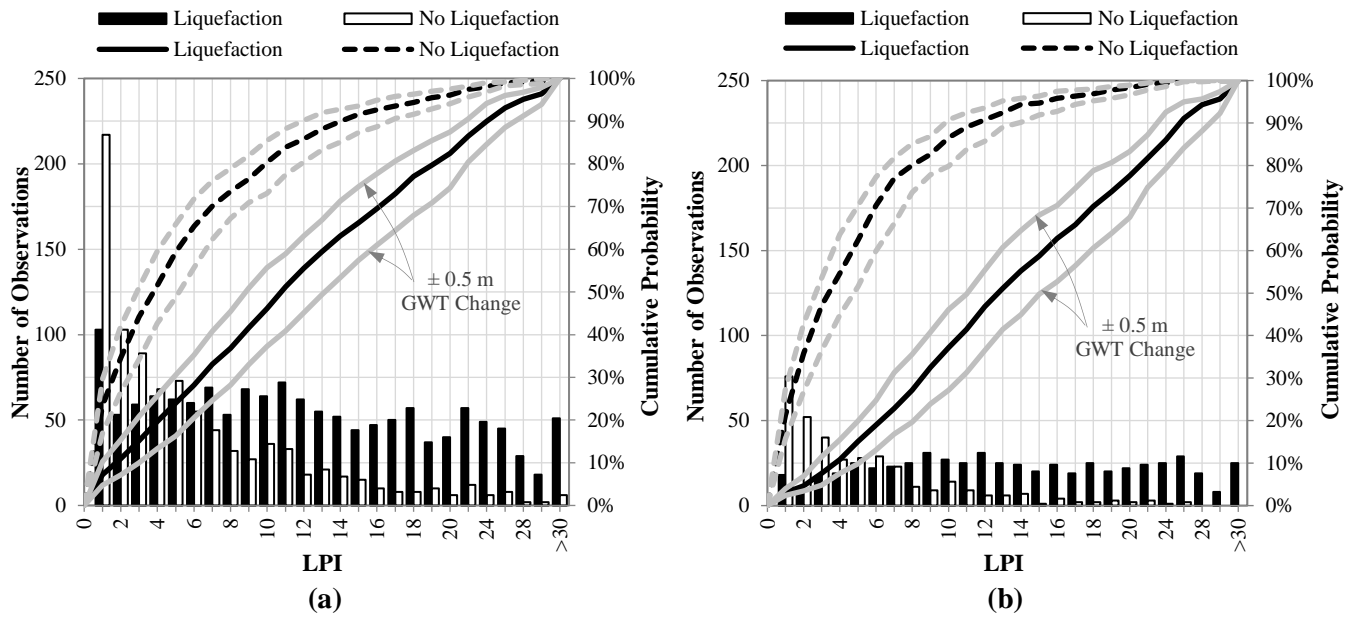


Figure 2.2 Histograms and cumulative probabilities of LPI values for CPT soundings at sites with and without liquefaction manifestations in the Darfield and Christchurch earthquakes: (a) all soundings; (b) sounding depths ≥ 20 m.

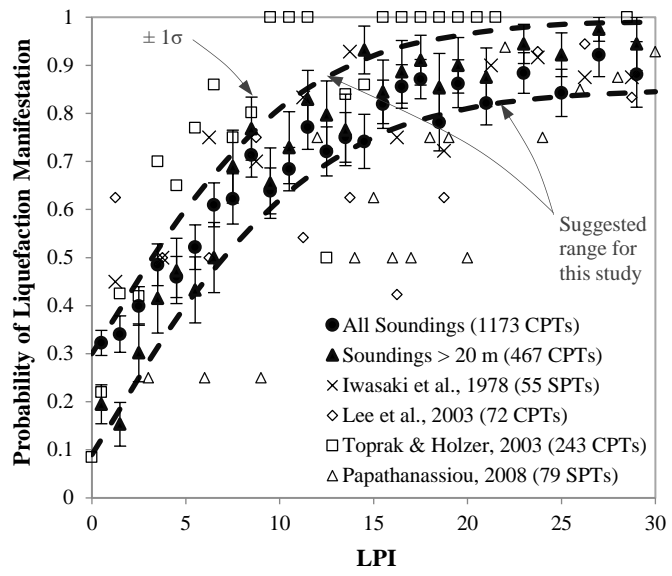


Figure 2.3 Probability of liquefaction manifestation.

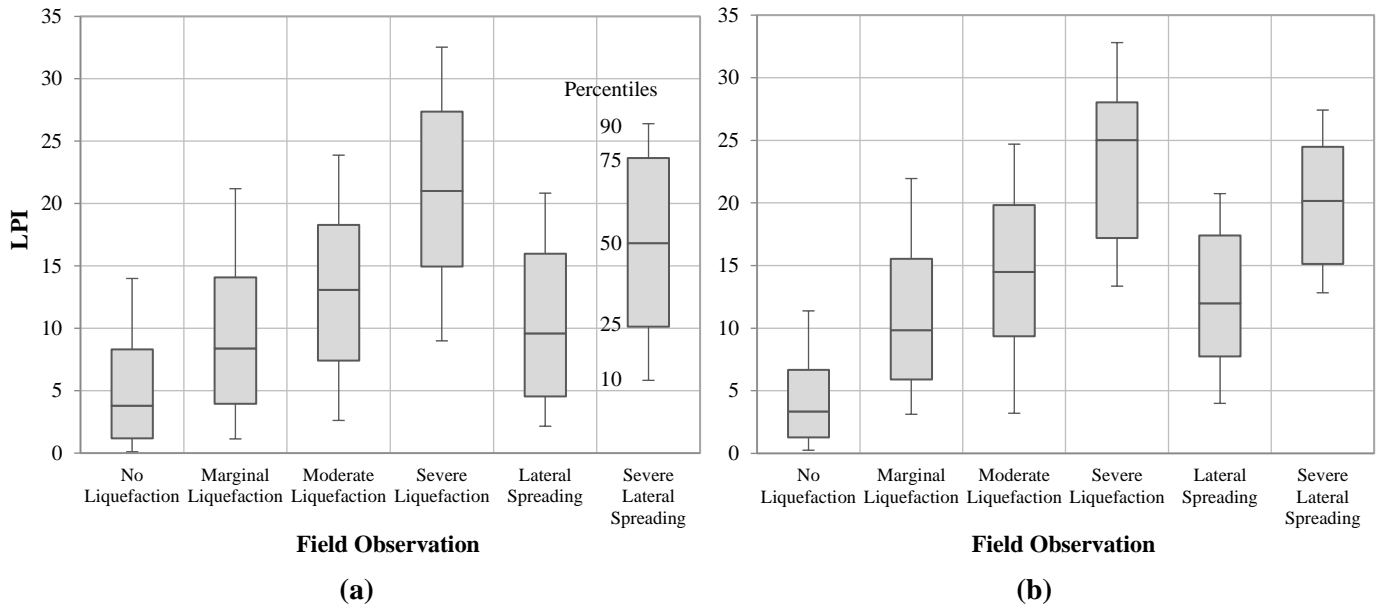


Figure 2.4 Correlation between LPI and severity of liquefaction manifestation in the Darfield and Christchurch earthquakes: (a) all soundings; (b) sounding depths ≥ 20 m.

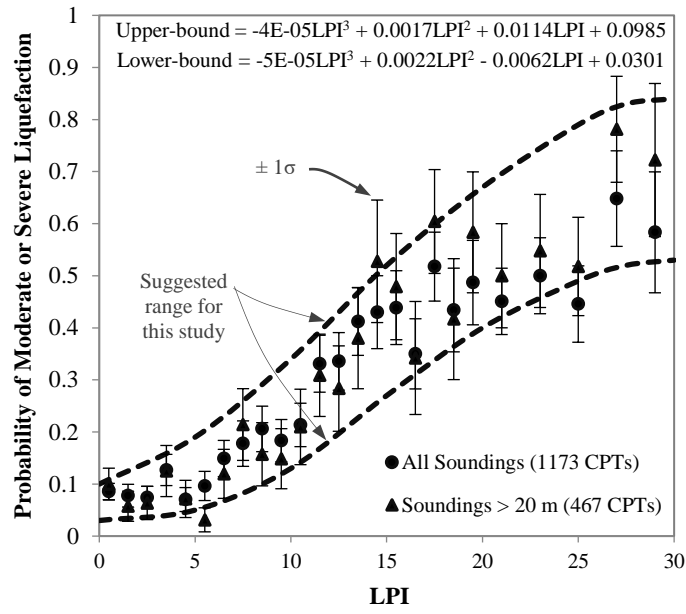
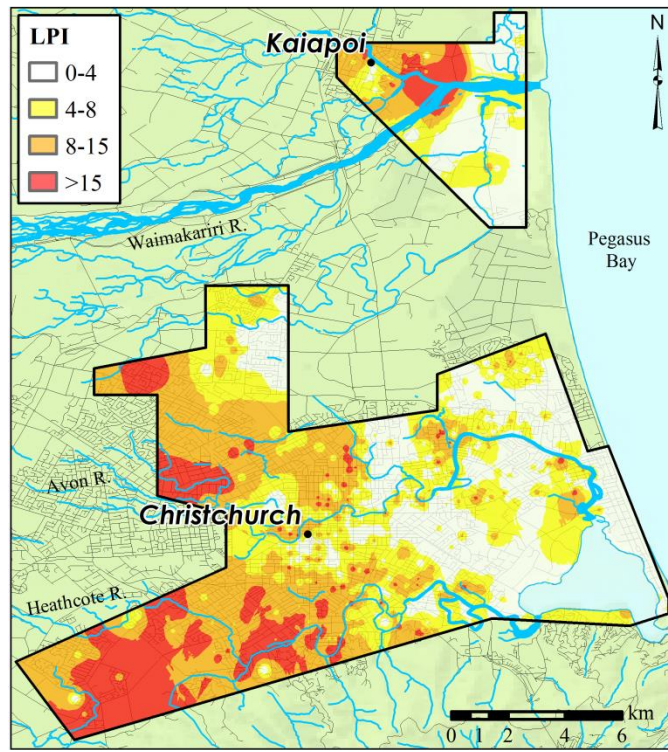
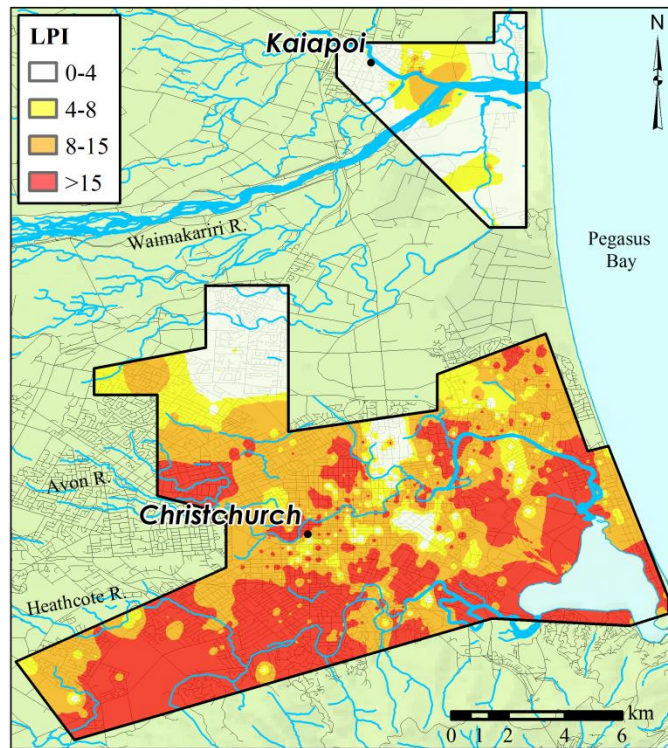


Figure 2.5 Probability of moderate or severe liquefaction (sand blows).

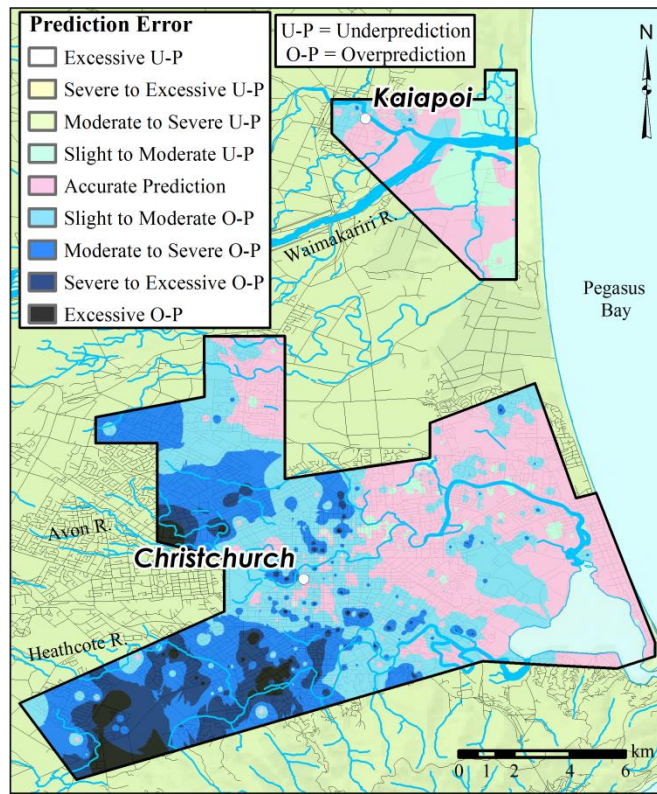


(a)

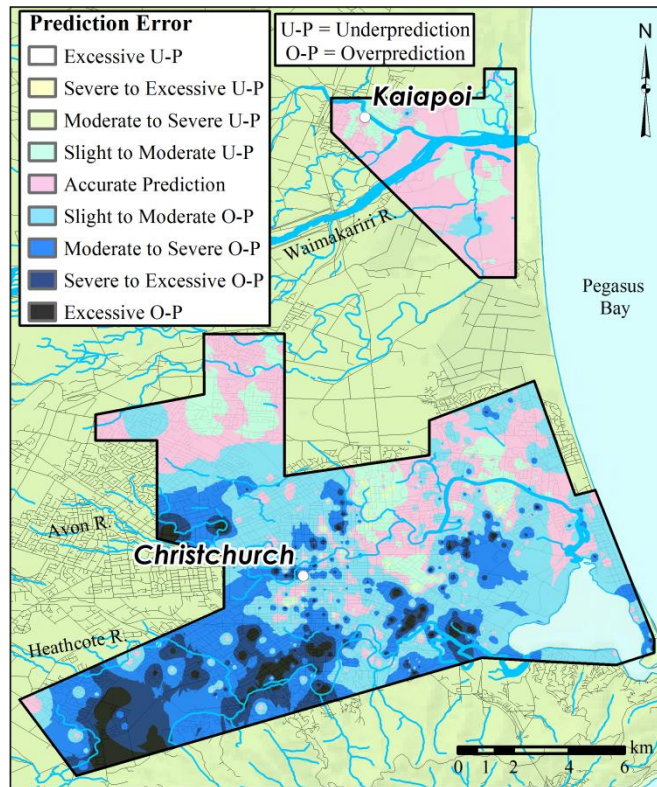


(b)

Figure 2.6 Computed LPI values for the (a) Darfield and (b) Christchurch earthquakes.



(a)



(b)

Figure 2.7 Prediction errors for the (a) Darfield and (b) Christchurch earthquakes.

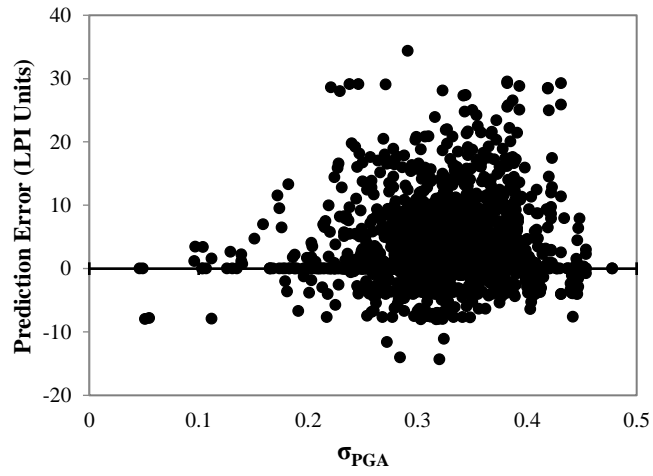
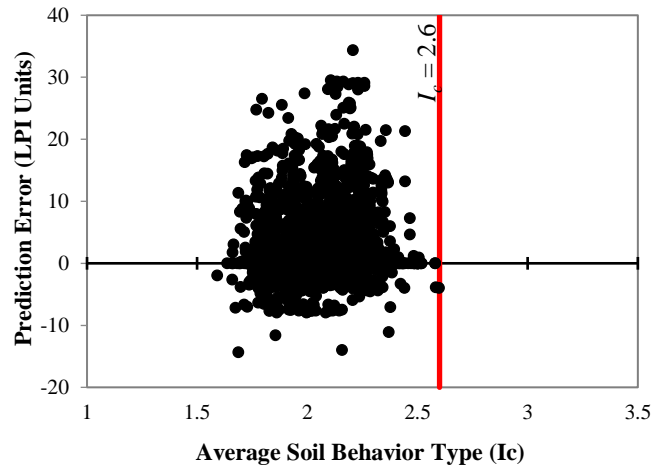
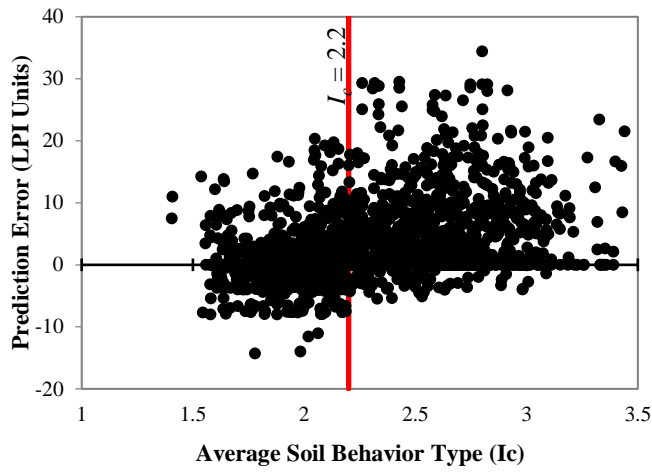


Figure 2.8 Correlation between liquefaction prediction error and uncertainty of conditional PGA.



(a)



(b)

Figure 2.9 Correlation between liquefaction prediction error and average soil behavior type index in the (a) strata predicted to have liquefied and (b) crust and/or interspaced strata predicted not to have liquefied.

2.7 Electronic Supplement

Notice

Figures 1, 6, 7, S1, S2, and S4a were created using inverse-distance-weighting interpolation (i.e., $1/R^2$) between CPT sites to show the spatial distribution of observations/results and are not intended for any other purpose. The accuracy of observations/results at sites other than those with CPT soundings is unknown. In addition, Figures 1, 6, 7, S1, S2, and S4a were created using basemap layers available under a Creative Commons Attribution 3.0 New Zealand License, the terms of which may be found at <http://creativecommons.org/licenses/by/3.0/nz/legalcode>; the source data was not modified in any way.

Figures 1-9 and S1-S4 were created from maps and/or data extracted from the Canterbury Geotechnical Database (<https://canterburygeotechnicaldatabase.projectorbit.com>), which were prepared and/or compiled for the Earthquake Commission (EQC) to assist in assessing insurance claims made under the Earthquake Commission Act 1993 and/or for the Canterbury Geotechnical Database on behalf of the Canterbury Earthquake Recovery Authority (CERA). The source maps and data were not intended for any other purpose. EQC, CERA, and their data suppliers and their engineers, Tonkin & Taylor, have no liability for any use of these maps and data or for the consequences of any person relying on them in any way.

Table 2.3 (S1) Liquefaction severity classification criteria

Classification	Criteria
No Liquefaction	No surficial liquefaction manifestation or lateral spread cracking
Marginal Liquefaction	Small, isolated liquefaction features; streets had traces of ejecta or wet patches less than a vehicle width; < 5% of ground surface covered by ejecta
Moderate Liquefaction	Groups of liquefaction features; streets had ejecta patches greater than a vehicle width but were still passable; 5-40% of ground surface covered by ejecta
Severe Liquefaction	Large masses of adjoining liquefaction features, streets impassible due to liquefaction, >40% of ground surface covered by ejecta
Lateral Spreading	Lateral spread cracks were predominant manifestation and damage mechanism, but crack displacements < 200 mm
Severe Lateral Spreading	Extensive lateral spreading and/or large open cracks extending across the ground surface with > 200 mm crack displacement

Classifications were made at each CPT site from observations within a 25 m² area centered on the test location. The classification criteria assume that increasing areal coverage of the ground surface by liquefaction ejecta is due to increasing ejecta volumes, and thus, to greater ground deformation and damage potential. While ground deformation is generally well correlated to areal ground coverage by liquefaction ejecta, exceptional cases do exist.

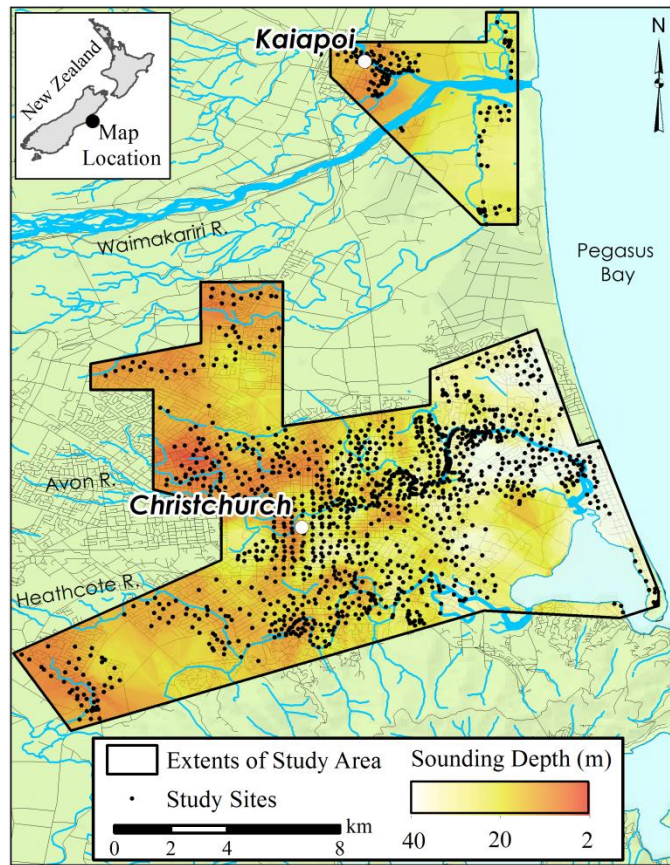


Figure 2.10 (S1) Depth of CPT soundings.

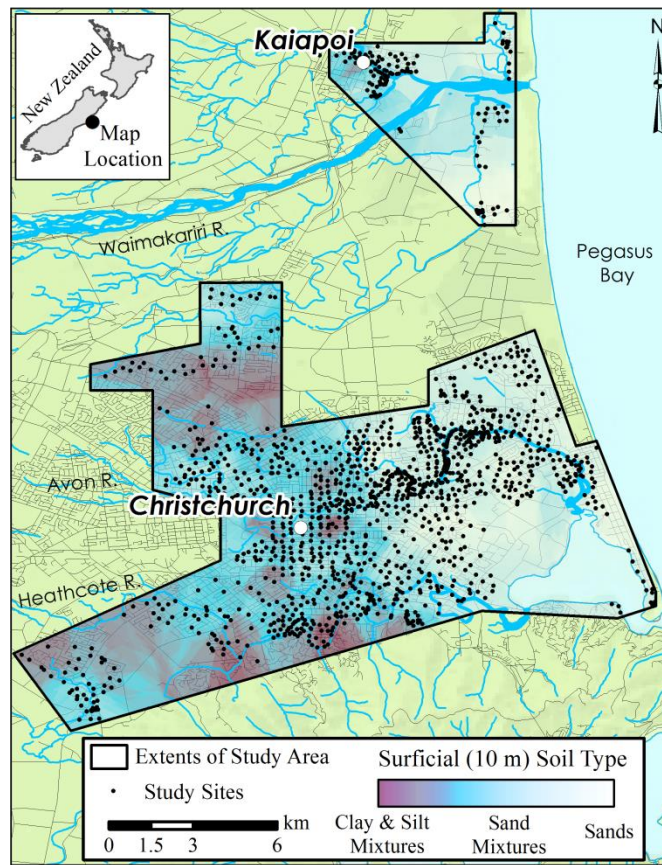


Figure 2.11 (S2) Surficial (10 m) Soil Type inferred from CPT data.



(a) Marginal Liquefaction



(b) Moderate Liquefaction



(c) Severe Liquefaction



(d) Severe Lateral Spreading

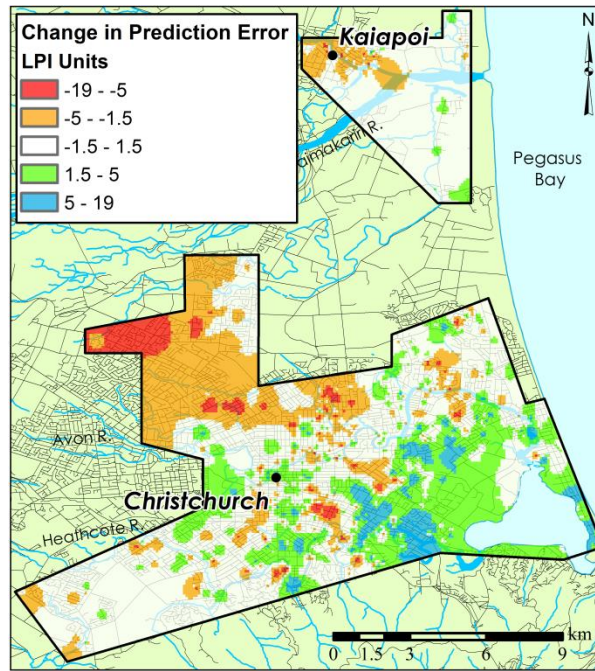
Figure 2.12 (S3) Representative observations of four liquefaction severity classes: (a) marginal liquefaction; (b) moderate liquefaction; (c) severe liquefaction; (d) severe lateral spreading (After CGD, 2012b).

Additional Analysis: Liquefaction Severity Prediction Errors, Darfield vs. Christchurch

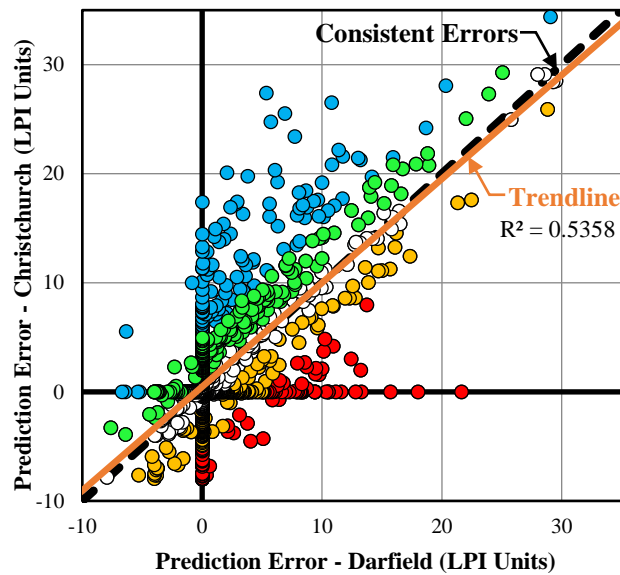
The change in liquefaction severity prediction error between the Darfield and Christchurch earthquakes is mapped in Figure S4a, where blue and green indicate an increase in the prediction error for the Christchurch earthquake relative to the Darfield earthquake (e.g., accurately predicted for Darfield but over-predicted for Christchurch), red and yellow indicate a relative decrease (e.g., over-predicted for Darfield but accurately predicted for Christchurch), and white indicates consistent prediction errors (i.e., under-, over-, or accurately-predicted in both events). In Figure S4b, liquefaction severity prediction errors in the Darfield earthquake are plotted vs. those in the Christchurch earthquake, and are color-coded to identify their respective locations as shown in Figure S4a.

While prediction errors trend towards being consistent between the two events, the spatial distribution of errors indicates that if a site is inherently not well represented by the LPI model, and is thus prone to a misprediction (say, due to the geometries and material characteristics of its liquefiable/non-liquefiable strata), then increasing or decreasing the seismic loading can be expected to change the magnitude of the prediction error. For example, from Figure 7a in the main text it can be seen that liquefaction severity was over-predicted in the Darfield earthquake for much of the study-area south and west of central Christchurch. Where seismic loading (considering both duration and amplitude of ground motions) is relatively similar between the two events, the over-predictions likewise tend to be similar. Conversely, where seismic loading was lesser in the Christchurch earthquake (e.g., areas northwest of central Christchurch), over-predictions diminish, and where seismic loading was greater in the Christchurch earthquake (e.g., areas southeast of central Christchurch), over-predictions are exacerbated.

Thus, as could be expected, where predictions of liquefaction severity are poor, the magnitude of the prediction error generally changes with a change in seismic loading, with the type of misprediction (i.e. under- or over-prediction) remaining generally constant. It can be seen in Figure S4b that of the 1176 investigation sites, there are only ~10 where the prediction error changed from an over-prediction for Darfield to an under-prediction for Christchurch, or vice versa. This suggests that some sites are inherently not well represented by the LPI model, which may not fully account for the variables and mechanisms affecting ground surface manifestation of liquefaction.



(a)



(b)

Figure 2.13 (S4) (a) Change in liquefaction severity prediction error from the Darfield earthquake to the Christchurch earthquake; (b) prediction error for Darfield earthquake vs. prediction error for Christchurch earthquake.

Chapter 3: Assessment of CPT-Based Methods for Liquefaction Evaluation in a Liquefaction Potential Index (LPI) Framework

Brett W. Maurer¹, Russell A. Green², Misko Cubrinovski³, Brendon A. Bradley⁴

¹ Graduate Research Assistant, Dept. of Civil and Environmental Engineering, Virginia Tech, Blacksburg, Virginia 24061, U.S.A.

² Professor, Dept. of Civil and Environmental Engineering, Virginia Tech, Blacksburg, Virginia 24061, U.S.A.

³ Professor, Dept. of Civil and Natural Resources Engineering, University of Canterbury, Private Bag 4800, Christchurch, New Zealand

⁴ Professor, Dept. of Civil and Natural Resources Engineering, University of Canterbury, Private Bag 4800, Christchurch, New Zealand

3.1 Abstract

In practice, several competing liquefaction evaluation procedures (LEPs) are used to compute factors of safety against soil liquefaction, often for use within a liquefaction potential index (LPI) framework to assess liquefaction hazard. At present, the influence of the selected LEP on the accuracy of LPI hazard assessment is unknown, and the need for LEP-specific calibrations of the LPI hazard-scale has never been thoroughly investigated. As such, this study aims to assess the efficacy of the Robertson & Wride (1998), Moss et al. (2006), and Idriss & Boulanger (2008) CPT-based LEPs, operating within the LPI framework, for predicting the severity of liquefaction manifestation. Utilizing more than 7,000 liquefaction case studies from the 2010-2011 Canterbury (NZ) earthquake sequence, this study found that: (1) The relationship between liquefaction manifestation severity and computed LPI values is LEP-specific; (2) Using a calibrated, LEP-specific hazard scale, the performance of the LPI models is essentially equivalent; and (3) The existing LPI framework has inherent limitations, resulting in inconsistent severity predictions versus field observations for certain soil profiles, regardless of which LEP is used. It is unlikely that revisions of the LEPs will resolve these erroneous assessments. Rather, a revised index which more adequately accounts for the mechanics of liquefaction manifestation is needed.

3.2 Introduction

The objective of this study is to assess the efficacy of three common CPT-based liquefaction evaluation procedures (LEPs), operating within a liquefaction potential index (LPI) framework, for predicting the severity of surficial liquefaction manifestation, which is commonly used as a proxy for liquefaction damage potential. Utilizing data from the 2010-2011 Canterbury Earthquakes, this study investigates the influence of the selected LEP on the accuracy of hazard assessments, and assesses the need for LEP-specific calibrations of the LPI hazard-scale. Towards this end, the deterministic LEPs of Robertson & Wride (1998) [R&W98], Moss et al. (2006) [MEA06], and Idriss & Boulanger (2008) [I&B08] are evaluated.

While the “simplified” LEP (Whitman, 1971; Seed & Idriss, 1971) is central to most liquefaction hazard assessments, the output from an LEP is not a direct quantification of liquefaction damage potential, but rather is the factor of safety against liquefaction triggering (FS_{liq}) in a soil stratum at depth. Iwasaki et al. (1978) proposed the LPI to link liquefaction triggering at depth to damage potential, where LPI is computed as:

$$LPI = \int_0^{20 \text{ m}} F \cdot w(z) dz \tag{1}$$

where $F = 1 - FS_{liq}$ for $FS_{liq} \leq 1$ and $F = 0$ for $FS_{liq} > 1$; $w(z)$ is a depth weighting function given by $w(z) = 10 - 0.5z$; and z is depth in meters below the ground surface. Thus, it is assumed that the severity of liquefaction manifestation is proportional to the thickness of a liquefied layer, the proximity of the layer to the ground surface, and the amount by which FS_{liq} is less than 1.0. Given this definition, LPI can range from 0 to a maximum of 100 (i.e., where FS_{liq} is zero over the entire 20 m depth). Analyzing SPT data from 55 sites in Japan, Iwasaki et al. (1978) proposed that severe liquefaction should be expected for sites where $LPI > 15$ but not where $LPI < 5$. This criterion for liquefaction manifestation, defined by two threshold values of LPI, is subsequently referred to as the *Iwasaki criterion*. However, in using the LPI framework to assess liquefaction hazard in current practice, it not always appreciated that the *Iwasaki criterion* is inherently linked to the LEP that was in common use in Japan in 1978, which differs significantly from those commonly used today. Also, it has been shown that the various LEPs used in today's practice can result in different FS_{liq} values for the same soil profile and earthquake scenario (e.g., Green et al., 2014), and thus different LPI values. These differences have led to confusion as to which LEP is the most accurate, and whether the *Iwasaki criterion* is equally effective for all LEPs.

The 2010-2011 Canterbury Earthquake Sequence (CES) resulted in a liquefaction dataset of unprecedented size and quality, presenting a unique opportunity to assess the efficacy of liquefaction-analytics (e.g., Cubrinovski & Green, 2010; Cubrinovski et al., 2011; Bradley & Cubrinovski, 2011). Towards this end, Maurer et al. (2014) evaluated LPI during the CES at approximately 1,200 sites using the R&W98 CPT-based LEP. While the *Iwasaki criterion* was found to be effective in a general sense, LPI hazard assessments were erroneous for a portion of the study area. In practice, several competing LEPs are used to assess liquefaction hazard in an LPI framework (e.g., Sonmez, 2003; Baise et al., 2006; Holzer et al., 2006a; 2006b; Lenz & Baise, 2007; Cramer et al., 2008; Hayati & Andrus, 2008; Holzer, 2008; Chung & Rogers, 2011; Kang et al., 2014), but the need for LEP-specific calibration of the LPI hazard-scale has never been thoroughly investigated. Therefore, the objective of this study is to assess the efficacy of the R&W98, MEA06, and I&B08 CPT-based LEPs, operating within the LPI framework, for predicting the severity of surficial liquefaction manifestation. Utilizing more than 7,000 liquefaction case studies from the CES, this study evaluates the influence of the selected LEP on the accuracy of hazard assessment, and assesses the need for LEP-specific calibrations of the LPI hazard-scale. This evaluation is performed using Receiver Operating Characteristic (ROC) analyses, which are commonly used to assess the performance of medical diagnostics (e.g., Zou, 2007).

In the following, the high-quality liquefaction case-history dataset resulting from the CES is briefly summarized. This is followed by a description of how LPI was computed using three common CPT-

based LEPs. An overview of ROC analyses is then presented, which is followed by the analysis of the LPI data. The influence of the LEP on the accuracy of LPI hazard assessment is then discussed.

3.3 Data and Methodology

The 2010-2011 CES began with the M_w 7.1, 4 September 2010 Darfield earthquake and includes up to ten events that are known to have induced liquefaction in the affected region (Quigley et al., 2013). However, most notably, widespread liquefaction was induced by the Darfield earthquake and the M_w 6.2, 22 February 2011 Christchurch earthquake (e.g., Green et al., 2014). Ground motions from these events were recorded by a dense network of strong motion stations (e.g., Bradley & Cubrinovski, 2011), and due to the extent of liquefaction, the New Zealand Earthquake Commission funded an extensive geotechnical reconnaissance and characterization program (Murahidy et al., 2012). The combination of densely-recorded ground motions, well-documented liquefaction response, and detailed subsurface characterization comprises the high-quality dataset used for this study. To evaluate the influence of the LEP operating in the LPI framework, a large database of Cone Penetration Test (CPT) soundings performed across Christchurch and its environs (CGD, 2012a) are analyzed in conjunction with liquefaction observations made following the Darfield and Christchurch events.

3.3.1 CPT Soundings

This study utilizes 3,616 CPT soundings performed at sites where the severity of liquefaction manifestation was well-documented following both the Darfield and Christchurch earthquakes, resulting in more than 7,000 liquefaction case studies. In the process of compiling these case studies, CPT soundings were first rejected from the study as follows. *First*, CPTs were rejected if the depth of “pre-drill” significantly exceeded the estimated depth of the ground water table (GWT), a condition arising at sites where buried utilities needed to be safely bypassed before testing could begin. *Second*, to identify soundings prematurely terminating on shallow gravels, termination depths of CPT soundings were geo-spatially analyzed using an Anselin Local Morans *I* analysis (Anselin, 1995) and soundings with anomalously shallow termination depths were removed from the study. For a complete discussion of CPT soundings and the geospatial analysis used herein, see Maurer et al. (2014).

3.3.3 Liquefaction Severity

Observations of liquefaction and the severity of manifestations were made by the authors for each of the CPT sounding locations following both the Darfield and Christchurch earthquakes. This was accomplished by ground reconnaissance and using high-resolution aerial and satellite imagery (CGD, 2012b) performed in the days immediately following each of the earthquakes. CPT sites were assigned

one of six damage classifications, as described in Table 1, where the classifications describe the predominant damage mechanism and manifestation of liquefaction. For example, some “severe liquefaction” sites also had minor lateral spreading, and likewise, many “lateral spreading” sites also had some amount of liquefaction ejecta present. Of the more than 7,000 cases compiled, 48% are cases of “no manifestation,” and 52% are cases where manifestations were observed and classified in accordance with Table 1.

3.3.4 Estimation of a_{max} (PGA)

To evaluate FS_{liq} using the three LEPs (i.e., R&W98, MEA06, and I&B08), the Peak Ground Accelerations at the ground surface (PGAs) were computed using the robust procedure discussed in detail by Bradley (2013a) and used by Green et al. (2011; 2014) and Maurer et al. (2014). The Bradley (2013a) procedure combines unconditional PGA distributions estimated by the Bradley (2013b) Ground Motion Prediction Equation, recorded PGAs from strong motion stations, and the spatial correlation of intra-event residuals to compute the conditional PGA distribution at sites of interest.

3.3.5 Estimation of ground water table (GWT) depth

Given the sensitivity of liquefaction hazard and computed LPI values to GWT depth (e.g., Chung and Rogers, 2011; Maurer et al., 2014), accurate measurement of GWT depth is critical. For this study, GWT depths were sourced from the robust, event-specific regional ground water models of van Ballegooy et al. (2014). These models, which reflect seasonal and localized fluctuations across the region, were derived in part using monitoring data from a network of ~1000 piezometers and provide a best-estimate of GWT depths immediately prior to the Darfield and Christchurch earthquakes.

3.3.6 Liquefaction Evaluation and LPI

FS_{liq} was computed using the deterministic CPT-based LEPs of R&W98, MEA06, and I&B08, where the soil behavior type index, I_c , was used to identify non-liquefiable strata; soils having $I_c > 2.6$ were considered too plastic to liquefy. Soil unit weights were estimated for each procedure using the method of Robertson & Cabal (2010). For the MEA06 procedure, the stress-reduction coefficient, r_d , was computed using the V_s -independent equation given in Moss et al. (2006); in addition, the probability of liquefaction (P_L) was set to 0.15, as proposed by Moss et al. (2006) for deterministic assessments of FS_{liq} . For the I&B08 procedure, fines content, FC, is required to compute normalized tip resistances (in lieu of FC, R&W98 and MEA06 use I_c and CPT friction ratio, R_f , respectively); as such, FC values were estimated using both the generic I_c -FC correlation proposed by Robertson & Wride (1998) and a Christchurch-soil-specific I_c -FC correlation developed by Robinson et al. (2013). Henceforth herein, I&B08¹ and I&B08² refer to the use of the generic and Christchurch-specific I_c -FC correlations, used in

conjunction with the I&B08 procedure. The two I_c -FC correlations are shown in Figure 1; it can be seen that the Christchurch-specific correlation suggests different I_c -FC trends for $I_c < 1.7$ and $I_c \geq 1.7$, where FC is estimated to be 10 for all $I_c \leq 1.7$. While thin layer corrections (i.e., adjustments to CPT data in thin strata to account for the influence of over- or underlying soils) are applicable to the LEPs used herein, their use requires judgment, and an automated implementation of these corrections does not yet exist. Given the quantity of case studies analyzed, thin layer corrections were not performed. FS_{liq} was computed at 1- or 2-cm depth intervals (i.e., the measuring rate of CPT soundings); LPI was then computed with each of the four LEPs per Eq. 1.

3.4 Overview of ROC Analyses

ROC analyses are used herein to assess: (1) the efficacy of each LEP for predicting the severity of liquefaction manifestation within the LPI framework; and (2) the need for LEP-specific calibrations of the LPI hazard-scale. ROC analyses have been extensively used in assessing medical diagnostic tests in clinical studies (e.g., imaging tests for identifying abnormalities), as well as in machine learning and data-mining research (e.g., Swets et al., 2000; Eng, 2005; Fawcett, 2006; Metz, 2006). In any ROC application, the distributions of “positives” (e.g., liquefaction is observed) and “negatives” (e.g., no liquefaction is observed) overlap when the frequency of the distributions are expressed as a function of index test results (e.g., LPI values). In such cases, threshold values for the index test results are selected considering the relative probabilities of true positives (i.e., liquefaction is observed, as predicted) and false positives (i.e., liquefaction is predicted, but is not observed). Setting the threshold too low will result in numerous false positives, which is not without consequences, while setting the threshold unduly high will result in many false negatives (i.e., liquefaction is observed when it is predicted not to occur), which comes with a different set of consequences. ROC analyses are particularly valuable for evaluating the relative efficacy of competing diagnostic tests, independent of the thresholds used, and for selecting an optimal threshold for a given diagnostic test.

In this study, the competing diagnostic tests are the LEPs, and the index test results are the computed LPI values. Accordingly, in analyzing the case histories, true and false positives are scenarios where surficial liquefaction manifestations are predicted, but were and were not observed, respectively. Figure 2 illustrates the relationship among the positive and negative distributions, the selected threshold value, and the corresponding ROC curve, where the ROC curve plots the true positive rate (TPR) and false positive rate (FPR) for varying threshold values. Figure 3 illustrates how a ROC curve is used to assess the efficiency of LPI hazard assessment, where TPR and FPR are synonymous with “True Positive Probability” and “False Positive Probability”, respectively. In ROC curve space, random guessing is indicated by a 1:1 line through the origin (i.e., equivalent correct and incorrect predictions), while a perfect model plots as a point at (0,1), indicating the existence of a threshold value which perfectly

segregates the dataset (e.g., all sites with manifestation have LPI above the selected threshold; all sites without manifestation have LPI below the same selected threshold). While no single parameter can fully characterize model performance, the area under a ROC curve (AUC) is commonly used for this purpose, where AUC is equivalent to the probability that sites with manifestation have higher computed LPI than sites without manifestation (e.g., Fawcett, 2005). As such, increasing AUC indicates better model performance. The optimum operating point (OOP) is defined herein as the threshold LPI value which minimizes the rate of misprediction (i.e., $FPR + (1-TPR)$, where TPR and FPR are the rates of true and false positives, respectively). As such, contours of the quantity $[FPR + (1-TPR)]$ represent points of equivalent performance in ROC space. Thus, in plotting the LPI data as ROC curves for each LEP, we may assess both the influence of LEPs on the accuracy of hazard assessments, and the need for LEP-specific calibrations of the LPI hazard-scale.

3.5 Results and Discussion

Utilizing more than 7,000 combined case studies from the Darfield and Christchurch earthquakes, LPI values were computed using the LEPs of R&W98, MEA06, I&B08¹, and I&B08².

3.5.1 Prediction of Liquefaction Occurrence

In Figure 4, ROC curves are plotted to evaluate the performance of each LPI model in segregating sites with and without liquefaction manifestation; this initial analysis assesses only whether LPI accurately predicts the occurrence of manifestations and does not yet consider manifestation severity. Included in Figure 4 is data from both the Darfield and Christchurch earthquakes for all investigation sites, except for those where lateral spreading was the predominant manifestation (the separate assessment of lateral spreading is discussed later in this paper). It can be seen in Figure 4 that while the four LPI models perform similarly, MEA06 and I&B08¹ are respectively the least and most efficacious, with AUC ranging from 0.71 (MEA06) to 0.78 (I&B08¹). To place this performance in context, AUCs of 0.5 and 1.0 respectively indicate random guessing and a perfect model. Also, as highlighted in Figure 4, the optimum threshold LPI values for the R&W98, MEA06, I&B08¹, and I&B08² models are 4.0, 5.5, 6.0, and 4.5, respectively. Thus, while the lower *Iwasaki criterion* (i.e., $LPI = 5$) is generally appropriate for predicting liquefaction manifestation in Christchurch, the optimum threshold is LEP-dependent. The presence of different optimum threshold LPI values for each LEP is not surprising given that different LEPs have been shown to commonly compute notably different FS_{liq} values for the same soil profile (e.g., Green et al., 2014). Though not unexpected, these findings may have important implications for liquefaction hazard assessment, as the risks corresponding to particular LPI values depend on the LEP used to compute LPI.

Also of interest is the influence of the $I_c - FC$ correlation used within the I&B08 LEP. As shown in Figure 1, the Christchurch-specific correlation infers a higher FC than does the generic correlation for all values of I_c , resulting in higher computed FS_{liq} values, and thus, lower computed LPI. As a result, the LPI hazard-scale computed using I&B08² (i.e., using the Christchurch-specific correlation) is shifted towards lower values relative to the hazard-scale computed using I&B08¹ (i.e., using the generic correlation) such that the median LPI values computed using I&B08¹ and I&B08² are 7.2 and 4.1, respectively. In addition to influencing the LPI hazard scale, the $I_c - FC$ correlation affects model efficacy (i.e., efficiency segregating sites with and without liquefaction manifestations), with I&B08¹ correctly classifying 3% more cases than I&B08² when operating at their respective OOPs. The slightly weaker performance of I&B08² might be due to the fact that the Robinson et al. (2013) Christchurch-specific $I_c - FC$ correlation was developed using data from along the Avon River only, while the database assessed herein consists of sites distributed throughout Christchurch, although further analysis is needed to evaluate this hypothesis. As research continues in Christchurch, refined region-specific $I_c - FC$ correlations, which might improve the efficacy of LPI hazard assessment in Christchurch, are likely to be developed.

While the preceding ROC analysis showed that optimum threshold LPI values are LEP-dependent, the implications for liquefaction hazard assessment are not intuitively clear. For example, it was shown that for the considered dataset the R&W98 and I&B08¹ LPI models have optimum threshold LPI values of 4.0 and 6.0, respectively, but the potential consequence of failing to account for different optimum thresholds is not easily discerned. To elucidate the significance of these differences, the probability of surficial liquefaction manifestation is computed herein using the Wilson (1927) interval for a binomial proportion. This assessment also allows for application to risk-based frameworks, complementing the prior evaluation of deterministic threshold values. The resulting probabilities are plotted in Figure 5 where each data point represents one 20th of the corresponding dataset (~350 case histories) and is plotted as a function of the median-percentile for each data bin (i.e., 2.5th-percentile, 7.5th-percentile, etc.); also shown are 3rd-order polynomial regressions for each LPI model. It can be seen from these regressions that at an LPI value of 5.0, the probabilities of liquefaction manifestation corresponding to the I&B08¹, MEA06, R&W98, I&B08² LPI models are 0.44, 0.53, 0.58, and 0.58, respectively. Conversely, using the optimum threshold LPI values found previously, the probabilities corresponding to the respective LPI models are 0.50, 0.55, 0.53, and 0.55. Thus, the optimum thresholds correspond to roughly the same probability of manifestation, whereas failing to account for the influence of the LEP could result in different risk levels for the same LPI value, particularly with I&B08¹.

3.5.2 Prediction of Liquefaction Severity

While predicting the occurrence of surficial manifestation is an important component of liquefaction hazard analysis, the severity of manifestation is of greater consequence to the built environment and is thus of added importance for hazard mapping and engineering design. To investigate the capacity of each LPI model for predicting manifestation severity, additional ROC analyses were performed for each classification of severity in Table 1; the results are summarized in Table 2 in the form of AUC and recommended threshold LPI values. Where the prior ROC analysis assessed each model's capacity for predicting any surficial manifestation (i.e., having *at least* marginal severity), the additional analyses assess their ability to predict that manifestations will be of a particular severity (e.g., moderate vs. marginal). As mentioned previously, lateral spreading is treated separately in this study, and the "marginal", "moderate", and "severe" classifications refer only to sand-blow manifestations. This distinction is made because lateral spreading is a unique manifestation associated with large permanent ground displacements, and because there are separate criteria for assessing its severity (e.g., Youd et al., 2002), including the ground slope and height of the nearest free-face (e.g., river bank), among others. Consequently, while site profiles with thin liquefiable layers may have low LPI values, these sites are susceptible to lateral spreading if located on sloping ground or near rivers. Since the factors pertinent to lateral spreading cases are not considered in the formulation of LPI, such cases should not be used to assess its performance.

From Table 2, the following observations are made: (1) Relative trends in model performance, as suggested by AUC, are consistent for each classification of manifestation severity. While the LPI models perform similarly, the I&B08 and MEA06 models are consistently the most and least efficacious, respectively. (2) Unsurprisingly, the models are more efficient predicting the incidence of liquefaction manifestation than predicting the severity of manifestation (e.g., distinguishing between marginal and moderate manifestations); nonetheless, the expected severity of manifestation increases with increasing LPI. (3) Differences in optimum threshold LPI values extend throughout the LPI hazard-scale, indicating that the utility of the *Iwasaki criterion* varies amongst LEPs. (4) Considering the potential for damage to infrastructure, lateral spreading manifestations have relatively low optimum threshold LPI values. For example, lateral spreading and marginal sand-blow manifestations have similar OOPs for each respective LPI model (i.e., similar LPI distributions), but the potential for damage to infrastructure is generally much greater with lateral spreading. This illustrates that while LPI may be useful for hazard assessment, the influence of local conditions on the manifestation of liquefaction must also be considered. As such, the damage-potential of lateral spreading may not be well-estimated by LPI.

As was done previously, the probability of manifestation is computed to assess the significance of different optimum thresholds, and to allow for application to risk-based frameworks. Because damage to infrastructure (e.g., settlement of structures, failure of lifelines, and cracking of pavements) is more likely a consequence of moderate or severe liquefaction, these cases are used to compute the likelihood of damaging liquefaction due to sand blows, where marginal liquefaction is considered non-damaging. Using the methodology previously discussed, the probability of moderate or severe liquefaction is plotted in Figure 6 along with 3rd-order polynomial regressions for each LPI model. It can be seen from these regressions that at an LPI value of 15.0 (i.e., the upper *Iwasaki criterion*), the probabilities corresponding to the I&B08¹, MEA06, R&W98, I&B08² LPI models are 0.37, 0.40, 0.43, and 0.47, respectively. Conversely, using the threshold LPI values found previously for severe liquefaction (Table 2), the probabilities corresponding to the respective LPI models are 0.39, 0.39, 0.38, and 0.40. Thus, the optimum thresholds correspond to roughly the same probability of damaging manifestation, whereas failing to account for the influence of the LEP results in different risk levels. Similarly, the optimum thresholds for moderate liquefaction correspond to the same level of risk (~27%).

3.5.3 Comparative Performance in an Applied Framework

The preceding analyses have suggested the four LPI models may be equally-capable of assessing liquefaction hazard, but that LEP-specific correlations relating LPI values and severity of surficial liquefaction manifestations are required. To compare LEP performance in an applied setting, and to determine whether any LEP is superior for practical intents and purposes, deterministic “prediction errors” are computed for each case-history using both the *Iwasaki criterion* and the LEP-specific calibrations in Table 2. The prediction error (E) is computed using the thresholds assigned to each manifestation category, such that $E = \text{LPI} - (\text{min or max})$ of the relevant range. For example, using the *Iwasaki criterion*, if the computed LPI is 14 for a site with no manifestation, $E = 14 - 5 = 9$ (where 5 is the maximum of the range of LPI values for no manifestation), whereas if the computed LPI is 6 for a site with severe liquefaction, $E = 6 - 15 = -9$ (where 15 is the minimum of the range of LPI values for severe liquefaction). Thus, positive errors indicate over-predictions of manifestation severity, and conversely, negative errors indicate under-predictions. While there is no precedent for using a “moderate manifestation” threshold with the *Iwasaki criterion*, an LPI value of 8.0 is used herein to facilitate comparisons amongst models. Also, in light of the separate criteria for assessing lateral spreads, lateral spreading is assigned a wide range of expected LPI values consistent with any manifestation, independent of spreading severity (i.e., lateral spread sites are only expected to have $\text{LPI} \geq$ the threshold for marginal liquefaction).

The distributions of LPI prediction errors are shown for each model in Figure 7 using both the *Iwasaki* (Figure 7a) and LEP-specific (Figure 7b) hazard-scales. It can be seen in Figure 7a that the distributions of errors amongst LEPs vary using the *Iwasaki criterion*, as expected. Because the models have different LPI hazard-scales, applying the *Iwasaki criterion* to each results in dissimilar performance. For example, R&W98 and I&B08¹ under-predict manifestation severity for 38% and 18% of cases, respectively. Conversely, using the LEP-specific calibrations of the LPI hazard-scale (Figure 7b), the distributions of errors amongst LEPs are more similar. For example, R&W98 and I&B08¹ under-predict manifestation severity for 24% and 20% of cases, respectively. In addition, the rate of accurate prediction (i.e., zero-error) is improved for each LEP; R&W98, MEA06, I&B08¹, and I&B08² accurately predict 44%, 42%, 46%, and 44% of cases, respectively. These performance trends mirror those of the ROC analyses, which indicated that while the models performed similarly, I&B08¹ and MEA06 were respectively the most and least efficacious. However, though accurate predictions of manifestation severity are important, so too is limiting the rate of highly-erroneous predictions, which are not necessarily mutually inclusive. While I&B08¹ has the most zero-error predictions (46%), it also has the most predictions with $|E| > 15$ (5%). Conversely, MEA06 has the least zero-error predictions (42%), but it also has the fewest predictions with $|E| > 15$ (2.5%). Given these inconsistencies, and considering the variety of metrics that might be used to gauge performance, it is difficult to argue that any one LEP is superior in this applied framework. Thus, using the LEP-specific hazard-scales, and based on the prediction-errors computed herein, the performance of the LPI models is, for practical intents and purposes, equivalent.

While minor errors are to be expected in any deterministic analysis, each model produced significant errors with consequences for hazard assessment. For example, even with calibration, $|E|$ exceeded 10 at 9% of sites, on average, for each model (e.g., severe manifestation predicted, but no manifestation observed) and $|E|$ exceeded 5 at 22% of sites, on average, for each model (e.g., no manifestation predicted, but moderate manifestation observed). To determine whether certain models perform better in particular locations, prediction errors from the calibrated R&W98, MEA06, and I&B08² models are plotted against one another in Figure 8. It can be seen that prediction errors are generally equivalent; in all, the difference in prediction error between any two of the models exceeds 5 for only 12% of investigation sites. Thus, locations of under-, over-, and accurate prediction are generally consistent between models. In addition, maps showing the spatial distributions of errors to be very similar in both earthquakes are provided in an *Electronic Supplement*. Thus, some site profiles have very poor predictions, irrespective of the LEP used (note that Maurer et al., 2014 found no correlation between prediction errors and either PGA uncertainty, ground water fluctuation, or CPT termination depth). This suggests that LPI has inherent limitations in its formulation, such that the variables influencing surficial manifestation are not adequately accounted for. While liquefaction triggering has garnered significant

research and is a subject of frequent debate, the mechanics of liquefaction manifestation have received less attention. This study highlights that triggering and manifestation are two distinct phenomena contributing to liquefaction hazard, and that an improved framework providing clear separation and accounting of the two phenomena is needed.

Lastly, the 12% of cases with inconsistent prediction errors between models can be shown to correspond to “exceptional” site profiles. Since the LEP-specific calibrations are based on the entire dataset (i.e., predominant behaviour across Christchurch), predictions for site-profiles that diverge from typical conditions may be inconsistent amongst models. As an example, it can be seen in Figs. 8a and 8c that a number of cases exist where the MEA06 prediction error significantly differs from that of R&W98 and I&B08². One common cause of this discrepancy is shown in Figure 9, where r_d , $CSR_{M7.5}$, and LPI profiles are shown for one such case in the Darfield earthquake. Amongst the models, MEA06 computes a lower r_d below a depth of 10 m, and thus, lower $CSR_{M7.5}$. Consequently, LPI values computed using MEA06 tend to diverge from those of R&W98 and I&B08² when liquefiable strata are present at depths greater than 10 m. Considering all investigation sites, the median cumulative thickness of soil strata predicted to liquefy below 10 m depth is 0.35 m, according to I&B08². Conversely, the site shown in Figure 9 is predicted to have a more than 6 m thick liquefiable strata below a depth of 10 m; being an “exceptional” site-profile, the LEP-specific calibrations perform inconsistently. This emphasizes that assessments and/or calibrations of the LPI hazard-scale are a function not only of the selected LEP, but also of the chosen dataset, including the geometry and soil characteristics of site-profiles, as well as the amplitude and duration of ground shaking. As such, the applicability of findings derived herein to other datasets is unknown.

3.6 Summary and Conclusions

Utilizing high-quality case histories from the CES, this study evaluated the performance of the R&W98, MEA06, I&B08¹, and I&B08² CPT-based LEPs, operating within the LPI framework, for assessing liquefaction hazard. The findings are summarized as follows:

- For deterministic analyses, the optimum threshold LPI values for assessing liquefaction hazard were unique to the LEP used in the LPI framework; suggested optimum thresholds for the CES dataset are summarized in Table 2. The use of LPI for assessing lateral spread potential is not recommended.
- Taking these LEP-specific threshold values into account, receiver-operating-characteristic analyses indicated that while the models performed similarly, the I&B08 and MEA06 models were respectively the most and least efficacious.
- LPI probability curves were computed to assess the significance of different optimum thresholds, and to allow for application in probabilistic frameworks. The optimum thresholds were shown to correspond to roughly the same probability of manifestation, whereas failing to account for the

influence of the LEP (i.e., using the *Iwasaki criterion*) resulted in different risk levels for the same LPI value.

- To compare model performance in a practical setting, deterministic “prediction errors” were computed for each case history. Using the *Iwasaki criterion*, the distributions of errors amongst LEPs varied. These distributions became more similar using the LEP-specific hazard-scales given in Table 2, which also improved the rate of accurate prediction for all LEPs.
- Even with calibration, each model had significant prediction errors (e.g., severe manifestation predicted, but no manifestation observed). This suggests that LPI has inherent limitations in its formulation, such that the variables influencing surficial liquefaction manifestation are not adequately accounted for.
- The findings presented in this study are based on a dataset from the CES; the applicability of these findings to other datasets is unknown.

In conclusion: (1) The risk-levels corresponding to the *Iwasaki criterion* varied amongst LEPs. (2) Using a calibrated, LEP-specific hazard-scale, the performance of the LPI models was, for practical intents and purposes, equivalent; and (3) The existing LPI framework has inherent limitations such that all LEPs have very poor predictions for certain soil profiles. It is unlikely that revisions of the LEPs will resolve these erroneous assessments. Rather, a revised index which more adequately accounts for the mechanics of liquefaction manifestation is needed.

3.7 Acknowledgements

This study is based on work supported by the U.S. National Science Foundation (NSF) grants CMMI-1030564 and CMMI-1306261, and US Army Engineer Research and Development Center (ERDC) grant W912HZ-13-C-0035. The third and fourth authors would like to acknowledge the continuous financial support provided by the Earthquake Commission (EQC) and Natural Hazards Research Platform (NHRP), New Zealand, of the research and investigations related to the 2010-2011 Canterbury earthquakes. The authors also acknowledge the New Zealand GeoNet project and its sponsors EQC, GNS Science and LINZ for providing the earthquake occurrence data and the Canterbury Geotechnical Database and its sponsor EQC for providing the CPT soundings, lateral spread observations, and aerial imagery used in this study. However, any opinions, findings, and conclusions or recommendations expressed in this paper are those of the authors and do not necessarily reflect the views of NSF, ERDC, EQC, NHRP, or LINZ.

References

- Anselin, L. (1995). Local Indicators of Spatial Association—LISA. *Geographical Analysis* 27, No.2, 93–115.
- Baise, L.G., Higgins, R.B., & Brankman, C.M. (2006). Liquefaction hazard mapping-statistical and spatial characterization of susceptible units. *Journal of Geotechnical and Geoenvironmental Engineering* 132, No. 6, 705-715.
- Bradley, B.A. (2013b). A New Zealand-specific pseudo-spectral acceleration ground-motion prediction equation for active shallow crustal earthquakes based on foreign models. *Bulletin of the Seismological Society of America* 103, No. 3, 1801-1822.
- Bradley, B.A. (2013a). Estimation of site-specific and spatially-distributed ground motion in the Christchurch earthquakes: Application to liquefaction evaluation and ground motion selection for post-event investigation. *Proceedings of the 19th New Zealand Geotechnical Symposium*. 20-23 November 2013. Queenstown, New Zealand. 8pp.
- Bradley, B.A. & Cubrinovski, M., (2011). Near-source Strong Ground Motions Observed in the 22 February 2011 Christchurch Earthquake." *Seismological Research Letters* 82, 853-865.
- CDG - Canterbury Geotechnical Database (2012a). Geotechnical Investigation Data, Map Layer CGD0010, See: <https://canterburygeotechnicaldatabase.projectorbit.com>. Accessed 1/12/12.
- CDG - Canterbury Geotechnical Database (2012b). Aerial Photography, Map Layer CGD0010, See: <https://canterburygeotechnicaldatabase.projectorbit.com>. Accessed 1/12/12.
- Chung, J. & Rogers, J., (2011). Simplified method for spatial evaluation of liquefaction potential in the St. Louis Area. *Journal of Geotechnical and Geoenvironmental Engineering* 137, No. 5, 505-515.
- Cramer, C.H., Rix, G.J., & Tucker, K. (2008). Probabilistic liquefaction hazard maps for Memphis, Tennessee. *Seismological Research Letters* 79, No. 3, 416-423.
- Cubrinovski, M. & Green, R.A. (eds.) (2010). Geotechnical Reconnaissance of the 2010 Darfield (Canterbury) Earthquake, (contributing authors in alphabetical order: J. Allen, S. Ashford, E. Bowman, B. Bradley, B. Cox, M. Cubrinovski, R. Green, T. Hutchinson, E. Kavazanjian, R. Orense, M. Pender, M. Quigley, & L. Wotherspoon), *Bulletin of the New Zealand Society for Earthquake Engineering* 43, No. 4, 243-320.
- Cubrinovski, M., Bradley, B., Wotherspoon, L., Green, R., Bray, J., Woods, C., Pender, M., Allen, J., Bradshaw, A., Rix, G., Taylor, M., Robinson, K., Henderson, D., Giorgini, S., Ma, K., Winkley, A., Zupan, J., O'Rourke, T., DePascale, G., & Wells, D. (2011). Geotechnical aspects of the 22 February 2011 Christchurch earthquake. *Bulletin of the New Zealand Society for Earthquake Engineering*, 43, No. 4, 205-226.
- Eng, J. (2005). Receiver Operating Characteristic Analysis. *Academic Radiology* 12, 909-916.
- Fawcett, T. (2005). An introduction to ROC analysis. *Pattern Recognition Letters* 27, 861-874.

- Green, R.A., Allen, A., Wotherspoon, L., Cubrinovski, M., Bradley, B., Bradshaw, A., Cox, B., & Algie, T. (2011). Performance of levees (stopbanks) during the 4 September M_w 7.1 Darfield and 22 February 2011 M_w 6.2 Christchurch, New Zealand, earthquakes. *Seismological Research Letters* 82, No. 6, 939-949.
- Green, R.A., Cubrinovski, M., Cox, B., Wood, C., Wotherspoon, L., Bradley, B., & Maurer, B. (2014). Select Liquefaction Case Histories from the 2010-2011 Canterbury Earthquake Sequence. *Earthquake Spectra* 30, No. 1, 131-153.
- Hayati, H. & Andrus, R.D. (2008). Liquefaction potential map of Charleston, South Carolina based on the 1986 earthquake. *Journal of Geotechnical and Geoenvironmental Engineering* 134, No. 6, 815-828.
- Holzer, T.L., Bennett, M.J., Noce, T.E., Padovani, A.C., & Tinsley III, J.C. (2006). Liquefaction hazard mapping with LPI in the greater Oakland, California, area. *Earthquake Spectra* 22, No. 3, 693-708.
- Holzer, T.L., (2008). Probabilistic liquefaction hazard mapping, in Zeng, D., Manzari, M.T., & Hiltunen, D.R., *Geotechnical Earthquake Engineering and Soil Dynamics IV: Sacramento, CA*, ASCE Geotechnical Special Publication 181.
- Idriss, I.M. & Boulanger, R.W. (2008). Soil liquefaction during earthquakes. Monograph MNO-12, Earthquake Engineering Research Institute, Oakland, CA, 261 pp.
- Iwasaki, T., Tatsuoka, F., Tokida, K., & Yasuda, S. (1978). "A practical method for assessing soil liquefaction potential based on case studies at various sites in Japan." *Proceedings of the 2nd International Conference on Microzonation*, Nov 26-Dec 1, San Francisco, CA, USA.
- Kang, G.C., Chung, J.W., & Rogers, R.J. (2014). Re-calibrating the thresholds for the classification of liquefaction potential index based on the 2004 Niigata-ken Chuetsu earthquake. *Engineering Geology* 169, 30-40.
- Lenz, A. & Baise, L.G. (2007). Spatial variability of liquefaction potential in regional mapping using CPT and SPT data. *Soil Dynamics and Earthquake Engineering* 27, 690-702.
- Maurer, B.W., Green, R.A., Cubrinovski, M., & Bradley, B.A. (2014). Evaluation of the liquefaction potential index for assessing liquefaction hazard. *Journal of Geotechnical and Geoenvironmental Engineering* 140, No. 7, 04014032.
- Metz, C.E. (2006). Receiver Operating Characteristic Analysis: A Tool for the Quantitative Evaluation of Observer Performance and Imaging Systems. *Journal of the American College of Radiology* 3, No. 6, 413-422.
- Moss, R.E.S, Seed, R.B., Kayen, R.E., Stewart, J.P., Der Kiureghian, A., & Cetin, K.O. (2006). CPT-based probabilistic and deterministic assessment of in situ seismic soil liquefaction potential. *Journal of Geotechnical and Geoenvironmental Engineering* 132, No. 8, 1032-1051.

- Murahidy, K.M., Soutar, C.M., Phillips, R.A., & Fairclough, A. (2012). Post earthquake recovery - Development of a geotechnical database for Christchurch central city. *15th World Conference on Earthquake Engineering*, Lisbon, Portugal. p. 10.
- Papathanassiou, G. (2008). LPI-Based Approach for Calibrating the Severity of Liquefaction-Induced Failures and for Assessing the Probability of Liquefaction Surface Evidence. *Engineering Geology*, 96, 94-104.
- Robertson, P.K. & Cabal, K.L. (2010). Estimating soil unit weight from CPT. *2nd International Symposium on Cone Penetration Testing*, Huntington Beach, CA, USA, May 2010, Paper # 2-40.
- Robertson, P.K. & Wride, C.E. (1998). Evaluating cyclic liquefaction potential using cone penetration test. *Canadian Geotechnical Journal* 35, No. 3, 442-459.
- Robinson K, Cubrinovski M, & Bradley BA. Sensitivity of predicted liquefaction-induced lateral displacements from the 2010 Darfield and 2011 Christchurch Earthquakes. *Proc. New Zealand Soc. for Earthquake Eng. Annual Conf.* 2013, Wellington, New Zealand; 8p.
- Seed, H.B. & Idriss, I.M. (1971). Simplified procedure for evaluating soil liquefaction potential. *Journal of the Soil Mechanics and Foundation Division*, ASCE, 97, No. 9, 1249-1273.
- Sonmez, H. (2003). Modification of the liquefaction potential index and liquefaction susceptibility mapping for a liquefaction-prone area (Inegol, Turkey). *Environmental Geology* 44, No. 7, 862-871.
- Swets, J.A., Dawes, R.M., & Monahan, J. (2000). Better decisions through science. *Scientific American*, October, 82-87.
- Toprak, S. & Holzer, T. (2003). Liquefaction potential index: field assessment. *Journal of Geotechnical and Geoenvironmental Engineering* 129, No. 4, 315-322.
- van Ballegooy, S., Cox, S.C., Thurlow, C., Rutter, H.K., Reynolds T., Harrington, G., Fraser, J., and Smith, T. (2014). Median water table elevation in Christchurch and surrounding area after the 4 September 2010 Darfield earthquake: Version 2. GNS Science Report 2014/18.
- Whitman, R.V. (1971). Resistance of soil to liquefaction and settlement. *Soils and Foundations* 11, No. 4, 59-68.
- Wilson, E.B. (1927). Probable inference, the law of succession, and statistical inference. *Journal of the American Statistical Association* 22, 209-212.
- Youd, T.L., Hansen, C.M., & Bartlett, S.F. (2002). Revised multilinear regression equations for prediction of lateral spread displacement. *Journal of Geotechnical and Geoenvironmental Engineering* 128, No. 12, 1007-1017.
- Zou, K.H. (2007). Receiver operating characteristic (ROC) literature research. On-line bibliography: See <http://www.spl.harvard.edu/archive/spl-pre2007/pages/ppl/zou/roc.html>. Accessed 15/3/2014.

Tables

Table 3.1 Liquefaction severity classification criteria (after Green et al., 2014).

Classification	Criteria
No Manifestation	No surficial liquefaction manifestation or lateral spread cracking
Marginal Manifestation	Small, isolated liquefaction features; streets had traces of ejecta or wet patches less than a vehicle width; < 5% of ground surface covered by ejecta
Moderate Manifestation	Groups of liquefaction features; streets had ejecta patches greater than a vehicle width but were still passable; 5-40% of ground surface covered by ejecta
Severe Manifestation	Large masses of adjoining liquefaction features, streets impassible due to liquefaction; >40% of ground surface covered by ejecta
Lateral Spreading	Lateral spread cracks were predominant manifestation and damage mechanism, but crack displacements < 200 mm
Severe Lateral Spreading	Extensive lateral spreading and/or large open cracks extending across the ground surface with > 200 mm crack displacement

Table 3.2 Summary of Receiver Operator Characteristic (ROC) analyses^a

LPI Model	All Manifestations ^b		Marginal Manifestation ^b		Moderate Manifestation ^b		Severe Manifestation ^b		Lateral Spreading		Severe Lateral Spreading	
	OOP ^c	AUC ^d	OOP ^c	AUC ^d	OOP ^c	AUC ^d	OOP ^c	AUC ^d	OOP ^c	AUC ^d	OOP ^c	AUC ^d
R&W98	4.0	0.73	3.0	0.68	5.5	0.62	10.5	0.69	4.5	0.83	10.0	0.66
MEA06	5.5	0.71	5.0	0.66	7.5	0.60	14.0	0.68	5.0	0.83	12.0	0.64
I&B08¹	6.0	0.78	5.0	0.72	9.0	0.64	16.0	0.69	6.5	0.79	8.0	0.62
I&B08²	4.5	0.75	3.0	0.70	6.0	0.63	11.0	0.69	5.0	0.86	8.0	0.63

^a Where manifestation severity is characterized as described in Table 1.

^b Excludes sites where lateral spreading was predominant manifestation, as described in text.

^c Optimum operating point: recommended optimum threshold LPI value found from ROC analysis.

^d Area under ROC curve: general index of model efficacy, where higher AUC indicates better performance.

Figures

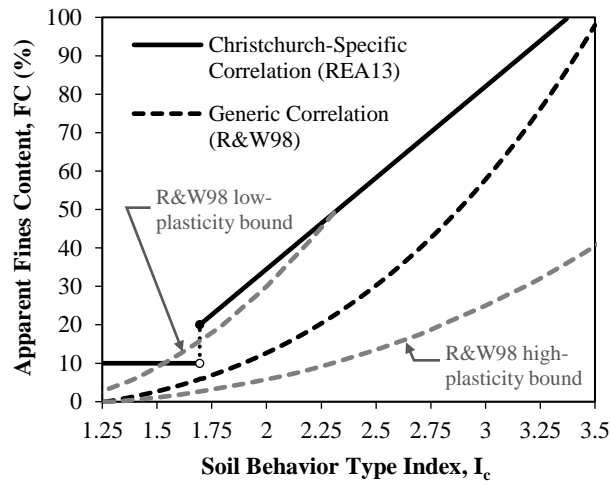


Figure 3.1 Correlations between I_c and apparent FC: Christchurch-specific correlation (Robinson et al., 2013) and generic correlation (Robertson & Wride, 1998).

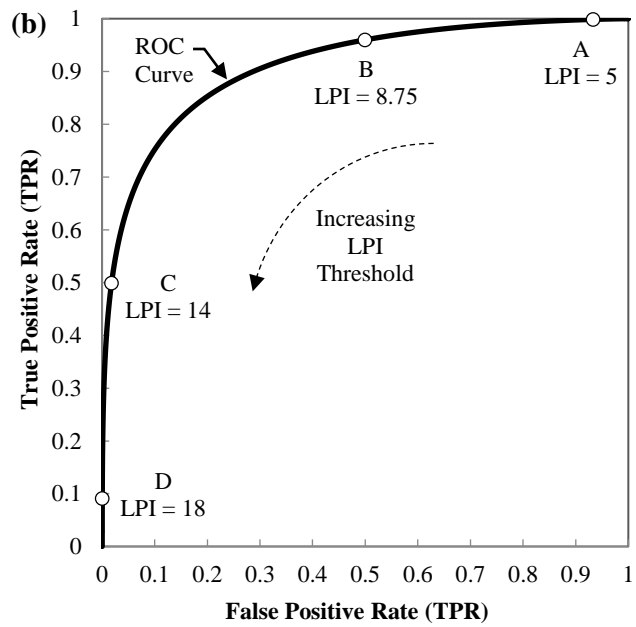
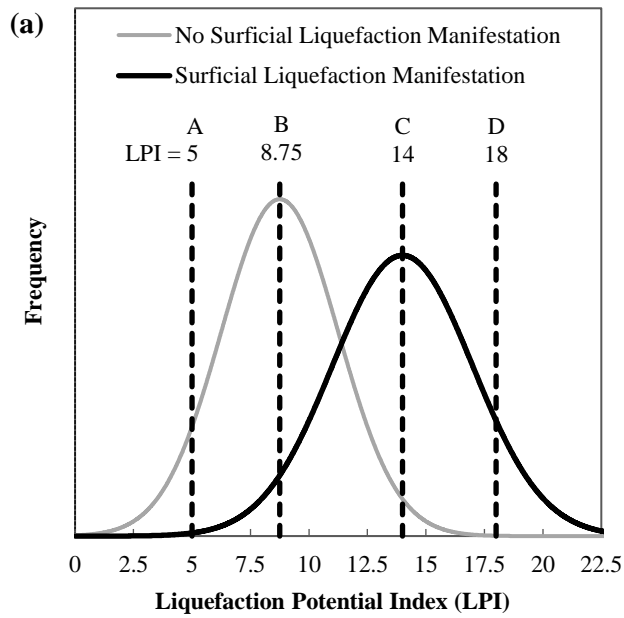


Figure 3.2 ROC analyses: (a) Frequency distributions of No Surficial Liquefaction Manifestation and Surficial Liquefaction Manifestations as a function of LPI, with four different threshold LPI values shown; and (b) Corresponding ROC curve.

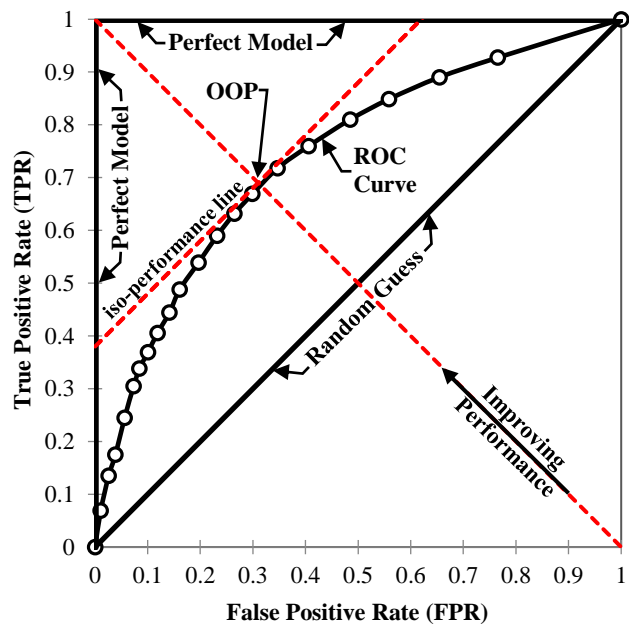


Figure 3.3 Illustration of how a ROC curve is used to assess the efficiency of a diagnostic test. The optimum operating point (OOP) indicates the threshold value for which the misprediction rate is minimized, as described in text.

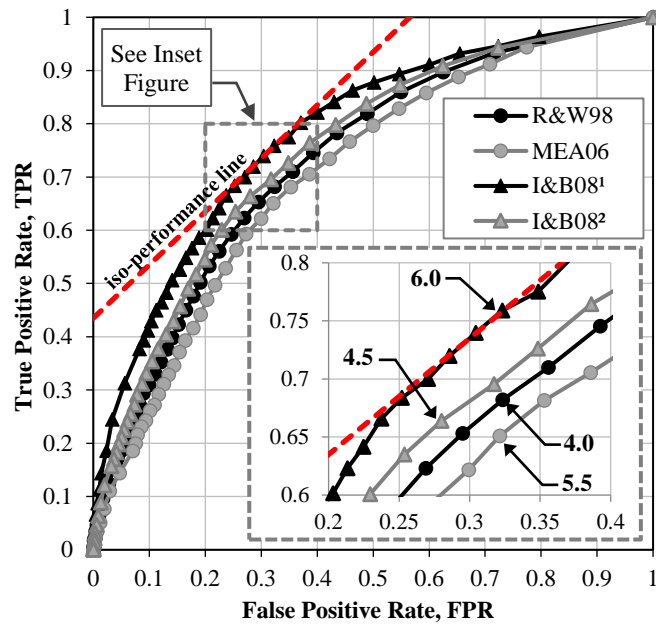


Figure 3.4 ROC analysis of LPI model performance in predicting the occurrence of surficial liquefaction manifestation. The optimum threshold LPI values (i.e., OOPs) for each LEP are highlighted in the inset figure.

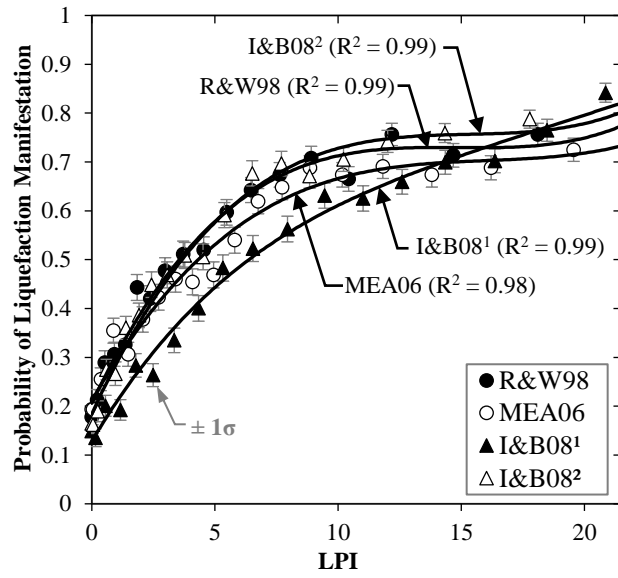


Figure 3.5 Probability of liquefaction manifestation.

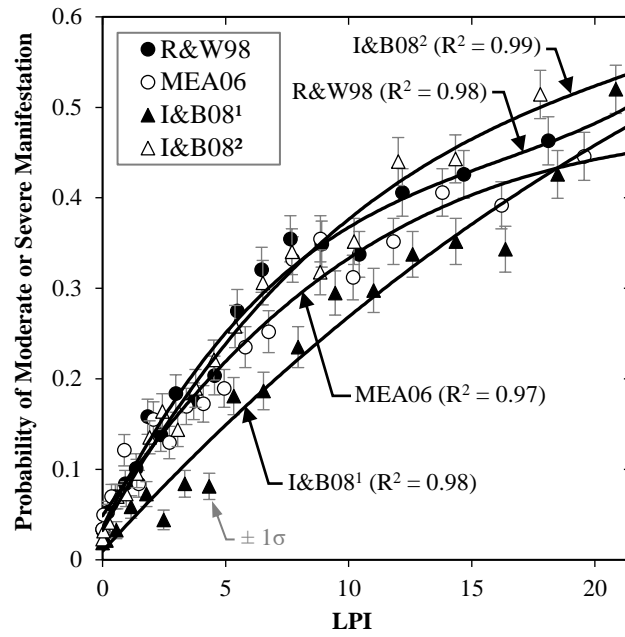


Figure 3.6 Probability of moderate or severe liquefaction manifestation.

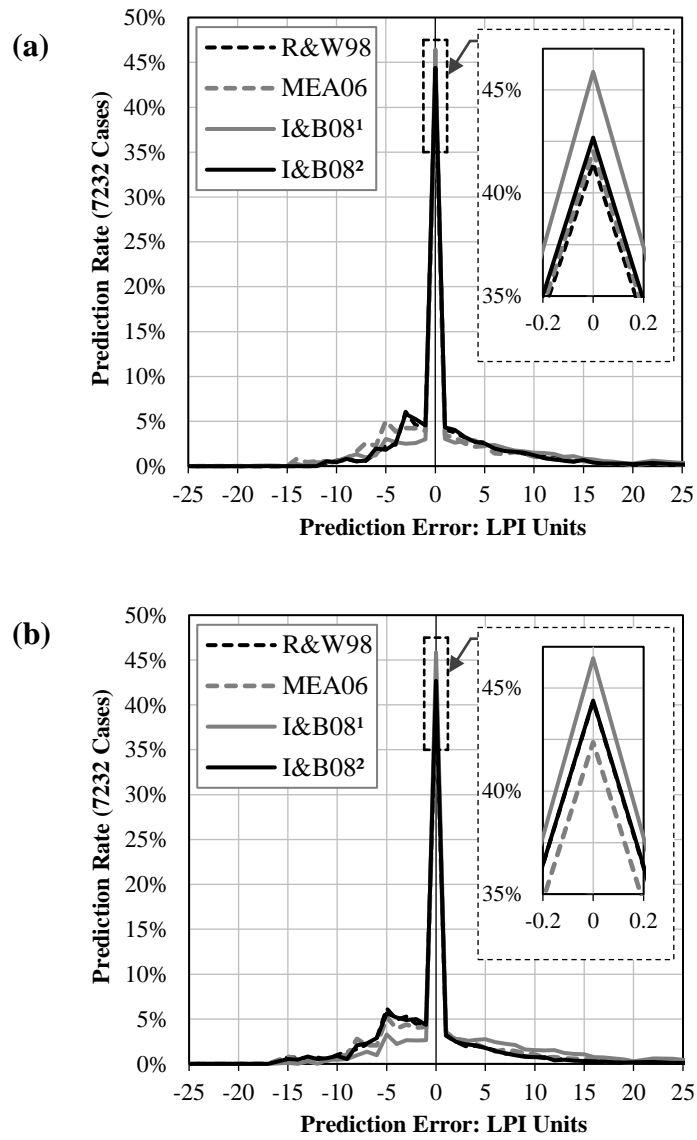


Figure 3.7 Distribution of LPI prediction errors, computed from the LPI hazard-scales defined by the (a) *Iwasaki criterion*; and (b) LEP-specific calibrations given in Table 2.

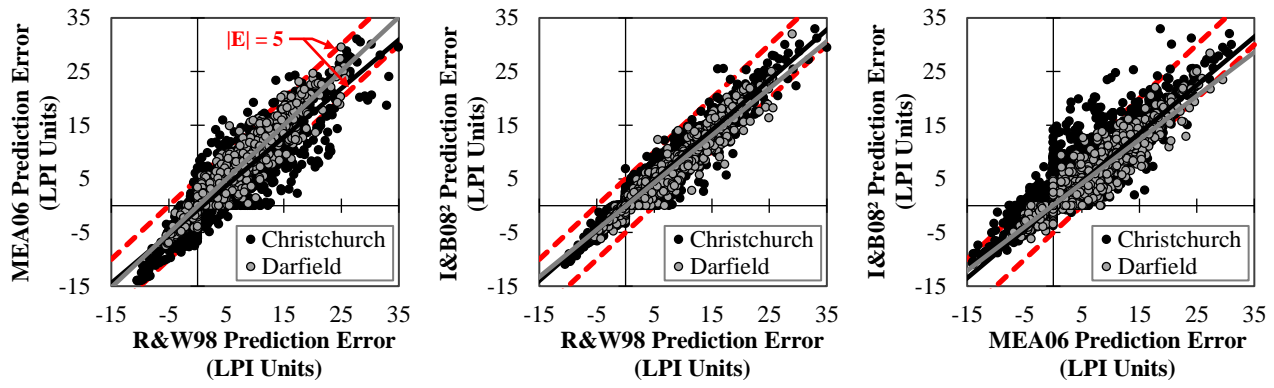


Figure 3.8 Comparison of LPI model prediction errors at each investigation site, as computed by (a) R&W98 vs. MEA06; (b) R&W98 vs. I&B08²; and (c) MEA06 vs. I&B08².

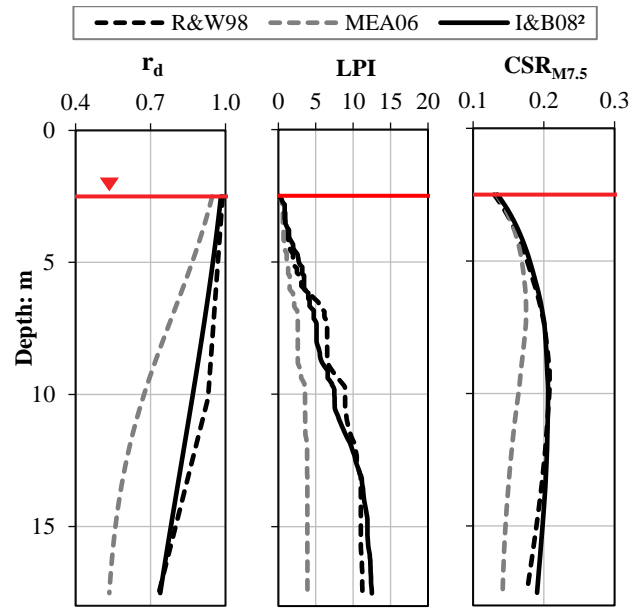


Figure 3.9 LEP/LPI model comparisons at site with inconsistent errors in the Darfield earthquake: (a) stress reduction coefficient, r_d ; (b) CSR_{M7.5}; and (c) LPI.

3.8 Electronic Supplement

The following are available in an Electronic Supplement: (1) aerial images representative of the liquefaction manifestation severity classes described in Table 1; and (2) map figures showing the spatial distribution of LPI prediction errors for each LPI model, for both the Darfield and Christchurch earthquakes.

Notice

Some of the data used in this study was extracted from the Canterbury Geotechnical Database (<https://canterburygeotechnicaldatabase.projectorbit.com>), which was prepared and/or compiled for the Earthquake Commission (EQC) to assist in assessing insurance claims made under the Earthquake Commission Act 1993 and/or for the Canterbury Geotechnical Database on behalf of the Canterbury Earthquake Recovery Authority (CERA). The source maps and data were not intended for any other purpose. EQC, CERA, and their data suppliers and their engineers, Tonkin & Taylor, have no liability for any use of these maps and data or for the consequences of any person relying on them in any way.

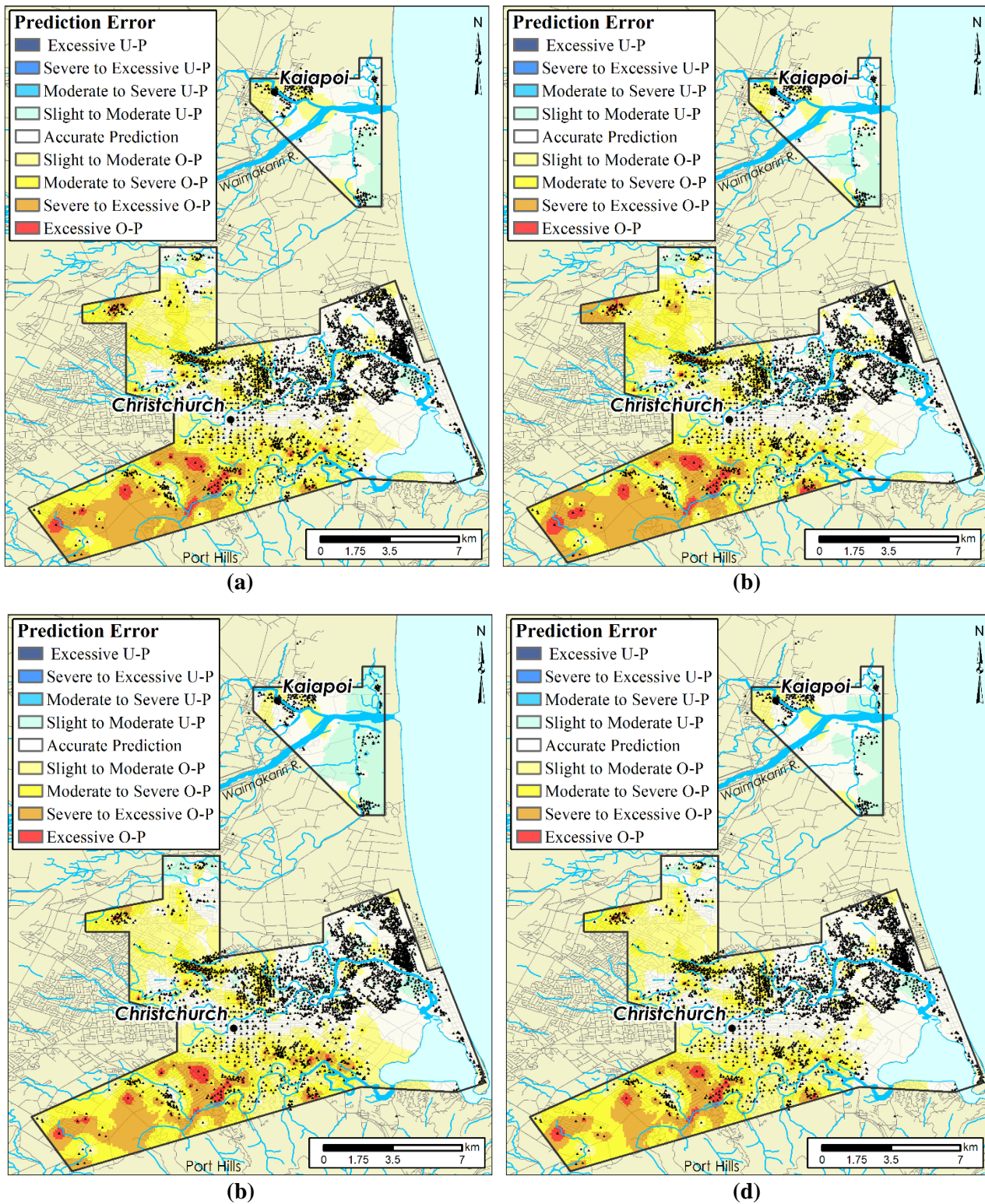


Figure 3.10 (S1) LPI prediction errors for the 4/9/2010 Darfield earthquake, using the calibrated (a) R&W98; (b) MEA06; (c) I&B08¹; and (d) I&B08² LPI models. The classification scheme is detailed in Table S1, where “U-P” indicates under-predictions of manifestation severity (i.e., severity was more than predicted), and “O-P” indicates over-predictions of manifestation severity (i.e., severity was less than predicted).

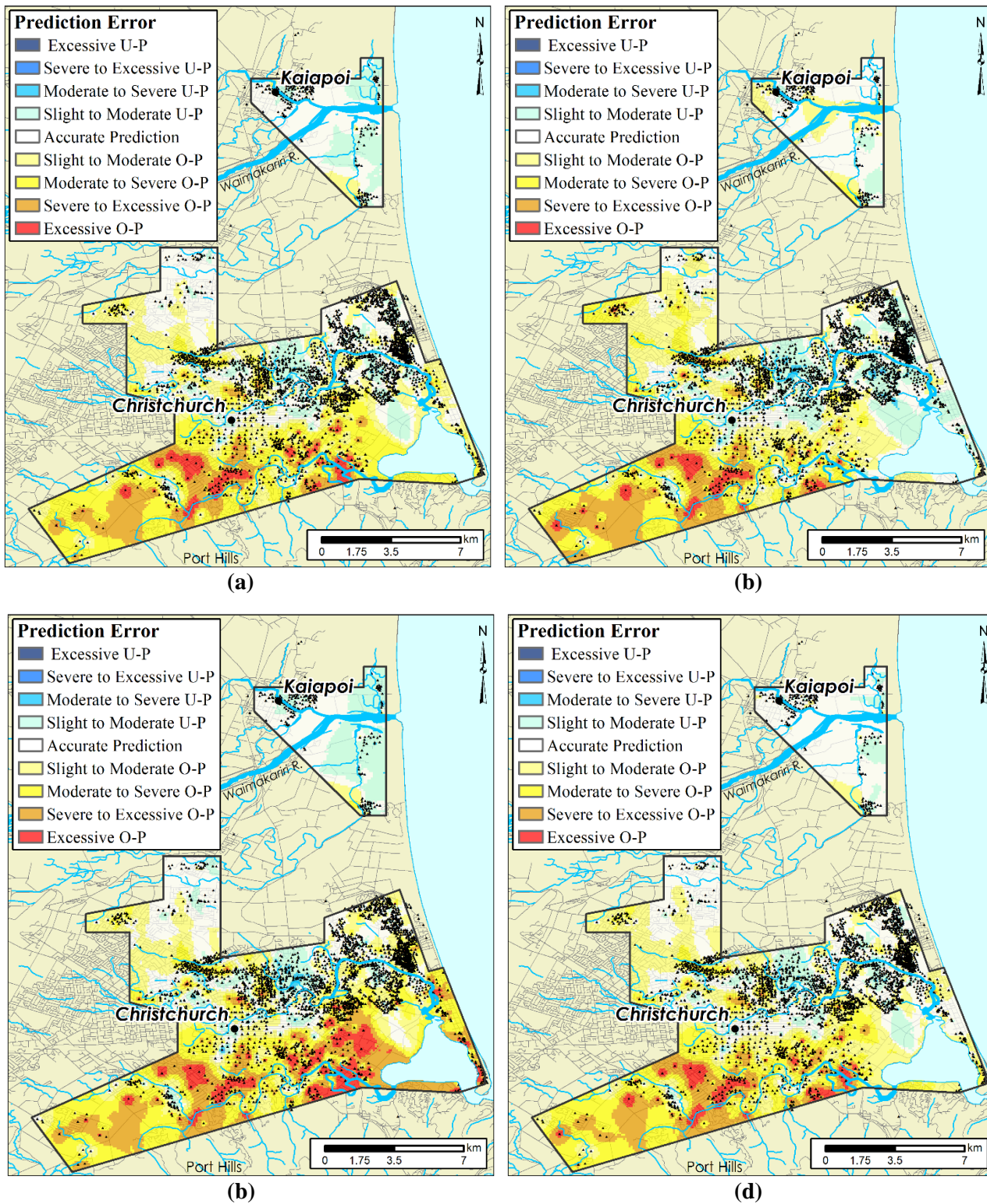


Figure 3.11 (S2) LPI prediction errors for the 22/2/2011 Christchurch earthquake, using the calibrated (a) R&W98; (b) MEA06; (c) I&B08¹; and (d) I&B08² LPI models. The classification scheme is detailed in Table S1, where “U-P” indicates under-predictions of manifestation severity (i.e., severity was more than predicted), and “O-P” indicates over-predictions of manifestation severity (i.e., severity was less than predicted).

Table 3.3 (S1) LPI prediction error classifications

Error (E) Classification	E (LPI units)
Excessive Underprediction	$E < -15$
Severe to Excessive Underprediction	$-15 \leq E < -10$
Moderate to Severe Underprediction	$-10 \leq E < -5$
Slight to Moderate Underprediction	$-5 \leq E < -1$
Accurate Prediction	$-1 \leq E \leq 1$
Slight to Moderate Overprediction	$1 < E \leq 5$
Moderate to Severe Overprediction	$5 < E \leq 10$
Severe to Excessive Overprediction	$10 < E \leq 15$
Excessive Overprediction	$E > 15$



(a) Marginal Liquefaction



(b) Moderate Liquefaction



(c) Severe Liquefaction



(d) Severe Lateral Spreading

Figure 3.12 (S3) Representative observations of four liquefaction severity classes: (a) marginal liquefaction; (b) moderate liquefaction; (c) severe liquefaction; (d) severe lateral spreading.

Chapter 4: Fines-Content Effects on Liquefaction Hazard Assessment for Infrastructure during the 2010-2011 Canterbury, New Zealand, Earthquake Sequence

Brett W. Maurer¹, Russell A. Green², Misko Cubrinovski³, Brendon A. Bradley⁴

¹ Graduate Research Assistant, Dept. of Civil and Environmental Engineering, Virginia Tech, Blacksburg, Virginia 24061, U.S.A.

² Professor, Dept. of Civil and Environmental Engineering, Virginia Tech, Blacksburg, Virginia 24061, U.S.A.

³ Professor, Dept. of Civil and Natural Resources Engineering, University of Canterbury, Private Bag 4800, Christchurch, New Zealand

⁴ Professor, Dept. of Civil and Natural Resources Engineering, University of Canterbury, Private Bag 4800, Christchurch, New Zealand

4.1 Abstract

To assess soil liquefaction hazards for civil infrastructure, several competing liquefaction evaluation procedures (LEPs) are used to estimate the potential for liquefaction triggering, often for use in a liquefaction potential index (LPI) framework. However, due to the relatively uncertain effects of fines-content (FC) on liquefaction behavior, LPI hazard assessments may be less accurate at sites with high FC. Accordingly, this study investigates “fines-content effects” on the accuracy of LPI hazard assessment during the 2010-2011 Canterbury Earthquake Sequence (CES). These effects are resolved into: (1) criteria based on the soil-behavior-type index (I_c) for identifying liquefaction-susceptible soils; (2) FC-corrections inherent to each LEP, used to adjust liquefaction resistance for the presence of fines; and (3) the potential for non-liquefied, high-FC soils to inhibit liquefaction manifestation. This investigation is performed using 7,000 liquefaction case studies from the CES, wherein LPI hazard assessments computed with the Robertson and Wride (1998), Moss et al. (2006), and Idriss and Boulanger (2008) LEPs are compared to field observations. For the assessed dataset, LPI hazard assessments were significantly and uniformly less accurate at sites with silty and clayey soil mixtures. For these sites, the existing LPI framework has inherent limitations, such that all LEPs produce erroneous hazard assessments. In particular, the capacity of plastic soils to inhibit liquefaction manifestation by affecting pore pressure development and redistribution should be further evaluated.

4.2 Introduction

The objective of this study is to investigate fines-content effects on the accuracy of liquefaction hazard assessment for infrastructure using data from the 2010-2011 Canterbury, New Zealand, earthquake sequence (CES). This investigation considers the performance of three popular cone penetration test (CPT) based liquefaction evaluation procedures (LEPs) for predicting the severity of liquefaction manifestation within the liquefaction potential index (LPI) framework. Utilizing data from the CES, this study examines the adequacy of commonly adopted liquefaction assessment criteria and methods, with special emphasis placed on silty and clayey soil mixtures. In particular, we examine: (1) criteria based on the soil behavior type index (I_c) used to identify liquefaction-susceptible soils; (2) the correction factors applied to liquefaction-susceptible soils to adjust liquefaction resistance for fines-content; and (3) the potential for inter-bedded, non-liquefied, high fines-content soils to inhibit liquefaction manifestation. Towards this end, the deterministic CPT-based LEPs of Robertson & Wride (1998) [R&W98], Moss et al. (2006) [MEA06], and Idriss & Boulanger (2008) [I&B08] are evaluated within the LPI framework using a database of 7,000 liquefaction case studies from the CES.

The 2010-2011 CES induced widespread, severe, and recurrent liquefaction throughout the city of Christchurch, resulting in large-scale damage to civil infrastructure (e.g., Cubrinovski and Green, 2010;

Cubrinovski et al., 2011; Green et al., 2012; Cubrinovski et al., 2012). The CES initiated with the $M_w7.1$, 4 September 2010 Darfield earthquake and was punctuated by the $M_w6.2$, 22 February 2011 Christchurch earthquake, each of which induced pervasive and damaging liquefaction. Observed manifestations of liquefaction included, among others: (1) spreading- and settlement-induced damage to bridges and bridge approaches (e.g., Wotherspoon et al., 2011; Cubrinovski et al., 2014); (2) widespread loss of road functionality due to cracking and fissuring of pavements and inundation by liquefaction ejecta (e.g., Cubrinovski and Green, 2010); (3) failure of buried lifelines due to flotation or differential settlements, to include water and wastewater distribution systems (e.g., O’Rourke et al., 2014), electric power networks (e.g., Kwasinski et al., 2014), and communication lines (e.g., Tang et al., 2014); (4) damage to levees (stopbanks) caused by spreading, slumping, and settlement (e.g., Green et al., 2011); (4) impairment of port structures caused by ground deformations, to include wharfs, seawalls, and fuel lines (e.g., Chalmers et al., 2013); (5) slumping- and spread-induced damage to railway embankments (e.g., Cubrinovski and Green, 2010); and (7) settlement and tilting of residential homes, commercial properties, and high-rise structures, resulting in widespread loss of building stock (e.g., Bray et al., 2014). In addition to direct effects on infrastructure, the ~500,000 tonnes of liquefaction ejecta collected throughout Christchurch posed a threat to stormwater systems and to human health if left unmanaged (Villemure et al., 2012).

As illustrated by the severe liquefaction-induced damage during the CES, there is a critical need to accurately assess liquefaction hazards for civil infrastructure. In current engineering practice, liquefaction hazard is commonly assessed using the liquefaction potential index (LPI) (Iwasaki et al. 1978), defined by:

$$LPI = \int_0^{20 \text{ m}} F \cdot w(z) dz \quad (1)$$

In Eq. (1), $F = 1 - FS_{liq}$ for $FS_{liq} \leq 1$ and $F = 0$ for $FS_{liq} > 1$, where FS_{liq} is the factor of safety against liquefaction “triggering” computed by an LEP (e.g., Robertson and Wride, 1998; Moss et al., 2006; Idriss and Boulanger, 2008); $w(z)$ is a depth weighting function given by $w(z) = 10 - 0.5z$; and z is depth in meters below the ground surface. Thus, it is assumed that the severity of liquefaction manifestation is proportional to the cumulative thickness of liquefied layers, the proximity of these layers to the ground surface, and the amount by which FS_{liq} in each layer is less than 1.0. Given this definition, LPI can range from 0 to a maximum of 100 (i.e., where FS_{liq} is zero over the entire 20 m depth). Analyzing standard-penetration-test (SPT) data from 55 sites in Japan, Iwasaki et al. (1978) proposed that severe liquefaction should be expected for sites where $LPI > 15$ but not where $LPI < 5$. This criterion for liquefaction manifestation, defined by two threshold values of LPI, is referred to as the *Iwasaki criterion*.

In the decades since its inception, LPI has been widely adopted as a predictive proxy for liquefaction damage potential and has been used worldwide in hazard mapping, urban planning, and the engineering design of infrastructure (e.g., Sonmez, 2003; Baise et al., 2006; Holzer et al., 2006a; 2006b; Lenz & Baise, 2007; Cramer et al., 2008; Hayati & Andrus, 2008; Holzer, 2008; Chung & Rogers, 2011; Kang et al., 2014). However, in using LPI to assess liquefaction hazard in current practice, it is not always appreciated that the efficacy of LPI hazard assessment (and the *Iwasaki criterion*) is inherently linked to the LEP used within the LPI framework. Although the LEPs used in today’s practice (e.g., Robertson and Wride, 1998; Moss et al., 2006; Idriss and Boulanger, 2008) are the cumulative result of 4-5 decades of research, it has been shown that they can compute different FS_{liq} values for the same soil profile and earthquake scenario (e.g., Green et al., 2014), and thus different LPI values. In addition, today’s LEPs are vastly different from that used by Iwasaki et al. (1978) to develop the *Iwasaki criterion*. These differences have led to confusion as to which LEP is the most accurate, and whether the LPI framework and *Iwasaki criterion* are equally effective for all LEPs.

Maurer et al. (2014a) addressed these uncertainties by assessing the efficacies of the R&W98, MEA06, and I&B08 LEPs, operating within the LPI framework, for evaluating the liquefaction hazard at 1,173 sites during the Darfield and Christchurch earthquakes. Maurer et al. (2014a) concluded that: (1) the utility of the *Iwasaki criterion* varied amongst LEPs (i.e., the optimum threshold LPI values for predicting liquefaction manifestation were LEP-dependent); and (2) LPI hazard assessments were highly erroneous for some sites, irrespective of the LEP used within the LPI framework.

While there are many potential sources of LEP discrepancy (and erroneous liquefaction hazard assessment), the uncertain liquefaction behavior of silty and clayey soil mixtures may be a predominate factor. For, while the behavior of clean sands is *relatively* established (e.g., Li et al., 2007), there are many conflicting opinions about the effects of fines-content on liquefaction resistance, and definitive guidance on the matter is lacking (e.g., Green et al., 2006; Prakash and Puri, 2010). Uncertainties pertaining to high fines-content soils could affect liquefaction hazard assessment in several ways. First, antecedent to using any LEP in the LPI framework, liquefaction-susceptible soils must be identified. For CPT-based liquefaction assessment (considered herein), the current state-of-practice is to use the soil behavior type index (I_c) for this purpose, defined as (Robertson and Wride, 1998):

$$I_c = \sqrt{(3.47 - \log_{10} Q)^2 + (1.22 + \log_{10} F)^2} \quad (2)$$

where Q and F are the normalized cone tip resistance and normalized friction ratio, respectively. A value of $I_c > 2.6$ is commonly considered to imply non-liquefiable soils (e.g., Robertson and Wride,

1998). However, because the relationship between I_c and soil type is approximate, the $I_c = 2.6$ cutoff may in some cases be inappropriate (e.g., Zhang et al., 2002). Accordingly, Youd et al. (2001) recommended that soils with $I_c \geq 2.4$ be sampled and tested to evaluate their liquefaction susceptibility. While these guidelines are widely used with I_c to gauge liquefaction susceptibility, their efficacy is uncertain (e.g., Boulanger and Idriss, 2006; Li et al., 2007; Pease, 2010).

Once liquefaction-susceptible soils are identified (e.g., $I_c \leq 2.6$), the LEPs used in today's practice apply differing correction factors to adjust liquefaction resistance for fines-content. These correction factors, unique to each LEP, were developed from relatively limited data using different approaches. For example, the R&W98, MEA06, and I&B08 procedures respectively use I_c , friction ratio (R_f), and fines-content (FC) to adjust liquefaction resistance for the presence of fines. Greater discrepancies may therefore exist amongst LEP predictions in the assessment of silty sands and sandy silts, relative to evaluations of clean sands. Lastly, field, laboratory, and numerical analyses have suggested that high fines-content soils in the capping or interbedded non-liquefiable strata may inhibit surficial liquefaction manifestations (Ozutsumi et al., 2002; Brennan, 2008; Maurer et al., 2014b). Thus, inherent limitations in the LPI framework to account for such effects may lead to erroneous hazard assessments even if the selected LEP is wholly competent. In summary, due to the relatively uncertain effects of fines on liquefaction behavior, referred to herein as "fines-content effects," the accuracy of liquefaction hazard assessment for infrastructure is uncertain.

Accordingly, the objective of this study is to investigate fines-content effects on the accuracy of LPI hazard assessment using data from the 2010-2011 CES. These effects are resolved into (1) criteria based on I_c for identifying liquefaction-susceptible soils; (2) fines-content corrections inherent to each LEP; and (3) the potential for non-liquefied, high fines-content soils to inhibit liquefaction manifestations. This investigation is performed using 7,000 liquefaction case studies from the CES, wherein LPI hazard assessments computed with the R&W98, MEA06, and I&B08 LEPs are compared to field observations.

In the following, the high-quality dataset from the CES is briefly summarized. This is followed by a description of how LPI was computed using three CPT-based LEPs. An overview of receiver-operating-characteristic (ROC) curves, which will be used in the analysis of the LPI data, is then provided. Lastly, fines-content effects on the accuracy of LPI hazard assessment are analyzed and discussed in detail.

4.2 Data and Methodology

The 2010-2011 CES resulted in a liquefaction dataset of unprecedented size and quality, presenting a unique opportunity to evaluate fines-content effects on the accuracy of liquefaction hazard assessment (e.g., Cubrinovski & Green, 2010; Cubrinovski et al., 2011; Bradley & Cubrinovski, 2011; Bradley,

2012). The study presented herein uses data from the $M_w7.1$, 4 September 2010 Darfield and $M_w6.2$, 22 February 2011 Christchurch earthquakes, which induced pervasive and damaging liquefaction (e.g., Green et al., 2012, 2014). Ground motions from these events were recorded by a dense network of strong motion stations (e.g., Bradley & Cubrinovski, 2011; Bradley, 2012), and due to the extent of liquefaction, the New Zealand Earthquake Commission (EQC) funded an extensive geotechnical reconnaissance and characterization program (Murahidy et al., 2012). The combination of densely-recorded ground motions, well-documented liquefaction response, and detailed subsurface characterization comprises the high-quality dataset used in this study. To assess the accuracy of LPI hazard assessment, a large database of CPT soundings performed across Christchurch and its environs are analyzed in conjunction with liquefaction observations made following the Darfield and Christchurch earthquakes. In the following, the components of the dataset and the computation of LPI are discussed in further detail.

4.2.1 CPT Soundings

As the rebuilding of Christchurch progresses, the number of CPT soundings performed in the region and available through the Canterbury Geotechnical Database (CGD, 2012a) continues to increase with presently in excess of 16,000 soundings (e.g., van Ballegooy et al., 2014). Drawing from a high-quality subset of this data performed under the direct auspices of the EQC, this study utilizes 3,500 CPT soundings performed at sites where the severity of liquefaction manifestation was well-documented following both the Darfield and Christchurch earthquakes, resulting in 7,000 case studies. In the process of compiling the 3,500 soundings to be analyzed herein, soundings were first rejected from the study for one of several reasons, as follows.

First, CPT soundings were rejected if performed at sites where the predominant manifestation of liquefaction was lateral spreading. This distinction is made because lateral spreading is a unique manifestation of liquefaction, and because there are separate criteria for assessing its severity (e.g., Youd et al., 2002), including the ground slope and height of the nearest free-face (e.g., river bank). Consequently, while site profiles with thin liquefiable layers may have low LPI values, these sites are susceptible to lateral spreading if located on sloping ground or near rivers. Since the factors pertinent to lateral spreading cases are not considered in the formulation of LPI, such cases should not be used to assess the accuracy of LPI hazard assessment. *Second*, CPTs were rejected if the depth of “pre-drill” significantly exceeded the estimated depth of the ground water table (GWT), a condition arising at sites where buried utilities needed to be safely bypassed before testing could begin. While CPT data in the pre-drill zone may be estimated using intra-CPT extrapolation or inter-CPT interpolation, doing so below the GWT could lead to erroneous hazard assessments if the soil profile is misrepresented. *Third*,

termination depths of CPT soundings were geo-spatially analyzed using an Anselin Local Morans I analysis (Anselin, 1995) and soundings with anomalously shallow termination depths were rejected. As shown in Eq. (1), LPI requires integration over 20 m depth. However, if the local subsurface geology is well-characterized, it may be known that dense, non-liquefiable soils are typically found at a particular depth and unlikely to be underlain by looser liquefiable deposits that contribute to LPI. Such is the case in Christchurch, where liquefiable deposits overlay the Riccarton Gravel formation. The Anselin (1995) analysis was thus used to identify soundings that may have terminated before reaching the Riccarton formation. For the remaining soundings, the termination depths were reasonably assumed to define the maximum depths of liquefiable strata. For further discussion of the geospatial analysis used herein and the geology of the Canterbury plains, see Maurer et al. (2014b).

4.2.2 Liquefaction Severity

Observations of liquefaction and the severity of manifestations were made by the authors for each of the CPT sounding locations following both the Darfield and Christchurch earthquakes. This was accomplished by ground reconnaissance and using high-resolution aerial and satellite imagery (CGD, 2012b) performed in the days immediately following each of the earthquakes. CPT sites were assigned one of four damage classifications, as described in Table 1 (after Green et al. (2014)), where the classifications describe the predominant manifestation of liquefaction at the ground surface in the immediate vicinity of the sounding location. Representative observations of the manifestation severity classifications are shown in Fig. 1. Of the 7,000 case studies compiled, 49% are cases of “no manifestation,” and 51% are cases where manifestation severity was classified as either “marginal,” “moderate,” or “severe.” The relationship between manifestation severity and damage to infrastructure is discussed later in this paper.

4.2.3 Estimation of a_{max} (PGA)

To evaluate FS_{liq} using the three LEPs, the Peak Ground Accelerations (PGAs) at the ground surface were computed using the robust procedure discussed in detail by Bradley (2014) and used by Green et al. (2011; 2014) and Maurer et al. (2014a,b). The Bradley (2014) procedure combines unconditional PGA distributions estimated by the Bradley (2013b) Ground Motion Prediction Equation (GMPE), recorded PGAs from strong motion stations, and the spatial correlation of intra-event residuals to compute the conditional PGA distribution at sites of interest.

4.2.4 Estimation of ground water table (GWT) depth

Given the sensitivity of liquefaction hazard and computed LPI values to GWT depth (e.g., Chung and Rogers, 2011; Maurer et al., 2014b), accurate measurement of GWT depth is critical. For this study, GWT depths were sourced from the robust, event-specific regional ground water models of van

Ballegooy et al. (2014b). These models, which reflect seasonal and localized fluctuations across the region, were derived in part using monitoring data from a network of ~1000 piezometers and provide a best-estimate of GWT depths immediately prior to the Darfield and Christchurch earthquakes. Considering the extent and density of monitoring, the van Ballegooy et al. (2014b) GWT models in Christchurch are likely amongst the most robust ever used for regional study of liquefaction hazard assessment.

4.2.5 Liquefaction Evaluation and LPI

FS_{liq} was computed using the deterministic CPT-based LEPs of R&W98, MEA06, and I&B08. Soil unit weights were estimated for each procedure using the method of Robertson & Cabal (2010). For the MEA06 procedure, the stress-reduction coefficient, r_d , was computed using the V_s -independent equation given in Moss et al. (2006). For the I&B08 procedure, fines content, FC, is required to compute normalized tip resistances (in lieu of FC, R&W98 and MEA06 use I_c and CPT friction ratio, R_f , respectively); as such, FC values were estimated using both the generic I_c -FC correlation proposed by Robertson & Wride (1998) and a Christchurch-soil-specific I_c -FC correlation developed by Robinson et al. (2013) from samples collected near the Avon River in Christchurch. Henceforth, herein I&B08¹ and I&B08² refer to the use of the generic and Christchurch-specific I_c -FC correlations, respectively, used in conjunction with the I&B08 procedure. The two I_c -FC correlations are shown in Fig. 2; it can be seen that the Christchurch-specific correlation suggests different I_c -FC trends for $I_c < 1.7$ and $I_c \geq 1.7$, where FC is estimated to be 10 for all $I_c \leq 1.7$. FS_{liq} was computed at 1- or 2-cm depth intervals (i.e., the measuring rate of CPT soundings); LPI was then computed with each of the four LEPs per Eq. 1.

4.3 Overview of Receiver-Operating-Characteristic (ROC) Analyses

To investigate fines-content effects on the accuracy of liquefaction hazard assessment in Christchurch, receiver-operating characteristic (ROC) analyses, or “ROC curves,” are used to assess the efficacy of each LEP for predicting the severity of liquefaction manifestation within the LPI framework. ROC curves have been widely adopted to analyze the performance of classifier systems, including extensive use in medical diagnostics (e.g., Zou, 2007), but by comparison, the use of ROC curves in geotechnical engineering is relatively limited (Chen et al., 2007; Oommen et al., 2010, Mens et al., 2012; Maurer et al., 2014a). In any ROC curve application, the distributions of “positives” (e.g., liquefaction is observed) and “negatives” (e.g., no liquefaction is observed) overlap when the frequency of the distributions are expressed as a function of index test results (e.g., LPI values). In such cases, threshold values for the index test results are selected considering the relative probabilities of true positives (i.e., liquefaction is observed, as predicted) and false positives (i.e., liquefaction is predicted, but is not

observed). Setting the threshold too low will result in numerous false positives, which is not without consequences, while setting the threshold unduly high will result in many false negatives (i.e., liquefaction is observed when it is predicted not to occur), which comes with different consequences. ROC analyses are particularly valuable for evaluating the relative efficacy of competing diagnostic tests, independent of the thresholds used, and for selecting an optimal threshold for a given diagnostic test.

In this study, the competing diagnostic tests are the LEPs, and the index test results are the computed LPI values. Accordingly, in analyzing the case histories, true and false positives are scenarios where surficial liquefaction manifestations are predicted, but were and were not observed, respectively. Fig. 3 illustrates the relationship among the positive and negative distributions, the selected threshold value, and the corresponding ROC curve, where the ROC curve plots the rates of true and false positives for varying threshold values. Fig. 4 illustrates how a ROC curve is used to assess the efficiency of LPI hazard assessment, where “True Positive Rate” and “False Positive Rate” are synonymous with “True Positive Probability” and “False Positive Probability”, respectively. In ROC curve space, random guessing is indicated by a 1:1 line through the origin (i.e., equivalent correct and incorrect predictions), while a perfect model plots as a point at (0,1), indicating the existence of a threshold value which perfectly segregates the dataset (e.g., all sites with manifestation have LPI above the selected threshold; all sites without manifestation have LPI below the same selected threshold). While no single parameter can fully characterize model performance, the area under a ROC curve (AUC) is commonly used for this purpose, where AUC is equivalent to the probability that sites with manifestation have higher computed LPI than sites without manifestation (e.g., Fawcett, 2005). As such, increasing AUC indicates better model performance. The *optimum operating point* (OOP) is defined herein as the threshold LPI value which minimizes the rate of misprediction (i.e., $FPR + (1-TPR)$, where TPR and FPR are the rates of true and false positives, respectively). As such, contours of the quantity $[FPR + (1-TPR)]$ represent points of equivalent performance in ROC space. Thus, in plotting the LPI data as ROC curves for each LEP, we may investigate fines-content effects on (1) the efficacy of each model, as indicated by AUC; and (2) the optimum threshold LPI value (i.e., the OOP).

4.4 Results and Discussion

Utilizing 7,000 combined case studies from the Darfield and Christchurch earthquakes, LPI values were computed using the LEPs of R&W98, MEA06, I&B08¹, and I&B08². To illustrate how ROC curves will be used to study the LPI data, a full example is first provided, and thereafter, only ROC summary statistics (i.e., AUC; OOP) will be presented. In Fig. 5, ROC curves are plotted to evaluate the

performance of each LPI model in segregating sites with and without liquefaction manifestations, to include manifestations of all severities and cases from both earthquakes (i.e., all 7,000 cases). For this analysis, an I_c “cutoff” value of 2.6 is used within the LPI framework, as is commonly done in practice, such that soils with $I_c \geq 2.6$ are assumed to be unsusceptible to liquefaction. It can be seen in Fig. 5 that while the four LPI models perform similarly, MEA06 and I&B08¹ are respectively the least and most efficacious, with AUC ranging from 0.71 (MEA06) to 0.78 (I&B08¹). To place this performance in context, AUCs of 0.5 and 1.0 respectively indicate random guessing and a perfect model. Also, as highlighted in Fig. 5, the optimum threshold LPI values for the R&W98, MEA06, I&B08¹, and I&B08² models are 4.0, 5.5, 6.0, and 4.5, respectively. Thus, while the optimum thresholds are LEP-dependent, the lower *Iwasaki criterion* (i.e., LPI = 5) is generally an appropriate threshold for predicting liquefaction manifestation in Christchurch. Operating at this threshold, the models have overall accuracy (OA) ranging from 0.66 (MEA06) to 0.72 (I&B08¹), where the OA indicates the percentage of the cases correctly classified.

To investigate how the accuracy of LPI hazard assessment is influenced by the I_c -cutoff used within the LPI framework, the previous analysis is repeated using I_c -cutoff values ranging from 1.6 to 3.0, such that soils with I_c greater than the cutoff are assumed not to be susceptible to liquefaction; the results of these 32 ROC curves, summarized in terms of AUC and the corresponding OOP, are shown in Fig. 6a. From this summary, it can be seen that irrespective of the I_c -cutoff used, MEA06 and I&B08¹ are generally the least and most efficacious models, respectively, as indicated by AUC. Also, as could be expected, the OOPs increase as the I_c -cutoff is raised. This is due to the fact that as the I_c -cutoff increases, some soils previously assumed to be too plastic to liquefy are treated as liquefaction-susceptible, often resulting in higher computed LPI values for a given soil profile. With the distributions of computed LPI values shifting towards higher values, the OOPs segregating cases with and without liquefaction manifestations likewise increase, as reflected in Fig. 6a. Also of interest is the influence of the I_c -FC correlation used within the I&B08 LEP. As shown in Fig. 2, the Christchurch-specific correlation infers a higher FC than does the generic correlation for all values of I_c , resulting in higher computed FS_{liq} values, and thus, lower computed LPI. As a result, the OOPs using I&B08² (i.e., using the Christchurch-specific correlation) are less than those using I&B08¹ (i.e., using the generic correlation) for all I_c -cutoff values. In addition to influencing the OOPs, the I_c -FC correlation affects model efficacy (i.e., efficiency segregating sites with and without liquefaction manifestations), as shown in Fig. 6a. For example, using an I_c -cutoff value of 2.6, I&B08¹ correctly classifies 3% more cases than I&B08². The slightly weaker performance of I&B08² might be due to the fact that the Robinson et al. (2013) Christchurch-specific I_c -FC correlation was developed using data from along the Avon River only, while the database assessed herein extends throughout Christchurch and into surrounding areas, although further research would be needed to confirm this.

Returning to the performance of all LEPs, the relationship between AUC and the I_c -cutoff can be described by three loosely-defined zones of behavior, designated in Fig. 6a as Zones A, B, and C. As the I_c -cutoff drops below 2.0 in Zone A, many liquefaction-susceptible soils are treated as non-liquefiable, which in general reduces computed LPI values at a given site; as the I_c -cutoff continues to decrease, a point is reached where LPI is zero for all sites. As such, the distributions of LPI values for cases with and without liquefaction manifestations become increasingly similar, thereby reducing model performance. Conversely, as the I_c -cutoff value increases above 2.6 in Zone C, soils that are likely too plastic to liquefy are treated as being susceptible to liquefaction. The resistance to liquefaction of such a soil is then computed by each LEP to predict whether it will liquefy in a particular earthquake. Inherent to this process, the factors used to adjust liquefaction resistance for the presence of fines are critical. However, these fines-correction factors are not intended for use with soils that classify as either clayey silt, silty clay, or clay, and limited case-history data exists for such cases (e.g., Robertson and Wride, 1998). Thus, the use of LEPs on high-FC soils could result in erroneous estimates of liquefaction resistance and loss of model efficiency, as suggested by the more marked decline in AUC through Zone C. Lastly, it can be seen that AUC is relatively insensitive to the I_c -cutoff value in Zone B, with the exception of MEA06, for which AUC declines steadily. In addition, the LPI models reach optimum performance at I_c -cutoff values between 2.0 and 2.2, in contrast to the values of 2.4 to 2.6 typically used in practice. However, it will be shown that Zone B behavior, and thus the optimum I_c -cutoff, is both closely connected to other “fines-effects” discussed herein, and is strongly influenced by a relatively small fraction of the database.

First, however, the analysis summarized in Fig. 6a is repeated with instances of marginal manifestation removed from the dataset. While it is important that all manifestations of liquefaction (or the lack thereof) are accurately predicted, the consequences of misprediction increase with increasing liquefaction severity. As shown in Fig. 1, marginal manifestations are characterized by a trace amount of water or ejecta and typically do not result in damage to the built environment. Failure to predict such manifestations may therefore be relatively inconsequential. Conversely, moderate to severe manifestations of liquefaction are more likely to coincide with damage to infrastructure. Failure to accurately assess such hazards could thus result in either: (1) superfluous spending on engineering design and construction (e.g., ground-improvement), in the case of a false-positive prediction; or (2) severe damage to infrastructure, in the case of a false-negative prediction. Accordingly, considering only moderate to severe manifestations of liquefaction may provide a more “true” measure of LPI performance. The results of this re-analysis, summarized in terms of AUC and the corresponding OOP, are shown in Fig. 6b. The trends and outcomes exhibited are the same as those discussed for Fig. 6a, with two notable exceptions. *First*, the OOPs have in most cases increased slightly, mirroring the

upward shift in the distribution of computed LPI values for cases of manifestation. *Second*, the LPI models are more efficient in segregating cases with and without manifestations of liquefaction, as indicated by the increase in AUC. Nonetheless, 20% of cases are still incorrectly classified (i.e., OA = 0.80) using the best performing model, indicating erroneous LPI hazard assessments for a significant portion of sites.

To investigate whether fines-effects may be contributing to these erroneous assessments, the database is next parsed into sites having predominantly clean sand or silty sand, and sites having predominantly silty and clayey soil mixtures. This characterization is made using the average I_c value for the uppermost 10 m of each soil-profile, termed I_{c10} . Using an I_{c10} value of 2.05, the database is parsed into 5033 cases for which $I_{c10} < 2.05$, of which 49% are cases of “no manifestation,” and 1967 cases for which $I_{c10} \geq 2.05$, of which 50% are cases of “no manifestation.” As shown in Fig. 7, resolving the database in this manner also loosely corresponds to a parsing by geographic location. It can be seen that the majority of sites with $I_{c10} < 2.05$ are located in the eastern suburbs of Christchurch, extending from the coast to the central business district (CBD), while the majority of sites with $I_{c10} \geq 2.05$ are located in the southern and western portions of the study area; the locations of $I_{c10} \geq 2.05$ sites generally reflect the extents of mid-Holocene coastal transgression, as well as the unique sediment lithology found near the Port Hills (Brown et al., 1995).

Following the same methodology used in Fig. 6a, a summary of ROC analyses is presented in Fig. 8, considering all severities of liquefaction manifestations, where the database has been parsed into sites with $I_{c10} < 2.05$ (Fig. 8a) and sites with $I_{c10} \geq 2.05$ (Fig. 8b). Several observations are made with respect to Fig. 8, as follows. *First*, at sites with $I_{c10} < 2.05$, the accuracy of LPI hazard assessment is generally unaffected by the I_c -cutoff within Zone B, as could be expected; with the exception of MEA06, model performance is consistent for I_c -cutoff values ranging from 2.2 to 2.6. Conversely, at sites with $I_{c10} \geq 2.05$, model performance is relatively sensitive to the I_c -cutoff. With the exception of MEA06, the maximum AUC is attained using an I_c -cutoff value of 2.4, a finding consistent with the recommendation in Youd et al. (2001).

Second, it can be seen that the accuracy of LPI hazard assessment is significantly better at sites with $I_{c10} < 2.05$ than at sites with $I_{c10} \geq 2.05$. For example, expressed in terms of OA, I&B08¹ incorrectly classifies 23% of cases with $I_{c10} < 2.05$ (using an I_c -cutoff value of 2.6); for cases with $I_{c10} \geq 2.05$, the percent of incorrectly classified cases increases to 36%. In addition, it can be seen that the models perform more similarly (i.e., uniformly poor) at sites with $I_{c10} \geq 2.05$.

Third, it can be seen that the OOPs are significantly higher at sites with higher I_{c10} . For example, using an I_c -cutoff value of 2.6, the average optimum threshold LPI value, considering all LEPs, is 4.9 for cases with $I_{c10} < 2.05$; on the other hand, this average increases to 13.0 for cases with $I_{c10} \geq 2.05$. This discrepancy is consistent with assessments of LPI performance in previous earthquakes. For example, Toprak and Holzer (2003) evaluated LPI at historic liquefaction sites in California (USA) and found LPI = 5 to be an appropriate threshold. In contrast, Lee et al. (2003) evaluated LPI during the 1999 Chi-Chi (Taiwan) earthquake and found the *Iwasaki criterion* to be a poor predictor of liquefaction manifestation. Finding that 85% of sites without manifestation had LPI > 5, Lee et al. (2003) concluded that LPI = 13 was the OOP. Juang et al. (2008) first noted that the sites studied by Toprak and Holzer (2003) were predominantly deposits of clean sands, while those examined by Lee et al. (2003) were mostly deposits of silty sands and sandy silts, postulating that the discrepancy in findings might be tied to fines-content. Papathanassiou (2008) similarly evaluated LPI at sites with relatively high fines-content during the 1999 Chi-Chi (Taiwan), 1999 Kocaeli (Turkey), and 2003 Lefkada (Greece) earthquakes, and concluded that LPI = 19 was the OOP for the assessed dataset.

For completeness, the prior analysis is repeated with cases of marginal liquefaction manifestation omitted from the dataset, the motivation for which is as previously discussed; the results are summarized in Fig. 9 for sites with $I_{c10} < 2.05$ (Fig. 9a) and sites with $I_{c10} \geq 2.05$ (Fig. 9b). As the results are very similar to those presented in Figs. 6 and 8, it is simply noted that the accuracy of LPI hazard assessment is notably better at sites with $I_{c10} < 2.05$.

The preceding analyses indicate that the accuracy of LPI hazard assessment diminishes at sites comprised predominantly of silty and clayey soil mixtures, and moreover, that the OOP at such sites is significantly higher relative to sites comprised predominantly of clean sands. For the dataset assessed herein, this could be caused by: (1) an inadequacy in the fines-correction factors inherent to each LEP, such that FS_{liq} is erroneously estimated for soils susceptible to liquefaction with high I_c (e.g., $2.05 < I_c < 2.6$); and/or, (2) the presence of high fines-content soils in the capping or interbedded non-liquefiable strata could affect the generation and dissipation of pore pressure, thereby suppressing surficial liquefaction manifestations at a site. Each of these possible causes is investigated, as follows.

To assess the possible inadequacy of the fines-correction factors inherent to each LEP, the database of 7,000 cases is parsed using the average I_c values in the soil strata predicted to have liquefied (i.e., $FS_{liq} < 1$) and to have not liquefied (i.e., $FS_{liq} > 1$) by the respective LEPs. For this assessment, only cases for which the average I_c is less than 2.05 in strata predicted not to have liquefied are considered; this dataset is then divided into cases for which the average I_c in strata predicted to have liquefied is greater than and less than 2.05. Thus, if the poor performance of LPI in high- I_c soils is tied to the fines-correction factors inherent to each LEP, LPI should perform worse at sites where the strata predicted to

have liquefied have high FC. To test this hypothesis, ROC analyses were performed for the specified dataset and are summarized in Table 2. From this summary, it can be seen that LPI performs equally well at sites where the strata predicted to have liquefied are high in fines; it can likewise be seen that the OOPs are relatively unaffected by the average I_c in strata predicted to have liquefied. These results suggest that fines-correction factors (i.e., adjustments to liquefaction resistance for the presence of fines) are unlikely the cause of poor LPI performance at sites where $I_{c10} \geq 2.05$.

Next, the possibility for non-liquefiable, high fines-content soils to inhibit liquefaction manifestation is evaluated. Since high- I_c soils are generally more resistant to piping and hydraulic fracture, these soils might affect water flow and pore pressure development/dissipation among liquefied strata within the profile, and between liquefied strata and the ground surface. This would diminish the cumulative effects assumed in the LPI framework and limit the severity of surficial liquefaction manifestation. For this assessment, only cases for which the average I_c is less than 2.05 in strata predicted to have liquefied are considered; this dataset is then divided into cases for which the average I_c in strata predicted not to have liquefied is greater than and less than 2.05. Thus, if the poor performance of LPI in high- I_c soils is due to the above effects, LPI should perform worse at sites where the strata predicted not to have liquefied have high FC. To test this hypothesis, ROC analyses were performed for the specified dataset and are summarized in Table 3. From this summary, it can be seen that LPI performs notably worse at sites where the strata predicted not to have liquefied have high- I_c , as indicated by lower AUC; it can likewise be seen that the OOPs increase significantly for such cases. These results indicate that the poor performance of LPI at sites with $I_{c10} \geq 2.05$ is more likely due to the suppression of surficial liquefaction manifestation by silty and clayey soil mixtures, resulting in over-predictions of manifestation severity at the ground surface.

In summary, the preceding analyses suggest that LPI has inherent limitations in its framework, such that factors influencing surficial manifestation are not adequately accounted for. While significant research has been focused on liquefaction triggering and the development of LEPs, the mechanics of liquefaction manifestation have received less attention. This study highlights that triggering and manifestation are two distinct phenomena contributing to liquefaction hazard, and that an improved framework providing clear separation and accounting of the two phenomena is needed.

4.5 Summary and Conclusions

Utilizing 7,000 high-quality case histories from the CES, this study investigated fines-content effects on the accuracy of LPI hazard assessment. The findings are summarized as follows:

- In general, the efficacy of LPI hazard assessment (i.e., ability to segregate sites with and without liquefaction manifestation) was relatively insensitive to the I_c -cutoff value used within the LPI

framework for I_c -cutoffs ranging from 2.2 to 2.6. However, for select site profiles having high FC, the performance of LPI was more sensitive to the chosen I_c -cutoff, and optimum threshold LPI values were affected significantly. As such, erroneous LPI hazard assessments could result from the uncertain liquefaction-susceptibility of soils with $2.2 < I_c < 2.6$.

- For the selected dataset, the I&B08 and MEA06 LPI models were generally the most and least efficacious, respectively. However, LPI hazard assessments were significantly and uniformly less accurate at sites with silty and clayey soil mixtures, irrespective of the I_c -cutoff value used; moreover, the optimum threshold LPI values were significantly higher for such cases, a finding consistent with assessments of LPI at similar site-profiles in previous earthquakes.
- Possible causes of LPI's poor performance at site-profiles having high FC were investigated. The effect of capping and/or interbedded plastic soils suppressing liquefaction manifestation, rather than an inadequacy in the fines-correction factors inherent to each LEP, was identified as the more likely cause. This hypothesis is consistent with laboratory and numerical studies showing that such soils can affect water flow and pore pressure development/dissipation among liquefied strata, and between liquefied strata and the ground surface.
- Assessments and/or calibrations of LPI are a function not only of the selected LEP, but also of the chosen dataset, including the geometry and soil characteristics of site-profiles, as well as the amplitude and duration of ground shaking. As such, the applicability of findings derived herein to other datasets is unknown.

In conclusion, the findings derived herein suggest that liquefaction hazard assessments for infrastructure are less accurate at sites having soils with high FC. For these sites, the existing LPI framework has inherent limitations, such that all LEPs produce erroneous hazard assessments for the case studies considered. As such, further research is needed to understand and quantify “fines-effects” on liquefaction hazard, especially with respect to the mechanics of liquefaction manifestation. In particular, the capacity of plastic soils to inhibit liquefaction manifestation by affecting pore pressure development and redistribution should be further evaluated.

4.6 Acknowledgements

This study is based on work supported by the U.S. National Science Foundation (NSF) grants CMMI-1030564 and CMMI-1306261, and US Army Engineer Research and Development Center (ERDC) grant W912HZ-13-C-0035. The third and fourth authors would like to acknowledge the continuous financial support provided by the Earthquake Commission (EQC) and Natural Hazards Research Platform (NHRP), New Zealand, of the research and investigations related to the 2010-2011 Canterbury earthquakes. The authors also acknowledge the New Zealand GeoNet project and its sponsors EQC,

GNS Science and LINZ for providing the earthquake occurrence data and the Canterbury Geotechnical Database and its sponsor EQC for providing the CPT soundings, lateral spread observations, and aerial imagery used in this study. However, any opinions, findings, and conclusions or recommendations expressed in this paper are those of the authors and do not necessarily reflect the views of NSF, ERDC, EQC, NHRP, or LINZ.

Notice

Some of the data used in this study was extracted from the Canterbury Geotechnical Database (<https://canterburygeotechnicaldatabase.projectorbit.com>), which was prepared and/or compiled for the Earthquake Commission (EQC) to assist in assessing insurance claims made under the Earthquake Commission Act 1993 and/or for the Canterbury Geotechnical Database on behalf of the Canterbury Earthquake Recovery Authority (CERA). The source maps and data were not intended for any other purpose. EQC, CERA, and their data suppliers and their engineers, Tonkin & Taylor, have no liability for any use of these maps and data or for the consequences of any person relying on them in any way.

References

- Anselin, L. (1995). Local Indicators of Spatial Association—LISA. *Geographical Analysis* 27(2): 93–115.
- Baise, L.G., Higgins, R.B., & Brankman, C.M. (2006). Liquefaction hazard mapping-statistical and spatial characterization of susceptible units. *Journal of Geotechnical and Geoenvironmental Engineering* 132(6): 705-715.
- Boulangier, R.W. and Idriss, I.M. (2006). Liquefaction susceptibility criteria for silts and clays. *Journal of Geotechnical and Geoenvironmental Engineering*, 132(11): 1413-1426.
- Brennan, A.J. (2008). Observations on sand boils from simple model tests. Geotechnical Special Publication 181: Geotechnical Earthquake Engineering and Soil Dynamics IV. Zeng, D., Manzari, M, Hiltunen, D. (eds). p 1-10.
- Bradley, B. A. (2012). Strong ground motion characteristics observed in the 4 September 2010 Darfield, New Zealand earthquake. *Soil Dynamics and Earthquake Engineering* 42: 32-46.
- Bradley, B.A. (2013). A New Zealand-specific pseudo-spectral acceleration ground-motion prediction equation for active shallow crustal earthquakes based on foreign models. *Bulletin of the Seismological Society of America* 103(3): 1801-1822.
- Bradley, B.A. (2014). Site-specific and spatially-distributed ground-motion intensity estimation in the 2010-2011 Canterbury earthquakes. *Soil Dynamics and Earthquake Engineering*, 61-61: 83-91.
- Bradley, B.A. & Cubrinovski, M., (2011). Near-source Strong Ground Motions Observed in the 22 February 2011 Christchurch Earthquake." *Seismological Research Letters* 82: 853-865.

- Bray, J., Cubrinovski, M., Zupan, J., and Taylor, M. (2014). Liquefaction effects on buildings in the central business district of Christchurch. *Earthquake Spectra*, 30(1): 85-109.
- Brown, L.J., Beetham, R.D., Paterson, B.R., and Weeber, J.H. (1995). Geology of Christchurch, New Zealand: Environmental and Engineering Geoscience, 1: 427–488.
- CDG - Canterbury Geotechnical Database (2012a). Geotechnical Investigation Data, Map Layer CGD0010, See: <https://canterburygeotechnicaldatabase.projectorbit.com>. Accessed 1/12/12.
- CDG - Canterbury Geotechnical Database (2012b). Aerial Photography, Map Layer CGD0010, See: <https://canterburygeotechnicaldatabase.projectorbit.com>. Accessed 1/12/12.
- Chalmers, G., McLennan, N., and Barsanti, L. (2013). Lyttelton port of Christchurch seismic resilience from an owners perspective. *Ports 2013: Success through Diversification*, p. 1405-1414. Ostbo, B. and Oates, D. (eds.).
- Chen, C.C., Tseng, C.Y., and Dong, J.J. (2007). New entropy-based method for variables selection and its application to the debris-flow hazard assessment. *Engineering Geology*, 94: 19-26.
- Chung, J. & Rogers, J., (2011). Simplified method for spatial evaluation of liquefaction potential in the St. Louis Area. *Journal of Geotechnical and Geoenvironmental Engineering* 137(5): 505-515.
- Cramer, C.H., Rix, G.J., & Tucker, K. (2008). Probabilistic liquefaction hazard maps for Memphis, Tennessee. *Seismological Research Letters* 79(3): 416-423.
- Cubrinovski, M. & Green, R.A. (eds.) (2010). Geotechnical Reconnaissance of the 2010 Darfield (Canterbury) Earthquake, (contributing authors in alphabetical order: J. Allen, S. Ashford, E. Bowman, B. Bradley, B. Cox, M. Cubrinovski, R. Green, T. Hutchinson, E. Kavazanjian, R. Orense, M. Pender, M. Quigley, & L. Wotherspoon), *Bulletin of the New Zealand Society for Earthquake Engineering* 43(4): 243-320.
- Cubrinovski, M., Bradley, B., Wotherspoon, L., Green, R., Bray, J., Woods, C., Pender, M., Allen, J., Bradshaw, A., Rix, G., Taylor, M., Robinson, K., Henderson, D., Giorgini, S., Ma, K., Winkley, A., Zupan, J., O'Rourke, T., DePascale, G., & Wells, D. (2011). Geotechnical aspects of the 22 February 2011 Christchurch earthquake. *Bulletin of the New Zealand Society for Earthquake Engineering*, 43(4): 205-226.
- Cubrinovski, M., Robinson, K., Taylor, M., Hughes, M., and Orense, R. (2012). Lateral spreading and its impacts in urban areas in the 2010-2011 Christchurch earthquakes. *New Zealand Journal of Geology and Geophysics*, 55(3): 255-269.
- Cubrinovski, M., Winkley, A., Haskell, J., Palermo, A., Wotherspoon, L. Robinson, K., Bradley, B., Brabharan, P., Hughes, M. (2014). Spreading-induced damage to short-span bridges in Christchurch, New Zealand. *Earthquake Spectra*, 30(1): 57-83.
- Fawcett, T. (2005). An introduction to ROC analysis. *Pattern Recognition Letters* 27: 861-874.

- Green, R.A., Olsen, S., and Polito, C. (2006). A comparative study of the influence of fines on the liquefaction susceptibility of sands: field versus laboratory. *Proceedings of the 8th U.S. National Conference on Earthquake Engineering*, 14: 8229-8238.
- Green, R.A., Allen, A., Wotherspoon, L., Cubrinovski, M., Bradley, B., Bradshaw, A., Cox, B., & Algie, T. (2011). Performance of levees (stopbanks) during the 4 September M_w7.1 Darfield and 22 February 2011 M_w6.2 Christchurch, New Zealand, earthquakes. *Seismological Research Letters* 82(6): 939-949.
- Green, R.A., Cubrinovski, M., Wotherspoon, L., Allen, J., Bradley, B., Bradshaw, A., Bray, J., DePascale, G., Orense, R., O'Rourke, T., Pender, M., Rix, G., Wells, D., Wood, C., Henderson, D., Hogan, L., Kailey, P., Robinson, K., Taylor, M., and Winkley, A. (2012). "Geotechnical Aspects of the M_w6.2 2011 Christchurch, New Zealand Earthquake", *State of the Art and Practice in Geotechnical Engineering* (R. Hryciw, A. Athanasopoulos-Zekkos, and N. Yesiller, eds.), ASCE Geotechnical Special Publication (GSP) 225: 1700-1709.
- Green, R.A., Cubrinovski, M., Cox, B., Wood, C., Wotherspoon, L., Bradley, B., & Maurer, B. (2014). Select Liquefaction Case Histories from the 2010-2011 Canterbury Earthquake Sequence. *Earthquake Spectra*, 30(1): 131-153.
- Hayati, H. & Andrus, R.D. (2008). Liquefaction potential map of Charleston, South Carolina based on the 1986 earthquake. *Journal of Geotechnical and Geoenvironmental Engineering* 134(6): 815-828.
- Holzer, T.L., Bennett, M.J., Noce, T.E., Padovani, A.C., Tinsley III, J.C. (2006a). "Liquefaction hazard mapping with LPI in the greater Oakland, California, area." *Earthquake Spectra*, 22(3): 693-708.
- Holzer, T.L., Blair, J.L., Noce, T.E., Bennett, M.J. (2006b). "Predicted liquefaction of east bay fills during a repeat of the 1906 San Francisco earthquake." *Earthquake Spectra*, 22(S2), S261-277.
- Holzer, T.L., (2008). Probabilistic liquefaction hazard mapping, in Zeng, D., Manzari, M.T., & Hiltunen, D.R., *Geotechnical Earthquake Engineering and Soil Dynamics IV: Sacramento, CA*, ASCE Geotechnical Special Publication 181.
- Idriss, I.M. & Boulanger, R.W. (2008). Soil liquefaction during earthquakes. Monograph MNO-12, Earthquake Engineering Research Institute, Oakland, CA, 261 pp.
- Iwasaki, T., Tatsuoka, F., Tokida, K., & Yasuda, S. (1978). "A practical method for assessing soil liquefaction potential based on case studies at various sites in Japan." *Proceedings of the 2nd International Conference on Microzonation*, Nov 26-Dec 1, San Francisco, CA, USA.
- Juang, C.H., Liu, C.N., Chen, C.H., Hwang, J.H., Lu, C.C., 2008. Calibration of liquefaction potential index: a re-visit focusing on a new CPTU model. *Engineering Geology* 102: 19–30.
- Kang, G.C., Chung, J.W., & Rogers, R.J. (2014). Re-calibrating the thresholds for the classification of liquefaction potential index based on the 2004 Niigata-ken Chuetsu earthquake. *Engineering Geology* 169: 30-40.

- Krzanowski, W.J. and Hand, D.J. (2009). *ROC Curves for Continuous Data*. CRC Press, London, 232 p.
- Kwasinski, A., Eidinger, J., Tang, A., and Tudo-Bornarel, C. (2014) Performance of electric power systems in the 2010-2011 Christchurch, New Zealand, earthquake sequence. *Earthquake Spectra*, 30(1): 205-230.
- Lee, D.H., Ku, C.S., and Yuan, H. (2003). "A study of liquefaction risk potential at Yuanlin, Taiwan." *Engineering Geology*, 71: 97-117.
- Lenz, A. & Baise, L.G. (2007). Spatial variability of liquefaction potential in regional mapping using CPT and SPT data. *Soil Dynamics and Earthquake Engineering* 27: 690-702.
- Li, D.K., Juang, C.H., Andrus, R.D., and Camp, W.M. (2007). Index properties-based criteria for liquefaction susceptibility of clayey soils: a critical assessment. *Journal of Geotechnical and Geoenvironmental Engineering*, 133: 110-115.
- Maurer, B.W., Green, R.A., Cubrinovski, M., & Bradley, B.A. (2014a). "Assessment of CPT-based methods for liquefaction evaluation in a liquefaction potential index framework." *Geotechnique, In Review*.
- Maurer, B.W., Green, R.A., Cubrinovski, M., & Bradley, B.A. (2014b). "Evaluation of the liquefaction potential index for assessing liquefaction hazard." *Journal of Geotechnical and Geoenvironmental Engineering, ASCE, In Press*.
- Mens, A.M.J., Korff, M., and van Tol, A.F. (2012). "Validating and improving models for vibratory installation of steel sheet piles with field observations." *Geotechnical and Geological Engineering*, 30(5): 1085-1095.
- Metz, C.E. (2006). Receiver Operating Characteristic Analysis: A Tool for the Quantitative Evaluation of Observer Performance and Imaging Systems. *Journal of the American College of Radiology* 3(6): 413-422.
- Moss, R.E.S, Seed, R.B., Kayen, R.E., Stewart, J.P., Der Kiureghian, A., & Cetin, K.O. (2006). CPT-based probabilistic and deterministic assessment of in situ seismic soil liquefaction potential. *Journal of Geotechnical and Geoenvironmental Engineering* 132(8): 1032-1051.
- Murahidy, K.M., Soutar, C.M., Phillips, R.A., & Fairclough, A. (2012). Post earthquake recovery - Development of a geotechnical database for Christchurch central city. *15th World Conference on Earthquake Engineering*, Lisbon, Portugal. p. 10.
- Oommen T., Baise, L.G., and Vogel, R. (2010). Validation and application of empirical liquefaction models. *Journal of Geotechnical and Geoenvironmental Engineering, ASCE*, 136: 1618-1633.
- O'Rourke, T., Jeon, S.S., Toprak, S., Cubrinovski, M., Huges, M., van Ballegooy, S., and Bouziou, D. (2014). Earthquake response of underground pipeline networks in Christchurch, NZ. *Earthquake Spectra*, 30(1): 183-204.

- Ozutsumi, O., Sawada, S., Iai, S., Takeshima, Y., Sugiyama, W., and Shimazu, T. (2002). "Effective stress analyses of liquefaction-induced deformation in river dikes." *Soil. Dyn. Earthquake Eng.*, 22(9–12), 1075–1082.
- Papathanassiou, G. (2008). LPI-Based Approach for Calibrating the Severity of Liquefaction-Induced Failures and for Assessing the Probability of Liquefaction Surface Evidence. *Engineering Geology*, 96: 94-104.
- Pease, J.W. (2010). Misclassification in CPT liquefaction evaluation. *2nd International Symposium on Cone Penetration Testing*, Huntington Beach, CA, USA, May 2010, Paper # 3-23.
- Prakash, S. and Puri, V.K. (2010). Recent advances in liquefaction of fine grained soils. *Fifth International Conference on Recent Advances in Geotechnical Earthquake Engineering and Soil Dynamics*, Paper No. 4.17a, 24-29 May 2010, San Diego, California.
- Robertson, P.K. & Cabal, K.L. (2010). Estimating soil unit weight from CPT. *2nd International Symposium on Cone Penetration Testing*, Huntington Beach, CA, USA, May 2010, Paper # 2-40.
- Robertson, P.K. & Wride, C.E. (1998). Evaluating cyclic liquefaction potential using cone penetration test. *Canadian Geotechnical Journal* 35(3): 442-459.
- Robinson K, Cubrinovski M, & Bradley BA. Sensitivity of predicted liquefaction-induced lateral displacements from the 2010 Darfield and 2011 Christchurch Earthquakes. *Proc. New Zealand Soc. for Earthquake Eng. Annual Conf.* 2013, Wellington, New Zealand; 8p.
- Sonmez, H. (2003). Modification of the liquefaction potential index and liquefaction susceptibility mapping for a liquefaction-prone area (Inegol, Turkey). *Environmental Geology* 44(7): 862-871.
- Tang, A., Kwasinski, A., Eidinger J., Foster, C., and Anderson, P. (2014). Telecommunication systems' performance: Christchurch earthquakes. *Earthquake Spectra*, 30(1): 231-252.
- Toprak, S. & Holzer, T. (2003). Liquefaction potential index: field assessment." *Journal of Geotechnical and Geoenvironmental Engineering* 129(4): 315-322.
- van Ballegooy, S., Malan, P., Lacrosse, V., Jacka, M.E., Cubrinovski, M., Bray, J.D., O'Rourke, T.D., Crawford, S.A., and Cowan, H. (2014a). Assessment of liquefaction-induced land damage for residential Christchurch. *Earthquake Spectra*, 30(1): 31-55.
- van Ballegooy, S., Cox, S.C., Thurlow, C., Rutter, H.K., Reynolds T., Harrington, G., Fraser, J., and Smith, T. (2014b). Median water table elevation in Christchurch and surrounding area after the 4 September 2010 Darfield earthquake: Version 2. GNS Science Report 2014/18.
- Villemure, M., Wilson, T.M., Bristow, D., Gallagher, M., Giovinazzi, S., and Brown, C. (2012). Liquefaction ejecta clean-up in Christchurch during the 2010-2011 earthquake sequence. *New Zealand Society for Earthquake Engineering Annual Technical Conference*, Paper 131, April 13-15, Christchurch, New Zealand.

- Wotherspoon, L., Bradshaw, A., Green, R.A., Wood, C., Palermo, A., Cubrinovski, M., and Bradley, B. (2011). Performance of bridges during the 2010 Darfield and 2011 Christchurch earthquakes. *Seismological Research Letters* 82(6): 950-964.
- Youd, T.L., Idriss, I.M., Andrus, R.D., Arango, I., Castro, G., Christian, J.T., Dobry, R., Finn, W.D.L., Harder, L.F., Hynes, M.E., Ishihara, K., Koester, J.P., Liao, S.S.C., Marcuson, W.F., Martin, G.R., Mitchell, J.K., Moriwaki, Y., Power, M.S., Robertson, P.K., Seed, R.B., and Stokoe, K.H. (2001). "Liquefaction Resistance of Soils: Summary Report from the 1996 NCEER and 1998 NCEER/NSF Workshops on Evaluation of Liquefaction Resistance of Soils." *Journal of Geotechnical and Geoenvironmental Engineering*, 127(4): 297-313.
- Youd, T.L., Hansen, C.M., & Bartlett, S.F. (2002). Revised multilinear regression equations for prediction of lateral spread displacement. *Journal of Geotechnical and Geoenvironmental Engineering* 128(12): 1007-1017.
- Zhang, G., Robertson, P.K., and Brachman, R.W.I. (2002). Estimating liquefaction-induced ground settlements from CPT for level ground. *Canadian Geotechnical Journal*, 39(5): 1168-1180.
- Zou, K.H. (2007). Receiver operating characteristic (ROC) literature research. On-line bibliography available from: <<http://www.spl.harvard.edu/archive/spl-pre2007/pages/ppl/zou/roc.html>> accessed 15 March 2014.

Tables

Table 4.1 Liquefaction severity classification criteria (after Green et al., 2014).

Classification	Criteria
No Manifestation	No surficial liquefaction manifestation or lateral spread cracking
Marginal Manifestation	Small, isolated liquefaction features; streets had traces of ejecta or wet patches less than a vehicle width; < 5% of ground surface covered by ejecta
Moderate Manifestation	Groups of liquefaction features; streets had ejecta patches greater than a vehicle width but were still passable; 5-40% of ground surface covered by ejecta
Severe Manifestation	Large masses of adjoining liquefaction features, streets impassible due to liquefaction; >40% of ground surface covered by ejecta

Table 4.2 Summary of ROC Analyses to Investigate Performance in High-FC Soils: Part A

Dataset Assessed	LPI MODEL							
	R&W98		MEA06		I&B08 ¹		I&B08 ²	
	AUC	OOP	AUC	OOP	AUC	OOP	AUC	OOP
No Liq¹: Ic < 2.05 & Liq²: Ic < 2.05	0.79	4.0	0.76	5.0	0.83	6.0	0.81	4.0
No Liq¹: Ic < 2.05 & Liq²: Ic > 2.05	0.79	4.0	0.76	5.0	0.82	5.0	0.81	4.5

¹ Strata predicted not to have liquefied by respective LEPs

² Strata predicted to have liquefied by respective LEPs

Table 4.3 Summary of ROC Analyses to Investigate Performance in High-FC Soils: Part B

Dataset Assessed	LPI MODEL							
	R&W98		MEA06		I&B08 ¹		I&B08 ²	
	AUC	OOP	AUC	OOP	AUC	OOP	AUC	OOP
No Liq¹: Ic < 2.05 & Liq²: Ic < 2.05	0.79	4.0	0.76	5.0	0.83	6.0	0.81	4.0
No Liq¹: Ic > 2.05 & Liq²: Ic < 2.05	0.67	11.5	0.69	13.5	0.69	14.0	0.66	10.5

¹ Strata predicted not to have liquefied by respective LEPs

² Strata predicted to have liquefied by respective LEPs

Figures

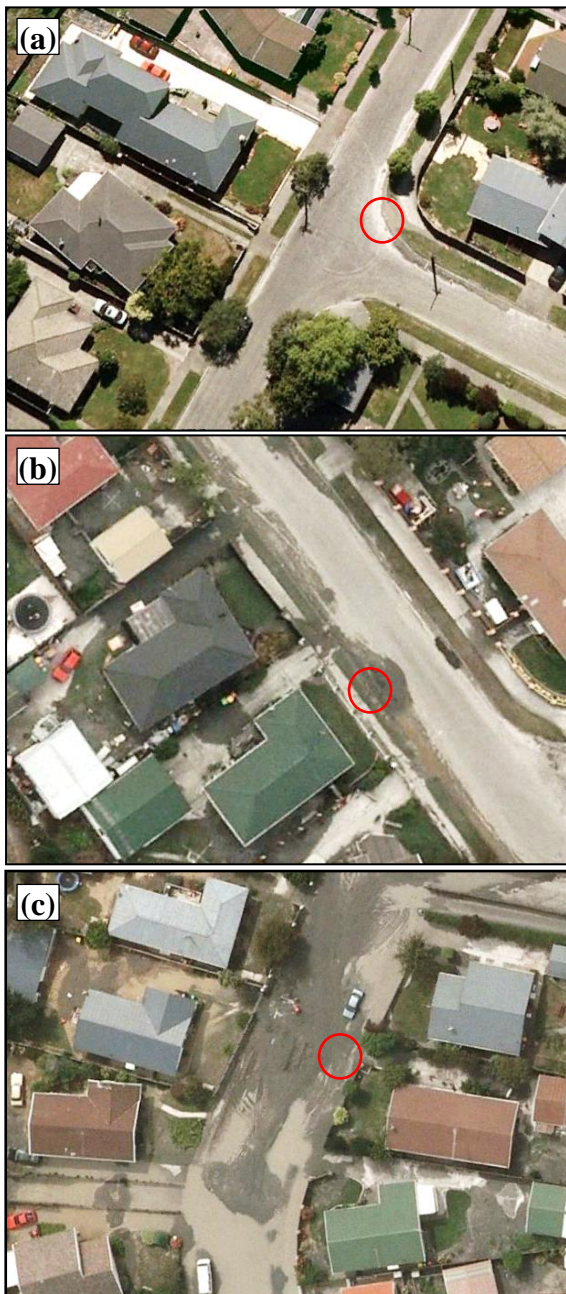


Figure 4.1 Representative observations of (a) marginal manifestation; (b) moderate manifestation; and (c) severe manifestation of liquefaction at the ground surface (after Green et al., 2014).

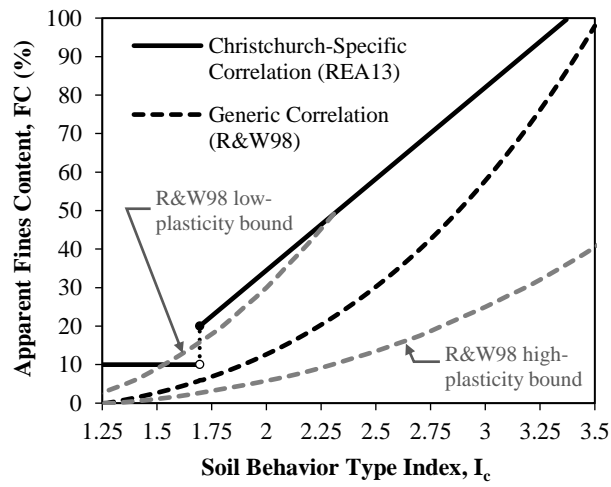


Figure 4.2 Correlations between I_c and apparent FC: Christchurch-specific correlation (Robinson et al., 2013) and generic correlation (Robertson & Wride, 1998).

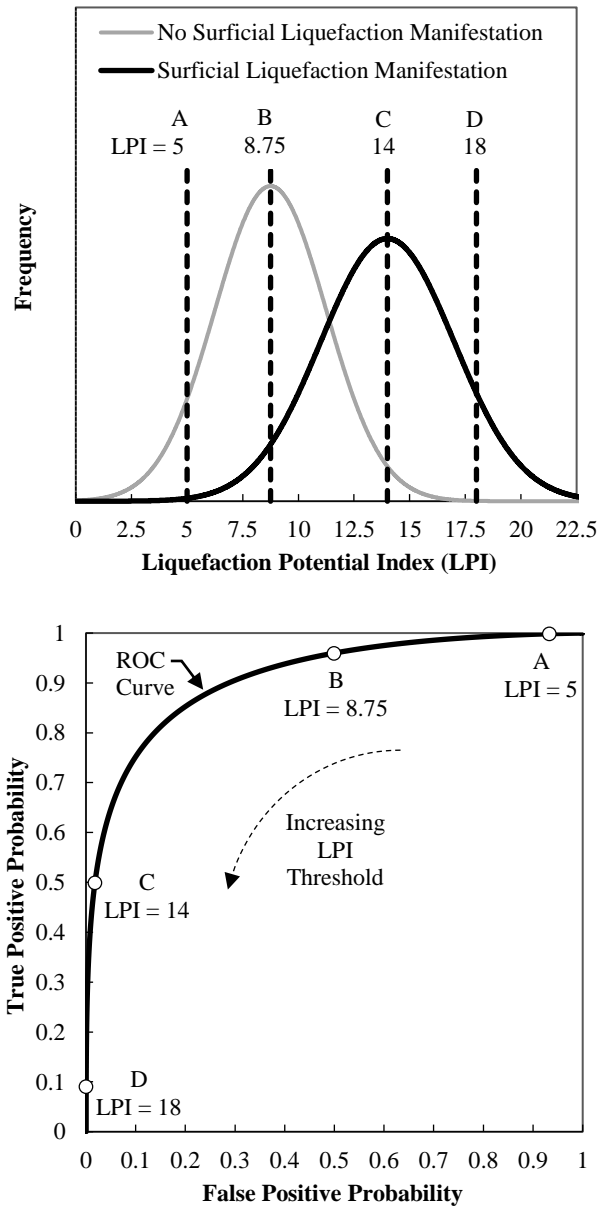


Figure 4.3 ROC analyses: (a) Frequency distributions of No Surficial Liquefaction Manifestation and Surficial Liquefaction Manifestations as a function of LPI, with four different threshold LPI values shown; and (b) Corresponding ROC curve

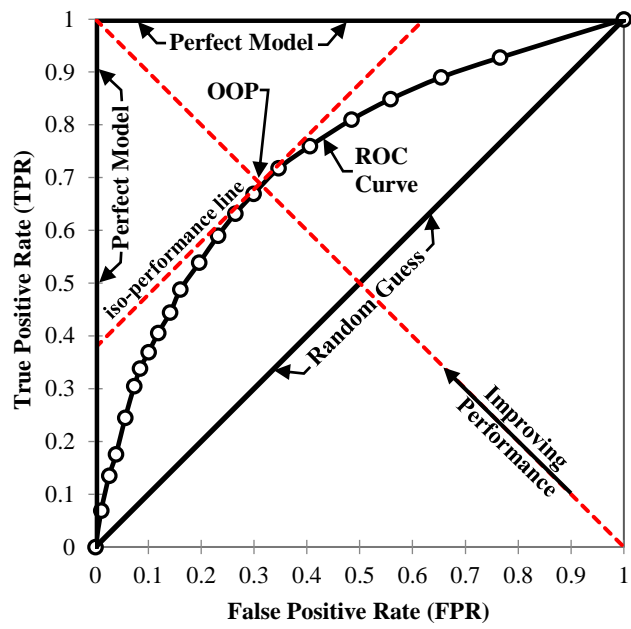


Figure 4.4 Illustration on how a ROC curve is used to assess the efficiency of a diagnostic test. The optimum operating point (OOP) indicates the threshold value for which the misprediction rate is minimized, as described in text.

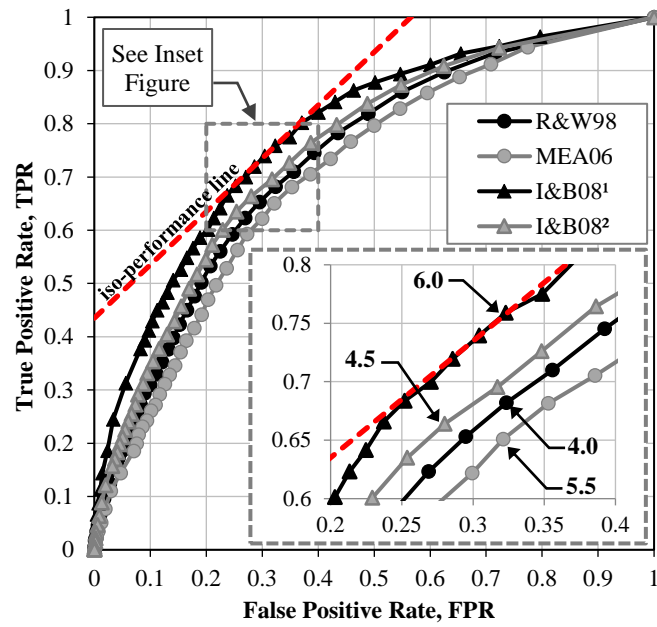


Figure 4.5 ROC analysis of LPI model performance in predicting the occurrence of surficial liquefaction manifestation (using I_c -cutoff value of 2.6). The optimum threshold LPI values (i.e., OOPs) for each LEP are highlighted in the inset figure.

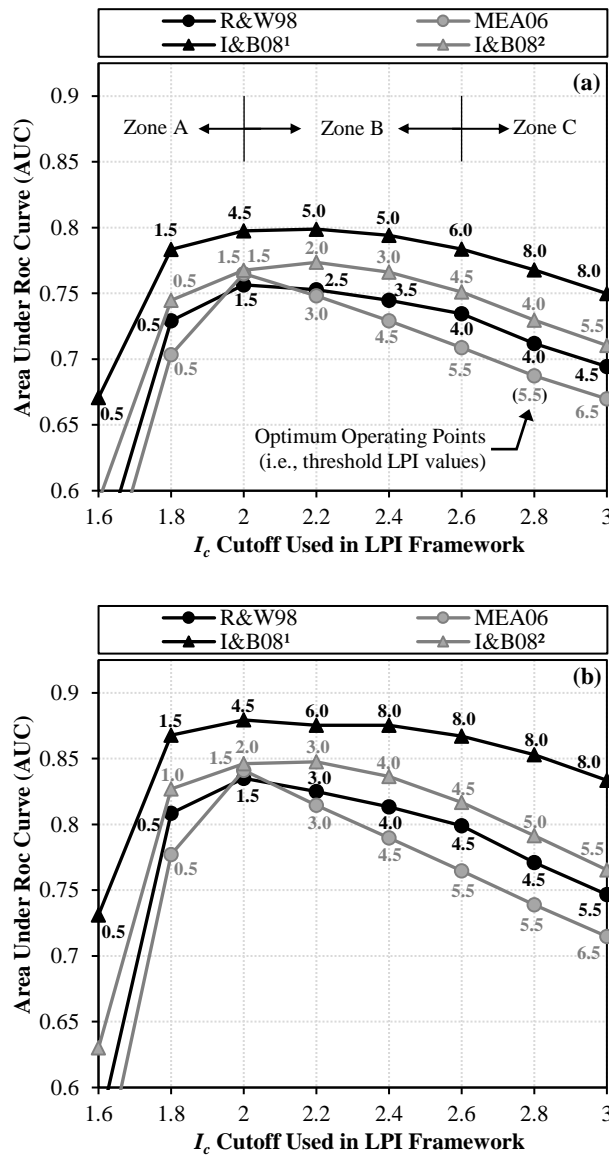


Figure 4.6 Area under ROC curve (AUC) vs. soil-behavior-type index (I_c) cutoff used in the LPI framework, considering (a) all manifestations of liquefaction, ranging from marginal to severe; and (b) manifestations of liquefaction more likely to damage infrastructure, ranging from moderate to severe. Increasing AUC indicates better model performance.

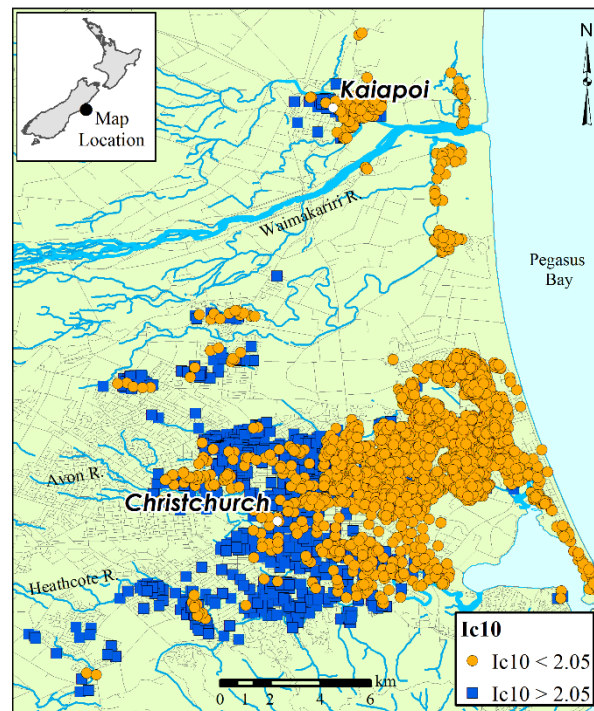


Figure 4.7 Map of study area showing locations of investigation sites, parsed by I_{c10} , the soil-behavior-type index (I_c) averaged over the uppermost 10 m of each site profile.

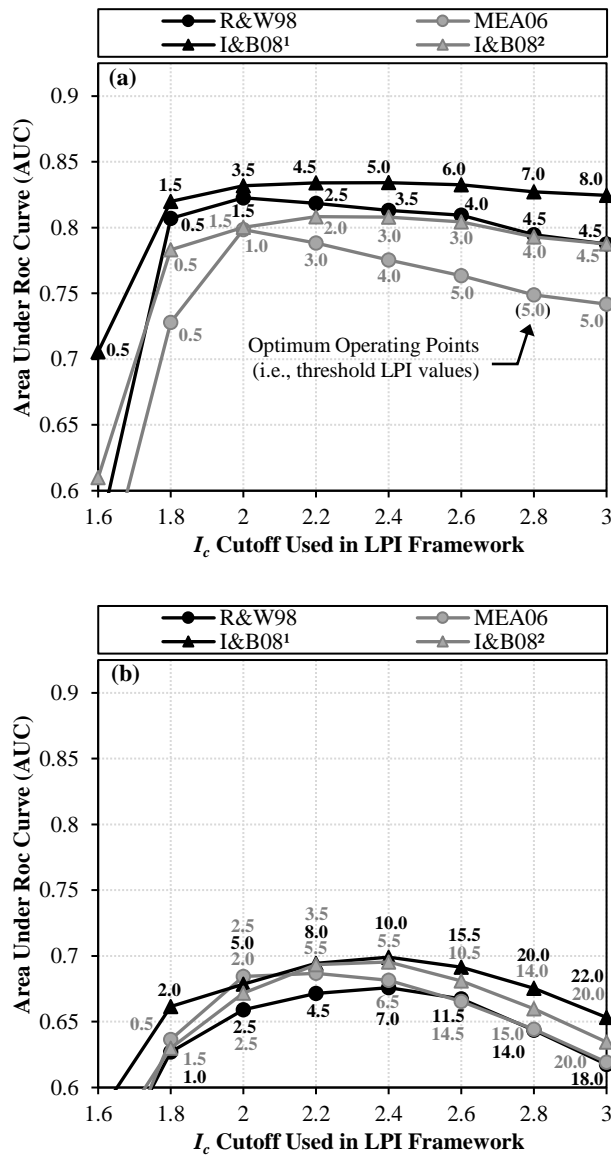


Figure 4.8 Area under ROC curve (AUC) vs. soil-behavior-type index (I_c) cutoff used in the LPI framework, considering all manifestations of liquefaction, ranging from marginal to severe, for cases with (a) $I_{c10} < 2.05$; and (b) $I_{c10} \geq 2.05$.

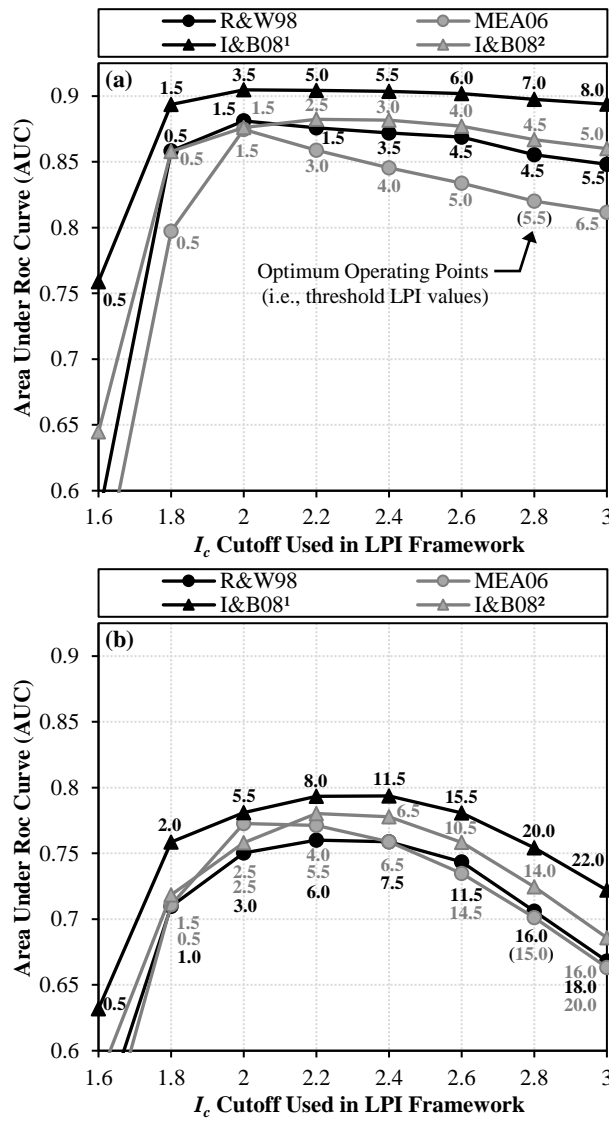


Figure 4.9 Area under ROC curve (AUC) vs. soil-behavior-type index (I_c) cutoff used in the LPI framework, considering manifestations of liquefaction more likely to damage infrastructure, ranging from moderate to severe, for cases with (a) $I_{c10} < 2.05$; and (b) $I_{c10} \geq 2.05$.

Chapter 5: Moving Towards an Improved Index for Assessing Liquefaction Hazard: Lessons from Historical Data

Brett W. Maurer¹, Russell A. Green², Oliver S. Taylor

¹ Graduate Research Assistant, Dept. of Civil and Environmental Engineering, Virginia Tech, Blacksburg, Virginia 24061, U.S.A.

² Professor, Dept. of Civil and Environmental Engineering, Virginia Tech, Blacksburg, Virginia 24061, U.S.A.

³ US Army Corps of Engineers, Engineering Research & Development Center, Vicksburg, MS 39180 USA

5.1 Abstract

While Liquefaction Potential Index (LPI) has been used to assess liquefaction hazards worldwide, evaluations of LPI during recent earthquakes have found its performance to be inconsistent. In 1985, Ishihara considered the influence of the non-liquefied surface layer on the manifestation of liquefaction, and proposed an empirical approach to predict liquefaction surface effects. The study presented herein investigates the insights the boundary curves proposed by Ishihara may provide for improving the existing LPI framework. The result of the investigation is a novel Ishihara-inspired index, LPI_{ISH} . Its performance is evaluated using select liquefaction case histories and is compared to that of the existing LPI framework. For the selected case studies, LPI_{ISH} was found to be consonant with observed surface effects and showed improvement over LPI in mitigating false-positive predictions. Ultimately, the influence of non-liquefiable layers on surficial manifestation is complex, and further research is needed to fully elucidate and quantify these effects.

5.2 Introduction

The objectives of this study are (1) to derive a novel liquefaction potential index (LPI) for assessing liquefaction hazard utilizing the Ishihara (1985) boundary curves for liquefaction surface effects; and (2) to evaluate the Ishihara-inspired index, LPI_{ISH} , using select liquefaction case histories, and compare its performance with that of the commonly-used Iwasaki et al. (1978) LPI procedure. While “simplified” liquefaction evaluation procedures (e.g., Robertson and Wride, 1998; Moss et al., 2006; Idriss and Boulanger, 2008) predict liquefaction triggering in particular strata, they do not predict the severity of liquefaction manifestation at the ground surface, which more directly correlates to damage potential and represents the cumulative response of a soil deposit. To serve this need, Iwasaki et al. (1978) proposed LPI, computed as:

$$LPI = \int_0^{20\text{ m}} F \cdot w(z) dz \quad (1)$$

In Equation 1, $F = 1 - FS$ for $FS \leq 1$ and $F = 0$ for $FS > 1$, where FS is the factor of safety against liquefaction computed by a liquefaction evaluation procedure, and $w(z)$ is a depth weighting function given by $w(z) = 10 - 0.5z$, where $z = \text{depth in meters}$. The severity of liquefaction manifestation is thus assumed to be proportional to the thickness of a liquefied layer, the proximity of the layer to the ground surface, and the amount by which FS is less than 1.0. Given this definition, LPI can range from 0 to 100. Based on Standard Penetration Test (SPT) data from 55 sites in Japan, Iwasaki et al. (1978) proposed that severe liquefaction should be expected at sites where $LPI > 15$ but not where $LPI < 5$. Using this criterion, LPI has been used to assess liquefaction hazards worldwide. However, researchers evaluating LPI during recent earthquakes have found its performance to be inconsistent, ranging from

largely erroneous (Lee et al., 2003) to generally consonant but inaccurate for a non-trivial percent of sites (Toprak and Holzer, 2003). For example, Maurer et al. (2014) assessed the performance of LPI during the 2010-2011 Canterbury (NZ) earthquake sequence; prediction-errors from the M_w 7.1 Darfield and M_w 6.2 Christchurch earthquake are shown in Figure 1, where over-predictions indicate the observed severity of liquefaction manifestation was less than predicted. It can be seen in Figure 1 that while LPI performance was generally good, liquefaction severity was significantly over-predicted for a portion of the study-area. Given the inconsistent efficacy of the existing LPI framework and criterion for assessing risk due to liquefaction, further research is warranted.

In evaluating the performance of LPI during the Canterbury earthquakes, Maurer et al. (2014) found that predictions might be improved if LPI accounted for the characteristics of the non-liquefied strata, in addition to those of the liquefied strata. As seen in Equation 1, the existing LPI framework assumes a simple form and does not account for the characteristics of non-liquefied soils, other than soils having an $FS \geq 1$ not contributing to the computed LPI value. Since LPI asserts only that the severity of manifestation is linearly related to the FS and depth of liquefied strata, LPI predictions may be inherently poor for some soil profiles and/or loading scenarios. While the findings of Maurer et al. (2014) are significant, they are not altogether novel. In 1985, Ishihara recognized the influence of the non-liquefied capping layer on mitigating the surficial manifestation of liquefaction. He plotted observations of liquefaction surface effects using the thicknesses of the non-liquefied capping layer, H_1 , and the liquefied strata, H_2 , and proposed boundary curves for predicting liquefaction manifestation as a function of H_1 , H_2 , and peak ground acceleration (PGA). Ishihara (1985) initially proposed a single boundary curve, shown in Figure 2a, using data from sites subjected to a PGA of 200 gal ($\sim 0.2g$); incorporating the work of others, a series of curves was then proposed corresponding to different PGAs, as shown in Figure 2b. The proposed boundary curves indicate that for a given PGA, there is a limiting H_1 beyond which surface manifestations do not form regardless of H_2 .

The boundary curves proposed by Ishihara (1985) for liquefaction surface effects may provide insight into how the existing LPI framework can be improved. Given the inconsistent performance of LPI for assessing liquefaction hazard, and considering its preeminent role in engineering practice, efforts to improve its efficacy are warranted. Accordingly, first a new index for assessing liquefaction hazard utilizing the Ishihara (1985) boundary curves for surficial manifestation of liquefaction is derived; and second the Ishihara-inspired index, LPI_{ISH} , is evaluated using select liquefaction case histories, and its performance is compared to that of the commonly-used Iwasaki et al. (1978) LPI procedure. As part of this comparison, case studies exemplifying the differences between the two LPI procedures are discussed in detail.

5.3 Derivation of LPI_{ISH}

In the following, LPI_{ISH} is derived using the Ishihara (1985) boundary curves shown in Figure 2. The derivation of LPI_{ISH} is separated into the following four sub-sections: (1) assumptions; (2) functional form; (3) determining constants; and (4) final form.

5.3.1 Assumptions

1. The penetration resistance of the liquefiable strata corresponding to each boundary curve is assumed to be the same. It will be shown that as such, PGA at the ground surface is proportional to FS in the liquefiable strata.
2. Each boundary curve, which separates cases of liquefaction manifestation from no manifestation, is assumed to represent the same LPI value (i.e., the threshold LPI value for surficial liquefaction manifestation). LPI is thus constant along each boundary curve.
3. It is assumed that each boundary curve may be approximated by two straight lines having slopes m and ∞ . These lines are shown in Figure 3a for the 0.2 g boundary curve. As such, the thickness of the liquefiable strata, H_2 , and the thickness of the non-liquefiable surface layer, H_1 , may be related through the slope (m) that is unique to each boundary curve.
4. The FS for liquefied strata is assumed to be uniform with depth. As such, the F parameter in Equation 1 (i.e., $F = 1 - FS$) is constant.

5.3.2 Functional Form

To determine how the existing LPI framework might be improved, the new Ishihara-inspired index is derived from the Iwasaki et al. (1978) functional form:

$$LPI_{ISH} = \int_{H_1}^{H_1+H_2} F w'(z) dz \quad (2)$$

In Equation 2, the bounds of the liquefiable layer are expressed in terms of H_1 and H_2 , where H_1 and H_2 are as illustrated in Figures 2 and 3; the parameter F is defined in Equation 1 by Iwasaki et al. (1978); and $w'(z)$ is a depth weighting function whose functional form is to be derived subsequently. Per assumption 4, the F-parameter (i.e., $F = 1 - FS$) is constant and is thus removed from the integral, as shown in Equation 3:

$$LPI_{ISH} = F \int_{H_1}^{H_1+H_2} w'(z) dz \quad (3)$$

Per assumption 2, LPI must be constant along each boundary curve, in which case the integral in Equation 3 must be constant for any combination of H_1 and H_2 that define a boundary curve. As will be shown in Equation 5, this is accomplished by assuming a power-law depth weighting function [i.e., $w'(z)$], given by Equation 4:

$$w'(z) = \frac{k}{z} \quad (4)$$

In Equation 4, z is the depth in meters below the ground surface, and k is a constant that is determined subsequently. Per assumption 3, H_1 and H_2 are related via the slope (m) unique to each boundary curve. From Figure 3a, it can be seen that $H_2 = H_1 \times m$. LPI_{ISH} can thus be simplified as follows:

$$LPI_{ISH} = F \int_{H_1}^{H_1(m+1)} kz^{-1} dz = Fk \ln \left(\frac{H_1(m+1)}{H_1} \right) = Fk \ln(m+1) = c \quad (5)$$

In Equation 5, c is the threshold LPI_{ISH} value for surficial manifestation; the value originally proposed by Iwasaki et al. (1978) (i.e., 5) is commonly used in practice. Rearranging the right side of Equation 5, the slope unique to each boundary curve can be expressed as follows:

$$m = \exp \left[\frac{c}{k(1-FS)} \right] - 1 \quad (6)$$

5.3.3 Determining Constants

As shown in Equation 6, a relationship exists between m , k , c and FS , where m is the initial slope unique to each boundary curve, k is a depth-weighting constant, c is the threshold LPI_{ISH} value for surficial manifestation, and FS is the factor of safety against liquefaction in the liquefiable strata. If we can relate m to FS , and define the threshold LPI_{ISH} value expected for manifestation, we may solve for the constant k . Using any of the simplified liquefaction evaluation procedures, FS for level ground conditions is expressed as follows:

$$FS = \frac{CRR \cdot K_\sigma}{CSR_{7.5}} \quad (7)$$

In Equation 7, CRR is the cyclic resistance ratio, K_σ is a dimensionless factor that accounts for the effect of overburden pressure on liquefaction resistance, and $CSR_{7.5}$ is the cyclic stress ratio normalized to an $M_w 7.5$ earthquake. Since CRR is expressed as function of normalized penetration resistance, CRR is

assumed to be the same for each boundary curve, per assumption 1. $CSR_{7.5}$ can be computed as follows (e.g., Seed and Idriss, 1971):

$$CSR_{M7.5} = 0.65 \frac{a_{max}}{g} \frac{\sigma_v}{\sigma'_{vo}} r_d \frac{1}{MSF} \quad (8)$$

where a_{max} = peak geometric-mean horizontal ground acceleration (PGA); g = coefficient of acceleration of due to gravity; σ'_{vo} = initial effective stress; σ_v = total stress; r_d = dimensionless stress reduction factor accounting for the non-rigid response of the soil column; and MSF = magnitude scaling factor to account for the duration of shaking. Thus, as can be seen from Equations 7 and 8 for the stated assumptions, FS in the liquefiable strata is inversely proportional to PGA at the ground surface. As such, the safety factors corresponding to the two extreme boundary curves shown in Figure 3 may be related as follows:

$$\frac{FS_{0.41g-0.51g}}{FS_{0.2g}} \approx \frac{0.2g}{0.45g} \approx 0.45 \quad \Rightarrow \quad FS_{0.45g} = 0.45 FS_{0.2g} \quad (9)$$

In Equation 9, $FS_{0.45g}$ is the safety factor in the liquefiable layer corresponding to the 0.45 g boundary curve, and $FS_{0.2g}$ is that corresponding to the 0.2 g boundary curve. Also, as shown in Figure 3b, the initial slopes corresponding to the 0.2 g, 0.3 g, and 0.45 g boundary curves are approximated as 1, 0.5, and 0.33, respectively.

Given the approximations shown in Figure 3b, and utilizing the relationships given by Equations 6 and 9, the slopes of the two extreme boundary curves are related as follows:

$$\frac{m_{0.2g}}{m_{0.45g}} \approx \frac{1}{0.33} = 3 = \frac{\exp\left[\frac{c}{k(1-FS_{0.2g})}\right]^{-1}}{\exp\left[\frac{c}{k(1-0.45FS_{0.2g})}\right]^{-1}} \quad (10)$$

In Equation 10, $m_{0.45g}$ is the initial slope of the 0.45 g boundary curve, and $m_{0.2g}$ is that of the 0.2 g boundary curve. As can be seen from Equation 10, three unknowns remain: c , k , and $FS_{0.2g}$. As stated, it is desirable to define the LPI_{ISH} threshold value expected for manifestation (c), and k is an unknown depth-weighting constant. Therefore, from the data used by Ishihara (1985) to propose his 0.2 g boundary curve, a reasonable value of $FS_{0.2g}$ will be determined. From his analysis of liquefaction sites following the 1983 $M_w 7.7$ Nihonkai-Chube (JPN) earthquake, Ishihara (1985) determined that the threshold SPT penetration resistance (i.e., $N_{1.60}$) for liquefaction triggering was approximately 12

blows/30 cm. Using this and other inputs consistent with the soil profiles given by Ishihara (1985), $FS_{0.2g}$ is estimated to be 0.72 using Equations 7 and 8 (Youd et al., 2001):

$$a_{max} = 0.2 \text{ g}; \frac{\sigma_v}{\sigma'_{v0}} = 1.35; r_d = 0.97; MSF = 0.93; N_{1,60} = 12 \xrightarrow{\text{Eqs. 7\&8}} FS_{0.2g} \approx 0.72 \quad (11)$$

For consistency with current practice, and to facilitate performance comparisons between LPI and LPI_{ISH} , the threshold value for manifestation (i.e., c) is set equal to 5. As such, liquefaction manifestation is expected where $LPI_{ISH} \geq 5$ and is not expected where $LPI_{ISH} < 5$. Next, from Equation 10, the depth weighting constant, k , is computed to be 25.56. To affirm compatibility between boundary curves and the constants determined herein, m is computed for each boundary curve shown in Figure 3 using Equation 6 and the proportionality demonstrated in Equation 9 (i.e., $FS \propto 1/PGA$):

$$m(0.2 \text{ g}) = \exp \left[\frac{5}{25.56(1-0.719)} \right] - 1 \approx 1 \quad (12)$$

$$m(0.3 \text{ g}) = \exp \left[\frac{5}{25.56(1-0.479)} \right] - 1 \approx 0.5 \quad (13)$$

$$m(0.45 \text{ g}) = \exp \left[\frac{5}{25.56(1-0.323)} \right] - 1 \approx 0.33 \quad (14)$$

As demonstrated by Equations 12-14, the derived relationship relating m , k , c and FS is consistent with the Ishihara (1985) boundary curves for surficial liquefaction manifestation. Lastly, the limiting surface layer thickness (H_1) is incorporated into the LPI_{ISH} framework. As can be seen from the three boundary curves shown in Figure 3b, when the quantity $H_1 \times m$ exceeds ~ 3 for a given PGA , surficial manifestations are not expected regardless of the liquefiable layer's thickness. Since m is a function of FS (see Equation 6), and the limiting value of H_1 is a function of m , the limiting surface layer thickness is easily computed for any value of FS . In summary, as the strength of shaking increases, reducing FS , the computed cap thickness required for suppressing manifestation increases via the proxy m .

5.4 Final Form

The final form of LPI_{ISH} is presented in Equation 15. As compared to the Iwasaki et al. (1978) LPI procedure, LPI_{ISH} incorporates the concept of a limiting cap thickness and also utilizes a power-law, rather than linear, depth weighting function. In Figure 4, the depth weighting function used in the existing LPI framework is compared to that proposed herein. It can be seen that LPI_{ISH} weighs the contribution of liquefaction triggering towards producing surficial manifestation more for depths between 0 and 3 meters, and less for depths between 3 and 17 meters. From Equation 15, it can be

shown that $LPI_{ISH} = 100$ for a profile with $FS = 0$ over the entire 20 meters, and with ground water at a depth of 0.4 meters. Because of the power-law form of the depth weighting function (Figure 4), it is recommended that a minimum H_1 of 0.4 m be used in computing LPI_{ISH} , regardless of whether liquefiable soils are present at shallower depths. [Note that only 0.8% of liquefaction case histories in the Boulanger and Idriss (2014) database are from sites with ground water depth less than 0.4 meters]. Thus, the limits of the LPI and LPI_{ISH} hazard-scales are consistent for all but extreme conditions.

$$LPI_{ISH} = \int_{H_1}^{20 \text{ m}} F(FS) \frac{25.56}{z} dz \quad (15)$$

Where:

$$F(FS) = \begin{cases} 1 - FS & \text{if } FS \leq 1 \cap H_1 \cdot m(FS) \leq 3 \\ 0 & \text{otherwise} \end{cases} \quad (16a)$$

and

$$m(FS) = \exp\left(\frac{5}{25.56(1-FS)}\right) - 1 \quad (16b)$$

5.3 Evaluation of LPI_{ISH}

LPI_{ISH} was evaluated using select liquefaction case histories, and its performance was compared with that of the commonly-used Iwasaki et al. (1978) LPI procedure. This evaluation was performed using a total of 60 liquefaction case studies from the 1989 Loma Prieta (USA), 1994 Northridge (USA), 1999 Kocaeli (Turkey), 1999 Chi-Chi (Taiwan), 2010 Darfield (New Zealand), and 2011 Christchurch (New Zealand) earthquakes; a summary of the select liquefaction case histories used herein is given in Table 1. Case-histories were selected from the literature based on the availability of CPT soundings in digital-format; in the future, the authors plan to further evaluate LPI_{ISH} using an expanded, high-quality case history database from the Canterbury, New Zealand earthquakes. Factors of safety against liquefaction (i.e., FS) were computed using the Cone Penetration Test (CPT) based liquefaction evaluation procedure of Robertson and Wride (1998) where the soil behavior type index, I_c , was used to identify non-liquefiable strata. Soils having $I_c > 2.6$ were considered too plastic to liquefy. In the following, example cases highlighting the differences between LPI and LPI_{ISH} are presented; complete results are then discussed.

In Figure 5, CPT sounding data are shown from site LEN-37 following the 1989 Loma Prieta

earthquake. Site LEN-37 had no surficial manifestations of liquefaction, which was correctly predicted by LPI_{ISH} (i.e., $LPI_{ISH} = 2.2$) but not by LPI (i.e., $LPI = 8.2$). This disparity can be attributed to both inclusion of the limiting cap thickness and to differences in depth weighting functions. For instance, in the 2.5 to 5-meter depth interval, it can be seen that LPI increases by 2.5 while LPI_{ISH} remains constant. This discrepancy is due to FS not being sufficiently low to overcome the mitigating influence of the non-liquefiable surface layer present at the site. It can also be seen that over the 5 to 6-meter depth interval, LPI increases at a faster rate than does LPI_{ISH} . This discrepancy is due to the differences in depth weighting functions, as shown in Figure 4, where for the depth interval in question, LPI weighs the influence of liquefaction triggering more than LPI_{ISH} does.

In Figure 6, CPT sounding data are shown from site SF-5 following the 1999 Kocaeli earthquake. Surficial manifestations of liquefaction were observed at site SF-5 as predicted to by LPI_{ISH} (i.e., $LPI_{ISH} = 6.7$), but not by LPI (i.e., $LPI = 3.8$). As seen in Figure 6, the site profile is generally too plastic to liquefy, aside for a shallow liquefiable layer in the 1 to 2-meter depth interval. According to LPI , this layer is too thin for liquefaction triggering to produce surficial manifestations. The observation of such manifestations therefore suggests the LPI depth weighting function may be insufficient for shallow depths. As a result of LPI_{ISH} weighing the influence of liquefaction triggering more than LPI does for the depth interval in question, its prediction was more accurate.

In Figure 7, CPT sounding data are shown from site AVD-49 following the 2010 Darfield earthquake. Site AVD-49 had no surficial manifestations of liquefaction, which was correctly predicted by LPI_{ISH} (i.e., $LPI_{ISH} = 4.6$) but not by LPI (i.e., $LPI = 10.8$). Similar to site LEN-37 (Figure 5), this disparity can be attributed to both inclusion of the limiting cap thickness and to differences in depth weighting functions. For instance, over several depth intervals (e.g., 2.8 to 3.2-meters depth), it can be seen that LPI increases while LPI_{ISH} remains constant. This discrepancy is due to FS not being sufficiently low to overcome the mitigating influence of the non-liquefiable surface layer present at the site. It can also be seen that over several other depth intervals (e.g., 8 to 11-meters depth), LPI increases at a faster rate than does LPI_{ISH} . This discrepancy is due to the differences in depth weighting factors, as shown in Figure 4 (i.e., LPI weighs the influence of liquefaction triggering more than LPI_{ISH} does at these depths).

While the majority of case-studies assessed herein demonstrate the relative efficacy of LPI_{ISH} , others serve as a reminder that continued research is needed. In Figure 8, CPT sounding data are shown from site WYN-5a following the 1994 Northridge earthquake. Surficial manifestations of liquefaction were present at Site WYN-5a, which was incorrectly predicted by both LPI_{ISH} (i.e., $LPI_{ISH} = 0.8$) and LPI (i.e., $LPI = 2.5$). These erroneous predictions could be due to a number of factors, including (1) erroneous characterization of soil type (i.e., liquefaction susceptibility) by the soil behavior type index,

I_c ; (2) erroneous measurement of ground water depth; (3) erroneous estimation of PGA; (4) limitations inherent to the liquefaction evaluation procedure of Robertson and Wride (1998), used to compute FS values; or (4) limitations inherent to the frameworks of both LPI and LPI_{ISH} to accurately represent the mechanics of liquefaction manifestation. Regardless of the error's source, cases such as WYN-5a suggest that further study of liquefaction hazard assessment is warranted.

In Figure 9, cumulative distribution functions of LPI and LPI_{ISH} values for soundings at sites with and without liquefaction manifestation are shown for the selected 60 case histories. It can be seen that LPI and LPI_{ISH} performed equally well in predicting true positives (i.e., cases where manifestations were observed as predicted), with 94% of such cases correctly identified with either index. However, it can also be seen that LPI_{ISH} demonstrated improvement over LPI in reducing false positives (i.e., cases where manifestations were predicted but not observed). The results shown in Figure 9a indicate that 31% of no-manifestation cases had $LPI \leq 5$, while the results shown in Figure 9b indicate that 100% of no-manifestation cases had $LPI_{ISH} \leq 5$.

5.4 Conclusions

The Ishihara (1985) boundary curves for surficial liquefaction manifestation were used to derive an alternative index for assessing liquefaction hazard, LPI_{ISH} . The boundary curves were shown to indicate that (1) a power-law depth weighting function may be more appropriate than the existing linear form; and (2) the F-parameter (see Equation 1) should account for the limiting thickness of the non-liquefiable surface layer, beyond which surface manifestations do not form regardless of the thickness of the underlying liquefiable strata. Using simplifying assumptions, LPI_{ISH} was derived to incorporate these improvements. Its performance was evaluated using select liquefaction case studies and compared to that of the commonly-used Iwasaki et al. (1978) LPI procedure. For the selected case studies, LPI_{ISH} was found to be consonant with observed surface effects and showed improvement over the existing LPI procedure in reducing false-positive predictions (i.e., cases where manifestations were predicted but not observed). In the future, the authors plan to further evaluate the performance of LPI_{ISH} using an expanded, high-quality case history database from the Canterbury, New Zealand earthquakes.

This study highlights deficiencies with existing liquefaction hazard assessment and presents an alternative hazard index for discussion. The need to account for the characteristics of both liquefied and non-liquefied strata, as suggested by recent field observations, is supported by the seminal work of Ishihara (1985). However, the influence of the capping and/or interbedded non-liquefiable layers on surficial manifestation is complex, and further research is needed to fully elucidate and quantify these effects.

5.5 Acknowledgements

This study is based on work supported by the US Army Engineer Research and Development Center (ERDC) grant W912HZ-13-C-0035 and U.S. National Science Foundation (NSF) grants CMMI-1030564, CMMI-1306261, CMMI-1407428, and CMMI-1435494. However, any opinions, findings, and conclusions or recommendations expressed in this paper are those of the author and do not necessarily reflect the views of ERDC or NSF.

References

- Bennett, M. J. and Tinsley, J. C. I., 1995. Geotechnical data from surface and subsurface samples outside of and within liquefaction-related ground failures caused by the October 17, 1989, Loma Prieta Earthquake, Santa Cruz and Monterey Counties, California. Open-File Report 95-663, U.S. Department of the Interior, U.S. Geological Survey, Menlo Park, California.
- Bennett, M. J., Ponti, D. J., Tinsley, J. C. I., Holzer, T. L., and Conaway, C. H., 1998. Subsurface geotechnical investigations near sites of ground deformation caused by the January 17, 1994, Northridge, California, Earthquake. Open File Report 98-373, U.S. Department of the Interior, U.S. Geological Survey, Menlo Park, California.
- Boulanger, R. W., and Idriss, I. M. (2014). CPT and SPT based liquefaction triggering procedures. Report No. UCD/CGM-14/01, Center for Geotechnical Modeling, Department of Civil and Environmental Engineering, University of California, Davis, CA, 134 pp.
- Bradley, B.A., 2014. Site-specific and spatially distributed estimation of ground motion intensity in the 2010-2011 Canterbury earthquakes. *Soil Dynamics and Earthquake Engineering*, 62-63, 83-91.
- Cetin, K. O., 2000. Reliability-based assessment of seismic soil liquefaction initiation hazard. Ph. D. Dissertation, University of California, Berkeley.
- CGD, 2012. Canterbury Geotechnical Database Layer CGD0010, <https://canterburygeotechnicaldatabase.projectorbit.com> [accessed 3/14/2014].
- Idriss, I.M. and Boulanger, R.W., 2008. Soil liquefaction during earthquakes. Monograph MNO-12, Earthquake Engineering Research Institute, Oakland, CA, 261 pp.
- Ishihara, K., 1985. Stability of natural deposits during earthquakes. In: Proceedings of the 11th International Conference on Soil Mechanics and Foundation Engineering, San Francisco, CA, USA, 1, 321-376.
- Iwasaki, T., Tatsuoka, F., Tokida, K., and Yasuda, S., 1978. A practical method for assessing soil liquefaction potential based on case studies at various sites in Japan. In: Proceedings of the 2nd International Conference on Microzonation, San Francisco, CA, USA, 885-896.

- Lee, D.H., Ku, C.S., and Yuan, H., 2003. A study of liquefaction risk potential at Yuanlin, Taiwan. *Engineering Geology*, 71, 97-117.
- Maurer, B.W., Green, R.A., Cubrinovski, M., and Bradley, B.A., 2014. Evaluation of the liquefaction potential index for assessing liquefaction hazard in Christchurch, New Zealand. *Journal of Geotechnical and Geoenvironmental Engineering*, 140(7), 04014032.
- Moss, R.E., Seed, R.B., Kayen, R.E., Stewart, J.P., Der Kiureghian, A., and Cetin, K.O., 2006. CPT-based probabilistic and deterministic assessment of in situ seismic soil liquefaction potential. *Journal of Geotechnical and Geoenvironmental Engineering*, 132(8), 1032-1051.
- PEER, 2000a. Documenting incidents of ground failure resulting from the Aug. 17, 1999, Kocaeli, Turkey Earthquake. <http://peer.berkeley.edu/publications/turkey/adapazari/> [accessed 3/14/ 2014].
- PEER, 2000b. Documentation of soil conditions at liquefaction sites from 1999 Chi-Chi, Taiwan Earthquake. http://peer.berkeley.edu/lifelines/research_projects/3A02/ [accessed 3/14/ 2014].
- Robertson, P.K. and Cabal, K.L., 2010. Estimating soil unit weight from CPT. In: *Proceedings of the 2nd International Symposium on Cone Penetration Testing*, Huntington Beach, CA, USA, paper #2-40.
- Robertson, P.K. and Wride, C.E., 1998. Evaluating cyclic liquefaction potential using cone penetration test. *Canadian Geotechnical Journal*, 35(3), 442-459.
- Toprak, S. and Holzer, T., 2003. Liquefaction potential index: field assessment. *Journal of Geotechnical and Geoenvironmental Engineering*, ASCE, 129(4), 315-322.

Tables

Table 1. Summary of select liquefaction case-histories used to evaluate LPI_{ISH} and LPI .

Case	Event	Study Site (CPT Sounding)	Field Investigation By:	GWT (m)	M_w	PGA (g)	PGA From:	Liquefaction Manifestation?	LPI_{ISH}	LPI
1	1989 Loma Prieta, USA	Leonardini 37 (LEN-37)	Bennett & Tinsley, 1995	2.50	7.0	0.17	Moss et al., 2006	No	2.2	8.2
2	1989 Loma Prieta, USA	Leonardini 39 (LEN-39)	Bennett & Tinsley, 1995	1.90	7.0	0.17	Moss et al., 2006	Yes	5.7	9.0
3	1989 Loma Prieta, USA	Leonardini 52a (LEN-52a)	Bennett & Tinsley, 1995	2.70	7.0	0.17	Moss et al., 2006	No	0.0	0.4
4	1989 Loma Prieta, USA	Marinovich 67 (MRR-67)	Bennett & Tinsley, 1995	6.20	7.0	0.28	Moss et al., 2006	No	0.0	0.1
5	1989 Loma Prieta, USA	Martella 111 (MAR-111)	Bennett & Tinsley, 1995	1.70	7.0	0.15	Moss et al., 2006	No	1.1	3.7
6	1989 Loma Prieta, USA	McGowan Farm 136 (MCG-136)	Bennett & Tinsley, 1995	2.40	7.0	0.26	Moss et al., 2006	No	3.5	5.6
7	1989 Loma Prieta, USA	Model Airport 18 (AIR-18)	Bennett & Tinsley, 1995	2.40	7.0	0.29	Moss et al., 2006	Yes	8.9	13.4
8	1989 Loma Prieta, USA	Model Airport 21 (AIR-21)	Bennett & Tinsley, 1995	2.40	7.0	0.29	Moss et al., 2006	Yes	7.7	10.9
9	1989 Loma Prieta, USA	Radovich 98 (RAD-98)	Bennett & Tinsley, 1995	3.50	7.0	0.28	Moss et al., 2006	No	2.1	7.1
10	1989 Loma Prieta, USA	Salinas R. Bridge 117 (SRB-117)	Bennett & Tinsley, 1995	6.40	7.0	0.12	Moss et al., 2006	No	0.0	0.0
11	1994 Northridge, USA	Wynne Avenue 5a (WYN-5a)	Bennett et al., 1998	4.30	6.7	0.54	Cetin, 2000	Yes	0.8	2.5
12	1999 Chi-Chi, Taiwan	Nantou Site C3 (CPT-3)	Peer, 2000b	1.00	7.6	0.38	Moss et al., 2006	Yes	8.3	7.3
13	1999 Chi-Chi, Taiwan	Nantou Site C7 (CPT-7)	Peer, 2000b	1.00	7.6	0.38	Moss et al., 2006	Yes	24.8	36.2
14	1999 Chi-Chi, Taiwan	Nantou Site C8 (CPT-8)	Peer, 2000b	1.00	7.6	0.38	Moss et al., 2006	Yes	10.4	18.0
15	1999 Chi-Chi, Taiwan	WuFeng Site B (WBC-1)	Peer, 2000b	1.12	7.6	0.60	Moss et al., 2006	Yes	21.1	26.1
16	1999 Chi-Chi, Taiwan	WuFeng Site C (WCC-6)	Peer, 2000b	1.20	7.6	0.60	Moss et al., 2006	Yes	28.0	27.7
17	1999 Chi-Chi, Taiwan	Yanlin Site C19 (CPT-19)	Peer, 2000b	0.57	7.6	0.25	Moss et al., 2006	Yes	18.7	19.3
18	1999 Chi-Chi, Taiwan	Yanlin Site C2 (CPT-2)	Peer, 2000b	0.56	7.6	0.25	Moss et al., 2006	Yes	13.9	17.4
19	1999 Chi-Chi, Taiwan	Yanlin Site C22 (CPT-22)	Peer, 2000b	1.13	7.6	0.25	Moss et al., 2006	Yes	26.0	28.0
20	1999 Chi-Chi, Taiwan	Yanlin Site C24 (CPT-24)	Peer, 2000b	1.20	7.6	0.25	Moss et al., 2006	Yes	29.3	32.9
21	1999 Chi-Chi, Taiwan	Yanlin Site C25 (CPT-25)	Peer, 2000b	3.52	7.6	0.25	Moss et al., 2006	Yes	10.6	17.9
22	1999 Chi-Chi, Taiwan	Yanlin Site C32 (CPT-32)	Peer, 2000b	0.74	7.6	0.25	Moss et al., 2006	Yes	19.3	24.7
23	1999 Chi-Chi, Taiwan	Yanlin Site C4 (CPT-4)	Peer, 2000b	0.66	7.6	0.25	Moss et al., 2006	Yes	17.7	23.1
24	1999 Kocaeli, Turkey	Adapazari Site B (CPT-B1)	Peer, 2000a	3.30	7.4	0.40	Moss et al., 2006	Yes	3.9	5.2
25	1999 Kocaeli, Turkey	Adapazari Site C2 (CPT-C4)	Peer, 2000a	0.44	7.4	0.40	Moss et al., 2006	Yes	14.5	22.0
26	1999 Kocaeli, Turkey	Adapazari Site D (CPT-D1)	Peer, 2000a	1.50	7.4	0.40	Moss et al., 2006	Yes	15.7	15.8
27	1999 Kocaeli, Turkey	Adapazari Site E (CPT-E1)	Peer, 2000a	0.50	7.4	0.40	Moss et al., 2006	Yes	34.1	24.5
28	1999 Kocaeli, Turkey	Adapazari Site F (CPT-F1)	Peer, 2000a	0.50	7.4	0.40	Moss et al., 2006	Yes	31.3	34.5
29	1999 Kocaeli, Turkey	Adapazari Site G (CPT-G1)	Peer, 2000a	0.45	7.4	0.40	Moss et al., 2006	Yes	38.2	38.8
30	1999 Kocaeli, Turkey	Adapazari Site H (CPT-H1)	Peer, 2000a	1.72	7.4	0.40	Moss et al., 2006	Yes	11.7	14.1
31	1999 Kocaeli, Turkey	Adapazari Site I (CPT-I2)	Peer, 2000a	0.71	7.4	0.40	Moss et al., 2006	Yes	14.5	16.8

Table 1 Cont. Summary of select liquefaction case-histories used to evaluate LPI_{ISH} and LPI .

Case	Event	Study Site (CPT Sounding)	Field Investigation By:	GWT (m)	M_w	PGA (g)	PGA From:	Liquefaction Manifestation?	LPI_{ISH}	LPI
32	1999 Kocaeli, Turkey	Adapazari Site J (CPT-J2)	Peer, 2000a	0.60	7.4	0.40	Moss et al., 2006	Yes	18.8	24.6
33	1999 Kocaeli, Turkey	Adapazari Site K (CPT-K1)	Peer, 2000a	0.80	7.4	0.40	Moss et al., 2006	Yes	11.1	12.4
34	1999 Kocaeli, Turkey	Adapazari Site L (CPT-L1)	Peer, 2000a	1.72	7.4	0.40	Moss et al., 2006	Yes	13.7	17.2
35	1999 Kocaeli, Turkey	Hotel Spanca (CPT-SH4)	Peer, 2000a	0.50	7.4	0.37	Moss et al., 2006	Yes	48.5	50.4
36	1999 Kocaeli, Turkey	Police Station (CPT-PS1)	Peer, 2000a	1.00	7.4	0.40	Moss et al., 2006	Yes	4.2	5.8
37	1999 Kocaeli, Turkey	Soccer Field (CPT-SF5)	Peer, 2000a	1.00	7.4	0.37	Moss et al., 2006	Yes	6.7	3.8
38	1999 Kocaeli, Turkey	Yalova Harbor (CPT-YH3)	Peer, 2000a	1.00	7.4	0.37	Moss et al., 2006	Yes	32.7	33.1
39	2010 Darfield, NZ	Avondale (AVD-10)	CGD, 2012 ¹	1.50	7.1	0.18	Bradley, 2014	No	3.1	7.0
40	2010 Darfield, NZ	Avondale (AVD-49)	CGD, 2012 ¹	1.70	7.1	0.18	Bradley, 2014	No	4.6	10.8
41	2010 Darfield, NZ	Avonside (AVS-23)	CGD, 2012 ¹	1.30	7.1	0.20	Bradley, 2014	Yes	8.0	7.4
42	2010 Darfield, NZ	Bexley (BEX-19)	CGD, 2012 ¹	1.00	7.1	0.18	Bradley, 2014	Yes	7.7	6.6
43	2010 Darfield, NZ	Burwood (BUR-12)	CGD, 2012 ¹	1.30	7.1	0.18	Bradley, 2014	Yes	7.2	9.0
44	2010 Darfield, NZ	Central Bus. Dist. (CBD-30)	CGD, 2012 ¹	2.40	7.1	0.21	Bradley, 2014	No	4.4	9.0
45	2010 Darfield, NZ	Halswell (HAL-32)	CGD, 2012 ¹	2.00	7.1	0.28	Bradley, 2014	Yes	5.8	7.0
46	2010 Darfield, NZ	Hoon Hay (HNN-30)	CGD, 2012 ¹	3.00	7.1	0.25	Bradley, 2014	No	4.7	7.3
47	2010 Darfield, NZ	Merivale (MRV-18))	CGD, 2012 ¹	1.80	7.1	0.21	Bradley, 2014	No	4.2	7.6
48	2010 Darfield, NZ	St Albans (STA-76)	CGD, 2012 ¹	0.40	7.1	0.22	Bradley, 2014	Yes	7.3	3.9
49	2010 Darfield, NZ	Wainoni (WAI-63)	CGD, 2012 ¹	3.00	7.1	0.19	Bradley, 2014	No	1.9	9.3
50	2011 Christchurch, NZ	Avondale (AVD-10)	CGD, 2012 ¹	1.50	6.2	0.35	Bradley, 2014	Yes	10.6	16.7
51	2011 Christchurch, NZ	Avondale (AVD-49)	CGD, 2012 ¹	1.70	6.2	0.36	Bradley, 2014	Yes	13.3	21.5
52	2011 Christchurch, NZ	Avonside (AVS-23)	CGD, 2012 ¹	1.30	6.2	0.44	Bradley, 2014	Yes	17.1	14.8
53	2011 Christchurch, NZ	Bexley (BEX-19)	CGD, 2012 ¹	1.00	6.2	0.47	Bradley, 2014	Yes	20.9	16.1
54	2011 Christchurch, NZ	Burwood (BUR-12)	CGD, 2012 ¹	1.30	6.2	0.35	Bradley, 2014	Yes	16.5	16.9
55	2011 Christchurch, NZ	Central Bus. Dist. (CBD-30)	CGD, 2012 ¹	2.40	6.2	0.46	Bradley, 2014	Yes	13.5	20.3
56	2011 Christchurch, NZ	Halswell (HAL-32)	CGD, 2012 ¹	2.00	6.2	0.38	Bradley, 2014	Yes	5.4	6.5
57	2011 Christchurch, NZ	Hoon Hay (HNN-30)	CGD, 2012 ¹	3.00	6.2	0.45	Bradley, 2014	Yes	6.9	9.7
58	2011 Christchurch, NZ	Merivale (MRV-18))	CGD, 2012 ¹	1.80	6.2	0.36	Bradley, 2014	Yes	7.0	10.9
59	2011 Christchurch, NZ	St Albans (STA-76)	CGD, 2012 ¹	0.40	6.2	0.44	Bradley, 2014	Yes	9.6	5.1
60	2011 Christchurch, NZ	Wainoni (WAI-63)	CGD, 2012 ¹	3.00	6.2	0.51	Bradley, 2014	Yes	22.8	32.8

¹Per terms of use, the following notice must appear: CPT soundings were prepared and/or compiled for the Earthquake Commission (EQC) to assist in assessing insurance claims made under the Earthquake Commission Act 1993 and/or for the Canterbury Geotechnical Database on behalf of the Canterbury Earthquake Recovery Authority (CERA). The data was not intended for any other purpose. EQC, CERA, and their data suppliers and their engineers, Tonkin & Taylor, have no liability for any use of this data or for the consequences of any person relying on it in any way.

Figures

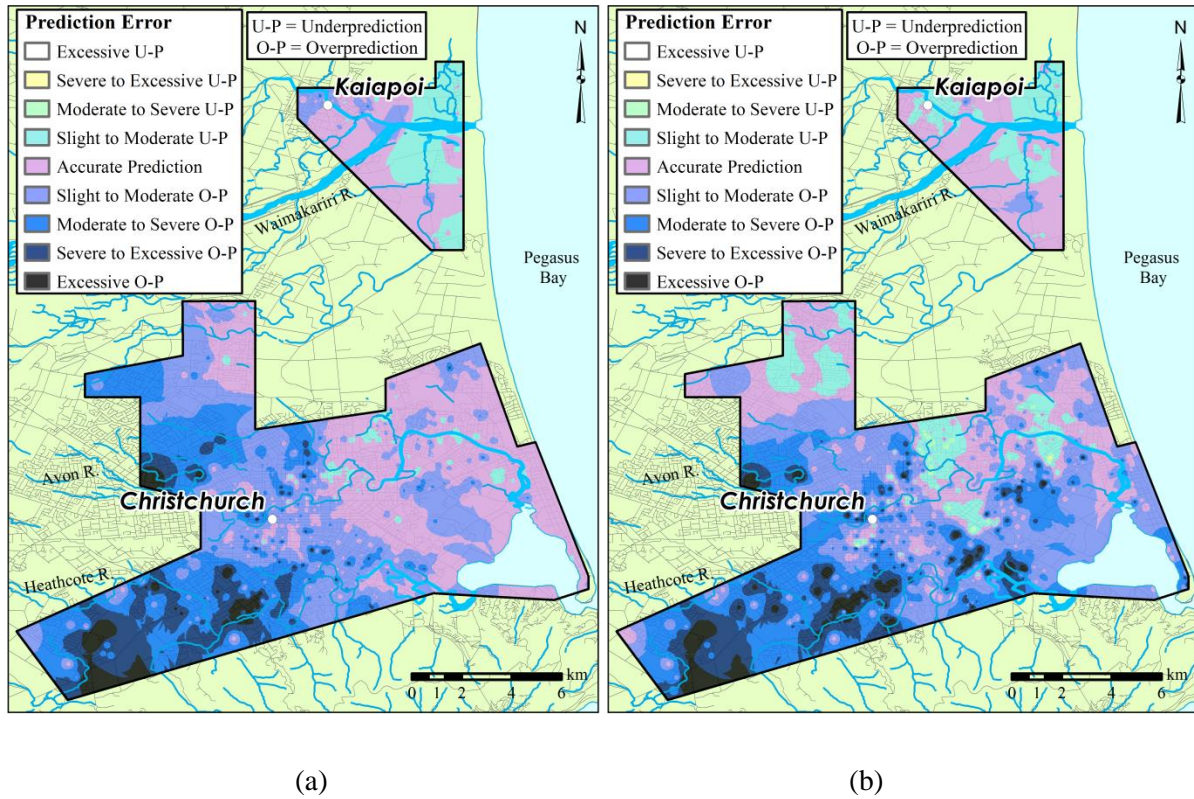
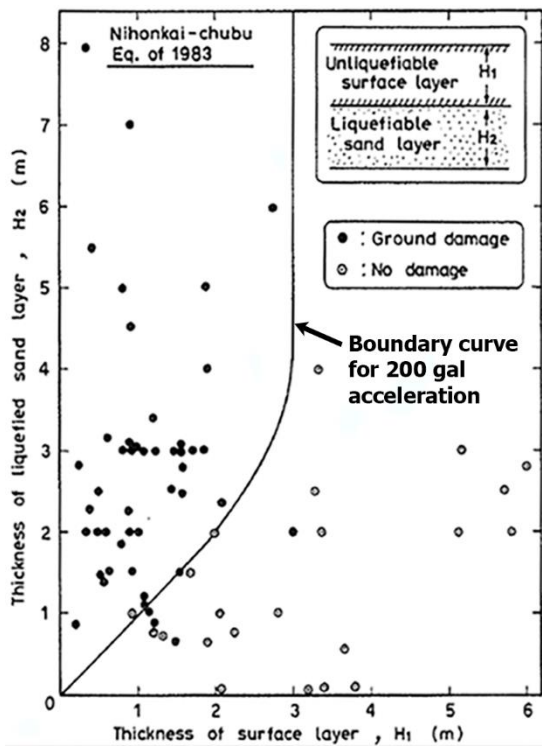
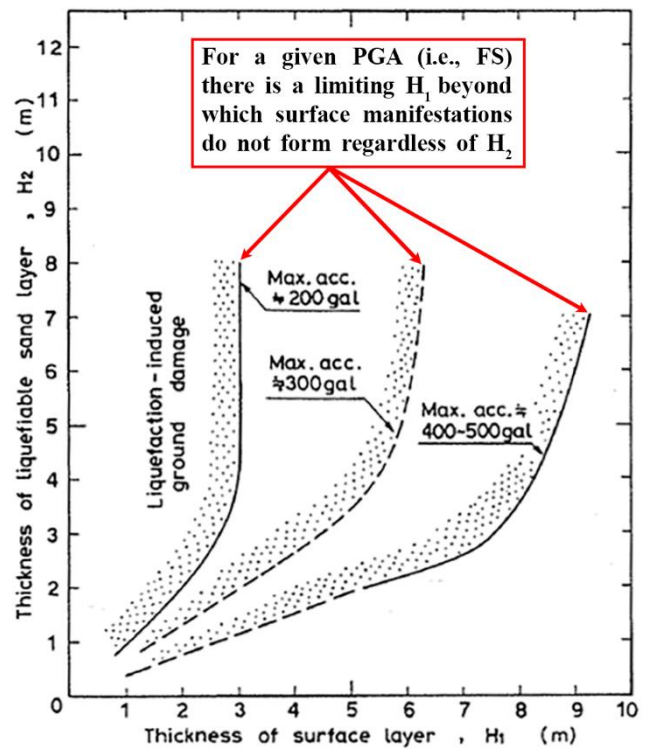


Figure 5.1 Liquefaction severity prediction errors for the (a) $M_w7.1$ Darfield and (b) $M_w6.2$ Christchurch New Zealand earthquakes. After Maurer et al. (2014).



(a)



(b)

Figure 5.2 a) Conditions of subsurface soil stratification discriminating between occurrence and non-occurrence of ground rupturing due to liquefaction (200 gal PGA); (b) Boundary curves proposed for identification of liquefaction-induced damage. After Ishihara (1985).

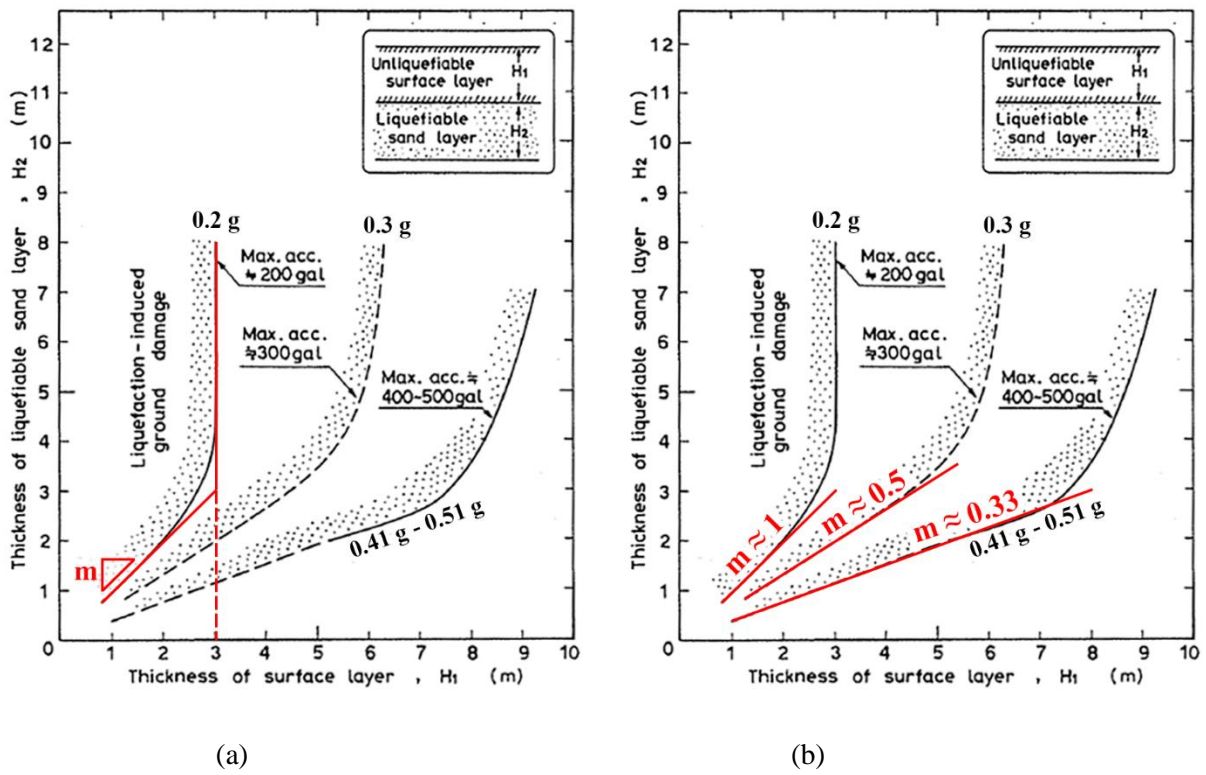


Figure 5.3 (a) Illustration of assumption #3, stated in the text, and used in the derivation of LPI_{ISH} . It can be seen that H_1 and H_2 are related via m , the slope unique to each boundary curve; (b) Assumed boundary curve slopes (m) used in the derivation of LPI_{ISH} .

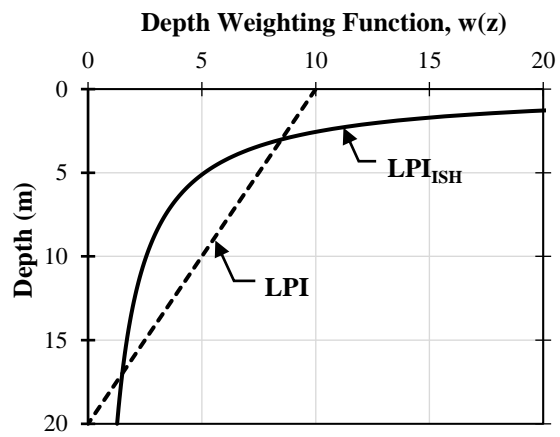


Figure 5.4 Comparison of depth weighting functions used in the LPI and LPI_{ISH} procedures.

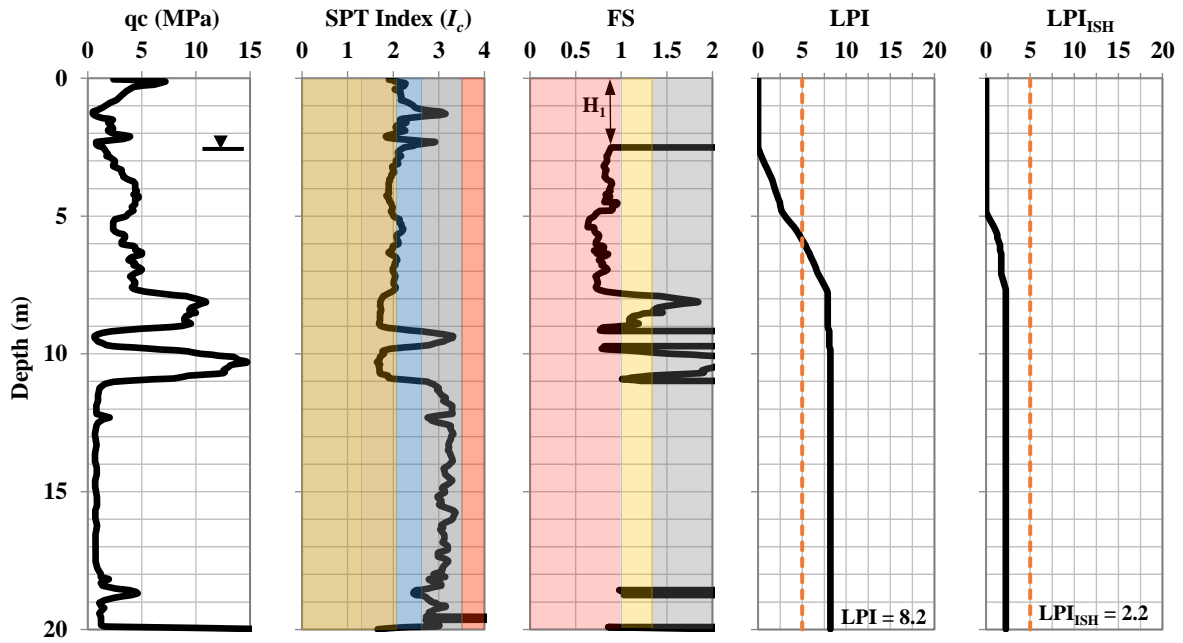


Figure 5.5 CPT data at site LEN-37 following the 1989 Loma Prieta earthquake. Site Len-37 had no surficial manifestations of liquefaction.

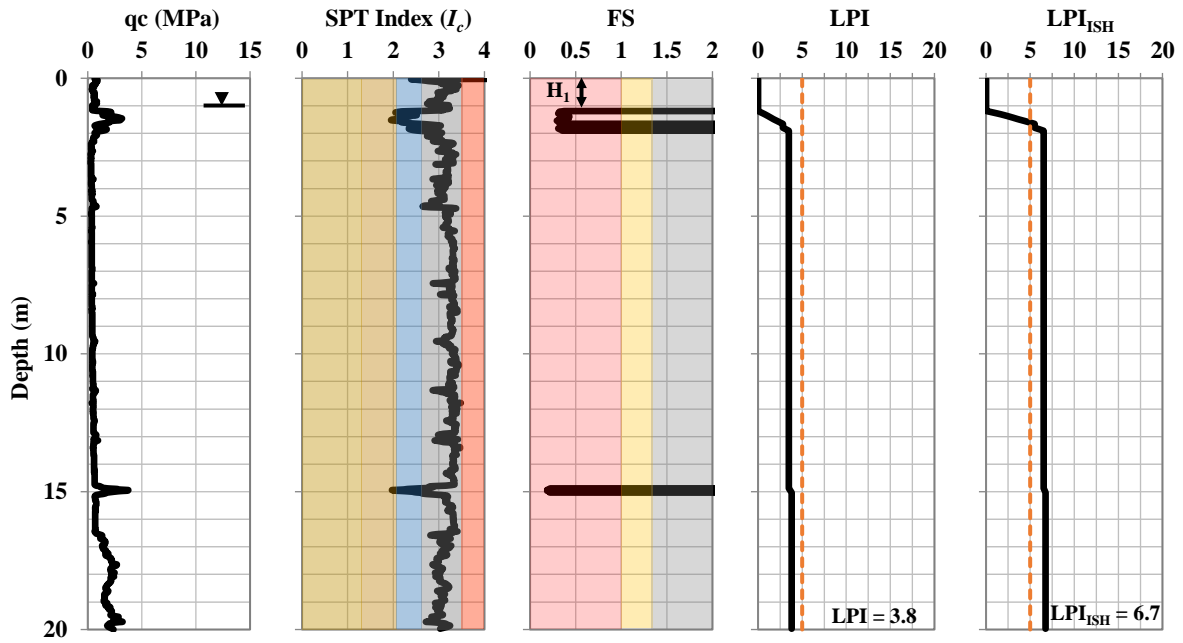


Figure 5.6 CPT data at site SF-5 following the 1999 Kocaeli earthquake. Surficial manifestations of liquefaction were present at site SF-5.

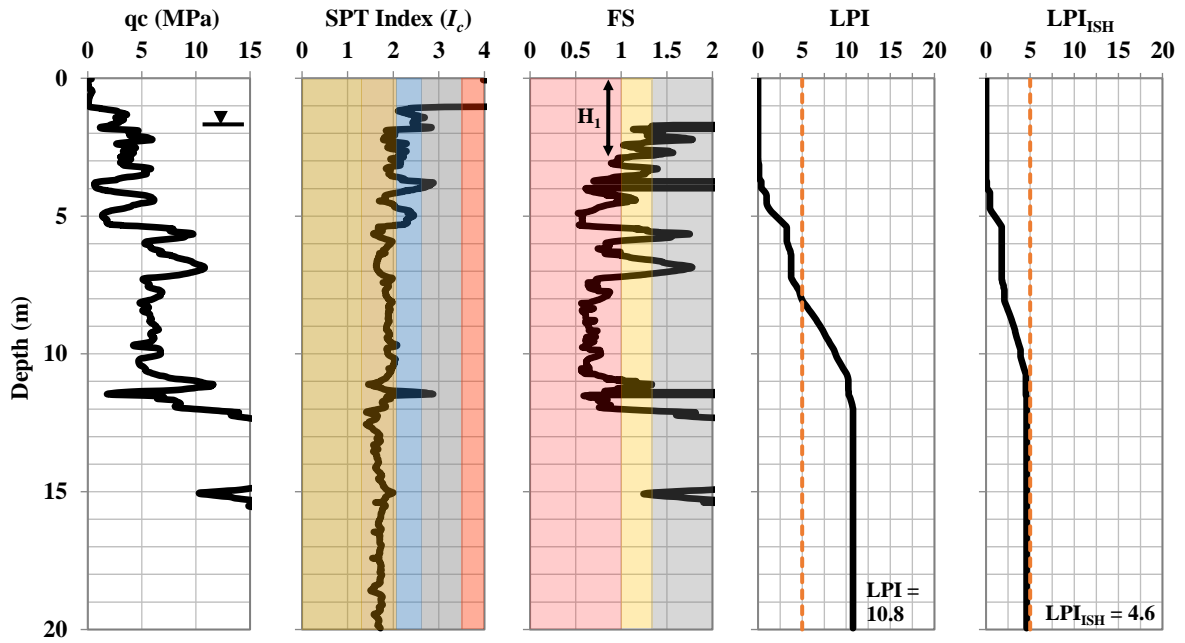


Figure 5.7 CPT data at site AVD-49 following the 2010 Darfield earthquake. Site AVD-49 had no surficial manifestations of liquefaction.

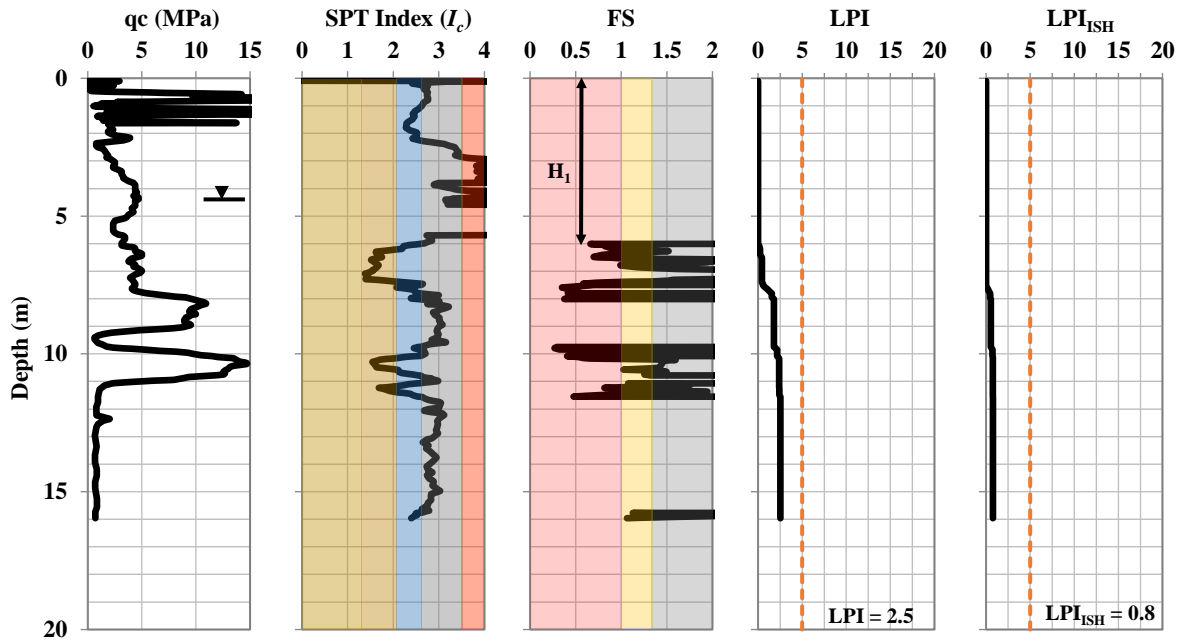


Figure 5.8 CPT data at site WYN-5a following the 1994 Northridge earthquake. Surficial manifestations of liquefaction were present at site WYN-5a.

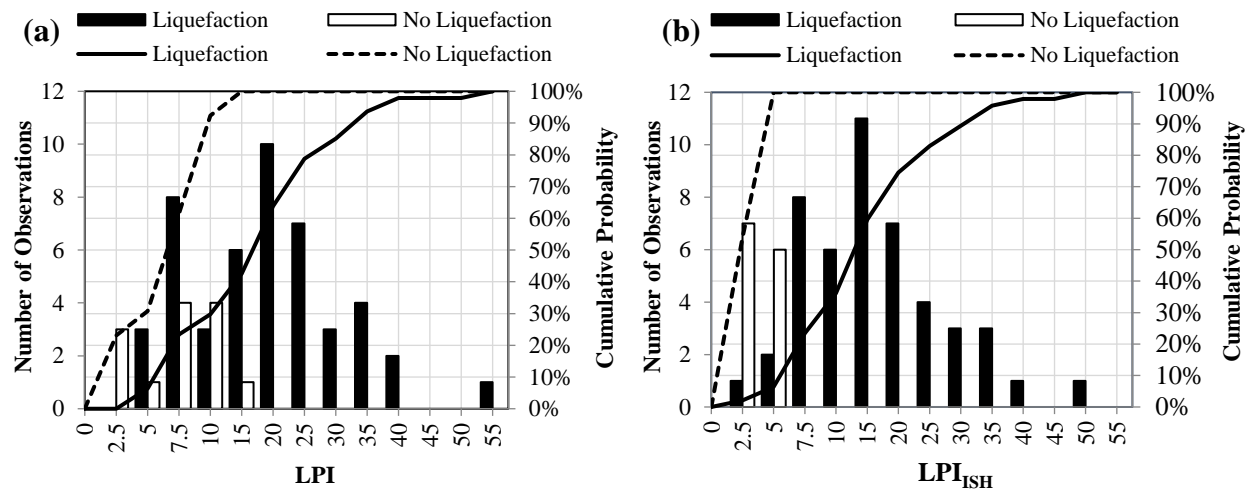


Figure 5.9 Histograms and cumulative probabilities of (a) LPI and (b) LPI_{ISH} values for CPT soundings at sites with and without surficial liquefaction manifestation.

Chapter 6: Investigating the Influence of Post-Liquefaction Strain Potential on the Accuracy of Liquefaction Severity Number (LSN) Hazard Assessments

Brett W. Maurer¹, Russell A. Green², Misko Cubrinovski³, Brendon A. Bradley⁴

¹ Graduate Research Assistant, Dept. of Civil and Environmental Engineering, Virginia Tech, Blacksburg, Virginia 24061, U.S.A.

² Professor, Dept. of Civil and Environmental Engineering, Virginia Tech, Blacksburg, Virginia 24061, U.S.A.

³ Professor, Dept. of Civil and Natural Resources Engineering, University of Canterbury, Private Bag 4800, Christchurch, New Zealand

⁴ Professor, Dept. of Civil and Natural Resources Engineering, University of Canterbury, Private Bag 4800, Christchurch, New Zealand

6.1 Abstract

The performance of any liquefaction hazard framework is intimately linked to the procedures used within it. For the Liquefaction Severity Number (LSN), post-liquefaction volumetric strain potential (ε_v) is one of several inputs used to assess the damage-potential of liquefaction. However, as with other inputs to the LSN framework, different techniques exist for estimating ε_v , each of which could lead to different computed LSN values, and by corollary, different assessments of liquefaction hazard. Accordingly, this study investigates six techniques for estimating ε_v using analyses of 7,000 liquefaction case-studies from the 2010-2011 Canterbury earthquakes. Results indicate that: (1) the LSN hazard scale (i.e. relationship between computed LSN and expected liquefaction hazard) is dependent on the ε_v estimation method; (2) accounting for these different hazard scales, the ε_v estimation method had no effect on the accuracy of LSN hazard assessment, such that all performed equally well; however (3) a control model in which ε_v was removed performed best, suggesting that ε_v either provides no statistically distinguishable benefits in terms of prediction accuracy, or is presently accounted for in such a way that is not optimal.

6.2 Introduction

The 2010-2011 Canterbury, New Zealand, earthquake sequence (CES) induced pervasive and severe soil liquefaction in the Christchurch region, resulting in widespread damage to civil infrastructure. As illustrated by the CES and other recent earthquakes, accurate assessment of liquefaction hazard is critical. Towards this end, hazard frameworks have been proposed to link the factor of safety against liquefaction triggering at depth (FS_{liq}) to the severity of liquefaction manifested at the ground surface, which serves as a pragmatic proxy for liquefaction damage potential. Within this realm, existing frameworks include: (1) the widely-used liquefaction potential index (LPI) (Iwasaki et al. 1978); (2) an Ishihara (1985) inspired variation of LPI, termed LPI_{ISH} (Maurer et al. 2015a); and (3) the liquefaction severity number (LSN) (van Ballegooy et al. 2014a), a variation of 1-D post-liquefaction settlement (e.g. Zhang et al. 2002). Central to all hazard frameworks are proposed decision thresholds corresponding to different levels of expected hazard. For example, Tonkin and Taylor (2013) proposed that little to no liquefaction manifestation is expected where $LSN < 20$; moderate to severe liquefaction manifestation is expected where $20 < LSN < 40$; and major manifestation of liquefaction is expected where $LSN > 40$.

Importantly, the efficacies of proposed threshold values are intimately linked to (Maurer et al., 2015b): (1) the approach used to select thresholds, and the assumed misprediction consequences

implicit to such selections; (2) the assessed dataset; and (3) the adopted procedures used within the liquefaction hazard framework. The focus of this study is on the latter as it pertains to the performance of LSN, which is now widely used in New Zealand. LSN is defined as (van Ballegooy et al. 2014a):

$$\text{LSN} = 10 \int_0^{20} \epsilon_v / z \, dz \quad (1)$$

where ϵ_v is the estimated post-liquefaction volumetric strain (%), and z is depth (m) below the ground surface. LSN thus assumes that the severity of liquefaction manifestation is a function of the cumulative thickness of liquefiable strata, the proximity of these strata to the ground surface, and the induced volumetric strain within these strata. Van Ballegooy et al. (2014a) proposed using the Zhang et al. (2002) approach to estimate ϵ_v , wherein values of equivalent-clean-sand-normalized CPT tip resistance (q_{c1Ncs}) and computed FS_{liq} are used to assess a soil's post-liquefaction strain potential. The performance of LN hazard assessment is therefore closely tied to the procedures used to determine FS_{liq} and ϵ_v . With respect to the former, several studies have investigated the influence of the procedure used to compute FS_{liq} on the accuracy of liquefaction hazard assessment. Among those commonly used in today's practice, the Idriss and Boulanger (2008) procedure has performed marginally better in analyzing data from the CES (Green et al. 2014; van Ballegooy et al. 2014a; Maurer et al. 2015c; 2015d) and is thus recommended by New Zealand Ministry of Business, Innovation, and Employment guidelines (MBIE, 2015).

Conversely, the influence of the procedure used to estimate ϵ_v is unknown. While significant differences exist among such procedures, the potential importance of these differences has never been thoroughly evaluated. Accordingly, this study investigates the influence of estimated ϵ_v on the accuracy of LSN hazard assessment using an analysis of 7,000 liquefaction case-studies from the CES, wherein six methods for estimating ϵ_v are used within the LSN framework. In the following, these six methods are first discussed in detail. The liquefaction case-studies to be analyzed, and additional methods used herein, are then summarized, followed by assessments of LSN performance.

6.2.1 Estimating Post-Liquefaction Volumetric-Strain (ϵ_v)

While attempts to estimate ϵ_v trace to earlier studies (e.g. Lee and Albaisa 1974), current CPT-based methods for estimating ϵ_v are often rooted in the work of Nagase and Ishihara (1988), who

conducted cyclic simple shear tests on saturated sands of varying relative density (D_r). Based largely on the results of Nagase and Ishihara (1988), Ishihara and Yoshimine (1992) proposed a series of curves, shown in Figure 1a, for estimating ε_v as a function of FS_{liq} and D_r . Using a correlation proposed by Tatsuoka et al. (1990) to convert from D_r to q_{c1N} , Zhang et al. (2002) converted the Ishihara and Yoshimine (1992) curves into a form suitable for use with CPT-based procedures for computing FS_{liq} , as shown in Figure 1b. However, to better capture trends identified by Ishihara and Yoshimine (1992), additional curves are developed in this study (Fig. 1b) for $FS_{liq} = 0.95$, $FS_{liq} = 0.96 \dots FS_{liq} = 0.99$ to supplement those of Zhang et al. (2002). As evident in Figure 1b, these curves are needed to accurately represent the behaviour identified by Ishihara and Yoshimine (1992), whereas linear interpolations between the $FS_{liq} = 0.9$ and $FS_{liq} = 1$ curves often fail to do so. It is also noteworthy that the Zhang et al. (2002) curves were developed using a correlation to q_{c1N} (i.e. normalized tip resistance, *uncorrected* for fines), but are proposed for use with values of q_{c1Ncs} . This simplification, justifications for which are given by Zhang et al. (2002) and Idriss and Boulanger (2008), is used throughout this study.

Problematically, while the Zhang et al. (2002) method for estimating ε_v is widely used in practice, it is rigidly tied to the Tatsuoka et al. (1990) correlation developed for Toyoura (Japan) sand, defined as:

$$D_r (\%) = -85 + 76 \log(q_{c1N}) \quad (2)$$

where D_r and q_{c1N} are as previously defined. Thus, if Equation (2) performs poorly for soils elsewhere, the resulting ε_v estimates could be inaccurate. Alternative correlations include that of Idriss and Boulanger (2003), adapted from Salgado et al. (1997), and defined as:

$$D_r = 0.465 \left(\frac{q_{c1N}}{C} \right)^{0.264} - 1.063 \quad (3)$$

where C is a soil-specific constant. Idriss and Boulanger (2003) used $C = 0.9$ in analyzing global liquefaction case studies, whereas C ranged from 0.64 to 1.55 for soils studied by Salgado et al. (1997). Plotted in Figure 2 are Equations (2) and (3), wherein 3 values of C are adopted for the latter ($C = 0.64, 0.9, 1.55$). It can be seen that large differences exist among the selected correlations, which could lead to different estimates of ε_v , and thus, different LSN hazard assessments.

Accordingly, utilizing variants of Equation (3), four alternatives to the Zhang et al. (2002) method are derived from Ishihara and Yoshimine (1992). *First*, as shown in Figure 3a, curves are developed a la Zhang et al. (2002) utilizing Equation (3) with $C = 0.9$, as adopted by Idriss and Boulanger (2003). These curves generally result in higher ε_v estimates relative to Zhang et al. (2002). *Second*, as shown in Figure 3b, curves are developed using the continuous function proposed by Yoshimine et al. (2006) which approximates the Ishihara and Yoshimine (1992) relations, wherein Equation (3) is again used with $C = 0.9$. Notably, the Zhang et al. (2002) approach suffers from two limitations solved by the Yoshimine et al. (2006) function: (1) it is laborious, such that developing curves for multiple $D_r - q_{cIN}$ correlations is impractical; and (2) the resulting curves are defined by discrete functions, such that interpolation is required to estimate ε_v . It can be seen in Figure 3a and 3b that ε_v estimates are very similar using these two approaches, but that ε_v is not bound to the Ishihara and Yoshimine (1992) parameter space (i.e. $30\% < D_r < 90\%$) in the latter. The Yoshimine et al. (2006) function is thus recommended for its pragmatic benefits. *Third* and *fourth*, ε_v is estimated using the Yoshimine et al. (2006) function and Equation (3) with respective C values of 0.64 and 1.55, the significance of which are as mentioned previously.

In addition, a “control” method is developed. To assess the possibility that manifestation severity is not influenced explicitly by D_r (i.e. beyond its influence in procedures that compute FS_{liq}), ε_v is set to an arbitrary value of 1% for all $FS_{liq} < 1$, and 0 otherwise. The six aforementioned methods for estimating ε_v are summarized in Table 1 and henceforth referred to as S1, S2, S3, S4, S5, and C1, respectively (Table 1, column 1).

6.3 Data and Methodology

6.3.1 CPT Soundings

This study utilizes 3,500 CPT soundings performed at sites where the severity of liquefaction manifestation was well-documented following both the Darfield and Christchurch earthquakes, resulting in 7,000 liquefaction case studies. Soundings were performed on various dates following the start of the CES, to include dates prior to, and following, the Christchurch earthquake. The CPT data is assumed to be unaffected by the date of the sounding (i.e., by the quantity and relative timing of prior earthquakes), as supported by Lees et al. (2015). In compiling the 7,000 case studies, CPT soundings were first rejected if: (1) performed at sites where the predominant manifestation of liquefaction was lateral spreading; (2) the depth of “pre-drill” significantly exceeded the estimated depth to ground water, or (3) believed to have prematurely terminated on shallow gravels, as

inferred from an Anselin (1995) Local Morans I analysis. For further discussion of CPTs and this geostatistical analysis, see Maurer et al. (2014).

6.3.2 Liquefaction Severity

Observations of liquefaction and the severity of manifestation were made by the authors for each CPT sounding location following both the Darfield and Christchurch earthquakes. CPT sites were assigned one of six damage classifications, as described in Green et al. (2014). Of the 7,000 cases compiled, 49% are cases of “no manifestation,” and 51% are cases where manifestations were observed and classified.

6.3.3 Estimation of Peak Ground Acceleration (PGA)

To evaluate FS_{liq} for use in computing LSN values, PGAs at the ground surface were computed using the Bradley (2013a) model, which combines unconditional PGA distributions estimated by the Bradley (2013b) ground motion prediction equation, recorded PGAs from strong motion stations, and the spatial correlation of intra-event residuals to compute conditional PGA distributions at sites of interest.

6.3.4 Estimation of Ground Water Table (GWT) Depth

Given the sensitivity of liquefaction hazard to GWT depth (e.g. Maurer et al. 2014), accurate estimates of the GWT are critical. For this study, GWT depths were sourced from the event-specific regional ground water models of van Ballegooy et al. (2014b). These models, which reflect seasonal and localized fluctuations across the region, were derived in part using monitoring data from ~1000 piezometers and provide a best-estimate of GWT depths immediately prior to the Darfield and Christchurch earthquakes.

6.3.5 Liquefaction Evaluation and LSN

FS_{liq} was computed using the deterministic procedure proposed by Idriss and Boulanger (2008), where the soil behavior type index, I_c , was used to identify non-liquefiable strata; soils with $I_c > 2.4$ were assumed non-liquefiable, per Maurer et al. (2015d). For I&B08, fines content (FC) is required to compute normalized tip resistances; as such, FC values were estimated using the I_c -FC

correlation proposed by Boulanger and Idriss (2014). LSN was computed for each of the 7,000 case studies per Equation (1), wherein ε_v was estimated using each of the six methods summarized in Table 1.

6.3.6 Receiver Operating Characteristic (ROC) Analyses

To investigate the significance of the ε_v estimation method used in the LSN framework, a standard analysis is needed to assess the performance of LSN hazard assessment. More specifically, for the six LSN variants, this analysis must: (1) evaluate their relative efficacies, independent of LSN decision thresholds; and (2) identify for each the optimum threshold value at which performance is optimized. Receiver operating characteristic (ROC) analyses are herein adopted for this purpose. In using LSN to predict liquefaction manifestation, the distributions of “positives” (i.e. liquefaction manifestation is observed) and “negatives” (i.e. no liquefaction manifestation is observed) overlap when the frequencies of the distributions are expressed in terms of computed LSN values. Optimal LSN decision thresholds are selected considering the rates of true positives (R_{TP}) (i.e. liquefaction is observed, as predicted) and false positives (R_{FP}) (i.e. liquefaction is predicted, but is not observed). Setting the threshold too low will result in a higher R_{FP} , the cost of which could be excessive spending on engineering design and construction (e.g. ground improvement costs). Conversely, setting the threshold too high results in a higher rate of false negatives (i.e. liquefaction is observed when it is predicted not to occur), the cost of which is liquefaction-induced damage (e.g. lost productivity, property damage, and reconstruction costs, among others). Thresholds should thus be selected so as to minimize these costs.

ROC curves plot R_{TP} versus R_{FP} for varying threshold values. Figures 4a and 4b illustrate the relationship among the positive and negative distributions, the threshold value, and the ROC curve. Figure 4b also illustrates how a ROC curve is used to assess the efficiency of a diagnostic test and select an optimum threshold. In ROC space, random guessing is indicated by a 1:1 line through the origin (i.e. equivalent correct and incorrect predictions), while a perfect model plots as a point at (0,1), indicating the existence of a threshold value which perfectly segregates the dataset (i.e. all cases with manifestation have LSN above the threshold; all cases without manifestation have LSN below the threshold). While no single parameter can fully characterize model performance, the area under a ROC curve (AUC) is commonly used for this purpose, where AUC is statistically equivalent to the probability that sites with manifestation have higher computed LSN than sites without manifestation (e.g. Fawcett 2005). As such, increasing AUC indicates better model performance. The optimum decision threshold, or optimum operating point (OOP), is defined

herein as the threshold LSN value which minimizes the rate of misprediction [i.e. $R_{FP} + (1 - R_{TP})$]. As such, contours of the quantity $[R_{FP} + (1 - R_{TP})]$ represent points of equivalent performance in ROC space, as shown in Figure 4b. For further overview of ROC analyses, and for demonstration of how project-specific misprediction consequences can be incorporated into ROC analyses, the reader is referred to Fawcett (2005) and Maurer et al. (2015b), respectively.

6.4 Results and Discussion

In Figure 5a, ROC curves are plotted to evaluate the accuracy of LSN hazard assessment for 7,000 liquefaction case studies from the CES, wherein six variants for estimating ε_v are assessed. More specifically, the performance evaluated in Figure 5 is that of LSN to predict liquefaction manifestations likely to damage infrastructure. In the adopted classification scheme (Green et al. 2014), “marginal” manifestations are characterized by a trace amount of water or ejecta and are likely to be non-damaging, whereas “moderate” to “severe” manifestations are likely to coincide with damage. Shown in Figure 5b is a magnified view of the optimal-performance area in ROC space, wherein the optimal LSN decision threshold is identified for models S1 through S5.

It can be seen in Figure 5a that models S1 through S5 have nearly identical performance, such that none of the five methods for estimating ε_v result in more (or less) accurate LSN hazard assessments for the considered case studies. In this regard, the measured AUCs range from 0.78 (S2, S3, S4) to 0.79 (S1 and S5). To place this performance in context, AUCs of 0.5 and 1.0 respectively indicate random guessing and a perfect model. However, it can be seen in Figure 5b that the LSN threshold at which performance is optimal varies significantly, ranging from LSN = 14.6 for S4, to LSN = 38.4 for S5. Thus, if optimal thresholds obtained from an analysis using one ε_v estimation method are applied to forward analyses wherein a different method is used, the resulting hazard assessments could be erroneous. Notably, the optimal thresholds for models S1 through S4 are reasonably consistent with that proposed by Tonkin and Taylor (2013) for predicting “moderate to severe” liquefaction manifestations (i.e. LSN = 20).

Interestingly, it can be seen in Figures 5a and 5b that “control” model C1 performs best, with measured AUC of 0.80. The leading performance of C1 indicates that the utility of ε_v is unclear. More specifically, this result suggests that: (1) ε_v is not a statistically significant variable for predicting liquefaction manifestation (i.e. beyond its inherent accounting for by procedures that compute FS_{liq} , see Dobry 1989); and/or (2) ε_v is accounted for in the LSN framework in such a way that is not optimal; and/or (3) the methods adopted for estimating ε_v (i.e. S1 through S5) do not

accurately portray the behavior of soils in the case studies assessed herein. With respect to the latter, additional methods for estimating ε_v in the LSN framework could be assessed in future studies. Importantly, even the best-performing model has potential for significant improvement. Operating at its optimum threshold, C1 has overall accuracy of 71%, indicating that 29% of liquefaction case studies are predicted incorrectly. While liquefaction triggering has garnered significant research and debate, the mechanics of liquefaction manifestation have received less attention, and seemingly, are less well understood. In this regard, further research is needed to fully elucidate and quantify influential factors.

6.5 Conclusions

Utilizing 7,000 liquefaction case-studies from the CES, this study investigated the influence of the method used to estimate ε_v within the LSN framework on the accuracy of resultant hazard assessments. The results are as follows: (1) the LSN hazard scale (i.e. relationship between computed LSN and expected liquefaction hazard) is dependent on the ε_v estimation method, and as such, LSN thresholds obtained from analyses using one method should not be applied to forward analyses wherein a different method is used; (2) accounting for these different hazard scales, the selected ε_v estimation method had no effect on the accuracy of LSN hazard assessment, such that all methods performed equally well; however, (3) a control model in which ε_v was removed from the LSN framework performed best, suggesting that ε_v either provides no statistically distinguishable benefits in terms of prediction accuracy, or is presently accounted for in such a way that is not optimal. Of course, the findings presented are based on a dataset from the CES, and their applicability to other datasets, or to methodologies different from that used herein, is unknown.

6.6 Acknowledgements

This study is based on work supported by the US National Science Foundation (NSF) grants CMMI 1030564, CMMI 1407428, and CMMI 1435494, and US Army Engineer research and Development Center (ERDC) grant W912HZ-13-C-0035. The authors also acknowledge the Canterbury Geotechnical Database and its sponsor EQC for providing data used in this study. However, any opinions, findings, and conclusions or recommendations expressed in this paper are those of the authors and do not necessarily reflect the views of NSF, ERDC, or EQC.

References

Anselin L. 1995. Local Indicators of Spatial Association—LISA, *Geographical Analysis*; 27(2):

93–115.

- Boulanger RW & Idriss IM. 2014. CPT and SPT based liquefaction triggering procedures, *Report No. UCD/CGM.-14/01*, Center for Geotech. Modelling, Dept. of Civil and Environ. Eng., UC Davis, CA, USA.
- Bradley BA. 2013a. Site-specific and spatially-distributed ground motion intensity estimation in the 2010-2011 Christchurch earthquakes, *SDEE*, 48: 35-47.
- Bradley BA. 2013b. A New Zealand-specific pseudo-spectral acceleration ground-motion prediction equation for active shallow crustal earthquakes based on foreign models, *BSSA*, 103(3): 1801-1822.
- Dobry R. 1989. Some basic aspects of soil liquefaction during earthquakes, *Earthquake Hazards and The Design of Constructed Facilities in the Eastern United States* (KH Jacob and CJ Turkstra, eds.), *Annals of the New York Academy of Sciences*, 558: 172-182.
- Fawcett T. 2005. An introduction to ROC analysis, *J of Pattern Recognition Letters*, 27(8): 861-874.
- Green RA, Cubrinovski, M, Cox, B, Wood, C, Wotherspoon, L, Bradley, B, Maurer, B. 2014. Select Liquefaction Case Histories from the 2010-2011 Canterbury Earthquake Sequence, *Earthquake Spectra*, 30(1): 131-153.
- Idriss IM & Boulanger RW. 2008. Soil liquefaction during earthquakes, *Monograph MNO-12*, Earthquake Engineering Research Institute, Oakland, CA, 261 pp.
- Idriss IM & Boulanger RW. 2003. Relating K_α and K_σ to SPT blow count and to CPT tip resistance for use in evaluating liquefaction potential, *2003 Dam Safety Conference*, Minneapolis, MN, USA.
- Ishihara K. 1985. Stability of natural deposits during earthquakes, *11th International Conference on Soil Mechanics and Foundation Engineering*, San Francisco, CA, USA, 1: 321-376.
- Iwasaki T, Tatsuoka F, Tokida K, Yasuda S. 1978. A practical method for assessing soil liquefaction potential based on case studies at various sites in Japan, *2nd Int. Conf. on Microzonation*, San Francisco, USA, 1978.
- Lee KL and Albaisa A. 1974. Earthquake induced settlements in saturated sands, *J Soil Mechanics and Foundations*, 100(4): 387-406.
- Lees JJ, Ballagh RH, Orense RP, van Ballegooy S. 2015. CPT-based analysis of liquefaction and re-liquefaction following the Canterbury earthquake Sequence, *SDEE*, *In Press*.
- Maurer BW, Green RA, Cubrinovski M, Bradley B. 2014. Evaluation of the liquefaction potential index for assessing liquefaction hazard in Christchurch, New Zealand. *J Geotech Geoenviron Eng.*, 140(7), 04014032.

- Maurer BW, Green RA, Cubrinovski M, Bradley B. 2015a. Moving towards an improved index for assessing liquefaction hazard: lessons from historical data, *Soils and Foundations*, 55(4): 778-787.
- Maurer BW, Green RA, Cubrinovski M, Bradley B. 2015b. Calibrating the liquefaction severity number (LSN) for varying misprediction economies: a case study in Christchurch, New Zealand, *6th Int. Conf. on Geotechnical Earthquake Engineering*, Christchurch, New Zealand, *In Press*.
- Maurer BW, Green RA, Cubrinovski M, Bradley B. 2015c. Assessment of CPT-based methods for liquefaction evaluation in a liquefaction potential index (LPI) framework, *Geotechnique*, 65(5): 328-336.
- Maurer BW, Green RA, Cubrinovski M, Bradley B. 2015d. Fines-content effects on liquefaction hazard evaluation for infrastructure during the 2010-2011 Canterbury, New Zealand earthquake sequence, *SDEE 76*: 58-68.
- MBIE. 2015. Repairing and rebuilding houses affected by the Canterbury earthquakes, Ver. 3a, Ministry of Business, Innovation, and Employment, Wellington, New Zealand.
- Nagase H, Ishihara K. 1988. Liquefaction-induced compaction and settlement of sand during earthquakes, *Soils and Foundations*, 28(1):66–76.
- Salgado R, Mitchell JK, Jamiolkowski, M. 1997. Cavity expansion and penetration resistance in sands, *J Geotech Geoenviron Eng*, 123(4): 344-354.
- Tatsuoka F, Zhou S, Sato T, Shibuya S. 1990. Evaluation method of liquefaction potential and its application. Report on seismic hazards on the ground in urban areas. Ministry of Education of Japan, Tokyo, Japan.
- Tonkin & Taylor (2013). Liquefaction vulnerability study, *T&T Ref: 52020.0200/v.1.0*, Christchurch, NZ.
- van Ballegooy, S, Malan, P, Lacrosse, V, Jacka, ME, Cubrinovski, M, Bray, JD, O'Rourke, TD, Crawford, SA, and Cowan, H. 2014a. Assessment of liquefaction-induced land damage for residential Christchurch, *Earthquake Spectra*, 30(1): 31-55.
- van Ballegooy S, Cox SC, Thurlow C, Rutter HK, Reynolds T, Harrington G, Fraser J, and Smith T. 2014b. Median water table elevation in Christchurch and surrounding area after the 4 September 2010 Darfield earthquake: Version 2, *GNS Science Report 2014/18*, 2014b.
- Yoshimine M, Nishizaki H, Amano K, Hosono Y. 2006. Flow deformation of liquefied sands under constant shear load and its application to analysis of flow slide in infinite slope. *SDEE*, 26: 253-264.
- Zhang G, Robertson PK, Brachman R. 2002. Estimating Liquefaction Induced Ground Settlements from CPT, *Canadian Geotechnical Journal*, 39: 1168-1180.

Tables

Table 6.1 Summary of ε_v estimation methods to be assessed in the LSN framework.

ID	Derived from Ishihara & Yoshimine 1992	$D_r - q_{c1N}$ Correlation Utilized	Function(s)
S1	✓	Eq. (2)	Zhang et al. 2002
S2	✓	Eq. (3); C = 0.9	Available on request (a la Zhang et al. 2002)
S3	✓	Eq. (3); C = 0.9	Yoshimine et al. 2006
S4	✓	Eq. (3); C = 0.64	Yoshimine et al. 2006
S5	✓	Eq. (3); C = 1.55	Yoshimine et al. 2006
C1	✗	N/A	$\varepsilon_v (\%) = \begin{cases} 1 & \text{for } FS_{liq} < 1 \\ 0 & \text{for } FS_{liq} \geq 1 \end{cases}$

Figures

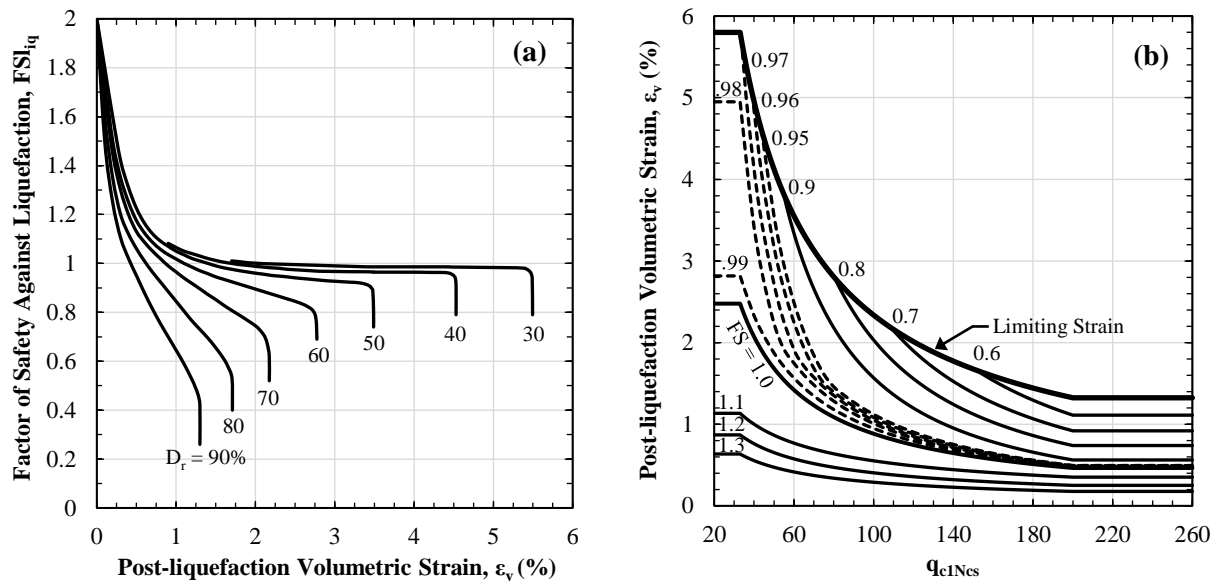


Figure 6.1 (a) Curves for estimating post-liquefaction volumetric-strain (ϵ_v) as a function of the factor of safety against liquefaction (FS_{liq}) and initial relative density (D_r) (after Ishihara and Yoshimine 1992); (b) curves derived from (a) for estimating ϵ_v as a function of FS_{liq} and equivalent clean sand normalized CPT tip resistance (q_{c1Ncs}), as proposed by Zhang et al. (2002) utilizing Equation (2), with curves added for this study (after Zhang et al. 2002).

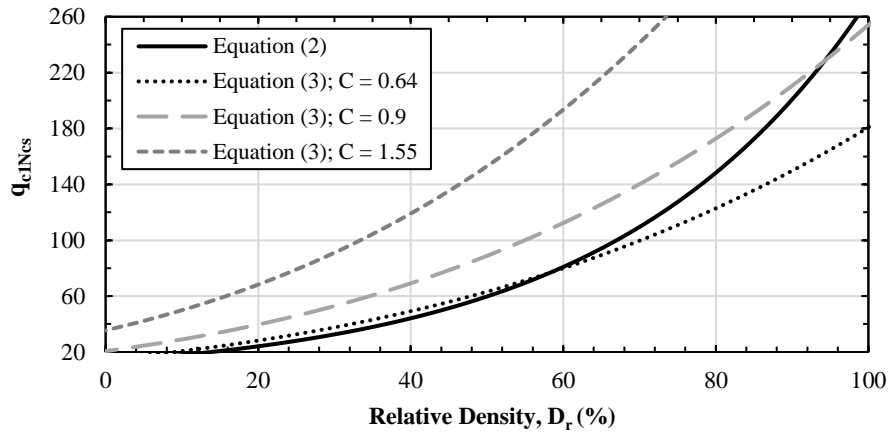


Figure 6.2 Correlations relating equivalent clean sand normalized CPT tip resistance (q_{c1Ncs}) to relative density (D_r).

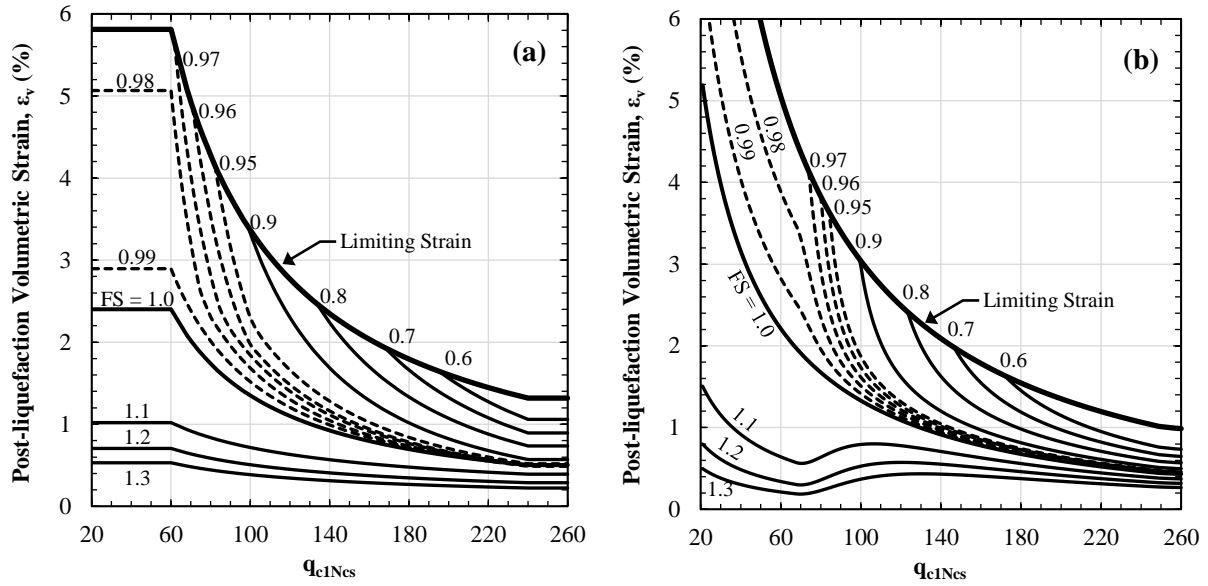


Figure 6.3 Curves derived from Figure 1a for estimating post-liquefaction volumetric-strain (ϵ_v) as a function of the factor of safety against liquefaction (FS_{liq}) and equivalent clean sand normalized CPT tip resistance (q_{c1Ncs}), herein developed utilizing Equation (3) with $C = 0.9$: (a) in the style of Zhang et al. (2002); and (b) using approximate, continuous solutions proposed by Yoshimine et al. (2006).

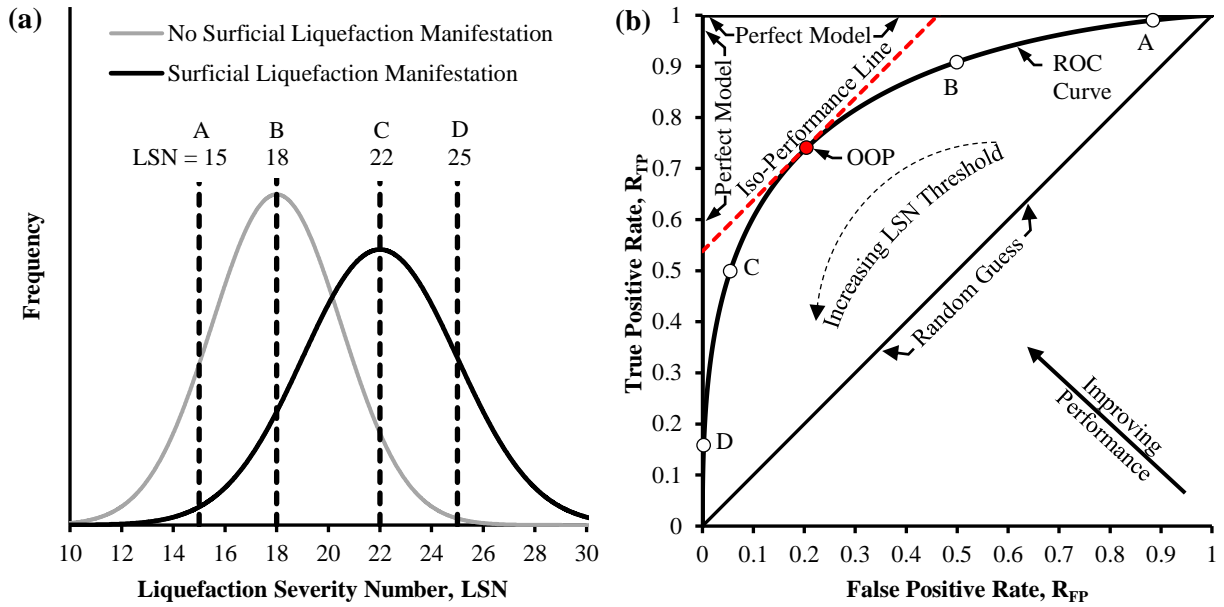


Figure 6.4 ROC analyses: (a) frequency distributions of liquefaction manifestation and no liquefaction manifestation as a function of LSN; (b) corresponding ROC curve, and illustration of how a ROC curve is used to assess the efficiency of a diagnostic test. The optimum operating point (OOP) indicates the LSN decision threshold for which the rate of misprediction is minimized.

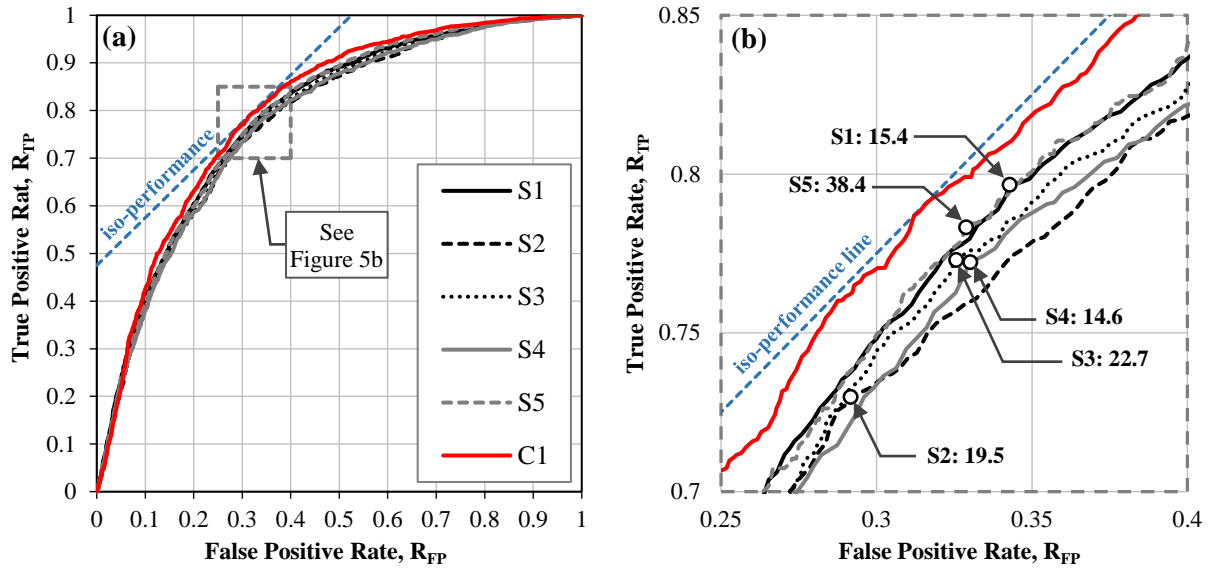


Figure 6.5 (a) ROC analyses of six LSN variants in predicting liquefaction likely to cause damage; (b) magnified view of optimal-performance area, wherein optimal LSN thresholds are identified for S1 through S5.

Chapter 7: Deterministic and Probabilistic Correlations for Predicting Liquefaction Susceptibility and Fines Content: A Study of the Cone Penetration Test in Christchurch, New Zealand

Brett W. Maurer¹, Russell A. Green², and Sjoerd van Ballegooy³

¹ Graduate Research Assistant, Dept. of Civil and Environmental Engineering, Virginia Tech, Blacksburg, Virginia 24061, U.S.A.

² Professor, Dept. of Civil and Environmental Engineering, Virginia Tech, Blacksburg, Virginia 24061, U.S.A.

³ Technical Director, Tonkin & Taylor Ltd, Auckland, New Zealand

7.1 Abstract

Continuous soil sampling is often impractical for liquefaction hazard assessments using the cone penetration test (CPT). The need thus arises to infer soil properties from CPT data without physical confirmation. Utilizing an unprecedented database of field and laboratory test data from Christchurch, New Zealand, this study proposes deterministic and probabilistic correlations relating the soil behavior type index (I_c) to liquefaction susceptibility and fines content; the relationship between I_c and USCS classification is also investigated. The findings presented herein represent an extensive case study of CPT-based soil characterization and are particularly pertinent to liquefaction-related research using data from Christchurch. Moreover, the approach demonstrated herein to develop deterministic and probabilistic I_c correlations is not limited to parts of New Zealand, but rather, can be applied worldwide.

7.2 Introduction

The undrained cyclic strength of soil is a critical input for assessing liquefaction hazard and can be measured directly from advanced laboratory tests (e.g., cyclic triaxial tests; cyclic simple shear tests) on high-quality undisturbed samples. However, owing to the difficulty and expense of obtaining and testing such samples, this approach is reserved for exceptional hazard assessments with compelling misprediction costs; even then, differences between field and laboratory conditions obfuscate the interpretation of test results.. The pragmatic and economic benefits of approaches based on in-situ tests measurements are thus widely recognized, as evidenced by the popularity of liquefaction evaluation procedures based on the standard penetration test (SPT), cone penetration test (CPT), and shear wave velocity (V_s). Using these procedures, a soil's cyclic strength is correlated to an in-situ parameter (e.g., SPT blow count), and the potential for liquefaction triggering is evaluated using the “simplified” stress-based framework initiated originally proposed by Whitman (1971) and Seed and Idriss (1971). Attributable to their relative simplicity and low cost, these procedures play a central role in today's state-of-practice approach to assessing liquefaction hazard.

While the SPT was the in-situ test used first in developing liquefaction correlations, the CPT has several advantages (e.g., near-continuous data sampling; repeatability; economic efficiency) that have made it a preferred in-situ test method in certain geomorphic settings. For example, following damaging liquefaction in Christchurch, New Zealand, induced by the 2010 - 2011 Canterbury earthquake sequence (CES) (e.g., Green et al., 2011; Wotherspoon et al., 2011; Bray et al., 2014;

Cubrinovski et al., 2014), an extensive geotechnical characterization program was initiated to assess regional liquefaction hazards and inform land-use planning. An unprecedented number of CPT soundings were performed in the affected region (presently in excess of 22,000) and compiled in the Canterbury Geotechnical Database (CERA, 2013). A beneficial consequence of the CES, this database has spawned numerous studies on CPT-based liquefaction hazard assessment and will play a transformative role in geotechnical research for many years.

Notwithstanding its popularity, challenges unique to the CPT persist in today's practice, introducing uncertainties to CPT-based analyses. Namely, because soil samples are not recovered during CPT sounding, soils are often not characterized directly or tested further in the laboratory. While discrete, disturbed soil specimens may be obtained selectively using a CPT-push sampler at sounding sites (Robertson, 2009), continuous sampling is impractical for studies involving many sites. For this reason, the need arises to infer certain soil properties and behaviors from CPT data without physical confirmation, to include soil type/classification; fines content (*FC*); and susceptibility to liquefaction.

For each of these closely related inferences, the state-of-practice approach relies on the soil behavior type index (I_c), defined as (Robertson and Wride, 1998):

$$I_c = \sqrt{(3.47 - \log_{10} Q)^2 + (1.22 + \log_{10} F)^2} \quad (1)$$

where Q and F are the normalized CPT penetration resistance and normalized CPT friction ratio, respectively. First proposed by Jeffries and Davies (1993) to define soil type boundaries, I_c was subsequently modified by Robertson and Wride (1998) to better fit the Robertson (1990) $Q - F$ classification scheme, with the latter version becoming widely used in practice. However, because the CPT is affected by many factors influencing soil behavior, such as soil plasticity, sensitivity, mineralogy, friction angle, age, cementation, and stress history (Robertson, 1990), the relationship between I_c and soil type is approximate and regionally dependent. I_c correlations derived from global data could therefore perform poorly on local scales, to include correlations relating I_c to liquefaction susceptibility and *FC*. The applicability of such correlations to regional datasets, such as that compiled after the CES, should therefore be evaluated, and the correlations calibrated as necessary. Moreover, to assess liquefaction hazards in a fully probabilistic manner, the uncertainties of inferred soil properties must also be known.

Accordingly, this study investigates CPT-based soil characterization in Christchurch, New Zealand, with emphasis on obtaining accurate inputs for liquefaction hazard assessment. In particular, deterministic and probabilistic I_c correlations are developed for predicting liquefaction susceptibility and FC . To assess the potential benefits of regional calibration, the proposed Christchurch-specific functions are compared to general correlations common in practice. This paper adds an extensive case study to the CPT-based soil characterization literature and is particularly pertinent to liquefaction-related research using data from the CES. In this regard, homage is owed to the many individuals providing data to the Canterbury Geotechnical Database, and to Robinson et al. (2013), Lees et al. (2015), and Leeves et al. (2015) for their seminal research on I_c correlations in Christchurch. Moreover, the approach demonstrated herein to develop deterministic and probabilistic I_c correlations is not limited to parts of New Zealand, but rather, can be applied worldwide. In the following, the role of I_c correlations in CPT-based liquefaction hazard assessment is first reviewed. The field and laboratory data used herein are then discussed, followed by the development of the deterministic and probabilistic correlations.

7.3 Background: Role of I_c Correlations in CPT-Based Liquefaction Hazard Assessment

Antecedent to using any CPT-based liquefaction evaluation procedure (e.g., Robertson and Wride, 1998; Moss et al., 2006; Boulanger and Idriss, 2014), liquefaction-susceptible soils must first be identified. In short, these procedures are intended to evaluate the potential for liquefaction triggering in sand-like soils susceptible to liquefaction, as it is “classically” defined. They should not be applied to high plasticity, fine grained, “non-liquefiable” soils, which could result in less accurate liquefaction hazard assessments (Maurer et al., 2015a), and for which more appropriate methods exist to predict cyclic shear strains (e.g., Boulanger and Idriss, 2007). However, because existing CPT-based procedures are not explicitly designed to screen for applicable soils, towards this end, an $I_c = 2.6$ threshold is commonly used for this purpose, such that soils with $I_c < 2.6$ are inferred to be liquefiable (Robertson and Wride, 1998). But, however, because I_c boundaries between soil types are approximate and may need regional refinement (e.g., Yi, 2014), the $I_c < 2.6$ criterion may in some cases be inappropriate (e.g., Zhang et al., 2002; Li et al., 2007; Pease et al., 2010). For this reason, Youd et al. (2001) recommended that soils with $I_c > 2.4$ be sampled and tested to evaluate their susceptibility.

Alternatively, researchers have proposed susceptibility criteria based on Atterberg limits. These criteria provide a more advanced screening tool, following which the potential benefits of cyclic

laboratory testing can be evaluated. Four such criteria applicable to data available from the CES will be investigated:

- 1) Polito (2001) proposed that soils with (i) $PI < 7$ and (ii) $LL < 25$ are liquefiable, where LL and PI are the liquid limit and plasticity index, respectively; soils with (i) $7 < PI < 10$ and (ii) $25 < LL < 35$ are potentially liquefiable and require further testing; and soils whose properties lie outside these bounds are susceptible to cyclic mobility only.
- 2) Seed et al. (2003) proposed that soils with (i) $PI \leq 12$ and (ii) $LL \leq 37$ are potentially liquefiable if $w_n / LL > 0.8$, where w_n is the natural moisture content; soils with (i) $PI \leq 20$ and (ii) $LL \leq 47$ are transitional and require further testing if $w_n / LL > 0.85$, and soils whose properties lie outside these bounds are not susceptible to liquefaction but may be vulnerable to strength loss.
- 3) Bray and Sancio (2006) proposed that soils with (i) $PI < 12$ and (ii) $w_n / LL > 0.85$ are susceptible to liquefaction; soils with (i) $12 < PI < 18$ and (ii) $w_n / LL > 0.8$ may be moderately susceptible to liquefaction and require further testing; and soils whose properties fall outside these bounds are not susceptible to liquefaction but may undergo deformation.
- 4) Boulanger and Idriss (2006) proposed that soils with $PI < 3$ have sand-like behavior; soils with $PI \geq 7$ have clay-like behavior, but if a soil classifies as CL-ML according to the Unified Soil Classification System (USCS) (ASTM D-2487), this criterion may be reduced to $PI \geq 5$; and soils with $3 < PI < 6$ may exhibit intermediate behavior and should be tested further.

The Polito (2001), Seed et al. (2003), Bray and Sancio (2006), and Boulanger and Idriss (2006) criteria are henceforth referred to as P01, SEA03, B&S06, and B&I06, respectively, and are illustrated in Figure 1. Notably, the terminologies and definitions used to characterize liquefaction susceptibility vary among authors, which may in part explain differences between these proposed criteria (Armstrong and Malvick, 2014; Green and Ziotopoulou, 2015). Nonetheless, it has been argued that I_c thresholds be discontinued in favor of Atterberg-limit criteria (and/or cyclic strength tests), which provide a more direct characterization of soil behavior. However, continuous sampling and testing is prohibitively expensive for many CPT-based studies most projects, including hazard assessments with low misprediction-costs and those involving many sites. The use of I_c , calibrated against Atterberg-limit criteria via select sampling, would be significantly less costly. This study investigates the efficacy of using such an approach.

Once liquefaction-susceptible soils are identified (e.g., $I_c < 2.6$), the liquefaction evaluation procedures used in today's practice apply correction factors to adjust computed liquefaction resistance for the quantity and/or nature of fines in the soil. Of these procedures, the Idriss and Boulanger (2008) procedure has performed better in analyzing data from the CES (Green et al., 2014; van Ballegooy et al., 2014a; Maurer et al., 2015a,b) and is thus recommended by New Zealand Ministry of Business, Innovation, and Employment guidelines (MBIE, 2015). Because FC is a required input to the Idriss and Boulanger (2008) fines-correction, $I_c - FC$ correlations are typically used to estimate FC throughout the soil profile. The efficacy of liquefaction hazard assessment could thus depend on the suitability of the selected correlation.

7.4 Field and Laboratory Testing

Following the Canterbury earthquake sequence, an unprecedented geotechnical investigation was initiated. A subset of the resulting data is utilized to investigate CPT-based soil characterization. This data is comprised of (a) standard penetration test (SPT) borings performed at 825 sites throughout Christchurch, from which 2,620 SPT samples were obtained in the split-spoon sampler; (b) laboratory measurements performed on each SPT sample, to include FC , LL , PI , and w_n ; and (c) CPT soundings performed adjacent to each of the 825 SPTs. With respect to (b), Atterberg Limits were measured determined for 2,097 of the 2,620 samples collected. All field and laboratory data was were obtained from the Canterbury Geotechnical Database (CERA, 2013). The near-continuous nature of CPT sounding data (i.e., 1 or 2 cm measurement intervals) can result in significant changes in the measured I_c over short depth intervals. Accordingly, to study relationships between I_c and laboratory measurements, the measured I_c was averaged over a 300 mm depth interval, centered on the midpoint of the split-spoon SPT sample. In addition, samples with large variation in I_c were identified by computing the standard deviation (σ) of I_c within the SPT sample interval was computed to identify data with large uncertainty. Example FC and I_c profiles from a site in Christchurch are shown in Figure 2. The locations of all test sites are mapped later in this paper (Figure 9).

7.5 Predicting Liquefaction Susceptibility from I_c

7.5.1 Deterministic Correlations

This study seeks to determine (a) how well the I_c index segregates soils susceptible to liquefaction from soils unsusceptible to liquefaction, as defined by the P01, SEA03, B&S06, and B&I06 criteria (i.e., the degree to which I_c is correlated to these criteria); and (b) the I_c thresholds, or cutoffs, at

which the efficiencies of these segregations are optimized. To make these determinations, a standard analysis is needed to assess the performance of diagnostic tests. Receiver operating characteristic (ROC) analyses are herein adopted for this purpose. ROC analyses have been widely used to study the performance of classifier systems, including extensive use in medical diagnostics (e.g., Zou, 2007), but by comparison, their use in geotechnical engineering is limited (Chen et al., 2007; Oommen et al., 2010; Maurer et al., 2015a; Zhu et al., 2015). In any ROC curve application, the distributions of “positives” (e.g., soil is susceptible to liquefaction) and “negatives” (e.g., soil is unsusceptible to liquefaction) overlap when the frequency of the distributions are expressed as a function of index test results (e.g., I_c values). In such cases, optimal decision thresholds for the index test are selected considering the rates of true positives (R_{TP}) (e.g., susceptibility is observed, as predicted) and false positives (R_{FP}) (e.g., susceptibility is predicted, but is not observed). Setting the threshold too high will result in a higher R_{FP} , the cost of which could be excessive spending on site remediation. Conversely, setting the threshold too low results in a higher rate of false negatives (e.g., liquefaction is observed when it is predicted not to occur), the cost of which is liquefaction-induced damage. Thresholds should thus be selected to minimize these costs.

ROC curves plot R_{TP} versus R_{FP} for varying threshold values. Figures 3a and 3b illustrate the relationship among the positive and negative distributions, the threshold value, and the ROC curve. Figure 3b also illustrates how a ROC curve is used to assess the efficiency of a diagnostic test and select an optimum threshold. In ROC space, random guessing is indicated by a 1:1 line through the origin (i.e., equivalent number of correct and incorrect predictions), while a perfect model plots as a point at (0,1), indicating the existence of a threshold value which perfectly segregates the dataset (e.g., all soils susceptible to liquefaction have I_c below the threshold; all soils unsusceptible to liquefaction have I_c above the threshold). While no single parameter can fully characterize model performance, the area under a ROC curve (AUC) is commonly used for this purpose, where AUC is statistically equivalent to the probability that “positives” have higher index test values than “negatives” (e.g., Fawcett 2005). As such, increasing AUC indicates better model performance. The optimum decision threshold is defined herein as the threshold which minimizes the rate of misprediction [i.e., $R_{FP} + (1 - R_{TP})$]. As such, contours of the quantity [$R_{FP} + (1 - R_{TP})$] map points of equivalent performance in ROC space, as shown in Figure 3b. Notably, this definition implicitly treats the costs of false positives and false negatives to be approximately equal. For further overview of ROC analyses, and for demonstration of how project-specific misprediction consequences can be incorporated into ROC analyses, the reader is referred to Fawcett (2005) and Maurer et al. (2015c).

Using the approach described above, ROC analyses were performed to determine how well the I_c index correlates to liquefaction susceptibility, as defined by criteria based on Atterberg limits. Soil samples were first classified by the P01, SEA03, B&S06, and B&I06 criteria as “susceptible,” “unsusceptible,” or “transition (test).” However, as previously discussed, the exact terminologies proposed by these criteria vary, as do the definitions they adopt for classifying soil behavior. For example, in lieu of “susceptible” vs “unsusceptible,” the B&I06 criteria classifies soil as having “sand-like” vs “clay-like” response to cyclic loading. Thus, while a unified terminology is adopted herein for simplicity, it should be understood, for example, that “susceptible” refers to a more nuanced, criteria-specific definition. Shown in Figure 4 are frequency distributions of the 2,097 classified samples, plotted as a function of measured I_c . ROC analyses of the “susceptible” and “unsusceptible” distributions are plotted in Figure 5. It can be seen that the performance of I_c in assessing liquefaction-susceptibility is similar using any of the four criteria, with AUC ranging from 0.89 (SEA03) to 0.92 (B&I06) (i.e., there is about a 90% probability that the measured I_c of an “unsusceptible” soil is greater than that of a “susceptible” soil). In other words, I_c is well-correlated to the Atterberg-limit criteria, with B&I06 exhibiting the strongest correlation.

As highlighted in Figures 4 and 5, the optimal I_c thresholds corresponding to the P01, SEA03, B&S06, and B&I06 criteria are 2.55, 2.60, 2.75, and 2.50, respectively, which are generally consistent with common I_c criteria used in practice. However, it should be recognized that these thresholds are those minimizing the misprediction rate and are only optimal if false positives and false negatives have equal cost. That is to say, the proposed thresholds are not conservative in nature. For example, if the costs of false negatives were instead greater than the costs of false positives, the optimum I_c threshold would increase in response. Operating at their respective optimal thresholds, the I_c classifiers have overall accuracy (OA) ranging from 0.76 (SEA03) to 0.86 (B&I06), where OA indicates the percentage of samples correctly classified. The superior performance of B&I06 should not be interpreted to mean that it is more appropriate for assessing liquefaction susceptibility, but rather, that it better correlates to I_c . It should be emphasized that while Atterberg-limit criteria offer a more direct characterization of soil behavior, they are not a definitive test of susceptibility. Ideally, more-advanced laboratory tests would also be performed to corroborate or re-calibrate susceptibility thresholds; this will be done in Christchurch as results become available. Nonetheless, these analyses suggest that I_c can be an efficient and cost-effective index of liquefaction-susceptibility.

7.5.2 Probabilistic Correlations

To assess liquefaction hazards in a fully probabilistic manner, the probability of liquefaction-susceptibility should be adequately accounted for. A probabilistic correlation is developed herein using an approach similar to that described by Porter et al. (2007) to create fragility functions for performance-based earthquake engineering. While the adopted approach is outlined below, the reader is referred to Porter et al. (2007) for complete details.

The probability that a soil is “unsusceptible” to liquefaction, given a measured I_c value, is denoted by $F_{unsusceptible}(I_c)$ and idealized by a log-normal distribution:

$$F_{unsusceptible}(I_c) = \Phi \left[\frac{\ln\left(\frac{I_c}{x_m}\right)}{\beta} \right] \quad (2)$$

where Φ denotes the Gaussian cumulative distribution function; x_m is the median value of the distribution, and β is the logarithmic standard deviation. The probability that a soil is “susceptible” to liquefaction, denoted as $F_{susceptible}(I_c)$, is then given by:

$$F_{susceptible}(I_c) = 1 - F_{unsusceptible}(I_c) \quad (3)$$

The data are first placed in bins of similar I_c , where each bin contains approximately the same number of samples. For each bin, the fraction of “unsusceptible” soils and bin-averaged I_c are computed. Eq. 2 is then converted to a linear regression problem by taking the inverse Gaussian cumulative distribution function of each side of the equation; x_m and β can be determined by fitting a line $y = mx + b$ to the resulting data:

$$\beta = \frac{1}{m} = \left(\sum_{j=1}^N (x_j - \bar{x})^2 \right) / \left(\sum_{j=1}^N (x_j - \bar{x})(y_j - \bar{y}) \right)$$

$$x_m = \exp(-b\beta) = \exp(\bar{x} - \bar{y}\beta) \quad (4)$$

In Eq. 4, N is the total number of bins; j is the bin number; x_j is the natural logarithm of the average I_c value in bin j ; \bar{x} is the average x_j across all bins; and \bar{y} is the average y_j among all bins, where y_j is given by:

$$y_j = \Phi^{-1}\left(\frac{m_j+1}{M_j+1}\right) \quad (5)$$

In Eq. 5, m_j and M_j are respectively the number of “unsusceptible” samples, and total samples, in bin j ; 1 is added to the numerator and denominator to handle bins in which all samples are “susceptible.” The coefficients β and x_m may be solved either directly by Eq. 4, or by plotting x_j vs. y_j and fitting a trendline; β is the inverse of the trendline slope, and x_m is the I_c value at which the line has a y of zero (i.e., $x_m = e^{-b/m}$).

Using the approach outlined above, probabilistic correlations were developed from the “susceptible” and “unsusceptible” distributions shown in Figure 4. The resulting functions are plotted in Figure 6 and defined by Eqs. 2 and 3 in conjunction with the criteria-specific coefficients in Table 1. The proposed functions allow for the uncertainty of whether a soil is susceptible to liquefaction to be incorporated into fully probabilistic hazard assessments. It can be seen from Figure 6 that the I_c values corresponding to a 50% probability of susceptibility are approximately equal to the deterministic thresholds developed from ROC analysis. For I_c thresholds traditionally used in practice (i.e., $2.4 \leq I_c \leq 2.6$), the probability of susceptibility ranges from 0.60 (B&I06) to 0.78 (B&S04) at $I_c = 2.4$, and from 0.40 (B&I06) to 0.61 (B&S04) at $I_c = 2.6$. It can therefore be expected that the rates of false positives and false negatives will be roughly equal using thresholds in this range. As with the deterministic approach, it should be emphasized that Atterberg-limit criteria are not a definitive test of susceptibility. Ideally, cyclic laboratory tests would also be used to classify susceptibility and develop I_c functions

7.6 Predicting FC from I_c

7.6.1 Deterministic and Probabilistic Correlations

Plotted in Figure 7 are I_c vs. FC data from 2,620 soil samples, from which a Christchurch-specific correlation is developed using the classical (Eisenhart, 1939) approach to calibration and the least squares estimator of a linear model having the form:

$$FC = \beta_0 + \beta_1 I_c + \varepsilon \quad (6)$$

In Eq. 6, FC and I_c are as previously defined; β_0 and β_1 are regression coefficients; and ε is a random error term. With the goal of developing an unbiased model (i.e., one for which prediction errors

sum to zero), ε is assumed to have an approximately normal distribution about the mean prediction. The standard deviation of ε (σ_ε) is unknown, however, and is thus estimated by the residual standard error. The resulting Christchurch-specific correlation is given by Eq. 7.

$$\mu_{FC} = 80.645 I_c - 128.5967 \quad (7)$$

where μ_{FC} is the mean estimate of FC (%), limited to $0 \leq FC \leq 100$, and I_c is as previously defined. The uncertainty in this prediction, represented by the standard deviation of ε , is $\sigma_\varepsilon = 16.56$. This indicates that approximately 68% of the samples have FC within ± 16.56 of the mean prediction (Eq. 7); approximately 95% have FC within ± 33.1 of this prediction. The proposed mean, $\pm 1\sigma$, and $\pm 2\sigma$ correlations are plotted in Figure 7a.

To demonstrate potential uses of the proposed correlation, two example cases are given below. For each case, an I_c measurement of 2.05 has been obtained from CPT sounding data in a given soil stratum. From Eq. 4, the mean (i.e., deterministic) estimate of FC is 36.73%.

- Case I: When performing fully probabilistic liquefaction hazard assessments, it may be desirable to account for the uncertainty in the estimated FC . Using such an approach in conjunction with the total probability theorem, the probabilities of various FC intervals can be computed from a Gaussian probability density function. As an example, the probability of the soil stratum having $49.5\% \leq FC \leq 50.5\%$ is estimated to be 0.0175, as illustrated by Eq. 8, for which the corresponding Microsoft Excel command is also given.

$$P (FC = 50) = \varphi_{FC} \left[\frac{50-36.73}{16.56} \right] = \text{NORM.DIST} (50, 36.73, 16.56, \text{FALSE}) = 0.0175 \quad (8)$$

- Case II: For soil classification or other probabilistic applications, it may be desirable to compute the probability of the FC being less than or greater than a particular value. In this case, the desired probabilities are computed from a Gaussian cumulative distribution function. As an example, the probability of the soil stratum having $FC \leq 50\%$ (i.e., a coarse-grained soil) is estimated to be 0.7886, as illustrated by Eq. 9, for which the corresponding Microsoft Excel command is also given.

$$P (FC \leq 50) = \Phi_{FC} \left[\frac{50-36.73}{16.56} \right] = \text{NORM.DIST} (50, 36.73, 16.56, \text{TRUE}) = 0.7886 \quad (9)$$

In Figure 7b, the mean Christchurch-specific $I_c - FC$ correlation is compared with the Robertson and Wride (1998) and Boulanger and Idriss (2014) general correlations developed from global data. The Robertson and Wride (1998) correlation is defined by Eq. 10 and has been widely used since its inception:

$$FC = 1.75 I_c^{3.25} - 3.7 \quad (10)$$

The Boulanger and Idriss (2014) correlation is defined by Eq. 8 and was developed largely from liquefaction case history data:

$$FC = 80 (I_c + C_{FC}) - 137 \quad (11)$$

In Eq. 11, C_{FC} is a calibration parameter, such that the general correlation (i.e., $C_{FC} = 0$) may be calibrated to site- or region-specific conditions. The Boulanger and Idriss (2014) correlation thus recognizes the uncertainty of global correlations and the need for site-specific $I_c - FC$ investigations. On this note, Eq. 7 may be closely approximated using $C_{FC} = 0.13$ in Eq. 11. To compare the performance of the three correlations shown in Figure 7b, the Nash-Sutcliffe model efficiency coefficient, E , is adopted. Commonly used in hydrology, the Nash-Sutcliffe efficiency is defined as (Nash and Sutcliffe, 1970):

$$E = 1 - \frac{\sum_{i=1}^n (O_i - P_i)^2}{\sum_{i=1}^n (O_i - \bar{O})^2} \quad (12)$$

where O_i and P_i are the measured and predicted values of FC , respectively; \bar{O} is the mean of the measured values of FC ; and n is the number of data points (2,620). An efficiency of 1.0 indicates a perfect model, while an efficiency less than zero indicates that the mean FC of the dataset (30.2) would have been a better predictor than the correlation. For the compiled dataset, the Christchurch-specific, Boulanger and Idriss (2014), and Robertson and Wride (1998) correlations have efficiencies of 0.69, 0.66, and 0.37, respectively. Thus, estimates of FC inferred from measurements of I_c may be significantly more accurate using regional correlations.

Though not a direct requirement for assessing liquefaction hazard, closely related to the prediction of FC from CPT data is the prediction of soil classification, often of general interest to geotechnical

engineers. Of the 2,620 soil samples collected, 2,097 had sufficient data to be classified in accordance with the Unified Soil Classification System (USCS) (ASTM D2487). In Figure 8, samples are grouped by USCS classification and plotted in terms of I_c vs. FC . To determine approximate, Christchurch-specific I_c boundaries between soil types, ROC analyses were performed on three pairs of sample data. The three I_c transitions investigated: (1) clean or borderline-clean sands to silty or clayey sands; (2) silty or clayey sands to ML or OL soils; and (3) ML or OL soils to CL-ML, CL, MH, or OH soils. The results of these analyses, summarized in Table 2, indicate the above transitions occur at approximate I_c values of 1.8, 2.0, and 2.5, respectively. Furthermore, the measured AUC values indicate that I_c is relatively effective in segregating fine grained soils from coarse grained soils, but less effective in discriminating more nuanced classification changes within these groups (e.g., ML vs. CL).

Plotted in Figure 9 (a-e) are the locations of all SPT samples classified per the USCS and parsed by soil type. In Figure 9f, the approximate Christchurch-specific I_c boundaries discussed above are used in conjunction with 3,500 CPT soundings to produce a continuous map of surficial soils. This characterization is made using the average I_c value for the uppermost 10 m of each soil profile, termed I_{c10} . It can be seen in Figure 9f that a spatial correlation exists among soil types, such that soils with higher I_{c10} are generally found in the western (i.e., inland) half of the study area, reflecting the extents of mid-Holocene coastal transgression, as well as the unique sediment lithology found near the Port Hills (Brown et al., 1995). For further discussion of Christchurch's surface geology and its relationship with liquefaction hazard, the reader is referred to Maurer et al. (2014).

7.7 Conclusions

Utilizing an unprecedented database of field and laboratory test data, this study investigated CPT-based soil characterization in Christchurch, New Zealand, with emphasis on obtaining accurate inputs for liquefaction hazard assessment. In particular, deterministic and probabilistic I_c correlations were developed for predicting liquefaction susceptibility and FC from CPT data. To predict liquefaction susceptibility, deterministic I_c thresholds of 2.55, 2.60, 2.75, and 2.50 were proposed for the P01, SEA03, B&S06, and B&I06 susceptibility criteria, respectively. Probabilistic correlations were proposed in Eqs. 2 and 3, and are plotted in Figure 6. The proposed deterministic thresholds approximately correspond to a 50% probability that the tested soil is liquefaction-susceptible. To predict FC , Eq. 7 can be used both deterministically and probabilistically. The proposed correlation is plotted in Figure 7 and scenarios demonstrating its use were presented. The

correlations developed in this study are particularly pertinent to liquefaction-related research derived from the Canterbury Earthquakes, which will play a transformative role in geotechnical research for many years. However, the methods demonstrated herein to develop deterministic and probabilistic correlations are not limited to parts of New Zealand, but rather, can be applied worldwide.

7.8 Acknowledgements

This study is based on work supported by the U.S. National Science Foundation (NSF) grants CMMI-1030564 and CMMI-1306261, and US Army Engineer Research and Development Center (ERDC) grant W912HZ-13-C-0035. The authors also acknowledge the the Canterbury Geotechnical Database and its sponsor EQC for providing the geotechnical data used in this study. However, any opinions, findings, and conclusions or recommendations expressed in this paper are those of the authors and do not necessarily reflect the views of NSF, ERDC, or EQC.

Notice

Some of the data used in this study was extracted from the Canterbury Geotechnical Database (<https://canterburygeotechnicaldatabase.projectorbit.com>), which was prepared and/or compiled for the Earthquake Commission (EQC) to assist in assessing insurance claims made under the Earthquake Commission Act 1993 and/or for the Canterbury Geotechnical Database on behalf of the Canterbury Earthquake Recovery Authority (CERA). The source maps and data were not intended for any other purpose. EQC, CERA, and their data suppliers and their engineers, Tonkin & Taylor, have no liability for any use of these maps and data or for the consequences of any person relying on them in any way.

References

- Armstrong, R.J. and Malvick, E.J. (2014). "Comparison Of liquefaction susceptibility criteria." *Dams and Extreme Events – Reducing Risk of Aging Infrastructure under Extreme Loading Conditions*. 34th Annual USSD Conference, San Francisco, California, April 7-11, 2014 29-38.
- Boulanger, R.W. and Idriss, I.M. (2006). "Liquefaction susceptibility criteria for silts and clays." *Journal of Geotechnical and Geoenvironmental Engineering*, 132(11): 1413-1426.
- Boulanger, R. W. and Idriss, I. M. (2007). "Evaluation of cyclic softening in silts and clays." *Journal of Geotechnical and Geoenvironmental Engineering*, 133(6): 641-652.

- Boulanger, R. W. and Idriss, I. M. (2014). "CPT and SPT based liquefaction triggering procedures." Report No. UCD/CGM-14/01, Center for Geotechnical Modeling, Department of Civil and Environmental Engineering, University of California, Davis, CA, 134 pp.
- Bray, J., Cubrinovski, M., Zupan, J., Taylor, M. (2014). "Liquefaction effects on buildings in the central business district of Christchurch." *Earthquake Spectra* 30(1): 85–109.
- Bray, J.D. and Sancio, R.B. (2006). "Assessment of the liquefaction susceptibility of fine-grained soils." *Journal of Geotechnical and Geoenvironmental Engineering*, 132(9): 1165-1177.
- Brown, L.J., Beetham, R.D., Paterson, B.R., Weeber, J.H. (1995). Geology of Christchurch. *New Zealand: Environmental and Engineering Geoscience* 427–88.
- CERA (2013). "Purpose and scope of the Canterbury geotechnical database." *Canterbury Earthquake Recovery Authority*; See: <https://canterburygeotechnicaldatabase.projectorbit.com>. Accessed 9/3/16.
- Chen, C.C., Tseng, C.Y, and Dong, J.J. (2007). New entropy-based method for variables selection and its application to the debris-flow hazard assessment. *Engineering Geology* 94: 19-26.
- Cubrinovski, M., Winkley, A., Haskell, J., Palermo, A., Wotherspoon, L., Robinson, K., et al. (2014). "Spreading-induced damage to short-span bridges in Christchurch, New Zealand." *Earthquake Spectra* 30(1): 57–83.
- Eisenhart, C. (1939). "The Interpretation of Certain Regression Methods and Their Use in Biological and Industrial Research." *The Annals of Mathematical Statistics* 10: 162-186.
- Fawcett, T. (2005). "An introduction to ROC analysis." *Pattern Recognition Letters* 27: 861-874.
- Green, R.A., Allen, A., Wotherspoon, L., Cubrinovski, M., Bradley, B., Bradshaw, A., et al. (2011). "Performance of levees (stopbanks) during the 4 September M_w 7.1 Darfield and 22 February 2011 M_w 6.2 Christchurch, New Zealand, earthquakes." *Seismological Research Letters* 82(6): 939–949.
- Green, R.A., Cubrinovski, M., Cox, B., Wood, C., Wotherspoon, L., Bradley, B., & Maurer, B. (2014). "Select Liquefaction Case Histories from the 2010-2011 Canterbury Earthquake Sequence." *Earthquake Spectra* 30(1): 131-153.
- Green, R.A. and Ziotopoulou, K. (2015). "Overview of screening criteria for liquefaction triggering susceptibility." *Proceedings of the 10th Pacific Conference on Earthquake Engineering*, Nov 6-8, Sydney, Australia. Australian Earthquake Engineering Society; Paper No. 35.
- Idriss, I.M. & Boulanger, R.W. (2008). "Soil liquefaction during earthquakes." Monograph MNO-12, Earthquake Engineering Research Institute, Oakland, CA, 261 pp.
- Jeffries, M.G., and Davies, M.P. (1993). "Use of CPTu to estimate equivalent SPT N_{60} ." *Geotechnical Testing Journal*, 16(4): 458-468.

- Li., D.K, Juang, C.H., Andrus, R.D., and Camp, W.M. (2007). "Index properties-based criteria for liquefaction susceptibility of clayey soils: a critical assessment." *Journal of Geotechnical and Geoenvironmental Engineering*, 133(1): 110-115.
- Lees, J., Van Ballegooy, S., and Wentz, F.J. (2015). "Liquefaction susceptibility and fines content correlations of the Christchurch soils." *Proceedings of the 6th International Conference on Earthquake Geotechnical Engineering*, Nov 2-4; Christchurch, New Zealand; Paper No. 491. International Society of Soil Mechanics and Geotechnical Engineering.
- Leeves, J., Van Ballegooy, S., Lees, J., and Wentz, F. (2015). "Effect of fines content correlations and liquefaction susceptibility thresholds on liquefaction consequence assessments." *Proceedings of the 6th International Conference on Earthquake Geotechnical Engineering*, Nov 2-4; Christchurch, New Zealand; Paper No. 491. International Society of Soil Mechanics and Geotechnical Engineering.
- Maurer, B.W., Green, R.A., Cubrinovski, M., & Bradley, B.A. (2014). Evaluation of the liquefaction potential index for assessing liquefaction hazard. *Journal of Geotechnical and Geoenvironmental Engineering* 140(7): 04014032.
- Maurer, B.W., Green, R.A., Cubrinovski, M., and Bradley, B. A. (2015a). "Fines-content effects on liquefaction hazard evaluation for infrastructure during the 2010-2011 Canterbury, New Zealand earthquake sequence." *Soil Dynamics and Earthquake Engineering*, Elsevier, 76: 58-68.
- Maurer, B.W., Green, R.A., Cubrinovski, M., and Bradley, B. A. (2015b). "Assessment of CPT-based methods for liquefaction evaluation in a liquefaction potential index (LPI) framework." *Geotechnique* 65(5): 328-336.
- Maurer, B.W., Green, R.A., Cubrinovski, M., and Bradley, B.A. (2015c). "Calibrating the liquefaction severity number (LSN) for varying misprediction economies: a case study in Christchurch, New Zealand." *Proceedings of the 6th International Conference on Earthquake Geotechnical Engineering*, Nov 2-4; Christchurch, New Zealand; Paper No. 491. International Society of Soil Mechanics and Geotechnical Engineering.
- MBIE (2015). "Repairing and rebuilding houses affected by the Canterbury earthquakes." Version 3a, Ministry of Business, Innovation, and Employment, Wellington, NZ.
- Moss, R.E.S, Seed, R.B., Kayen, R.E., Stewart, J.P., Der Kiureghian, A., & Cetin, K.O. (2006). "CPT-based probabilistic and deterministic assessment of in situ seismic soil liquefaction potential." *Journal of Geotechnical and Geoenvironmental Engineering* 132(8): 1032-1051.
- Nash, J.E. and Sutcliffe, J.V. (1970). "River flow forecasting through conceptual models part I -A discussion of principles." *Journal of Hydrology* 10(3): 282-290.

- Oommen T., Baise, L.G., and Vogel, R. (2010). "Validation and application of empirical liquefaction models." *Journal of Geotechnical and Geoenvironmental Engineering*, ASCE, 136: 1618-1633.
- Pease, J.W. (2010). "Misclassification in CPT liquefaction evaluation." *2nd International Symposium on Cone Penetration Testing*, Huntington Beach, CA, USA, May 2010, Paper # 3-23.
- Polito, C. (2001). "Plasticity Based Liquefaction Criteria." *Proceedings of the Fourth International Conference on Recent Advances in Geotechnical Earthquake Engineering and Soil Dynamics and Symposium in Honor of Professor W.D. Liam Finn*, San Diego, California, March 26-31, 2001. Paper 25.
- Porter, K., Kennedy, R., and Bachman, R. (2007). "Creating fragility functions for performance-based earthquake engineering." *Earthquake Spectra* 23(2): 471–489.
- Robertson, P.K. (1990). "Soil classification using the cone penetration test." *Canadian Geotechnical Journal* 27(1): 151-158.
- Robertson, P.K. (2009). "Interpretation of cone penetration tests - a unified approach." *Canadian Geotechnical Journal* 46: 1337-1355.
- Robertson, P.K. & Wride, C.E. (1998). "Evaluating cyclic liquefaction potential using cone penetration test." *Canadian Geotechnical Journal* 35 (3): 442-459.
- Robinson, K., Cubrinovski, M., and Bradley, B.A. (2013). "Sensitivity of predicted liquefaction-induced lateral displacements from the 2010 Darfield and 2011 Christchurch Earthquakes." *Proceedings of the New Zealand Society for Earthquake Engineering Annual Conference*, Wellington, New Zealand.
- Seed, R.B., Cetin, K.O., Moss, R.E.S., Kammerer, A.M., Wu, J., Pestana, J.M., Riemer, M.F., Sancio, R.B., Bray, J.D., Kayen, R.E., and Faris, A. (2003). "Recent advances in soil liquefaction engineering: a unified and consistent framework." *26th Annual ASCE Los Angeles Geotechnical Spring Seminar*, 30 April 2003, Long Beach, California.
- van Ballegooy, S., Malan, P., Lacrosse, V., Jacka, M.E., Cubrinovski, M., Bray, J.D., O'Rourke, T.D., Crawford, S.A., and Cowan, H. (2014a). "Assessment of liquefaction-induced land damage for residential Christchurch." *Earthquake Spectra*, 30(1): 31-55.
- Wotherspoon, L., Bradshaw, A., Green, R.A., Wood, C., Palermo, A., Cubrinovski, M., et al. (2011). "Performance of bridges during the 2010 Darfield and 2011 Christchurch earthquakes." *Seismological Research Letters* 82(6): 950–964.
- Yi, F. (2014). "Estimating soil fines contents from CPT data." *3rd International Symposium on Cone Penetration Testing*, Las Vegas, Nevada, USA.

- Whitman, R.V. (1971). "Resistance of soil to liquefaction and settlement." *Soils and Foundations* 11(4): 59-68.
- Seed, H.B. & Idriss, I.M. (1971). Simplified procedure for evaluating soil liquefaction potential. *Journal of the Soil Mechanics and Foundation Division* 97(9): 1249-1273.
- Youd, T.L., Idriss, I.M., Andrus, R.D., Arango, I., Castro, G., Christian, J.T., Dobry, R., Finn, W.D.L., Harder, L.F., Hynes, M.E., Ishihara, K., Koester, J.P., Liao, S.S.C., Marcuson, W.F., Martin, G.R., Mitchell, J.K., Moriwaki, Y., Power, M.S., Robertson, P.K., Seed, R.B., and Stokoe, K.H. (2001). "Liquefaction Resistance of Soils: Summary Report from the 1996 NCEER and 1998 NCEER/NSF Workshops on Evaluation of Liquefaction Resistance of Soils." *Journal of Geotechnical and Geoenvironmental Engineering*, 127(4): 297-313.
- Zhang, G., Robertson, P.K., and Brachman, R.W.I. (2002). "Estimating liquefaction-induced ground settlements from CPT for level ground." *Canadian Geotechnical Journal*, 39(5): 1168-1180.
- Zhu, J., Daley, D., Baise, L.G., Thompson, E.M., Wald, D.J., and Knudsen, K.L. (2015). "A Geospatial Liquefaction Model for Rapid Response and Loss Estimation." *Earthquake Spectra*, 31(3): 1813-1837.
- Zou, K.H. (2007). "Receiver operating characteristic (ROC) literature research." On-line bibliography available from: <<http://www.spl.harvard.edu/archive/spl-pre2007/pages/pppl/zou/roc.html>> accessed 10 March 2016.

Tables

Table 7.1 Criteria-specific coefficients for use in Eq 2.

Criteria	β	x_m
P01	0.1741	2.5646
SEA03	0.1982	2.6078
B&S04	0.1676	2.7295
B&I06	0.1658	2.5020

Table 7.2 Summary of ROC analyses to investigate I_c -based soil classification

USCS Soil Type Transition	Optimal I_c Threshold	Area Under ROC Curve (AUC)
Clean or Borderline Clean Sands ($FC < 12$) to Silty or Clayey Sands ($12 < FC < 50$)	1.8	0.783
Silty or Clayey Sands ($12 < FC < 50$) to ML or OL ($FC > 50$)	2	0.967
ML or OL to CL-ML, CL, MH, or OH	2.5	0.756

Figures

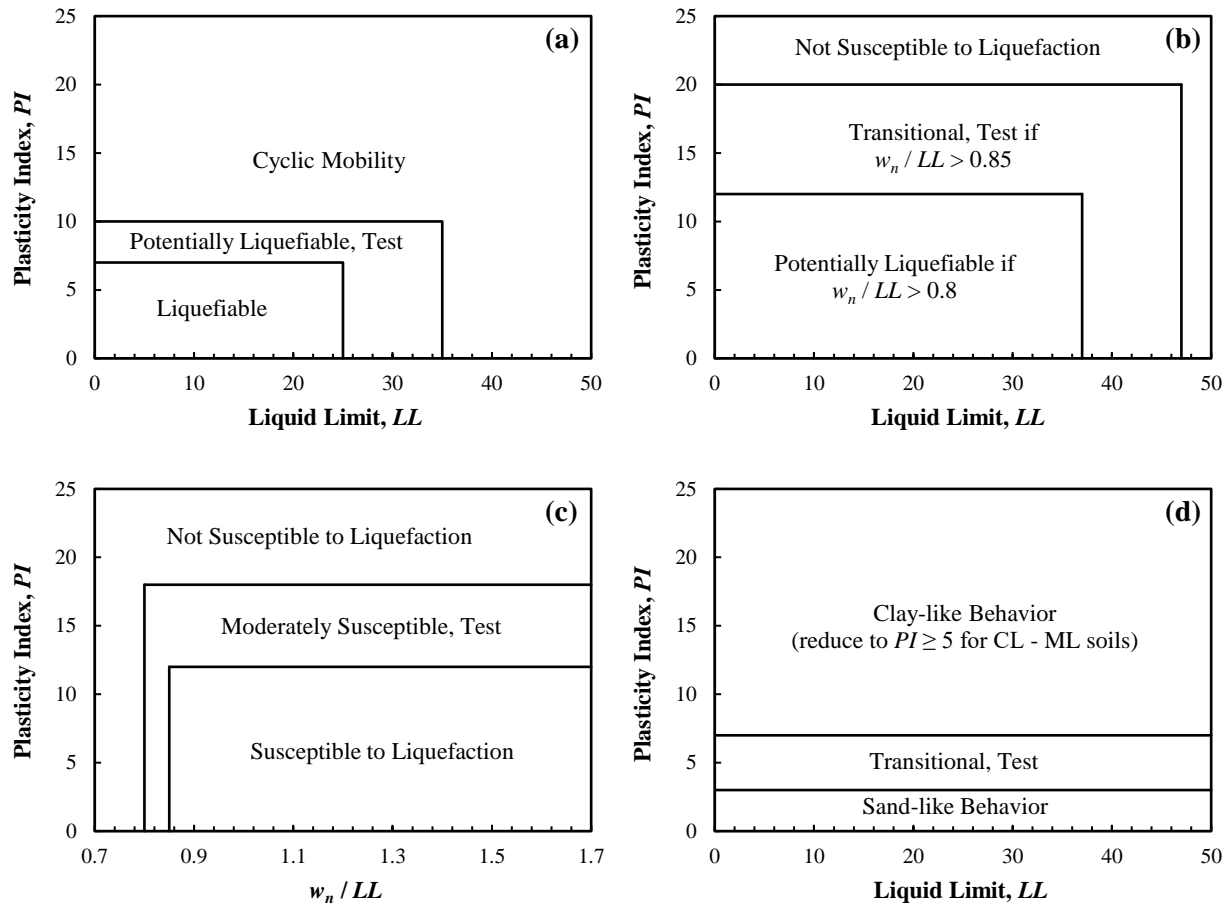


Figure 7.1 Liquefaction susceptibility criteria proposed by (a) Polito (2001) [P01]; (b) Seed et al. (2003) [SEA03]; (c) Bray and Sancio (2006) [B&S06]; and (d) Boulanger and Idriss (2006) [B&I06].

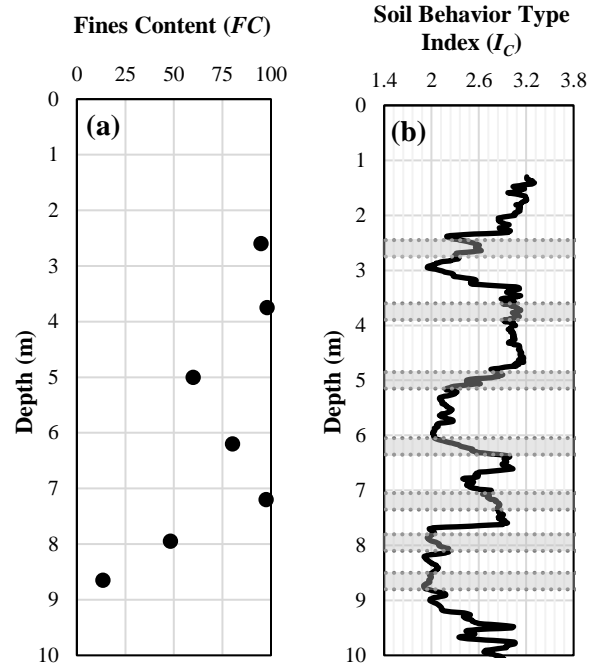


Figure 7.2 Example FC (a) and I_c (b) profiles from a site in Christchurch; 300 mm intervals over which I_c statistics were recorded, each corresponding to a soil sampling location, are shown in (b).

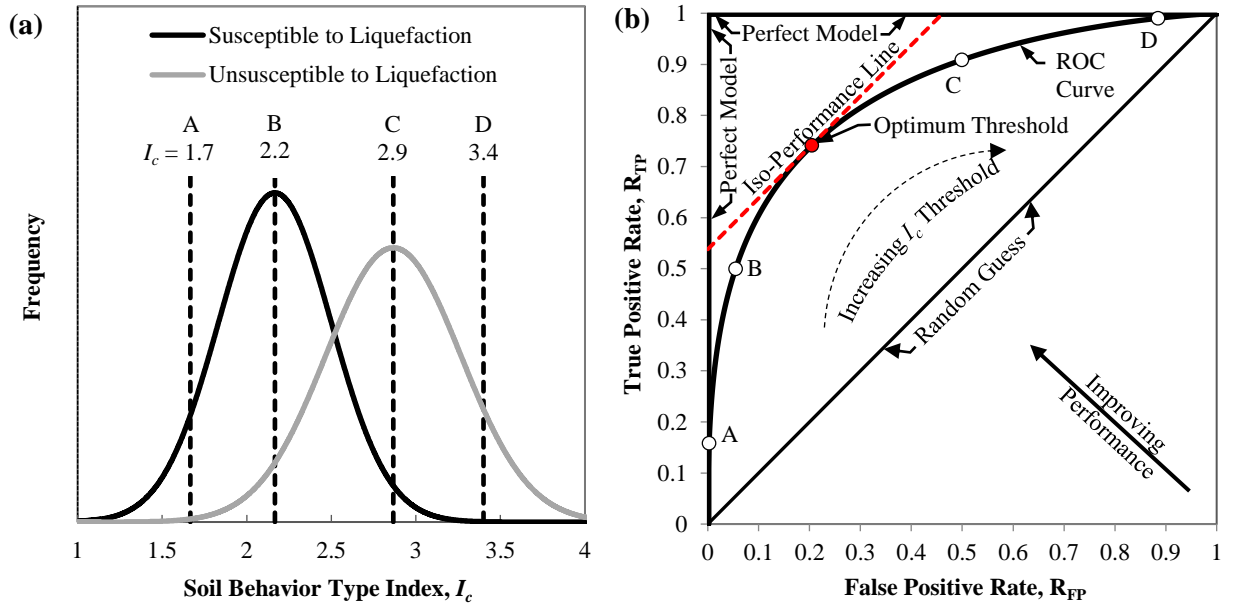


Figure 7.3 ROC analyses: (a) frequency distributions of soils susceptible and unsusceptible to liquefaction as a function of measured I_c , with four different threshold I_c values shown; (b) corresponding ROC curve, and illustration of how a ROC curve is used to assess the efficiency of a diagnostic test. The optimum decision threshold is that for which the rate of misprediction is minimized.

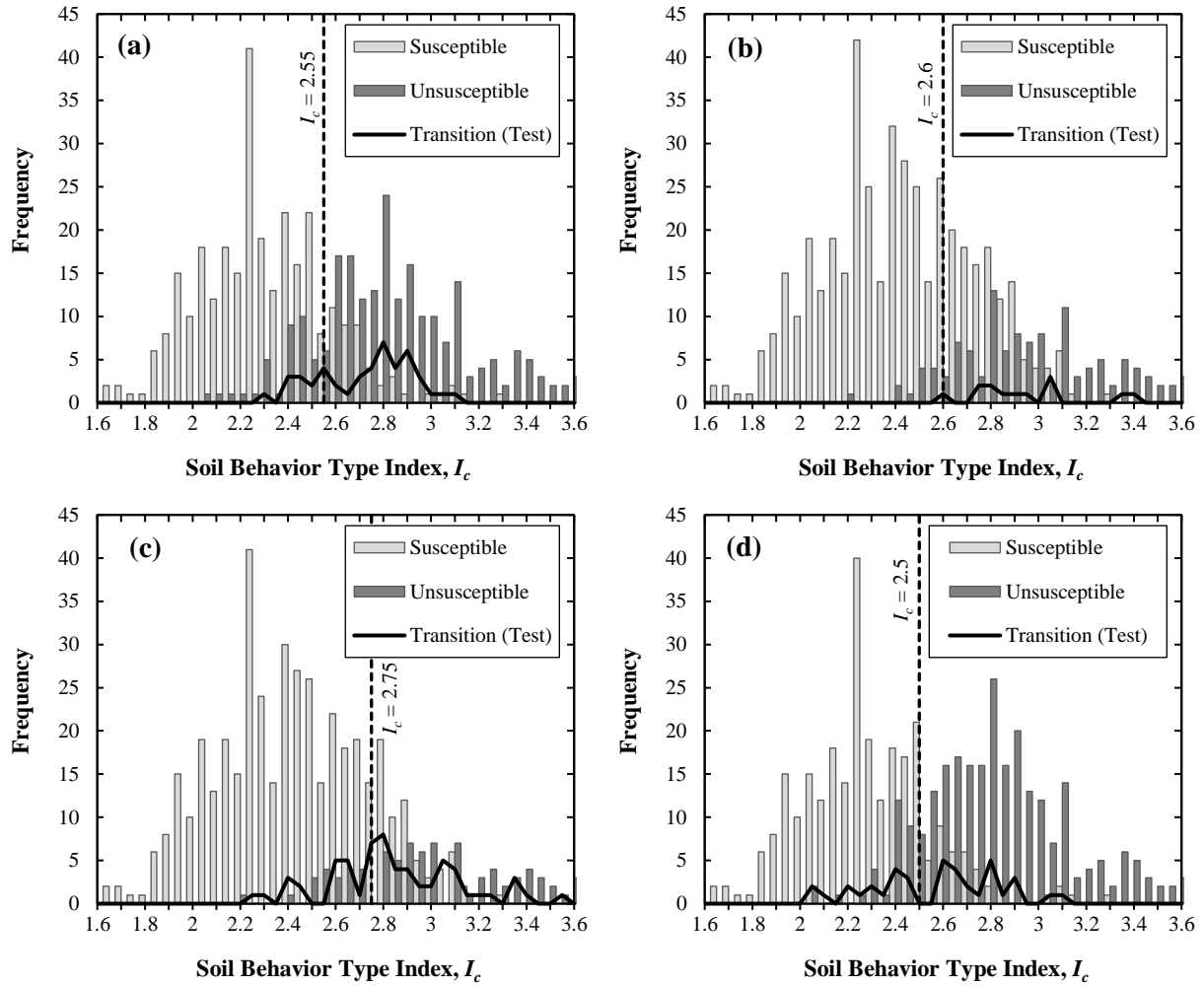


Figure 7.4 Frequency distributions of samples classified by liquefaction-susceptibility criteria based on Atterberg limits, plotted as a function of measured I_c : (a) Polito (2001); (b) Seed et al. (2003); (c) Bray and Sancio (2006); and (d) Boulanger and Idriss (2006). Classifications in (a) – (d) are as defined in the text. Optimal I_c thresholds for identifying liquefaction-susceptible soils are also identified in (a) – (d).

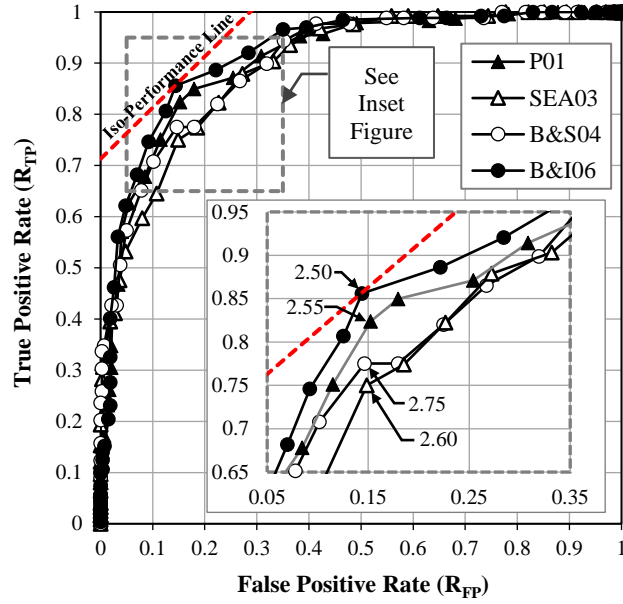


Figure 7.5 ROC analysis of I_c index performance in segregating soils susceptible to liquefaction from soils unsusceptible to liquefaction, as defined by the Polito (2001) [P01], Seed et al. (2003) [SEA03], Bray and Sancio (2006) [B&S06], and Boulanger and Idriss (2006) [B&I06] criteria. Optimum I_c thresholds are identified for each criteria in the inset figure.

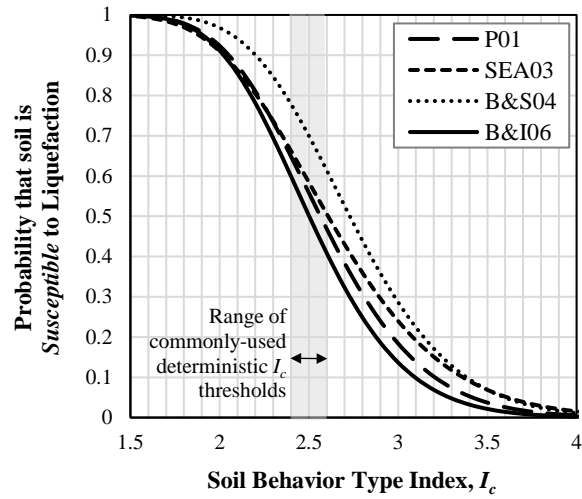


Figure 7.6 The probability of liquefaction susceptibility as a function of measured I_c . Susceptibility is as defined by the Polito (2001) [P01], Seed et al. (2003) [SEA03], Bray and Sancio (2006) [B&S06], and Boulanger and Idriss (2006) [B&I06] criteria. The range of deterministic I_c thresholds commonly used in practice is also highlighted.

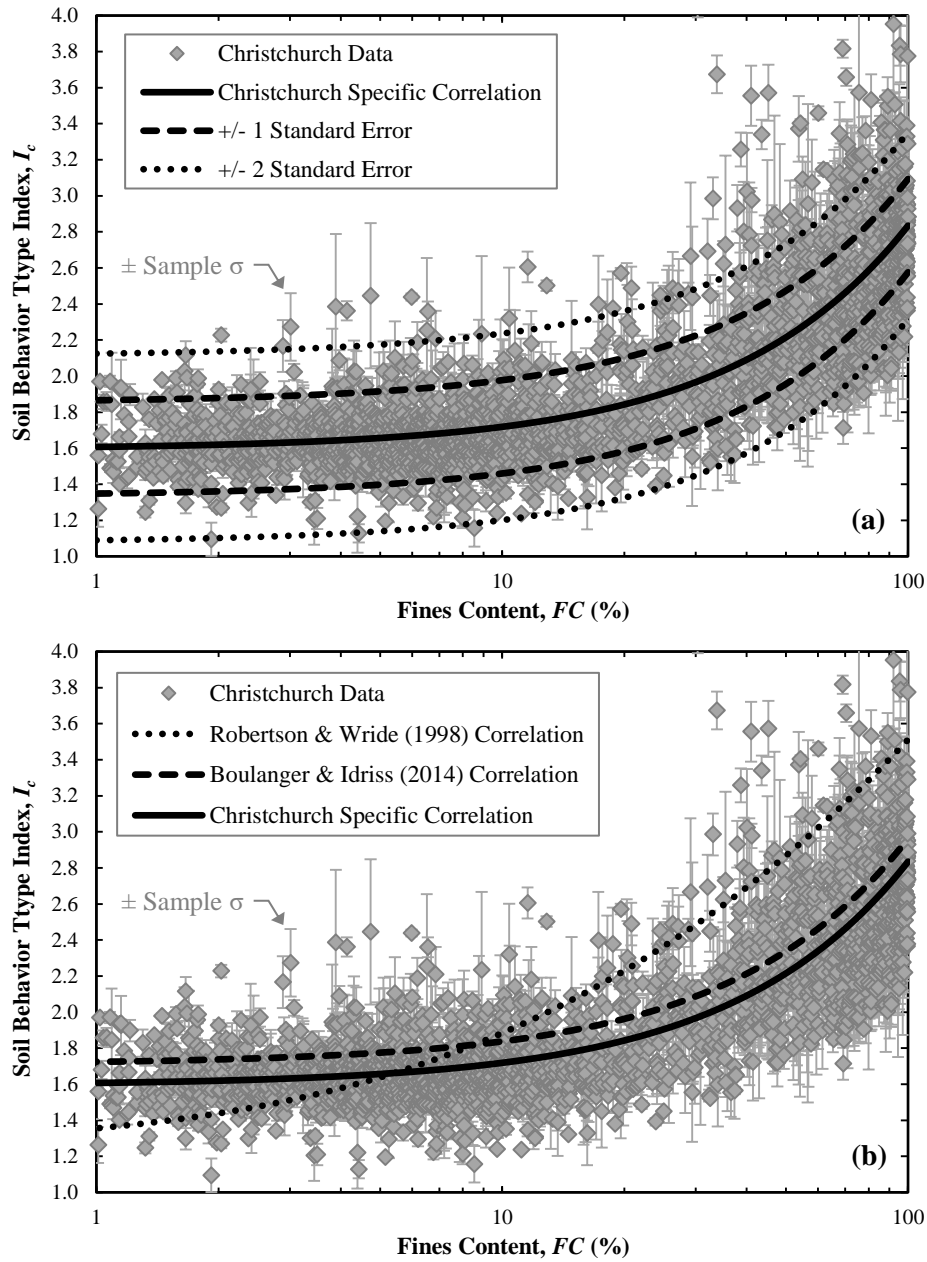


Figure 7.7 (a) Christchurch-specific $I_c - FC$ data and proposed correlation (Eq 7); (b) Comparison with the Robertson and Wride (1998) and Boulanger and Idriss (2014) generic $I_c - FC$ correlations.

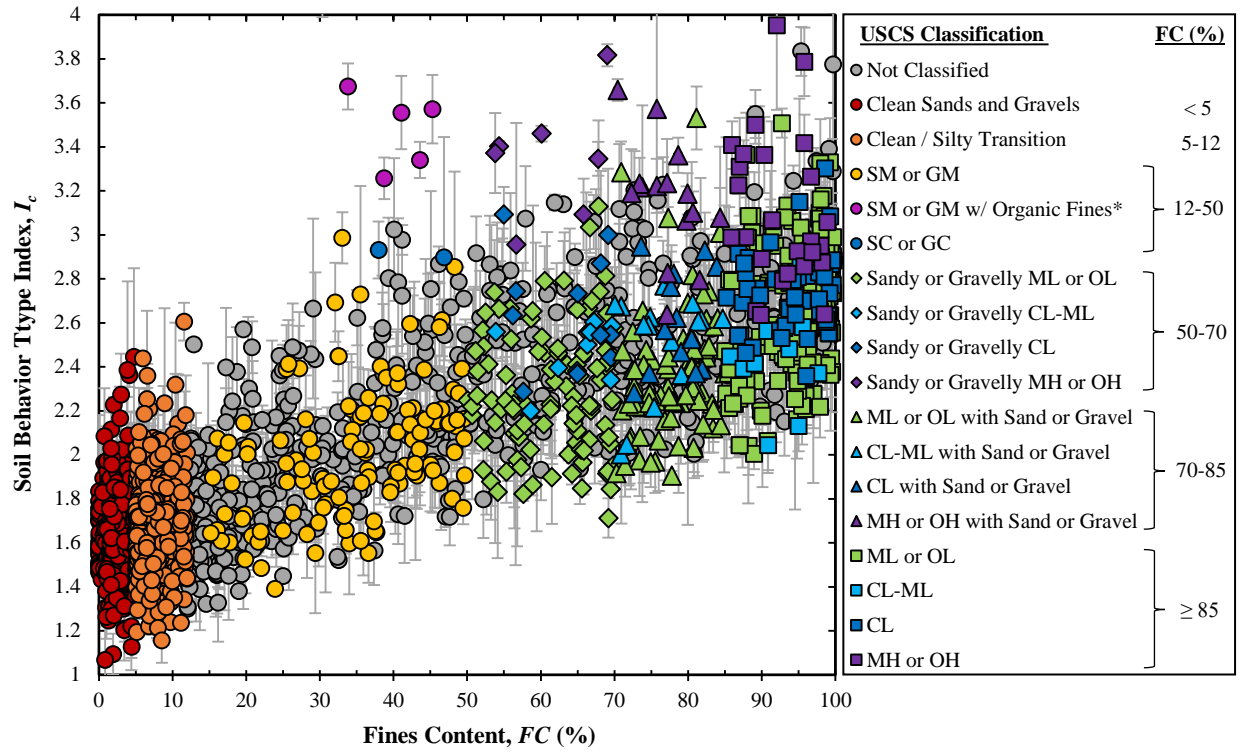


Figure 7.8 Soil behavior type index, I_c , vs. fines content, FC , color-coded by unified soil classification system (USCS) characterization.

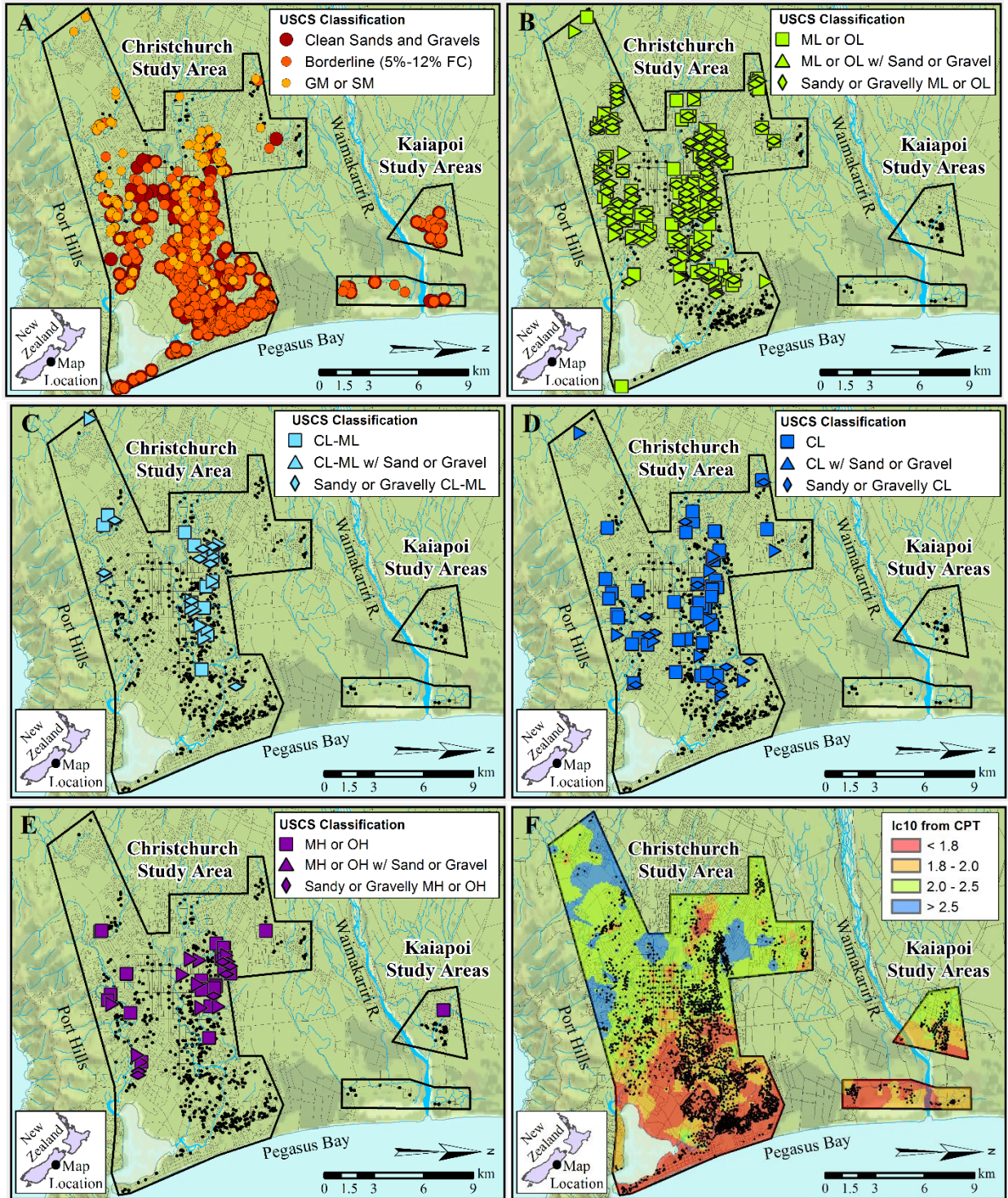


Figure 7.9 Locations of samples classified as: (a) clean sands to silty sands; (b) ML or OL variants; (c) CL-ML variants; (d) CL variants; and (e) MH or OH variants. The soil behavior type index computed from CPT data and averaged over the uppermost 10 m, I_{c10} , is mapped in (f) using inverse-distance-weighting interpolation between CPT locations. Black dots represent all soil sampling locations in (a-e) and all CPT locations in (f).

Chapter 8: Liquefaction Hazard Assessment Considering Misprediction Economies: A Study of 4 Hazard Frameworks and 10,000 Global Case Histories

Brett W. Maurer¹, Russell A. Green², Sjoerd van Ballegooy³,
Brendon A. Bradley⁴, and Sneha Upadhyaya¹

¹ Graduate Research Assistant, Dept. of Civil and Environmental Engineering, Virginia Tech, Blacksburg, Virginia 24061, U.S.A.

² Professor, Dept. of Civil and Environmental Engineering, Virginia Tech, Blacksburg, Virginia 24061, U.S.A.

³ Technical Director, Tonkin & Taylor Ltd, Auckland, New Zealand

⁴ Professor, Dept. of Civil and Natural Resources Engineering, University of Canterbury, Private Bag 4800, Christchurch, New Zealand

8.1 Abstract

Analyzing nearly 10,000 liquefaction case histories from 23 earthquakes, this study evaluates the performance of four liquefaction hazard frameworks using an objective and standardized methodology that considers the consequences of misprediction. Though often unappreciated, the performance of liquefaction hazard assessment is intimately linked to these site-specific consequences, or economies. In particular, this study determines, for the liquefaction potential index (*LPI*) and three alternative frameworks: (a) optimal decision thresholds for classifying liquefaction hazard; and (b) prediction efficiencies, both overall, and for particular misprediction economies encountered in practice. It is shown that optimal decision thresholds are inherently tied to underlying economic assumptions, since the threshold that is “optimal” for one project, or one category of land-use, may be inappropriate for others. The proposed thresholds can be used to inform strategies for assessing and/or mitigating liquefaction hazards. Additionally, for the assessed dataset, *LPI* alternatives provided predictions that were more efficient for particular misprediction economies. However, with respect to overall efficiency, improvements were minimal. The development of a more reliable framework for assessing liquefaction hazard thus remains a critical need for the geotechnical earthquake engineering profession.

8.2 Introduction

The severity of soil liquefaction manifested at the ground surface acts as a pragmatic proxy for liquefaction damage potential, particularly for pavement systems, buried lifelines, structures on shallow foundations, and other near-surface infrastructure. The greater the severity of surface manifestation, the greater the likelihood of damage to infrastructure. By way of this simplifying proxy, hazard frameworks have been proposed to link predictions of liquefaction triggering to damage potential. Iwasaki et al. (1978) proposed the first such framework: the liquefaction potential index (*LPI*), which has been used to assess liquefaction hazard in seismic regions around the world (e.g., among many, Sonmez 2003; Papathanassiou et al. 2005; Baise et al. 2006; Cramer et al. 2008; Hayati and Andrus 2008; Holzer et al. 2006; 2008; 2009; Yalcin et al. 2008; Chung and Rogers 2011; Dixit et al. 2012; Sana and Nath, 2016).

Though widely used, evaluations of *LPI* following recent liquefaction events have shown that it performs inconsistently (e.g., Maurer et al. 2014). This inconsistency inspired the development of alternative hazard frameworks, to include an Ishihara (1985) inspired variation of *LPI*, termed *LPI_{ISH}* (Maurer et al., 2015a), and the liquefaction severity number (*LSN*) (van Ballegooy et al.

2014a), an adaptation of one dimensional post-liquefaction reconsolidation settlement (*IDS*) (e.g., Zhang et al. 2002). Importantly, however, the performance of these frameworks has yet to be rigorously assessed in the field using a standardized and objective methodology. As a result, it is unknown whether any framework more accurately assesses liquefaction hazard than *LPI*, the current state-of-practice procedure. Moreover, the question of “which liquefaction hazard framework performs best?” is intimately linked to the site-specific consequences, or “economies,” of misprediction. As will be demonstrated herein, two prediction models with equivalent overall efficiency can perform very differently in certain scenarios. It is thus of interest to determine not only which framework performs best overall, but also which framework is best for particular misprediction economies. Additionally, central to all liquefaction hazard frameworks are proposed decision thresholds used to classify hazard. For example, based on recommendations by Iwasaki et al. (1982), $LPI = 5.0$ is commonly used in today’s practice to predict surficial manifestations of liquefaction, such that manifestations are expected at sites with $LPI \geq 5$. However, it is often unappreciated that proposed thresholds are inherently tied to underlying economic assumptions, such that the threshold that is “optimal” for one project, or one category of land-use, may be inappropriate for others. While misprediction economies strongly influence strategies for assessing and mitigating liquefaction hazards, they are not formally accounted for in the existing literature.

Accordingly, this study investigates the performance of the *LPI*, *LPI_{ISH}*, *LSN*, and *IDS* frameworks using analyses of 9,908 high-quality liquefaction case histories resulting from 23 earthquakes. In particular, the objectives of this performance assessment are to determine, for each framework: (a) optimal decision thresholds for classifying liquefaction hazard; and (b) prediction efficiencies (i.e., ability to predict the occurrence and non-occurrence of liquefaction manifestation). Each of these investigations carefully considers the importance of misprediction economies. In the following, an overview of the *LPI*, *LPI_{ISH}*, *LSN*, and *IDS* liquefaction hazard frameworks is first presented. The components of the 9,908 liquefaction case histories analyzed herein, and the methods used to analyze them, are then discussed. Lastly, the performance of the hazard frameworks are analyzed and discussed in detail.

8.3 Overview of Liquefaction Hazard Frameworks

8.3.1 Liquefaction Potential Index (LPI)

In current U.S. practice, liquefaction hazard is commonly assessed using *LPI*, defined as (Iwasaki et al. 1978; 1982):

$$LPI = \int_0^{20 \text{ m}} F(FS_{liq}) \cdot w(z) dz \quad (1a)$$

Where:

$$F(FS_{liq}) = \begin{cases} 1 - FS_{liq} & \text{if } FS_{liq} \leq 1 \\ 0 & \text{otherwise} \end{cases} \quad (1b)$$

$$w(z) = 10 - z/2 \quad (1c)$$

In Eq. (1), $F(FS_{liq})$ and $w(z)$ are functions weighting the respective influences of FS_{liq} and depth on surface manifestation, where FS_{liq} is the computed factor of safety against liquefaction triggering, and z is depth below the ground surface. Thus, *LPI* assumes the severity of liquefaction manifestation is proportional to the cumulative thickness of liquefied strata, the proximity of these strata to the ground surface, and the amount by which FS_{liq} in each stratum is less than 1.0. Given this definition, *LPI* can range from zero to a maximum of 100 (i.e., where FS_{liq} is zero over the entire 20 m depth).

8.3.2 Modified Liquefaction Potential Index (LPI_{ISH})

Compiling liquefaction observations following earthquakes in Japan, Ishihara (1985) recognized the importance of the non-liquefied capping stratum, or crust, on mitigating liquefaction manifestations at the ground surface. Parameterizing the Peak Ground Acceleration (*PGA*) and thicknesses of the crust (H_1) and underlying liquefied stratum (H_2), Ishihara (1985) proposed boundary curves for predicting liquefaction surface effects. These curves suggest that for a given *PGA*, there is a limiting H_1 beyond which surface manifestations are not expected, independent of H_2 . Motivated by the inconsistent performance of *LPI* during the CES, Maurer et al. (2015a) proposed modifications to better capture trends observed by Ishihara (1985). In consideration of its provenance, the modified *LPI* framework was termed LPI_{ISH} , defined as (Maurer et al., 2015a):

$$LPI_{ISH} = \int_{H_1}^{20 \text{ m}} F(FS_{liq}) \cdot w(z) dz \quad (2a)$$

Where:

$$F(FS_{liq}) = \begin{cases} 1 - FS_{liq} & \text{if } FS_{liq} \leq 1 \cap H_1 \cdot m(FS_{liq}) \leq 3 \\ 0 & \text{otherwise} \end{cases} \quad (2b)$$

$$m(FS_{liq}) = \exp\left(\frac{5}{25.56(1-FS_{liq})}\right) - 1 \quad (2c)$$

$$w(z) = 25.56/z \quad (2d)$$

In Eq. (2), $F(FS_{liq})$ and $w(z)$ have the same objective as in LPI , but are functionally different, such that: (1) $F(FS_{liq})$ accounts for the crust thickness via an additional constraint; and (2) $w(z)$ is a power-law function, weighting the contribution of liquefaction triggering more for depths between 0 and 3 m, and less for depths between 3 and 17 m. Parameters $FS_{liq, z}$, and H_1 are as previously defined, with Maurer et al. (2015a) recommending a minimum H_1 of 0.4 m be used in computing LPI_{ISH} , even when liquefiable soils are present at shallower depths. Given this constraint, LPI_{ISH} has the same range as LPI (i.e., 0 to 100).

8.3.3 One Dimensional Post-Liquefaction Reconsolidation Settlement (IDS)

The potential for volumetric post-liquefaction strain (ε_v) is inversely related to the initial relative density (D_r) of soil. All else being equal, ε_v decreases as D_r increases. By corollary, and assuming ε_v a sufficient index of liquefaction response, surface manifestations should diminish as the D_r of soil liquefying within the profile increases. This expected trend, however, may not be adequately accounted for by FS_{liq} alone. Accordingly, liquefaction hazard might be more accurately assessed using ε_v as a predictive variable.

While attempts to estimate ε_v trace to earlier studies (e.g., Lee and Albaisa, 1974), current CPT-based methods for estimating ε_v are often rooted in the cyclic simple shear tests of Nagase and Ishihara (1988). Based largely on the results of Nagase and Ishihara (1988), Ishihara and Yoshimine (1992) proposed a series of curves for estimating ε_v as a function of FS_{liq} and D_r . Using a correlation to convert D_r to normalized CPT penetration resistance (q_{c1N}), the Ishihara and Yoshimine (1992) curves may be adapted for use with CPT-based procedures that compute FS_{liq} . Integrating the

resultant ε_v over depth, an estimate of one dimensional post-liquefaction reconsolidation settlement (*IDS*) is obtained, defined as (e.g., Ishihara and Yoshimine, 1992):

$$IDS = \int \varepsilon_v dz \quad (3)$$

IDS thus assumes that ground settlement is proportional to ε_v and the cumulative thickness of affected strata, independent of depth (i.e., no depth weighting function is used). In Eq. (3) ε_v is in decimal form and z is as previously defined; for consistency with other hazard frameworks, a maximum integration depth of 20 m is imposed for this study. Assuming the largest possible ε_v is 0.05, *IDS* can range from zero to a maximum of 100 cm (i.e., where $\varepsilon_v = 0.05$ over the entire 20 m depth). While *IDS* is conventionally used to estimate free-field settlement, it is herein evaluated as a predictor of manifestation severity, as classified in this study, and its performance is compared to that of *LPI*, *LPI_{ISH}*, and *LSN*.

8.3.4 Liquefaction Severity Number (*LSN*)

As with *LPI_{ISH}*, the development of *LSN* was motivated by the need for a more reliable index of liquefaction hazard, as evidenced by the CES. *LSN* is an adaptation of *IDS*, modified to include a power-law depth weighting function, and defined as (van Ballegooy et al., 2014):

$$LSN = \int \varepsilon_v \cdot w(z) dz \quad (4a)$$

Where:

$$w(z) = 10/z \quad (4b)$$

In Eq. (4) ε_v is expressed in percent and z is as previously defined; as with *IDS*, an integration limit of 20 m is imposed for this study. *LSN* values can far surpass 100 when saturated, liquefiable soils are present at the immediate ground surface. Outside this rare occurrence, however, *LSN* values are typically between zero and 100 at sites commonly encountered in practice. Unlike *IDS* or modified *IDS* functions that include depth weighting (e.g., Cetin et al., 2009), the output from *LSN* is not a quantity of predicted ground settlement, but rather, is a hazard value á la *LPI* and *LPI_{ISH}*.

8.4 Data and Methodology

This study analyzes 9,908 liquefaction case histories resulting from 23 earthquakes, as summarized in Table 1. However, because the majority of these cases were compiled from three events during the CES, results are separately presented for these and the collective remaining 20 earthquakes, henceforth respectively referred to as the “CES dataset” and “global dataset.” These datasets are discussed subsequently, followed by a summary of the methods used to analyze them.

8.4.1 *Canterbury Earthquake Sequence (CES) Dataset*

The CES has resulted in a case history dataset of unprecedented size and quality, presenting a unique opportunity to advance the science of liquefaction hazard assessment. Beginning with the M_w 7.1, 4 Sept. 2010 Darfield earthquake, the CES includes approximately ten events known to have induced liquefaction manifesting at the ground surface (Quigley et al., 2013). The most notable of these induced pervasive liquefaction in the city of Christchurch and its environs, severely damaging infrastructure. Liquefaction-induced effects are documented in Cubrinovski and Green (2010), Cubrinovski et al. (2011a, 2011b, 2012, 2014), Wotherspoon et al. (2011), Green et al. (2012, 2014), O’Rourke et al. (2014), and van Ballegooy et al. (2014), among others. A comprehensive summary of the CES, to include tectonic and geologic settings, seismology, and environmental effects, is provided by Quigley et al. (2016). The present study uses data from the aforementioned M_w 7.1 Darfield earthquake, the M_w 6.2, 22 Feb. 2011 Christchurch earthquake, and the M_w 5.7, 14 Feb. 2016 Christchurch earthquake. Ground motions from these events were recorded by a dense network of strong motion stations (e.g., Bradley and Cubrinovski, 2011; Bradley, 2012) and due to the impacts of liquefaction, the New Zealand Earthquake Commission (EQC) initiated an extensive geotechnical reconnaissance and characterization effort (CERA, 2013). The combination of densely recorded ground motions, well-documented liquefaction response, and detailed subsurface characterization comprises the CES dataset used in this study.

8.4.1.1 *CPT Soundings*

Drawing from a high-quality subset of data collected under the auspices of the EQC and available in the New Zealand Geotechnical Database (NZGD, 2016), this study utilizes 3,834 CPT soundings performed at sites where the severity of liquefaction manifestation was well-documented following the 4 Sept 2010 Darfield and/or 22 Feb 2011 Christchurch and/or 14 Feb 2016 Christchurch earthquakes, resulting in a combined 10,881 case histories. In the process of compiling these cases,

CPTs were first rejected: (1) if performed at sites where the only manifestation of liquefaction was lateral spreading, a uniquely damaging manifestation driven by factors not considered in the *LPI*, *LPI_{ISH}*, *IDS*, or *LSN* frameworks; (2) if the depth of “pre-drill” significantly exceeded the depth of the ground water table, a condition arising where buried utilities needed to be safely bypassed before testing could begin; and (3) if believed to have prematurely terminated on shallow gravels, as inferred from an Anselin (1995) Local Morans I analysis. Extended coverage of CPT data and the exclusion criteria summarized above is provided in Maurer et al. (2014, 2015b).

8.4.1.2 Peak Ground Acceleration (PGA)

To compute FS_{liq} for use in each of the four hazard frameworks, Peak Ground Accelerations (PGAs) at the ground surface were computed using the procedure discussed in detail by Bradley (2013a) and used by several CES studies (e.g., Green et al. 2015; Maurer et al., 2015c; van Ballegooy et al. 2015). The Bradley (2013a) procedure combines unconditional PGA distributions estimated by the Bradley (2013b) ground motion prediction equation, recorded PGAs from strong motion stations, and the spatial correlation of intra-event residuals to compute the conditional PGA distribution at sites of interest. In addition to the exclusion criteria described above, cases with $PGA < 0.15g$ were removed from the dataset, resulting in the omission of 1,258 cases, nearly all from the $M_w 5.7$ Christchurch earthquake. This criteria was applied because sites with PGAs below a certain threshold have negligible probability of liquefaction triggering, and thus, do not provide meaningful assessments of prediction performance. In particular, 0.15g was selected because no site experiencing a PGA below this threshold had liquefaction manifestations in any CES event. Following the removal of cases with $PGA < 0.15g$, a final total of 9,623 cases remained.

8.4.1.3 Ground Water Table (GWT) Depth

Given the sensitivity of liquefaction hazard to GWT depth (e.g., Chung and Rogers, 2011; Maurer et al., 2014), accurate measurement of the GWT is critical. For this study, GWT depths were sourced from the robust, event-specific regional ground water models of van Ballegooy et al. (2014b). These models, which reflect seasonal and localized fluctuations across the region, were derived in part using monitoring data from a network of ~1000 piezometers and provide a best-estimate of GWT depths immediately prior to each CES earthquake. Considering the extent and density of monitoring, the van Ballegooy et al. (2014b) GWT models are likely among the most robust ever used for regional study of liquefaction hazard.

8.4.1.4 Liquefaction Severity

Observations of liquefaction and the severity of manifestation were made by the authors for each of the CPT sounding locations following at least one of the three aforementioned earthquakes. CPT sites were assigned one of four damage classifications, as described in Table 2, where the classifications describe the predominant manifestation of liquefaction at the ground surface in the immediate vicinity of the sounding location. Representative observations of the manifestation severity classifications are shown in Figure S1 in the Supplemental Data. Of the 9,623 cases compiled from the CES, 58% are cases of “no manifestation,” and 42% are cases where manifestations were observed and classified in accordance with Table 2 as “marginal,” moderate,” or “severe.”

8.4.2 Global Dataset

To compare performance findings in Christchurch with regions worldwide, 265 liquefaction case histories resulting from 23 global earthquakes in 9 countries are compiled and assessed in parallel. These case histories are largely sourced from the existing literature, to include CPT sounding data, observations of manifestation severity, and estimation of GWT depth and PGA, as generally reported by original investigators. In some cases, refined estimates of PGA and/or GWT depth are adopted. In this regard, homage is owed to the case history assemblages of Moss et al. (2005) and Boulanger and Idriss (2014), whose reference and data compilations greatly assisted the present study. In compiling these 265 cases, those with $PGA < 0.15g$ were first removed for consistency with the CES dataset. Provided in the Supplemental Data is an expanded version of Table 1 listing all pertinent details and references for each global case history. Notably, the CES and global datasets deviate in the classification of manifestation severity. Whereas CES liquefaction was intensively cataloged via reconnaissance and remote sensing, the global cases are often insufficiently documented for manifestations to be classified in the same level of detail (i.e., in accordance with Table 2). Surficial manifestations are therefore classified binomially as “yes” or “no” without categorizing the nature or severity of expression. Of the 265 cases compiled, 39% are “no” and 61% are “yes.” Within this domain, cases with evidence of liquefaction at depth but not at the ground surface (e.g., liquefaction inferred from ground motion or pore pressure records) are classified as “No.”

8.4.3 Liquefaction Triggering and Hazard Assessment

Intrinsic to the LPI , LPI_{ISH} , IDS , and LSN hazard frameworks, FS_{liq} vs. depth profiles are developed from a liquefaction triggering procedure. For this study, FS_{liq} values are separately computed by the Idriss and Boulanger (2008)[IB08] and Boulanger and Idriss (2014)[BI14] procedures, whose use is mandated in New Zealand (MBIE, 2015) and widespread in the United States and elsewhere. Soils susceptible to liquefaction are first identified using the soil-behavior-type-index (I_c) proposed by Robertson and Wride (1998), such that soils with $I_c < 2.50$ are treated as susceptible. This criterion was developed specifically for Christchurch soils from laboratory testing of more than 2,000 soil samples (Maurer et al., 2016). However, because an I_c threshold of 2.50 is within the range of values commonly used in practice, this criterion is also used in all analyses of the global dataset. Once liquefaction-susceptible soils are identified, the IB08 and BI14 procedures use fines content (FC) to adjust q_{c1N} for the quantity of fines in the soil. Accordingly, FC is herein estimated for the CES dataset using a Christchurch-specific $I_c - FC$ correlation (Maurer et al., 2016), and for the global dataset using a general $I_c - FC$ correlation (Boulanger and Idriss, 2014). Once FS_{liq} profiles are developed, LPI and LPI_{ISH} are computed per Eqs. 1 and 2, respectively. IDS and LSN are computed per Eqs. 3 and 4, respectively, where ε_v is estimated by the Zhang et al. (2002) procedure, as modified by Maurer et al. (2015d). This approach was previously shown to result in more accurate LSN hazard assessments when compared to four alternatives (Maurer et al., 2015d).

8.5 Receiver Operating Characteristic (ROC) Analyses

Using the data and methodologies described above, LPI , LPI_{ISH} , IDS , and LSN values are computed for each liquefaction case study. To compare the performance of these hazard frameworks, a standard approach is needed to assess the efficiency of binomial classifiers. Specifically, this study seeks to answer two fundamental questions: what are the optimal classification thresholds (referred to as decision thresholds) for each framework, and which framework is most efficient?

Receiver operating characteristic (ROC) analyses, which are widely used in biostatistics and medical diagnostics (e.g., Zou, 2007), are herein adopted to answer these questions. In any ROC application, the distributions of “positives” (e.g., liquefaction manifestation is observed) and “negatives” (e.g., no liquefaction manifestation is observed) overlap when the frequency of the distributions are expressed as a function of index test results (e.g., LPI , LPI_{ISH} , IDS , or LSN values). To demonstrate, distributions of liquefaction observations are shown in Figure 1a, plotted as a function of computed LSN . In such cases, decision thresholds should ideally be selected considering

both the rate and consequence of mispredictions (i.e., false positives and false negatives). Setting the decision threshold too low or too high will result in a greater number of mispredictions; the degree to which these mispredictions are acceptable is a function of their consequences, or costs. The cost of a false positive could be the superfluous spending on engineering design and construction (e.g., ground improvement costs), while the cost of a false negative might be the costs of liquefaction-induced damage (e.g., lost productivity, property damage, and reconstruction costs, among others). Importantly, these costs are a function of the assessed liquefaction hazard and the type of infrastructure at risk. Optimal decision thresholds, which minimize prediction cost, are thus site-specific.

ROC curves plot the rates of true positive predictions (R_{TP}) (e.g., liquefaction manifestation is observed, as predicted) and false positive predictions (R_{FP}) (e.g., liquefaction is predicted, but is not observed). Figure 1B depicts the relationship among the distributions in Figure 1a, the decision threshold, and the ROC curve. The optimum decision threshold is defined herein as the hazard value that minimizes the total cost of prediction, where cost is computed as:

$$Cost = C_{FP} \times R_{FP} + C_{FN} \times R_{FN} \quad (5)$$

where C_{FP} and R_{FP} are the cost and rate of false positive predictions, respectively, and C_{FN} and R_{FN} are the cost and rate of false negative predictions, respectively. Normalizing with respect to C_{FN} , Equation (5) may alternatively be expressed as:

$$Cost' = Cost/C_{FN} = R_{FP} \times CR + R_{FN} \quad (6)$$

where CR is the *cost ratio*, $CR = C_{FP} / C_{FN}$, and is synonymous with “misprediction economy.” In Equations (5) and (6), the rates of false negatives (R_{FN}) and false positives (R_{FP}) are respectively defined by:

$$R_{FN} = Q_{FN} / (Q_{FN} + Q_{TP}) \quad (7a)$$

$$R_{FP} = Q_{FP} / (Q_{FP} + Q_{TN}) \quad (7b)$$

where Q_{TP} , Q_{FP} , Q_{TN} , and Q_{FN} are respectively the quantities of true positives, false positives, true negatives, and false negatives. Thus, the denominators of Eqs. (7a) and (7b) equal the total number

of sites with and without observed surficial liquefaction manifestations, respectively. Accordingly, the rate of true positives (R_{TP}) is equal to $1-R_{FN}$ and the rate of true negatives (R_{TN}) is equal to $1-R_{FP}$. Since cost-contours represent points of equivalent performance (i.e., equal Cost') in ROC space, it follows from Equations (1-3) that two points in ROC space, (R_{FP1}, R_{TP1}) and (R_{FP2}, R_{TP2}) have equivalent performance if:

$$\frac{R_{TP1} - R_{TP2}}{R_{FP1} - R_{FP2}} = \frac{C_{FP}}{C_{FN}} = CR = m \quad (8)$$

Equation (8) defines the slope, m , of an iso-performance line, such that all points defining the line have the same expected Cost' (Provost and Fawcett, 2001). Thus, each unique CR corresponds to a different iso-performance line in ROC space. One such line is shown in Figure 1b. With 1:1 slope, this line corresponds to the case where false positives and false negatives have equivalent costs (i.e., $CR = 1$). Iso-performance points tangent to the ROC curve correspond to optimum decision thresholds at which Cost' is minimized. Thus, the optimum decision threshold identified in Figure 1b accounts for both the rates and consequences of misprediction. Repeating for different values of CR , optimal decision thresholds can be identified for various misprediction economies, which may be thought of as different levels of desired conservatism.

To evaluate the efficiencies of liquefaction hazard assessments, two different approaches will be used. The first approach evaluates the overall model efficiency across all misprediction economies. While no single parameter can fully characterize performance, the area under a ROC curve (AUC) is commonly used, where AUC is statistically equivalent to the probability that sites with manifestations have higher computed hazard values than sites without manifestations (e.g., Fawcett, 2005). As such, increasing AUC indicates better model performance. Figure 1b illustrates the relationship between AUC and model efficiency. In ROC space, random guessing is indicated by a 1:1 line through the origin, for which $AUC = 0.5$ (i.e., equivalent correct and incorrect predictions). A perfect model, for which $AUC = 1.0$, plots as a point at $(0,1)$, indicating the existence of a decision threshold that perfectly segregates the dataset (e.g., all cases with manifestation have LSN above the threshold; all cases without manifestation have LSN below the threshold). Thus, the closer a ROC point is to the $(0,1)$ coordinate, the lower the misprediction rate.

However, while AUC is a popular performance measure, it is an average efficiency across all misprediction economies. In cases where only a certain range of CR 's is of interest, AUC could be misleading. For example, models with equal AUC could perform very differently in specific regions

of ROC space. Such a case is shown in Figure 2a: models A and B have identical AUC , but each is better in certain scenarios. Consider the case in which false positives are $1/5^{\text{th}}$ as costly as false negatives. By Eq. 8, iso-performance lines have slope $m = 1/5$, on which all points have equal prediction cost. What that cost *is* depends on the lines' R_{TP} -intercepts and can be computed by Eq. 5 (the greater the R_{TP} -intercept, the lower the cost). Since a tangent to B with slope $m = 1/5$ has a greater R_{TP} -intercept than a similar tangent to A, B is better for these conditions. In other words, B is better in the “conservative” ROC region, in which models correctly classify most positives, but at the expense of high false-positive rates. Conversely, and by the same logic, A is preferred when false positives are 5 times as costly as false negatives. A is thus better in the “liberal” region, in which models make few false-positive predictions, but at the expense of also having low true-positive rates. Lastly, it can be seen that when false positives and false negatives have equal cost, A and B perform equally well. Similarly, a model with higher AUC could be less efficient in a specific region of ROC space than a model with lower AUC . Such a case is shown in Figure 2b: model A has higher AUC and is better than model B for $CR > 0.27$. However, for $CR < 0.27$, A performs slightly better.

Thus, while AUC provides a general measure of prediction efficiency, it cannot capture the nuances described above. Accordingly, the second approach adopted herein is to identify the best model for particular misprediction economies. To do so, the normalized cost, $Cost'$, is computed by Eq. 6 for each liquefaction hazard framework at the optimal decision threshold for different CR values. The hazard framework with lowest $Cost'$ at a given CR is most optimal. This approach is equivalent to the graphical approach demonstrated above, in which the ROC curve plotting closer to coordinate (0,1) has lower cost. Using these two approaches, it can be determined not only which framework performs best overall, but which framework is best for particular misprediction economies.

8.6 Results and Discussion

8.6.1 Demonstration ROC Curves

Utilizing 9,908 liquefaction case histories, LPI , LPI_{ISH} , LSN , and IDS values were separately computed using the I&B08 and B&I14 liquefaction triggering procedures. To demonstrate how ROC analyses will be used to study the case histories, a full example is first provided, and thereafter, only derivative statistics will be presented. In Figure 3, ROC curves are plotted to evaluate the performance of each framework in predicting liquefaction manifestations during the $M_w 7.1$ Darfield, New Zealand, Earthquake; for this demonstration, the I&B08 procedure was used within each framework. Optimal decision thresholds are first determined by Eq. 6, as identified in

Figure 3 for the scenario $CR = 1$. Given this misprediction economy, the LPI , LPI_{ISH} , LSN , and IDS frameworks have optimal decision thresholds of 1.6, 1.5, 15.7, and 6.0, respectively, where IDS is measured in cm. To determine which framework is optimal for a given CR , $Cost'$ is computed by Eq. 6 for each framework at its respective optimal threshold. Measured in this way, LSN is the least costly (i.e., most efficient) model at $CR = 1$, followed by LPI_{ISH} , LPI , and IDS . Based on these select results, and for an analysis in which $CR = 1$, it would thus be prudent to assess liquefaction hazard using LSN and a decision threshold of 15.7, such that sites with computed LSN values below this threshold are treated as “non-hazardous.” Finally, to evaluate overall model efficiencies, AUCs are computed for each ROC curve. It can be inferred from Figure 3 that while the four frameworks perform similarly, LSN and IDS respectively have the highest and lowest overall prediction efficiency. Ordered by improving performance, the IDS , LPI , LPI_{ISH} , and LSN frameworks have computed AUCs of 0.66, 0.68, 0.69, and 0.71. In this case, the performance rankings are the same for overall efficiency (measured by AUC) and efficiency at $CR = 1$ (measured by $Cost'$). To complete the performance investigation using the ROC curves plotted in Figure 3, the determinations of optimal decision thresholds and optimal hazard frameworks are repeated for various CR s. The process is then repeated using the I&B08 procedure in each framework, and again, for each CES event, the combined CES dataset, and the global dataset.

8.6.2 Optimal Decision Thresholds & Hazard Frameworks for Various Misprediction Costs

In Figure 4 (a-d), optimal decision thresholds are identified for various misprediction economies, wherein results are separately presented for the CES and global datasets, and for use with the I&B08 and B&I14 procedures in each framework. This analysis is performed for CR s ranging from 0.01 to 2.0, which correspond to misprediction economies likely to be encountered in engineering practice. It can be seen in Figure 4 that optimal thresholds strongly depend on underlying economic assumptions. As an example, if false negatives and false positives have equal costs, the optimal LPI threshold for the CES dataset is 4.7 using the B&I14 procedure. If, however, false negatives are three times as costly as false positives (a more reasonable CR for many engineering projects), the optimal LPI threshold drops to 1.9. Clearly, the conservatism desired in any hazard assessment must consider the consequences of misprediction, which vary amongst engineering projects. It follows that decision thresholds should be applied on a site-specific basis, since the threshold hazard value that is “optimum” for one project, or one category of land-use, may be inappropriate for others. These results also have implications for threshold hazard values previously proposed in the literature. For example, many studies have used the results of post-earthquake field

investigations to calibrate *LPI*. However, these studies have used different methods and justifications, generally without explicit accounting of misprediction consequences. *LPI* decision thresholds were first proposed by Iwasaki et al. (1982), who found that of 55 sites evaluated, 80% of sites with liquefaction manifestation had $LPI > 5$, and 70% of sites without manifestations had $LPI < 5$. This led Iwasaki et al. (1982) to propose $LPI = 5$ as an optimum threshold for predicting manifestations. In doing so, the costs of false positives and false negatives were implicitly treated similarly. Had Iwasaki et al. (1982) instead assumed that false negatives were more costly than false positives, the proposed *LPI* threshold would presumably have been less than 5. Authors assuming disubfferent misprediction economies will invariably propose different threshold values. For example, Iwasaki et al. (1982), Toprak and Holzer (2003), Lee et al. (2003), Papathanassiou (2008), Kang et al. (2014), Papathanassiou et al. (2015), and Maurer et al. (2015c) proposed *LPI* thresholds for predicting liquefaction manifestation of 5, 5, 13, 14, 14, ~13.5, and 5, respectively. While these discrepancies are potentially attributable to several factors, the lack of a standard approach to selecting thresholds, to include proper accounting of misprediction economies, makes comparisons amongst studies difficult. Most importantly, if the economic conditions assumed in the development of proposed thresholds are different from those existing in forward analyses, the resulting hazard assessments could be very inappropriate. It is thus recommended that ROC analyses, as used in this study, be adopted as the standard approach for studying threshold hazard values.

Returning to Figure 4, it can be seen that optimal thresholds are typically greater using the B&I14 procedure, relative to the I&B08 procedure. While there are several differences between the two procedures, this shift largely results from differences in the magnitude scaling factors (MSFs) inherent to each. The B&I14 MSF tends to result in lower computed FS_{liq} values, and thus, higher computed hazard values (to review the use of MSFs in liquefaction triggering mechanics, see Boulanger and Idriss, 2014). In response, the optimal thresholds segregating cases with and without liquefaction manifestation likewise increase, as reflected in Figure 4. It can also be seen that optimal thresholds for the CES and global datasets are generally consistent at lower CRs, but tend to deviate at $CR > 1$. This is due to the CES and global ROC curves having similar performance in the conservative (i.e., “northeast”) region of ROC space, but dissimilar performance elsewhere. Accordingly, for forward analyses outside the Canterbury region of New Zealand, a decision must be made as to which thresholds are used. One solution is to apply weighting factors to each dataset. For example, a 1:1 weighting could be justified: while the CES dataset is much larger, the more diverse global dataset represents a variety of geologic and seismologic conditions.

To identify the most efficient model for particular misprediction economies, $Cost'$ is computed for each framework at different CR values. The framework with lowest $Cost'$ is identified in Figure 5 for CR s ranging from 0.01 to 2.0. In addition to the CES and global datasets (5d and 5e), results are also presented for each of the three individual CES events (5a – 5c). Also, because multiple models could have nearly equivalent efficiency, and thus, be equally optimal, any framework whose $Cost'$ is within 1% of minimum is likewise treated as “optimal.” Importantly, a truly optimal framework must perform well for various earthquakes with different characteristics, in each case using the same decision threshold. Results from the CES and global datasets are therefore of most interest. However, those from individual CES events are also included to provide insights into the consistency of framework performance.

Several observations can be made from Figure 5, as follows. *First*, there is limited agreement between results based on the I&B08 and B&I14 procedures. As can be seen in Figure 5, the optimal framework is closely linked to which of these procedures is adopted. Using the CES dataset as an example (Figure 5D), LPI is optimal at all CR if I&B08 is used, while LPI_{ISH} is optimal at all CR if B&I14 is used. *Second*, there is similarly limited agreement between the CES and global datasets. This inconsistency might be resolved as additional cases are added to the global dataset. Owing to its size, a relatively small influx of additional cases could alter the results presented in Figure 5e. Due to this inconsistency, the decision to adopt a particular framework is unlikely to be easy or obvious. For example, approaching a scenario with $CR = 0.5$ and wishing to use the B&I14 procedure, the CES dataset suggests the use of LPI_{ISH} , while the global dataset suggests that LPI , LPI_{ISH} , and LSN would be equally effective. Accordingly, Figure 7 should be used to provide insight as to when a framework is likely to perform well, rather than as a definitive tool for framework selection. *Third*, the 1DS framework is optimal only for very low CR s, and only for the CES dataset. Given its notably poor performance, the use of 1DS is not recommended for predicting liquefaction manifestations, as classified in this study. *Fourth*, among CES events, the optimal framework at a given CR is highly variable. As an example, when using the B&I14 procedure, LSN is optimal for the largest range of CR values in the Sept 2010, $M_w7.1$ Darfield earthquake. The same can be said of LPI_{ISH} in the Feb 2011, $M_w6.2$ Christchurch earthquake, and of LPI in the Feb 2016, $M_w5.7$ Christchurch earthquake. This inconsistency may be the result of inherent limitations in (a) the assessed hazard frameworks, such that factors influencing liquefaction manifestation are not adequately accounted for; and/or (b) the liquefaction triggering procedures used within each framework, such that the mechanics of liquefaction triggering are not properly captured.

8.6.3 Using ROC Analyses to Inform Hazard Assessment and Mitigation Strategies

To demonstrate how the preceding results can be used to inform hazard assessment and mitigation decisions, several simplified example scenarios are provided. Each of these scenarios is based on the premise described as follows. Consider an infrastructure asset with 100-year design life. A liquefaction hazard assessment is to be performed for a 25-year return-period design earthquake, which, assuming a Poisson distribution has a 98% probability of occurring in 100 years. In addition, local codes mandate the B&I14 procedure be used. From CPT soundings at the site, LPI , LPI_{ISH} , LSN , and IDS are computed by B&I14 to be 5.0, 3.5, 9.0, and 4.5, respectively.

- Scenario 1: The infrastructure is a critical structure (e.g., a school building) and CR is estimated to be 0.15, indicating that liquefaction effects are estimated to be 6 to 7 times more costly than ground improvement and/or a robust foundation system that would mitigate the hazard to negligible levels. Results from the CES (Figure 5d) suggest that all four frameworks are likely to perform well for such an economy. From Figure 4, optimal thresholds for LPI , LPI_{ISH} , LSN , and IDS , averaged from the CES and global datasets, are 0.5, 0.2, 2.4, and 0.7, respectively. Since the computed hazard values exceed the optimal thresholds for each framework, it is prudent to mitigate the hazard. As could be expected for low- CR scenarios, hazard mitigation is warranted for essentially any measurable hazard. While this decision is easily reached by intuition, the appropriate decision is often less obvious.
- Scenario 2: The infrastructure is a large parking lot and CR is estimated to be 2.0; the cost of ground improvement performed over a large area is thus twice the cost of rebuilding the lot following liquefaction damage. Results from the CES and global datasets (Figures 5d and 5e) suggest that LPI_{ISH} is likely to perform well for such an economy. From Figure 4, the optimal LPI_{ISH} decision threshold, averaged from the CES and global datasets, is 4.8. Since the computed LPI_{ISH} is less than the decision threshold, it is prudent to treat the scenario as “non-hazardous.”
- Scenario 3: The premise described above occurs within a regional hazard-mapping project to inform land-use planning. The project aims to map locations where liquefaction manifestations are expected to occur. In this case, false-positives and false-negatives are assigned equal cost, corresponding a minimization of the misprediction rate. Based on results presented in Figure 5e, LSN performs well for a broad range of CR s centered on 1.0, and is

thus adopted. From Figure 4c, the average optimal LSN decision threshold is 13.0. Since the computed hazard ($LSN = 9$) is less than the optimal threshold, manifestations are not expected to occur at the site.

While these simple examples do not justly represent the complexity and probabilistic nature of life cycle cost analyses (e.g., consideration of earthquake motions for a range of return periods; consideration of different damage mechanisms and different damage severities), they clearly demonstrate that some consideration should be given to the relative consequences of misprediction when proposing or using a decision threshold. While far from an exact science, the approach demonstrated herein can be used to inform hazard mitigation strategies for scenario earthquakes.

8.6.4 Evaluating Overall Model Performance

While it has been shown that LPI alternatives provide more efficient predictions for particular CRs , the overall model efficiency is arguably most important. Ultimately, the objective of this research is to develop an improved and pragmatic liquefaction hazard framework providing more efficient predictions at all CRs . Towards this end, AUC values are plotted in Figure 6, as determined from ROC analyses of the CES and global datasets using the (a) I&B08 and (b) B&I14 procedures. In addition to the combined CES dataset, AUCs are also shown for each of the three individual CES events. Several observations can be made from Figure 6. *First*, the B&I14 procedure tends to result in slightly more efficient hazard assessments as compared to I&B08. This improvement is most significant for the LPI_{ISH} framework, for which AUCs for the CES and global datasets increase by 2% and 1%, respectively. 1DS is a notable exception to this trend: AUCs for these respective datasets *decrease* by 2% and 1%. *Second*, the framework that is most efficient varies among individual CES events. For example, using the I&B08 procedure, LSN is most efficient for the Sept 2010, $M_w7.1$ Darfield earthquake; LPI_{ISH} is most most efficient for the Feb 2011, $M_w6.2$ Christchurch earthquake; and LPI is most efficient for the Feb 2016, $M_w5.7$ Christchurch earthquake. As discussed previously, this inconsistency could be the result of limitations inherent to the assessed hazard frameworks and/or the liquefaction triggering procedures used within each framework.

Third, AUCs are higher for the CES dataset than for the global dataset (9.8% higher, on average). This may be due to the fact that the CES dataset is comprised of cases with relatively similar soil profiles situated in the same seismological setting, and/or because data was collected using consistent and relatively high-quality methods. Conversely, the global dataset contains cases

resulting from earthquakes over a 50 year timespan in a variety of geologic and seismologic settings, with data collected using different equipments and methods. It is thus unsurprising that hazard assessments are more efficient for the CES dataset. *Fourth*, it can be seen that overall, alternatives to *LPI* provide little to no statistical benefit in terms of AUC. For example, using the B&I14 procedure, *LPI_{ISH}* is the most efficient framework for both the CES and global datasets, but in each case, its efficiency is only ~0.5% better than *LPI*. Thus, while *LSN* and *LPI_{ISH}* have made notable improvements, resulting in more efficient predictions for particular misprediction economies, the development of an improved liquefaction hazard framework is still of profound consequence. Importantly, ROC analyses provide a standardized and objective methodology by which improvement can be tracked moving forward. In Figure 7, the results of Figure 6 are replotted in terms of AUC for the CES dataset vs. AUC for the global dataset. Figure 7 forms the basis for developing an improved liquefaction hazard framework: any framework whose performance plots in the shaded region performs better, relative to *LPI*, for both the CES and global datasets.

8.7 Conclusions

Analyzing 9,908 liquefaction case histories resulting from 23 earthquakes, this study investigated the performance of the *LPI*, *LPI_{ISH}*, *LSN*, and *IDS* liquefaction hazard frameworks, wherein the I&B08 and B&I14 liquefaction triggering procedures were separately utilized. The assessed case histories were parsed into those resulting from three events in the Canterbury Earthquake Sequence (“CES dataset”) and those resulting from 20 other global events (“global dataset”). The objectives of this performance assessment were to determine, for each framework: (a) optimal decision thresholds for classifying liquefaction hazard; and (b) the prediction efficiency (i.e., ability to predict the occurrence and non-occurrence of liquefaction manifestation). Moreover, these investigations considered the influence of misprediction economies, which play a significant role in liquefaction hazard assessment, but are not formally accounted for by existing methodologies. As illustrated herein, the relative consequences of misprediction strongly influence decision making when classifying and mitigating hazards. The findings of this study are summarized as follows:

- Receiver-operating-characteristic (ROC) analyses provide a standardized and objective methodology for investigating the performance of liquefaction hazard frameworks.
- Optimal thresholds for classifying liquefaction hazard are intimately linked to underlying economic assumptions, since the threshold hazard value that is “optimal” for one project, or

one category of land-use, may be inappropriate for others. Accordingly, LPI , LPI_{ISH} , LSN , and IDS decision thresholds were computed in Figure 4 for varying misprediction economies. While often unrealized, assumed costs are implicit to all proposed thresholds in the literature and could have significant implications for forward analyses using these thresholds to assess hazard. Additionally, optimal decision thresholds are typically greater using the B&I14 procedure relative to I&B08. This shift largely results from differences in the magnitude scaling factors inherent to each. As a result, the hazard corresponding to any particular LPI , LPI_{ISH} , LSN , or IDS value is dependent on the liquefaction triggering procedure used within the hazard framework.

- Optimal frameworks for particular misprediction economies were determined by Eq. 6 and presented in Figure 5. It was shown that LPI_{ISH} and LSN provide more efficient hazard assessments, relative to LPI , for particular misprediction economies. Conversely, IDS was generally inferior and is not recommended for predicting liquefaction manifestation, as classified in this study. Collectively, the results presented in Figures 4 and 5 can be used to guide strategies for assessing and mitigating hazard, as demonstrated for several simple scenarios.
- Overall prediction efficiency was evaluated in terms of AUC and presented in Figure 6. The B&I14 procedure tended to result in slightly more efficient hazard assessments as compared to I&B08. Moreover, it was shown that alternatives to LPI provide little to no statistical benefit in terms of AUC. Thus, while LSN and LPI_{ISH} have made notable improvements, resulting in more efficient predictions for particular misprediction economies, the development of an improved liquefaction hazard framework is still profoundly important.
- The findings presented in this study are based on analyses of 9,908 liquefaction case histories, predominately resulting from earthquakes in Canterbury, New Zealand; their applicability to other datasets, or to methodologies different from that used herein, is unknown.

References

- Anselin, L. (1995). "Local Indicators of Spatial Association—LISA." *Geographical Analysis*, 27(2): 93–115.
- Baise, L.G., Higgins, R.B., & Brankman, C.M. (2006). Liquefaction hazard mapping-statistical and spatial characterization of susceptible units. *Journal of Geotechnical and Geoenvironmental Engineering* 132(6): 705-715.
- Boulanger, R.W. and Idriss, I.M. (2014). "CPT and SPT based liquefaction triggering procedures." *Report No. UCD/CGM.-14/01*, Center for Geotech. Modelling, Department of Civil and Environmental Engineering, UC Davis, CA, USA.
- Bradley, B. A. (2012). "Strong ground motion characteristics observed in the 4 September 2010 Darfield, New Zealand earthquake." *Soil Dynamics and Earthquake Engineering*, 42: 32-46.
- Bradley, B.A. & Cubrinovski, M., (2011). "Near-source Strong Ground Motions Observed in the 22 February 2011 Christchurch Earthquake." *Seismological Research Letters*, 82: 853-865.
- Bradley, B.A. (2013a). "Site-specific and spatially-distributed ground motion intensity estimation in the 2010-2011 Christchurch earthquakes." *Soil Dynamics and Earthquake Engineering*, 48: 35-47.
- Bradley, B.A. (2013b). "A New Zealand-specific pseudo-spectral acceleration ground-motion prediction equation for active shallow crustal earthquakes based on foreign models." *Bulletin of the Seismological Society of America*; 103(3): 1801-1822.
- CERA (2013). "Purpose and scope of the Canterbury geotechnical database." *Canterbury Earthquake Recovery Authority*; See: <https://canterburygeotechnicaldatabase.projectorbit.com>. Accessed 9/3/16.
- Cetin, K., Bilge, H., Wu, J., Kammerer, A., and Seed, R. (2009). "Probabilistic Model for the Assessment of Cyclically Induced Reconsolidation (Volumetric) Settlements." *Journal of Geotechnical and Geoenvironmental Engineering*, 135(3): 387-398.
- Chung, J. & Rogers, J., (2011). Simplified method for spatial evaluation of liquefaction potential in the St. Louis Area. *Journal of Geotechnical and Geoenvironmental Engineering*, 137(5): 505-515.
- Cramer, C.H., Rix, G.J., & Tucker, K. (2008). Probabilistic liquefaction hazard maps for Memphis, Tennessee. *Seismological Research Letters* 79(3): 416-423.
- Cubrinovski, M. & Green, R.A. (eds.) (2010). "Geotechnical Reconnaissance of the 2010 Darfield (Canterbury) Earthquake", (contributing authors in alphabetical order: J. Allen, S. Ashford, E. Bowman, B. Bradley, B. Cox, M. Cubrinovski, R. Green, T. Hutchinson, E. Kavazanjian, R.

- Orense, M. Pender, M. Quigley, & L. Wotherspoon), *Bulletin of the New Zealand Society for Earthquake Engineering*, 43(4): 243-320.
- Cubrinovski, M., Bradley, B.A., Wotherspoon, L., Green, R.A., Bray, J., Woods, C., et al. (2011a) “Geotechnical aspects of the 22 February 2011 Christchurch earthquake”. *Bulletin of the New Zealand Society for Earthquake Engineering*, 44(4):205–226.
- Cubrinovski, M., Bray, J.D., Taylor, M., Giorgini, S., Bradley, B.A., Wotherspoon, L., Zupan, J. (2011b). “Soil liquefaction effects in the central business district during the February 2011 Christchurch earthquake.” *Seismological Research Letters*, 82: 893–904.
- Cubrinovski, M., Robinson, K., Taylor, M., Hughes, M., Orense, R. (2012). “Lateral spreading and its impacts in urban areas in the 2010–2011 Christchurch earthquakes.” *New Zealand Journal of Geology and Geophysics*, 55: 255–269.
- Cubrinovski, M., Winkley, A., Haskell, J., Palermo, A., Wotherspoon, L., Robinson, K., et al. (2014). “Spreading-induced damage to short-span bridges in Christchurch, New Zealand.” *Earthquake Spectra*, 30(1): 57–83.
- Dixit, J., Dewaikar, D. M., and Jangid, R. S. (2012). “Assessment of liquefaction potential index for Mumbai City.” *Natural Hazards and Earth Systems Sciences*, 12(9): 2759–2768.
- Fawcett, T. (2005). “An introduction to ROC analysis.” *Pattern Recognition Letters*, 27: 861-874.
- Green, R.A., Allen, A., Wotherspoon, L., Cubrinovski, M., Bradley, B., Bradshaw, A., Cox, B., & Algie, T. (2011). “Performance of levees (stopbanks) during the 4 September M_w 7.1 Darfield and 22 February 2011 M_w 6.2 Christchurch, New Zealand, earthquakes.” *Seismological Research Letters*, 82(6): 939-949.
- Green, R.A., Cubrinovski, M., Cox, B., Wood, C., Wotherspoon, L., Bradley, B., & Maurer, B.W. (2014). “Select Liquefaction Case Histories from the 2010-2011 Canterbury Earthquake Sequence.” *Earthquake Spectra*, 30(1): 131-153.
- Green, R.A., Maurer, B.W., Cubrinovski, M., and Bradley, B.A. (2015). “Assessment of the relative predictive capabilities of CPT-based liquefaction evaluation procedures: Lessons learned from the 2010-2011 Canterbury earthquake sequence.” *6th International Conference on Earthquake Geotechnical Engineering*, Nov 2-4; Christchurch, New Zealand; Paper No. 796. International Society of Soil Mechanics and Geotechnical Engineering.
- Hayati, H. & Andrus, R.D. (2008). Liquefaction potential map of Charleston, South Carolina based on the 1986 earthquake. *Journal of Geotechnical and Geoenvironmental Engineering* 134(6): 815-828.

- Holzer, T.L., Bennett, M.J., Noce, T.E., Padovani, A.C., Tinsley III, J.C. (2006). "Liquefaction hazard mapping with LPI in the greater Oakland, California, area." *Earthquake Spectra*, 22(3): 693-708.
- Holzer, T.L., (2008). Probabilistic liquefaction hazard mapping, in Zeng, D., Manzari, M.T., & Hiltunen, D.R., *Geotechnical Earthquake Engineering and Soil Dynamics IV: Sacramento, CA*, ASCE Geotechnical Special Publication 181.
- Holzer, T.L., Noce, T.E., and Bennett, M.J. (2009). "Scenario liquefaction hazard maps of Santa Clara Valley, Northern California." *Bulletin of the Seismological Society of America*, 99(1): 367-381.
- Idriss, I.M. & Boulanger, R.W. (2008). "Soil liquefaction during earthquakes." Monograph MNO-12, Earthquake Engineering Research Institute, Oakland, CA, 261 pp.
- Ishihara, K., 1985. "Stability of natural deposits during earthquakes." *Proceedings of the 11th International Conference on Soil Mechanics and Foundation Engineering*, San Francisco, CA, USA, 1, 321-376.
- Ishihara, K., and Yoshimine, M. (1992). "Evaluation of settlements in sand deposits following liquefaction during earthquakes." *Soils and Foundations*, 32(1): 173–188.
- Iwasaki, T., Tatsuoka, F., Tokida, K., & Yasuda, S. (1978). "A practical method for assessing soil liquefaction potential based on case studies at various sites in Japan." *Proceedings of the 2nd International Conference on Microzonation*, Nov 26-Dec 1, San Francisco, CA, USA.
- Iwasaki, T., Tokida, F., Tatsuoka, S., Watanabe, S., Yasuda, and H. Sato (1982). "Microzonation for soil liquefaction potential using simplified methods." *3rd International Earthquake Microzonation Conference*, Seattle, p. 1319-1330.
- Kang, G.C., Chung, J.W., Rogers, J.D. (2014). "Re-calibrating the thresholds for the classification of liquefaction potential index based on the 2004 Niigata-ken Chuetsu earthquake." *Engineering Geology*, 169: 30-40.
- Lee, K.L. and Albaisa, A. (1974). "Earthquake induced settlements in saturated sands." *Journal of Soil Mechanics and Foundations*, 100(4): 387-406.
- Lee, D.-H., Ku, C.-S., and Yuan, H. (2004). "A study of liquefaction risk potential at Yuanlin, Taiwan." *Engineering Geology*, 71(1–2): 97–117.
- Maurer, B.W., Green, R.A., Cubrinovski, M., and Bradley, B.A. (2014). "Evaluation of the liquefaction potential index for assessing liquefaction hazard in Christchurch, New Zealand." *Journal of Geotechnical and Geoenvironmental Engineering* 140(7): 04014032.

- Maurer, B.W., Green, R.A., and Taylor, O.S. (2015a). "Moving towards an improved index for assessing liquefaction hazard: lessons from historical data." *Soils and Foundations*, 55(4): 778-787.
- Maurer, B.W., Green, R.A., Cubrinovski, M., Bradley, B. (2015b). "Fines-content effects on liquefaction hazard evaluation for infrastructure during the 2010-2011 Canterbury, New Zealand earthquake sequence." *Soil Dynamics and Earthquake Engineering*, 76: 58-68.
- Maurer, B.W., Green, R.A., Cubrinovski, M., and Bradley, B. (2015c). "Assessment of CPT-based methods for liquefaction evaluation in a liquefaction potential index framework." *Géotechnique* 65(5): 328-336.
- Maurer, B.W., Green, R.A., Cubrinovski, M., and Bradley, B.A. (2015d). "Investigating the influence of post-liquefaction strain potential on the accuracy of Liquefaction Severity Number (LSN) hazard assessments." *10th Pacific Conference on Earthquake Engineering*, Nov 6-8; Sydney, Australia; Paper No. 796. Australian Earthquake Engineering Society.
- Maurer, B.W., Green, R.A., and van Ballegooy, S. (2016). "Deterministic and probabilistic correlations for predicting liquefaction susceptibility and fines content: a study of the cone penetration test in Christchurch, New Zealand" *Geotechnical Testing Journal*, American Society for Testing and Materials; *In Review*.
- MBIE (2015). "Repairing and rebuilding houses affected by the Canterbury earthquakes." Ver. 3a, Ministry of Business, Innovation, and Employment, Wellington, New Zealand.
- Moss, R.E.S, Seed, R.B., Kayen, R.E., Stewart, J.P., Der Kiureghian, A., & Cetin, K.O. (2006). "CPT-based probabilistic and deterministic assessment of in situ seismic soil liquefaction potential." *Journal of Geotechnical and Geoenvironmental Engineering* 132(8): 1032-1051.
- Nagase H, Ishihara K. (1988). "Liquefaction-induced compaction and settlement of sand during earthquakes." *Soils and Foundations*, 28(1): 66–76.
- NZGD (2016). "New Zealand Geotechnical Database." <<https://www.nzgd.org.nz/Default.aspx>> Accessed 8/24/16. New Zealand Earthquake Commission (EQC).
- O'Rourke, T., Jeon, S.S., Toprak, S., Cubrinovski, M., Huges, M., van Ballegooy, S., and Bouziou, D. (2014). "Earthquake response of underground pipeline networks in Christchurch, NZ." *Earthquake Spectra*, 30(1): 183-204.
- Papathanassiou, G., Pavlides, S., and Ganas, A. (2005). "The 2003 Lefkada earthquake: Field observation and preliminary microzonation map based on liquefaction potential index for the town of Lefkada." *Engineering Geology*, 82(1): 12–31.

- Papathanassiou, G. (2008). "LPI-based approach for calibrating the severity of liquefaction-induced failures and for assessing the probability of liquefaction surface evidence." *Engineering Geology*, 96(1–2): 94–104.
- Papathanassiou, G., Mantovani, A., Tarabusi, G., Rapti, D., and Caputo, R. (2015). "Assessment of liquefaction potential for two liquefaction prone areas considering the May 20, 2012 Emilia (Italy) earthquake." *Engineering Geology*, 189: 1-16.
- Provost, F. and Fawcett, T. (2001). "Robust classification for imprecise environments." *Machine Learning*, 42 (3): 203–231.
- Quigley, M.C., Bastin, S., and Bradley, B.A. (2013). "Recurrent liquefaction in Christchurch, New Zealand, during the Canterbury earthquake sequence." *Geology*, 41(4): 419-422.
- Quigley, M., Hughes, M.W., Bradley, B.A., Van Ballegooy S., Reid, C., Morgenroth, J., Horton, T., Duffy, B., Pettinga, J. (2016). "The 2010-2011 Canterbury earthquake sequence: Environmental effects, seismic triggering thresholds and geologic legacy." *Tectonophysics*, (672-673): 228-274.
- Robertson, P.K. & Wride, C.E. (1998). "Evaluating cyclic liquefaction potential using cone penetration test." *Canadian Geotechnical Journal*, 35(3): 442-459.
- Sana, H. and Nath, S.K. (2016). "Liquefaction potential analysis of the Kashmire valley alluvium, NW Himalaya." *Soil Dynamics and Earthquake Engineering*, 85: 11-18.
- Sonmez, H. (2003). "Modification of the liquefaction potential index and liquefaction severity mapping for a liquefaction-prone area (Inegol, Turkey)." *Engineering Geology*, 44(7): 862–871.
- Toprak, S., and Holzer, T. L. (2003). "Liquefaction potential index: Field assessment." *Journal of Geotechnical and Geoenvironmental Engineering*, 129(4): 315-322.
- van Ballegooy, S., Malan, P., Lacrosse, V., Jacka, M.E., Cubrinovski, M., Bray, J.D., O'Rourke, T.D., Crawford, S.A., and Cowan, H. (2014a). "Assessment of liquefaction-induced land damage for residential Christchurch." *Earthquake Spectra*, 30(1): 31-55.
- van Ballegooy, S., Cox, S.C., Thurlow, C., Rutter, H.K., Reynolds T., Harrington, G., Fraser, J., and Smith, T. (2014b). "Median water table elevation in Christchurch and surrounding area after the 4 September 2010 Darfield earthquake: Version 2." GNS Science Report 2014/18.
- Van Ballegooy, S., Green, R.A., Lees, J., Wentz, F., and Maurer, B.W. (2015). "Assessment of various CPT based liquefaction severity index frameworks relative to the Ishihara (1985) H₁-H₂ boundary curves." *Soil Dynamics and Earthquake Engineering*, 79: 347-364.
- Wotherspoon, L., Bradshaw, A., Green, R.A., Wood, C., Palermo, A., Cubrinovski, M., and Bradley, B. (2011). "Performance of bridges during the 2010 Darfield and 2011 Christchurch earthquakes." *Seismological Research Letters*, 82(6): 950-964.

- Yalcin, A., Gokceoglu, C., and Sönmez, H. (2008). “Liquefaction severity map for Aksaray city center (Central Anatolia, Turkey).” *Natural Hazards and Earth Systems Sciences*, 8(4): 641–649.
- Zhang, G., Robertson, P.K., and Brachman, R.W.I. (2002). “Estimating liquefaction-induced ground settlements from CPT for level ground.” *Canadian Geotechnical Journal*, 39(5): 1168-1180.
- Zou, K.H. (2007). “Receiver operating characteristic (ROC) literature research.” On-line bibliography available from: <<http://www.spl.harvard.edu/archive/spl-pre2007/pages/ppl/zou/roc.html>> accessed 15 March 2014.

Tables

Table 8.1 Summary of Liquefaction Case Histories Analyzed in this Study

Date	Event	Country	Magnitude (M _w)	Number of Case Histories
June 16, 1964	Niigata	Japan	7.60	3
February 9, 1971	San Fernando	United States	6.60	2
February 4, 1975	Haicheng	China	7.00	2
July 27, 1976	Tangshan	China	7.60	10
October 15, 1979	Imperial Valley	United States	6.53	5
June 9, 1980	Victoria (Mexicali)	Mexico	6.33	5
April 26, 1981	Westmoreland	United States	5.90	7
May 26, 1983	Nihonkai-Chubu	Japan	7.70	2
October 28, 1983	Borah Peak	United States	6.88	3
March 2, 1987	Edgcumbe	New Zealand	6.60	23
November 24, 1987	Superstition Hills	United States	6.54	8
October 18, 1989	Loma Prieta	United States	6.93	61
January 17, 1994	Northridge	United States	6.69	3
January 16, 1995	Hyogoken-Nambu	Japan	6.90	21
August 17, 1999	Kocaeli	Turkey	7.51	16
September 20, 1999	Chi-Chi	Taiwan	7.62	37
June 8, 2008	Achaia-Ilia	Greece	6.40	2
April 4, 2010	El Mayor-Cucapah	Mexico	7.20	2
September 4, 2010	Darfield	New Zealand	7.10	3647
February 22, 2011	Christchurch	New Zealand	6.20	3700
March 11, 2011	Tohoku	Japan	9.00	7
May 20, 2012	Emilia	Italy	6.10	46
February 14, 2016	Christchurch	New Zealand	5.70	2296
Total				9908

Table 8.2 Criteria for Classifying the Severity of Liquefaction Manifestation.

Classification	Criteria
No Manifestation	No surficial liquefaction manifestation or lateral spread cracking
Marginal Manifestation	Small, isolated liquefaction features; streets had traces of ejecta or wet patches less than a vehicle width; < 5% of ground surface covered by ejecta
Moderate Manifestation	Groups of liquefaction features; streets had ejecta patches greater than a vehicle width but were still passable; 5-40% of ground surface covered by ejecta
Severe Manifestation	Large masses of adjoining liquefaction features, streets impassible due to liquefaction; >40% of ground surface covered by ejecta

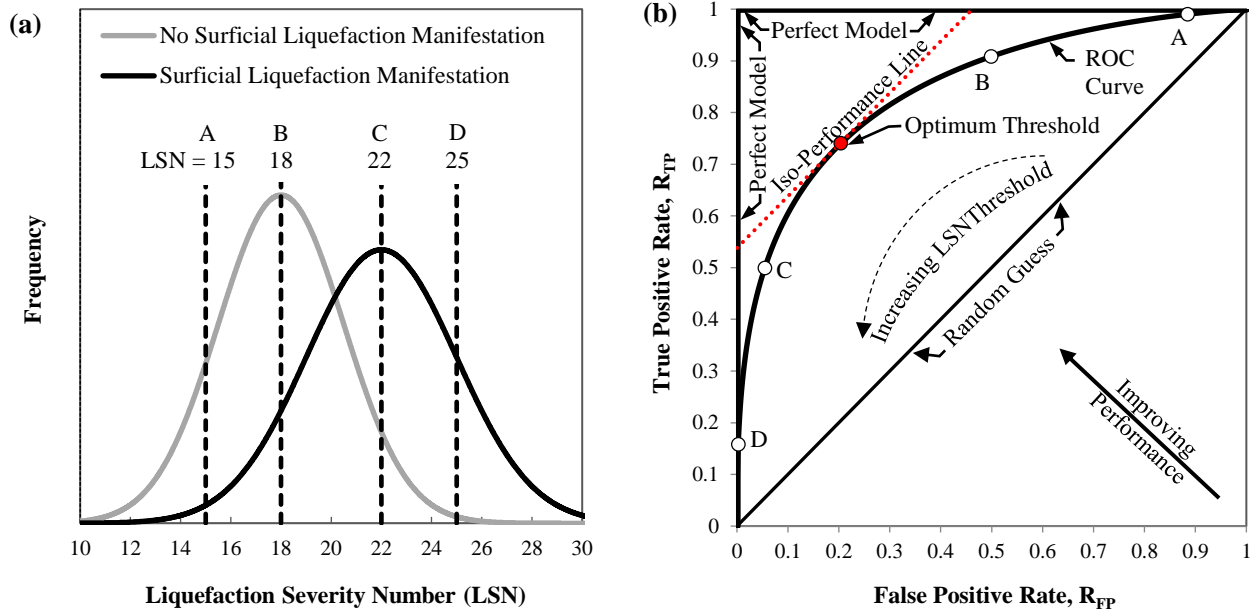


Figure 8.1 ROC analyses: (a) frequency distributions of liquefaction manifestation and no liquefaction manifestation as a function of LSN ; (b) corresponding ROC curve, and illustration of how a ROC curve is used to assess the performance of a diagnostic test. The optimum LSN decision threshold is that for which the misprediction cost is minimized.

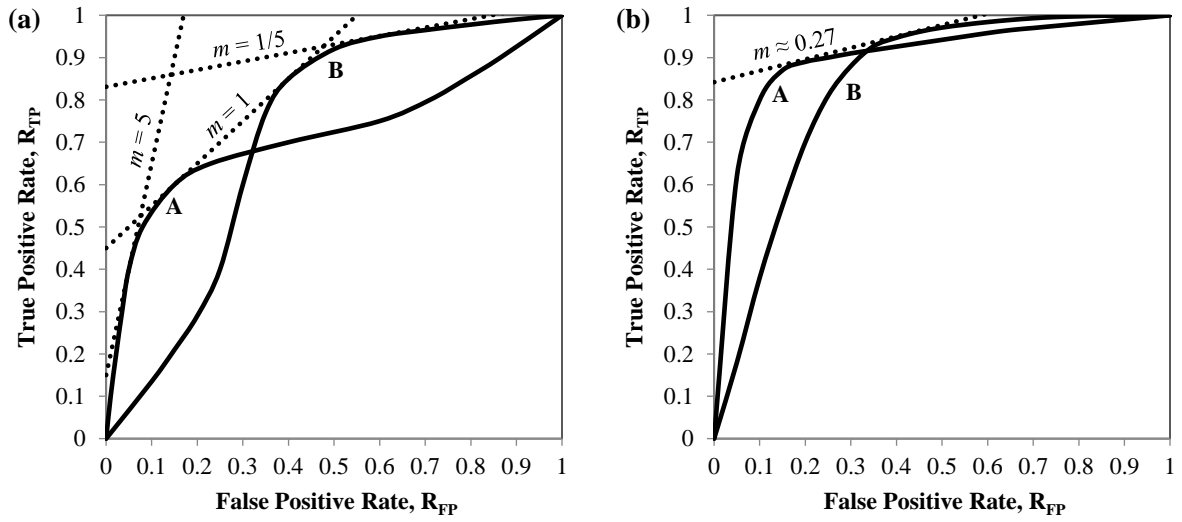


Figure 8.2 ROC analyses demonstrating that: (a) classifiers with equivalent AUC (i.e., equivalent overall efficiency) can perform very differently in specific regions of ROC space; (b) classifiers with higher AUC can, in specific regions of ROC space, perform worse than classifiers with lower AUC .

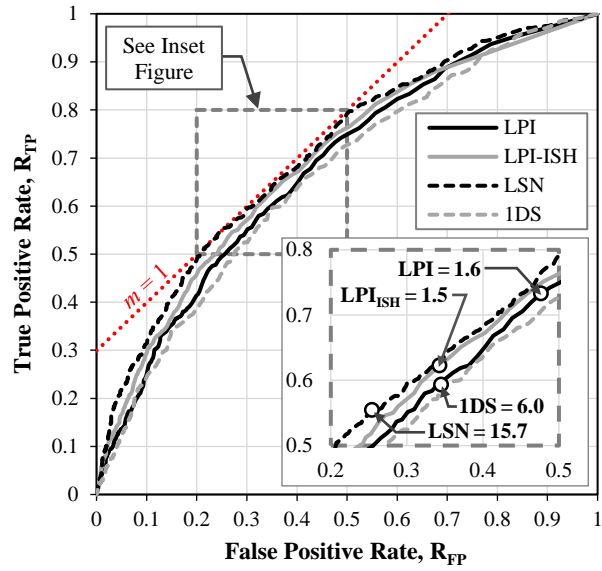


Figure 8.3 ROC analysis of LPI, LPI_{ISH}, LSN, and IDS performance in predicting the occurrence of surficial liquefaction manifestations, wherein the I&B08 procedure was used. Optimal decision thresholds for the scenario $CR = 1$ are highlighted for each liquefaction hazard framework in the inset figure.

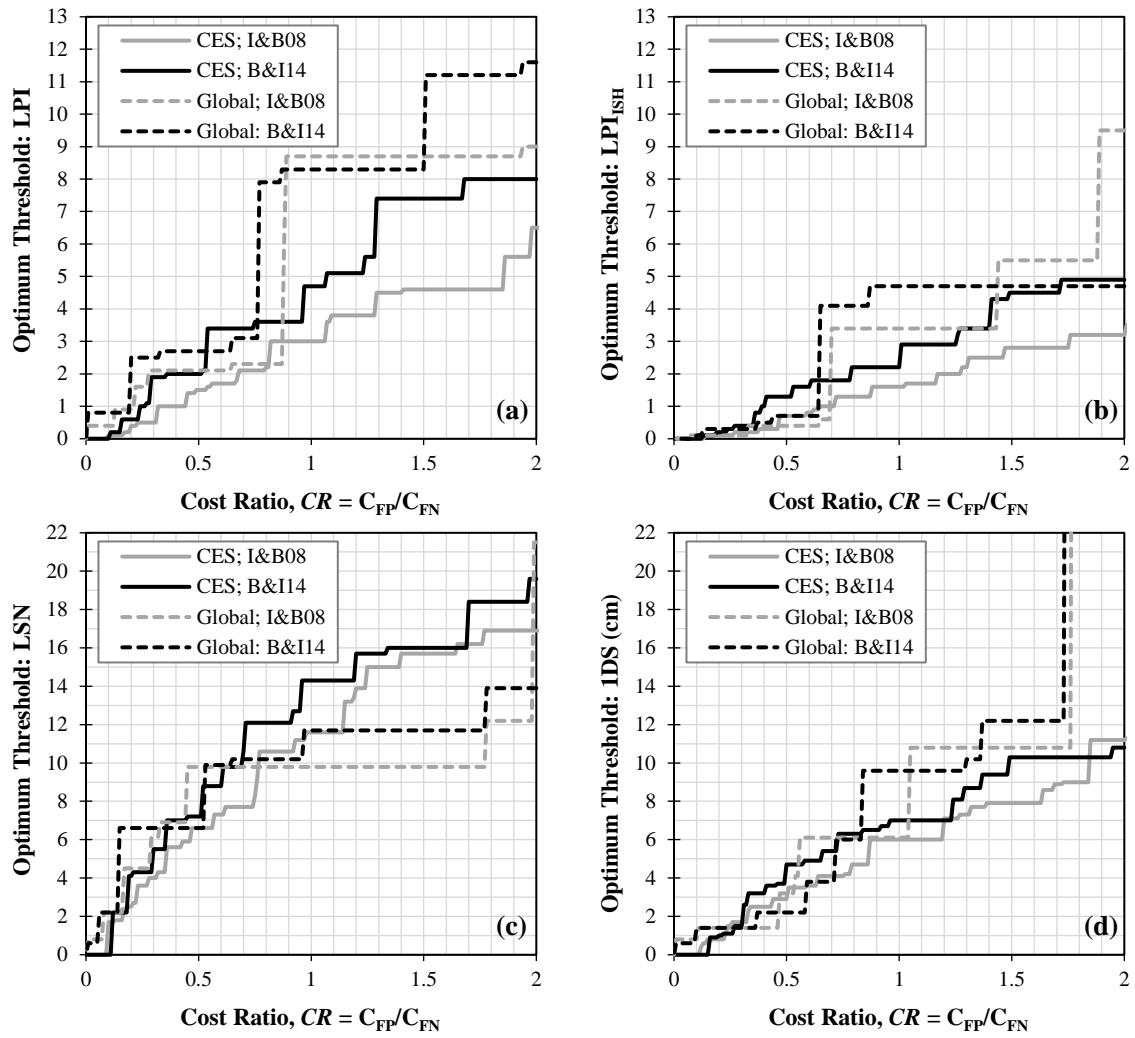


Figure 8.4 Optimal decision threshold vs. CR , as determined from analyses of the CES and global datasets using the I&B08 and B&I14 liquefaction triggering procedures within the frameworks of: (a) LPI ; (b) LPI_{ISH} ; (c) LSN ; and (d) IDS .

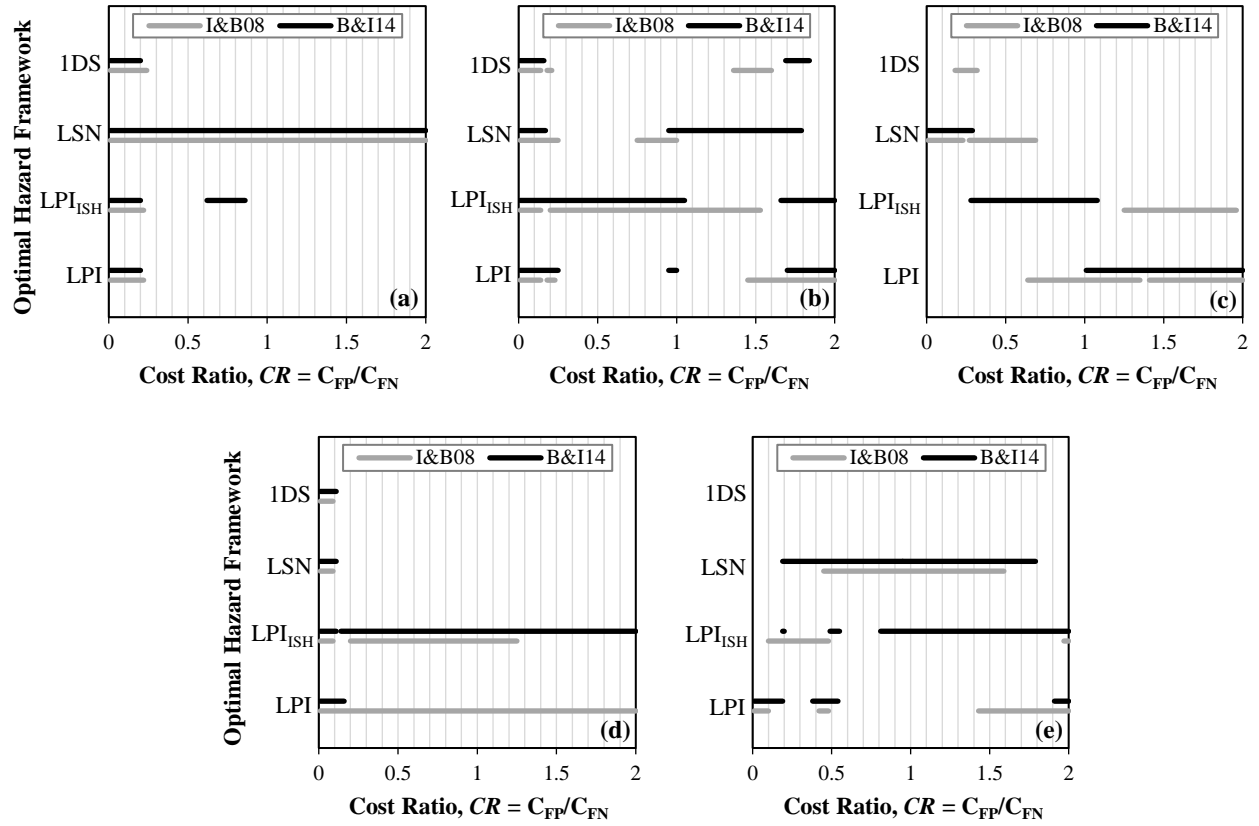


Figure 8.5 Optimal liquefaction hazard framework as a function of CR , as determined from ROC analyses of the: (a) Sept 2010 M_w 7.1 Darfield Earthquake; (b) Feb 2011 M_w 6.2 Christchurch Earthquake; (c) Feb 2016 M_w 5.7 Christchurch Earthquake; (d) CES dataset (i.e., a, b, and c combined); and (e) global dataset.

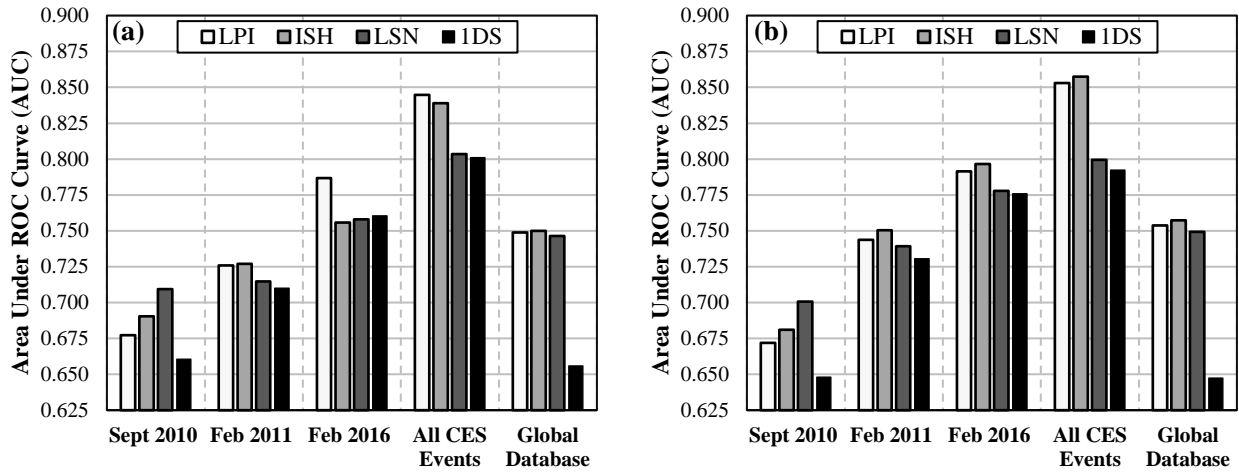


Figure 8.6 AUC values computed from ROC analyses of the CES and global datasets using the (a) I&B08 and (b) B&I14 liquefaction triggering procedures within the *LPI*, *LPI_{ISH}*, *LSN*, and *IDS* liquefaction hazard frameworks. AUC is a popular measure of overall prediction efficiency.

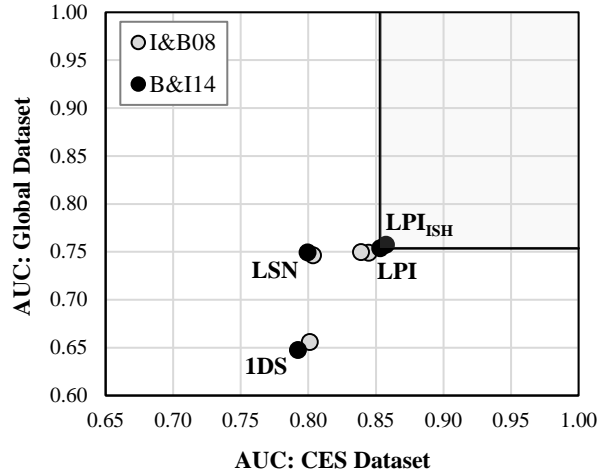


Figure 8.7 AUC computed from ROC analyses of the CES dataset vs. global dataset using the I&B08 and B&I14 procedures within the *LPI*, *LPI_{ISH}*, *LSN* and *IDS* liquefaction hazard frameworks. Figure 7 is an alternative visualization of data presented in Figure 6.

8.8 Electronic Supplement

Table 8.3 (S1) Global Dataset of Liquefaction Case Histories

No.	CPT ID	Date	Event	Country	Mag (M_w)	PGA (g)	GWT (mbg)	Y/N	References
1	D - Kawagisho-cho	16-Jun-1964	Niigata	Japan	7.60	0.162	1.10	Y	Ishihara and Koga (1981); Farrar (1990); Moss et al. (2003)
2	E - Showa Bridge (Left Bank)	16-Jun-1964	Niigata	Japan	7.60	0.162	1.40	Y	Ishihara and Koga (1981); Farrar (1990); Moss et al. (2003)
3	F - Showa Bridge (Right Bank)	16-Jun-1964	Niigata	Japan	7.60	0.162	1.70	N	Ishihara and Koga (1981); Farrar (1990); Moss et al. (2003)
4	Balboa Boulevard (BAL-10)	9-Feb-1971	San Fernando	United States	6.60	0.450	7.20	N	Bennett et al., 1998; Toprak and Holzer (2003)
5	Balboa Boulevard (BAL-11)	9-Feb-1971	San Fernando	United States	6.60	0.450	7.60	N	Bennett et al., 1998; Toprak and Holzer (2003)
6	17th Middle School	4-Feb-1975	Haicheng	China	7.00	0.300	1.00	N	Arulandan et al. (1986); Shengcong and Tatsuoka (1984)
7	Paper Mill	4-Feb-1975	Haicheng	China	7.00	0.300	1.52	Y	Arulandan et al. (1986); Shengcong and Tatsuoka (1984)
8	Tangshan (T1)	27-Jul-1976	Tangshan	China	7.60	0.640	3.70	Y	Shibata and Teparaska (1988); Moss et al. (2009; 2011)
9	Tangshan (T10)	27-Jul-1976	Tangshan	China	7.60	0.640	1.50	Y	Shibata and Teparaska (1988); Moss et al. (2009; 2011)
10	Tangshan (T11)	27-Jul-1976	Tangshan	China	7.60	0.610	0.90	Y	Shibata and Teparaska (1988); Moss et al. (2009; 2011)
11	Tangshan (T13)	27-Jul-1976	Tangshan	China	7.60	0.580	1.10	Y	Shibata and Teparaska (1988); Moss et al. (2009; 2011)
12	Tangshan (T16)	27-Jul-1976	Tangshan	China	7.60	0.260	3.50	N	Shibata and Teparaska (1988); Moss et al. (2009; 2011)
13	Tangshan (T4)	27-Jul-1976	Tangshan	China	7.60	0.640	1.10	N	Shibata and Teparaska (1988); Moss et al. (2009; 2011)
14	Tangshan (T6)	27-Jul-1976	Tangshan	China	7.60	0.640	1.50	Y	Shibata and Teparaska (1988); Moss et al. (2009; 2011)
15	Tangshan (T7)	27-Jul-1976	Tangshan	China	7.60	0.640	3.00	Y	Shibata and Teparaska (1988); Moss et al. (2009; 2011)

16	Tangshan (T8)	27-Jul-1976	Tangshan	China	7.60	0.640	2.20	Y	Shibata and Teparaska (1988); Moss et al. (2009; 2011)
17	Tangshan (T9-2)	27-Jul-1976	Tangshan	China	7.60	0.640	1.10	N	Shibata and Teparaska (1988); Moss et al. (2009; 2011)
18	McKim Ranch (MCK4)	15-Oct-1979	Imperial Valley	United States	6.53	0.510	1.50	N	Bennett et al. (1984); Seed et al. (1984)
19	McKim Ranch (MCK7)	15-Oct-1979	Imperial Valley	United States	6.53	0.510	1.50	Y	Bennett et al. (1984); Seed et al. (1984)
20	Radio Tower (Rad2)	15-Oct-1979	Imperial Valley	United States	6.53	0.200	2.10	Y	Bennett et al. (1984); Seed et al. (1984)
21	Radio Tower (Rad4)	15-Oct-1979	Imperial Valley	United States	6.53	0.200	2.10	N	Bennett et al. (1984); Seed et al. (1984)
22	River Park (RVP002)	15-Oct-1979	Imperial Valley	United States	6.53	0.160	0.30	Y	Moss et al. (2005)
23	Delta Site 1	9-Jun-1980	Victoria (Mexicali)	Mexico	6.33	0.190	2.30	N	Diaz-Rodriguez (1984); Diaz-Rodriguez and Armijo-Palaio (1991); Moss et al. (2003)
24	Delta Site 2	9-Jun-1980	Victoria (Mexicali)	Mexico	6.33	0.190	2.20	Y	Diaz-Rodriguez (1984); Diaz-Rodriguez and Armijo-Palaio (1991); Moss et al. (2003)
25	Delta Site 3	9-Jun-1980	Victoria (Mexicali)	Mexico	6.33	0.190	2.00	Y	Diaz-Rodriguez (1984); Diaz-Rodriguez and Armijo-Palaio (1991); Moss et al. (2003)
26	Delta Site 3'	9-Jun-1980	Victoria (Mexicali)	Mexico	6.33	0.190	2.20	Y	Diaz-Rodriguez (1984); Diaz-Rodriguez and Armijo-Palaio (1991); Moss et al. (2003)
27	Delta Site 4	9-Jun-1980	Victoria (Mexicali)	Mexico	6.33	0.190	2.00	Y	Diaz-Rodriguez (1984); Diaz-Rodriguez and Armijo-Palaio (1991); Moss et al. (2003)
28	Herber Road (HEB001)	26-Apr-1981	Westmoreland	United States	5.90	0.170	1.80	N	Moss et al. (2005)
29	Kornbloom (KOR4)	26-Apr-1981	Westmoreland	United States	5.90	0.320	2.70	Y	Bennett et al. (1984); Seed et al. (1984)
30	Kornbloom (KOR5)	26-Apr-1981	Westmoreland	United States	5.90	0.320	2.70	Y	Bennett et al. (1984); Seed et al. (1984)
31	Radio Tower (Rad2)	26-Apr-1981	Westmoreland	United States	5.90	0.200	2.10	Y	Bennett et al. (1984); Seed et al. (1984)
32	Radio Tower (Rad4)	26-Apr-1981	Westmoreland	United States	5.90	0.200	2.10	N	Bennett et al. (1984); Seed et al. (1984)
33	River Park (RVP002)	26-Apr-1981	Westmoreland	United States	5.90	0.170	0.30	N	Moss et al. (2005)
34	Wildlife B (3Cg)	26-Apr-1981	Westmoreland	United States	5.90	0.260	1.20	Y	Bennett et al. (1984); Cetin et al. (2000)

35	Akita B	26-May-1983	Nihonkai-Chubu	Japan	7.70	0.170	1.00	Y	Farrar (1990)
36	Akita C	26-May-1983	Nihonkai-Chubu	Japan	7.70	0.170	2.40	N	Farrar (1990)
37	Whiskey Springs Site 1 (CPT-1a)	28-Oct-1983	Borah Peak	United States	6.88	0.500	0.80	Y	Andrus (1986), Andrus & Youd (1987), Moss et al. (2003)
38	Whiskey Springs Site 2 (CPT-2)	28-Oct-1983	Borah Peak	United States	6.88	0.500	2.40	Y	Andrus (1986), Andrus & Youd (1987), Moss et al. (2003)
39	Whiskey Springs Site 3 (CPT-3)	28-Oct-1983	Borah Peak	United States	6.88	0.500	6.80	Y	Andrus (1986), Andrus & Youd (1987), Moss et al. (2003)
40	Awaroa Farm (AWA004)	2-Mar-1987	Edgecumbe	New Zealand	6.60	0.370	1.10	Y	Christensen (1995)
41	Brady Farm (BDY001)	2-Mar-1987	Edgecumbe	New Zealand	6.60	0.400	1.65	Y	Christensen (1995), Moss et al. (2003)
42	Brady Farm (BDY004)	2-Mar-1987	Edgecumbe	New Zealand	6.60	0.400	1.53	N	Christensen (1995), Moss et al. (2003)
43	Edgecumbe Pipe Breaks (EPB001)	2-Mar-1987	Edgecumbe	New Zealand	6.60	0.390	3.50	Y	Christensen (1995), Moss et al. (2003)
44	Gordon Farm (GDN001)	2-Mar-1987	Edgecumbe	New Zealand	6.60	0.430	0.50	Y	Christensen (1995), Moss et al. (2003)
45	Gordon Farm (GDN002)	2-Mar-1987	Edgecumbe	New Zealand	6.60	0.430	0.90	N	Christensen (1995), Moss et al. (2003)
46	James Street Loop (JSL006)	2-Mar-1987	Edgecumbe	New Zealand	6.60	0.280	2.00	Y	Christensen (1995), Moss et al. (2003)
47	Keir Farm (KER001)	2-Mar-1987	Edgecumbe	New Zealand	6.60	0.310	2.50	Y	Christensen (1995) Moss et al. (2003)
48	Landing Road Bridge (LRB007)	2-Mar-1987	Edgecumbe	New Zealand	6.60	0.270	1.20	Y	Christensen (1995), Moss et al. (2003)
49	Morris Farm (MRS001)	2-Mar-1987	Edgecumbe	New Zealand	6.60	0.420	1.60	Y	Christensen (1995), Moss et al. (2003)
50	Morris Farm (MRS002)	2-Mar-1987	Edgecumbe	New Zealand	6.60	0.420	1.89	N	Christensen (1995)
51	Morris Farm (MRS003)	2-Mar-1987	Edgecumbe	New Zealand	6.60	0.410	2.08	N	Christensen (1995), Moss et al. (2003)
52	Robinson Farm (RBN001)	2-Mar-1987	Edgecumbe	New Zealand	6.60	0.440	0.80	Y	Christensen (1995), Moss et al. (2003)

53	Robinson Farm (RBN002)	2-Mar-1987	Edgecumbe	New Zealand	6.60	0.440	0.70	N	Christensen (1995)
54	Robinson Farm (RBN003)	2-Mar-1987	Edgecumbe	New Zealand	6.60	0.440	0.90	N	Christensen (1995)
55	Robinson Farm (RBN004)	2-Mar-1987	Edgecumbe	New Zealand	6.60	0.440	0.61	Y	Christensen (1995), Moss et al. (2003)
56	Sewage Pumping Station (SPS001)	2-Mar-1987	Edgecumbe	New Zealand	6.60	0.260	1.30	Y	Christensen (1995), Moss et al. (2003)
57	Whakatane Board Mill (WBM001)	2-Mar-1987	Edgecumbe	New Zealand	6.60	0.270	1.44	N	Christensen (1995), Moss et al. (2003)
58	Whakatane Board Mill (WBM002)	2-Mar-1987	Edgecumbe	New Zealand	6.60	0.270	1.44	N	Christensen (1995), Moss et al. (2003)
59	Whakatane Hospital (HSP001)	2-Mar-1987	Edgecumbe	New Zealand	6.60	0.260	4.40	N	Christensen (1995), Moss et al. (2003)
60	Whakatane Pony Club (WPC001)	2-Mar-1987	Edgecumbe	New Zealand	6.60	0.270	2.35	Y	Christensen (1995), Moss et al. (2003)
61	Whakatane Pony Club (WPC002)	2-Mar-1987	Edgecumbe	New Zealand	6.60	0.270	2.20	Y	Christensen (1995)
62	Whakatane Pony Club (WPC003)	2-Mar-1987	Edgecumbe	New Zealand	6.60	0.270	2.20	N	Christensen (1995)
63	Herber Road (HEB001)	24-Nov-1987	Superstition Hills	United States	6.54	0.160	1.80	N	Moss et al. (2005)
64	Kornbloom (KOR4)	24-Nov-1987	Superstition Hills	United States	6.54	0.174	2.70	N	Bennett et al. (1984); Cetin et al. (2000)
65	Kornbloom (KOR5)	24-Nov-1987	Superstition Hills	United States	6.54	0.174	2.70	N	Bennett et al. (1984); Cetin et al. (2000)
66	McKim Ranch (MCK4)	24-Nov-1987	Superstition Hills	United States	6.54	0.200	1.50	N	Bennett et al. (1984); Toprak and Holzer (2003)
67	Radio Tower (Rad2)	24-Nov-1987	Superstition Hills	United States	6.54	0.200	2.10	N	Bennett et al. (1984); Cetin et al. (2000)
68	Radio Tower (Rad4)	24-Nov-1987	Superstition Hills	United States	6.54	0.180	2.10	N	Bennett et al. (1984); Cetin et al. (2000)
69	River Park (RVP002)	24-Nov-1987	Superstition Hills	United States	6.54	0.190	0.30	N	Moss et al. (2005)
70	Wildlife B (3Cg)	24-Nov-1987	Superstition Hills	United States	6.54	0.206	1.20	Y	Bennett et al. (1984); Holzer and Youd (2007); Cetin et al. (2000)

71	Alameda Bay Farm Island (Dike)	18-Oct-1989	Loma Prieta	United States	6.93	0.240	5.50	N	Mitchell et al. (1994)
72	Alameda Bay Farm Island (HBI-P6))	18-Oct-1989	Loma Prieta	United States	6.93	0.240	3.00	Y	Mitchell et al. (1994)
73	Farris Farm (FAR-58)	18-Oct-1989	Loma Prieta	United States	6.93	0.360	4.80	Y	Bennett & Tinsely (1995); Toprak & Holzer (2003)
74	Farris Farm (FAR-59)	18-Oct-1989	Loma Prieta	United States	6.93	0.360	4.80	Y	Bennett & Tinsely (1995); Toprak & Holzer (2003)
75	Farris Farm (FAR-61)	18-Oct-1989	Loma Prieta	United States	6.93	0.360	4.20	Y	Bennett & Tinsely (1995); Toprak & Holzer (2003)
76	General Fish (CPT-6)	18-Oct-1989	Loma Prieta	United States	6.93	0.280	1.70	N	Boulangier et al. (1995; 1997)
77	Granite Construction (GRA-123)	18-Oct-1989	Loma Prieta	United States	6.93	0.340	5.00	Y	Bennett & Tinsely (1995); Toprak & Holzer (2003)
78	Harbor Office (UC-12)	18-Oct-1989	Loma Prieta	United States	6.93	0.280	1.90	Y	Boulangier et al. (1995; 1997)
79	Harbor Office (UC-13)	18-Oct-1989	Loma Prieta	United States	6.93	0.280	1.90	Y	Boulangier et al. (1995; 1997)
80	Harbor Office (UC-20)	18-Oct-1989	Loma Prieta	United States	6.93	0.280	3.00	Y	Boulangier et al. (1995; 1997)
81	Harbor Office (UC-21)	18-Oct-1989	Loma Prieta	United States	6.93	0.280	2.70	Y	Boulangier et al. (1995; 1997)
82	Jefferson Ranch (JRR-141)	18-Oct-1989	Loma Prieta	United States	6.93	0.210	2.10	Y	Bennett & Tinsely (1995); Toprak & Holzer (2003)
83	Jefferson Ranch (JRR-148)	18-Oct-1989	Loma Prieta	United States	6.93	0.210	3.00	Y	Bennett & Tinsely (1995); Toprak & Holzer (2003)
84	KETT (KET-74)	18-Oct-1989	Loma Prieta	United States	6.93	0.470	1.50	Y	Bennett & Tinsely (1995); Toprak & Holzer (2003)
85	Leonardini (LEN-37)	18-Oct-1989	Loma Prieta	United States	6.93	0.220	2.50	N	Bennett & Tinsely (1995); Toprak & Holzer (2003)
86	Leonardini (LEN-39)	18-Oct-1989	Loma Prieta	United States	6.93	0.220	1.90	Y	Bennett & Tinsely (1995); Toprak & Holzer (2003)
87	Leonardini (LEN-51)	18-Oct-1989	Loma Prieta	United States	6.93	0.220	1.80	Y	Bennett & Tinsely (1995); Toprak & Holzer (2003)
88	Leonardini (LEN-52a)	18-Oct-1989	Loma Prieta	United States	6.93	0.220	2.70	N	Bennett & Tinsely (1995); Toprak & Holzer (2003)

89	Leonardini (LEN-53)	18-Oct-1989	Loma Prieta	United States	6.93	0.220	2.10	Y	Bennett & Tinsely (1995); Toprak & Holzer (2003)
90	Marine Lab (C4)	18-Oct-1989	Loma Prieta	United States	6.93	0.280	2.80	Y	Boullanger et al. (1995; 1997)
91	Marine Lab (UC-1)	18-Oct-1989	Loma Prieta	United States	6.93	0.280	2.40	Y	Boullanger et al. (1995; 1997)
92	Marine Lab (UC-7)	18-Oct-1989	Loma Prieta	United States	6.93	0.280	2.40	Y	Boullanger et al. (1995; 1997)
93	Marinovich (MRR-65)	18-Oct-1989	Loma Prieta	United States	6.93	0.400	5.60	Y	Bennett & Tinsely (1995); Toprak & Holzer (2003)
94	Marinovich (MRR-67)	18-Oct-1989	Loma Prieta	United States	6.93	0.400	6.20	N	Bennett & Tinsely (1995); Toprak & Holzer (2003)
95	MBARI 3 (RC-6)	18-Oct-1989	Loma Prieta	United States	6.93	0.280	2.60	N	Boullanger et al. (1995; 1997)
96	MBARI 3 (RC-7)	18-Oct-1989	Loma Prieta	United States	6.93	0.280	3.70	N	Boullanger et al. (1995; 1997)
97	MBARI 4 (CPT-1)	18-Oct-1989	Loma Prieta	United States	6.93	0.280	1.90	N	Boullanger et al. (1995; 1997)
98	McGowan Farm (MCG-136)	18-Oct-1989	Loma Prieta	United States	6.93	0.260	2.40	N	Bennett & Tinsely (1995); Toprak & Holzer (2003)
99	McGowan Farm (MCG-138)	18-Oct-1989	Loma Prieta	United States	6.93	0.260	1.80	N	Bennett & Tinsely (1995); Toprak & Holzer (2003)
100	Miller Farm (CMF-10)	18-Oct-1989	Loma Prieta	United States	6.93	0.360	3.00	N	Bennett & Tinsely (1995); Toprak & Holzer (2003)
101	Miller Farm (CMF-3)	18-Oct-1989	Loma Prieta	United States	6.93	0.360	4.90	Y	Bennett & Tinsely (1995); Toprak & Holzer (2003)
102	Miller Farm (CMF-5)	18-Oct-1989	Loma Prieta	United States	6.93	0.360	4.90	Y	Bennett & Tinsely (1995); Toprak & Holzer (2003)
103	Miller Farm (CMF-8)	18-Oct-1989	Loma Prieta	United States	6.93	0.360	4.90	Y	Bennett & Tinsely (1995); Toprak & Holzer (2003)
104	Model Airport (AIR-18)	18-Oct-1989	Loma Prieta	United States	6.93	0.260	2.40	Y	Bennett & Tinsely (1995); Toprak & Holzer (2003)
105	Model Airport (AIR-21)	18-Oct-1989	Loma Prieta	United States	6.93	0.260	2.40	Y	Bennett & Tinsely (1995); Toprak & Holzer (2003)
106	Pajaro Dunes (PD1-44)	18-Oct-1989	Loma Prieta	United States	6.93	0.220	3.40	Y	Bennett & Tinsely (1995); Toprak & Holzer (2003)
107	Port of Oakland (POO7-2)	18-Oct-1989	Loma Prieta	United States	6.93	0.280	3.00	Y	Mitchell et al. (1994); Kayen et al. (1998)
108	Port of Oakland (POO7-3)	18-Oct-1989	Loma Prieta	United States	6.93	0.280	3.00	M	Mitchell et al. (1994); Kayen et al. (1998)

109	Port of Richmond (POR-2)	18-Oct-1989	Loma Prieta	United States	6.93	0.180	2.40	Y	Mitchell et al. (1994); Kayen et al. (1998)
110	Port of Richmond (POR-3)	18-Oct-1989	Loma Prieta	United States	6.93	0.180	2.40	Y	Mitchell et al. (1994); Kayen et al. (1998)
111	Port of Richmond (POR-4)	18-Oct-1989	Loma Prieta	United States	6.93	0.180	2.40	Y	Mitchell et al. (1994); Kayen et al. (1998)
112	Radovich (RAD-98)	18-Oct-1989	Loma Prieta	United States	6.93	0.380	3.50	N	Bennett & Tinsely (1995); Toprak & Holzer (2003)
113	Radovich (RAD-99)	18-Oct-1989	Loma Prieta	United States	6.93	0.380	4.10	Y	Bennett & Tinsely (1995); Toprak & Holzer (2003)
114	Sandhold Road (UC-2)	18-Oct-1989	Loma Prieta	United States	6.93	0.280	1.70	N	Boulanger et al. (1995; 1997)
115	Sandhold Road (UC-3)	18-Oct-1989	Loma Prieta	United States	6.93	0.280	1.70	N	Boulanger et al. (1995; 1997)
116	Sandhold Road (UC-6)	18-Oct-1989	Loma Prieta	United States	6.93	0.280	1.70	N	Boulanger et al. (1995; 1997)
117	Sea Mist (SEA-31)	18-Oct-1989	Loma Prieta	United States	6.93	0.220	0.80	Y	Bennett & Tinsely (1995); Toprak & Holzer (2003)
118	Sea Mist (SIL-68)	18-Oct-1989	Loma Prieta	United States	6.93	0.380	3.50	Y	Bennett & Tinsely (1995); Toprak & Holzer (2003)
119	SFO Bay Bridge (SFOBB-1)	18-Oct-1989	Loma Prieta	United States	6.93	0.280	3.00	Y	Mitchell et al. (1994); Kayen et al. (1998)
120	SFO Bay Bridge (SFOBB-2)	18-Oct-1989	Loma Prieta	United States	6.93	0.280	3.00	Y	Mitchell et al. (1994); Kayen et al. (1998)
121	Southern Pacific Bridge (SPR-48)	18-Oct-1989	Loma Prieta	United States	6.93	0.330	5.30	Y	Bennett & Tinsely (1995); Toprak & Holzer (2003)
122	State Beach (UC-18)	18-Oct-1989	Loma Prieta	United States	6.93	0.280	3.40	N	Boulanger et al. (1995; 1997)
123	State Beach Kiosk (UC-14)	18-Oct-1989	Loma Prieta	United States	6.93	0.280	1.80	Y	Boulanger et al. (1995; 1997)
124	State Beach Path (UC-16)	18-Oct-1989	Loma Prieta	United States	6.93	0.280	2.50	Y	Boulanger et al. (1995; 1997)
125	Treasure Island Fire Station (CPTU1)	18-Oct-1989	Loma Prieta	United States	6.93	0.160	1.50	N	Pass (1994), Youd and Carter (2005)
126	Woodward Marine (14-A)	18-Oct-1989	Loma Prieta	United States	6.93	0.280	1.20	Y	Boulanger et al. (1995; 1997)
127	Woodward Marine (15-A)	18-Oct-1989	Loma Prieta	United States	6.93	0.280	1.30	Y	Boulanger et al. (1995; 1997)

128	Woodward Marine (UC-10)	18-Oct-1989	Loma Prieta	United States	6.93	0.280	1.00	Y	Boulanger et al. (1995; 1997)
129	Woodward Marine (UC-11)	18-Oct-1989	Loma Prieta	United States	6.93	0.280	1.00	Y	Boulanger et al. (1995; 1997)
130	Woodward Marine (UC-8)	18-Oct-1989	Loma Prieta	United States	6.93	0.280	1.30	Y	Boulanger et al. (1995; 1997)
131	Woodward Marine (UC-9)	18-Oct-1989	Loma Prieta	United States	6.93	0.280	1.20	Y	Boulanger et al. (1995; 1997)
132	Balboa Boulevard (BAL-10)	17-Jan-1994	Northridge	United States	6.69	0.840	7.20	Y	Bennett et al., 1998; Holzer et al. (1999); Moss et al. (2003)
133	Balboa Boulevard (BAL-11)	17-Jan-1994	Northridge	United States	6.69	0.840	7.60	Y	Bennett et al., 1998; Holzer et al. (1999); Moss et al. (2003)
134	Rory Lane (M-27)	17-Jan-1994	Northridge	United States	6.69	0.800	3.40	Y	Abdel-Haq & Hryciw (1998)
135	Dust Management Facility (DMC)	16-Jan-1995	Hyogoken-Nambu	Japan	6.90	0.370	2.00	Y	Suzuki et al. (2003)
136	Fukuzumi Park (FUP-1)	16-Jan-1995	Hyogoken-Nambu	Japan	6.90	0.650	3.10	N	Suzuki et al. (2003)
137	Hamakoshienn Housing Area (HAH-1)	16-Jan-1995	Hyogoken-Nambu	Japan	6.90	0.500	2.00	Y	Suzuki et al. (2003)
138	Honjyo Central Park (HCP-1)	16-Jan-1995	Hyogoken-Nambu	Japan	6.90	0.700	2.50	N	Suzuki et al. (2003)
139	Imazu Elementary School (IES-1)	16-Jan-1995	Hyogoken-Nambu	Japan	6.90	0.600	1.40	Y	Suzuki et al. (2003)
140	Kobe Art Institute (KAI-1)	16-Jan-1995	Hyogoken-Nambu	Japan	6.90	0.500	3.00	N	Suzuki et al. (2003)
141	Kobe Customs Maya Office A (KMO-A)	16-Jan-1995	Hyogoken-Nambu	Japan	6.90	0.600	1.80	Y	Suzuki et al. (2003)
142	Kobe Customs Maya Office A (KMO-B)	16-Jan-1995	Hyogoken-Nambu	Japan	6.90	0.600	1.80	Y	Suzuki et al. (2003)
143	Kobe Port Construction Office (KOP-2)	16-Jan-1995	Hyogoken-Nambu	Japan	6.90	0.600	2.50	Y	Suzuki et al. (2003)
144	Kobe Pump Station (KPS-1)	16-Jan-1995	Hyogoken-Nambu	Japan	6.90	0.450	2.60	Y	Suzuki et al. (2003)

145	Mikuska Park (MIP-1)	16-Jan-1995	Hyogoken-Nambu	Japan	6.90	0.650	2.00	Y	Suzuki et al. (2003)
146	Nagashi Park (NAP-1)	16-Jan-1995	Hyogoken-Nambu	Japan	6.90	0.650	1.00	N	Suzuki et al. (2003)
147	New Port No. 6 Pier (NPP-1)	16-Jan-1995	Hyogoken-Nambu	Japan	6.90	0.600	2.50	Y	Suzuki et al. (2003)
148	New Wharf Construction Offices (NWC-1)	16-Jan-1995	Hyogoken-Nambu	Japan	6.90	0.450	2.60	Y	Suzuki et al. (2003)
149	Nisseki Kobe Oil Tank A (NKO-2)	16-Jan-1995	Hyogoken-Nambu	Japan	6.90	0.600	2.40	Y	Suzuki et al. (2003)
150	Nisseki Kobe Oil Tank B (NKO-3)	16-Jan-1995	Hyogoken-Nambu	Japan	6.90	0.600	2.40	Y	Suzuki et al. (2003)
151	Shimonakajima Park (SHP-2)	16-Jan-1995	Hyogoken-Nambu	Japan	6.90	0.650	2.00	N	Suzuki et al. (2003)
152	Shiporex Kogyo Osaka Factory (SKF-1)	16-Jan-1995	Hyogoken-Nambu	Japan	6.90	0.400	1.50	Y	Suzuki et al. (2003)
153	Sumiyoshi Elementary (SES-1)	16-Jan-1995	Hyogoken-Nambu	Japan	6.90	0.600	1.90	N	Suzuki et al. (2003)
154	Tokuyama Concrete Factory (TCF-1)	16-Jan-1995	Hyogoken-Nambu	Japan	6.90	0.500	2.00	Y	Suzuki et al. (2003)
155	Yoshida Kogyo Factory (YKF-1)	16-Jan-1995	Hyogoken-Nambu	Japan	6.90	0.500	3.00	N	Suzuki et al. (2003)
156	Adapazari Site B	17-Aug-1999	Kocaeli	Turkey	7.51	0.400	3.30	Y	PEER (2000a)
157	Adapazari Site C2 (CPT-C4)	17-Aug-1999	Kocaeli	Turkey	7.51	0.400	0.40	Y	PEER (2000a)
158	Adapazari Site D (CPT-D1)	17-Aug-1999	Kocaeli	Turkey	7.51	0.400	1.50	Y	PEER (2000a)
159	Adapazari Site E (CPT-E1)	17-Aug-1999	Kocaeli	Turkey	7.51	0.400	0.50	Y	PEER (2000a)
160	Adapazari Site F (CPT-F1)	17-Aug-1999	Kocaeli	Turkey	7.51	0.400	0.50	Y	PEER (2000a)
161	Adapazari Site G (CPT-G1)	17-Aug-1999	Kocaeli	Turkey	7.51	0.400	0.50	Y	PEER (2000a)

162	Adapazari Site H (CPT-H1)	17-Aug-1999	Kocaeli	Turkey	7.51	0.400	1.70	Y	PEER (2000a)
163	Adapazari Site J (CPT-J2)	17-Aug-1999	Kocaeli	Turkey	7.51	0.400	0.60	Y	PEER (2000a)
164	Adapazari Site K (CPT-K1)	17-Aug-1999	Kocaeli	Turkey	7.51	0.400	0.80	Y	PEER (2000a)
165	Adapazari Site L (CPT-L1)	17-Aug-1999	Kocaeli	Turkey	7.51	0.400	1.72	Y	PEER (2000a)
166	Degirmendere DN-1	17-Aug-1999	Kocaeli	Turkey	7.51	0.400	1.70	Y	Youd et al. (2009)
167	Degirmendere DN-2	17-Aug-1999	Kocaeli	Turkey	7.51	0.400	2.50	N	Youd et al. (2009)
168	Hotel Spanca SH-4	17-Aug-1999	Kocaeli	Turkey	7.51	0.370	0.50	Y	PEER (2000a)
169	Police Station PS-1	17-Aug-1999	Kocaeli	Turkey	7.51	0.400	1.00	Y	PEER (2000a)
170	Soccer Field SF-5	17-Aug-1999	Kocaeli	Turkey	7.51	0.370	1.00	Y	PEER (2000a)
171	Yalova Harbor YH-3	17-Aug-1999	Kocaeli	Turkey	7.51	0.370	1.00	Y	PEER (2000a)
172	Nantou Site C (CPT-1)	20-Sep-1999	Chi-Chi	Taiwan	7.62	0.380	1.00	Y	PEER (2000b)
173	Nantou Site C13	20-Sep-1999	Chi-Chi	Taiwan	7.62	0.380	2.00	N	PEER (2000b)
174	Nantou Site C16	20-Sep-1999	Chi-Chi	Taiwan	7.62	0.380	5.30	N	PEER (2000b)
175	Nantou Site C2	20-Sep-1999	Chi-Chi	Taiwan	7.62	0.380	5.00	Y	PEER (2000b)
176	Nantou Site C3	20-Sep-1999	Chi-Chi	Taiwan	7.62	0.380	1.50	Y	PEER (2000b)
177	Nantou Site C6	20-Sep-1999	Chi-Chi	Taiwan	7.62	0.380	2.20	Y	PEER (2000b)
178	Nantou Site C7 (CPT-7)	20-Sep-1999	Chi-Chi	Taiwan	7.62	0.380	1.00	Y	PEER (2000b)
179	Nantou Site C8 (CPT-8)	20-Sep-1999	Chi-Chi	Taiwan	7.62	0.380	1.00	Y	PEER (2000b)
180	Nantou Site K1	20-Sep-1999	Chi-Chi	Taiwan	7.62	0.380	2.50	Y	PEER (2000b)
181	Nantou Site K5	20-Sep-1999	Chi-Chi	Taiwan	7.62	0.380	2.50	Y	PEER (2000b)
182	Nantou Site Y13	20-Sep-1999	Chi-Chi	Taiwan	7.62	0.380	2.20	Y	PEER (2000b)
183	Nantou Site Y14	20-Sep-1999	Chi-Chi	Taiwan	7.62	0.380	2.20	Y	PEER (2000b)
184	WuFeng Site B (WBC-1)	20-Sep-1999	Chi-Chi	Taiwan	7.62	0.600	1.10	Y	PEER (2000b)

185	WuFeng Site C (WCC-6)	20-Sep-1999	Chi-Chi	Taiwan	7.62	0.600	1.20	Y	PEER (2000b)
186	WuFeng Site C10 NCREE	20-Sep-1999	Chi-Chi	Taiwan	7.62	0.600	1.40	Y	PEER (2000b)
187	WuFeng Site C15 NCREE	20-Sep-1999	Chi-Chi	Taiwan	7.62	0.600	2.50	Y	PEER (2000b)
188	WuFeng Site C7 NCREE	20-Sep-1999	Chi-Chi	Taiwan	7.62	0.600	3.20	Y	PEER (2000b)
189	WuFeng Site C8 NCREE	20-Sep-1999	Chi-Chi	Taiwan	7.62	0.600	3.20	N	PEER (2000b)
190	WuFeng Site K5	20-Sep-1999	Chi-Chi	Taiwan	7.62	0.600	1.00	Y	Lee et al. (2000)
191	Yanlin Site 44	20-Sep-1999	Chi-Chi	Taiwan	7.62	0.250	1.40	N	PEER (2000b)
192	Yanlin Site C10	20-Sep-1999	Chi-Chi	Taiwan	7.62	0.250	1.90	N	PEER (2000b)
193	Yanlin Site C11	20-Sep-1999	Chi-Chi	Taiwan	7.62	0.250	2.90	N	PEER (2000b)
194	Yanlin Site C13	20-Sep-1999	Chi-Chi	Taiwan	7.62	0.250	1.10	N	PEER (2000b)
195	Yanlin Site C15	20-Sep-1999	Chi-Chi	Taiwan	7.62	0.250	1.50	N	PEER (2000b)
196	Yanlin Site C16	20-Sep-1999	Chi-Chi	Taiwan	7.62	0.250	2.50	N	PEER (2000b)
197	Yanlin Site C19	20-Sep-1999	Chi-Chi	Taiwan	7.62	0.250	0.60	Y	PEER (2000b)
198	Yanlin Site C2	20-Sep-1999	Chi-Chi	Taiwan	7.62	0.250	0.56	Y	PEER (2000b)
199	Yanlin Site C22	20-Sep-1999	Chi-Chi	Taiwan	7.62	0.250	1.10	Y	PEER (2000b)
200	Yanlin Site C24	20-Sep-1999	Chi-Chi	Taiwan	7.62	0.250	1.20	Y	PEER (2000b)
201	Yanlin Site C25	20-Sep-1999	Chi-Chi	Taiwan	7.62	0.250	3.50	Y	PEER (2000b)
202	Yanlin Site C32	20-Sep-1999	Chi-Chi	Taiwan	7.62	0.250	0.70	Y	PEER (2000b)
203	Yanlin Site C38	20-Sep-1999	Chi-Chi	Taiwan	7.62	0.250	1.40	N	PEER (2000b)
204	Yanlin Site C4	20-Sep-1999	Chi-Chi	Taiwan	7.62	0.250	0.70	Y	PEER (2000b)
205	Yanlin Site C5	20-Sep-1999	Chi-Chi	Taiwan	7.62	0.250	2.40	N	PEER (2000b)
206	Yanlin Site C7	20-Sep-1999	Chi-Chi	Taiwan	7.62	0.250	1.70	N	PEER (2000b)
207	Yanlin Site C8	20-Sep-1999	Chi-Chi	Taiwan	7.62	0.250	1.30	N	PEER (2000b)
208	Yanlin Site C9	20-Sep-1999	Chi-Chi	Taiwan	7.62	0.250	1.20	N	PEER (2000b)
209	Site I (CPT-2)	8-Jun-2008	Achaia-Ilia	Greece	6.40	0.180	0.40	Y	Batilas et al. (2014)
210	Site II (CPT-5)	8-Jun-2008	Achaia-Ilia	Greece	6.40	0.180	0.40	N	Batilas et al. (2014)

211	Herber Road (HEB001)	4-Apr-2010	El Mayor-Cucapah	Mexico	7.20	0.230	1.80	N	Moss et al. (2005); CESMD (2016)
212	San Felipe Bridges (CPT-1)	4-Apr-2010	El Mayor-Cucapah	Mexico	7.20	0.265	2.00	Y	Turner et al. (2016)
213	Akemi Elementary School	11-Mar-2011	Tohoku	Japan	9.00	0.169	1.20	N	Cox et al. (2013), Boulanger and Idriss (2014)
214	Hinode Elementary School	11-Mar-2011	Tohoku	Japan	9.00	0.199	1.20	Y	Cox et al. (2013), Boulanger and Idriss (2014)
215	Hinode Minami Elementary School	11-Mar-2011	Tohoku	Japan	9.00	0.170	1.10	N	Cox et al. (2013), Boulanger and Idriss (2014)
216	Hosoyama Nekki	11-Mar-2011	Tohoku	Japan	9.00	0.180	2.50	N	Cox et al. (2013), Boulanger and Idriss (2014)
217	Irifune Nursery School	11-Mar-2011	Tohoku	Japan	9.00	0.256	1.60	Y	Cox et al. (2013), Boulanger and Idriss (2014)
218	Takasu Chuou Park	11-Mar-2011	Tohoku	Japan	9.00	0.210	1.10	Y	Cox et al. (2013), Boulanger and Idriss (2014)
219	Takasu Kaihin Park	11-Mar-2011	Tohoku	Japan	9.00	0.220	1.30	Y	Cox et al. (2013), Boulanger and Idriss (2014)
220	184050U015	20-May-2012	Emilia	Italy	6.10	0.220	4.20	N	Papathanassiou et al. (2015); Servizio Geologico (2016)
221	184050U016	20-May-2012	Emilia	Italy	6.10	0.220	4.20	N	Papathanassiou et al. (2015); Servizio Geologico (2016)
222	184050U017	20-May-2012	Emilia	Italy	6.10	0.220	2.65	N	Papathanassiou et al. (2015); Servizio Geologico (2016)
223	184050U018	20-May-2012	Emilia	Italy	6.10	0.220	3.45	N	Papathanassiou et al. (2015); Servizio Geologico (2016)
224	184060U001	20-May-2012	Emilia	Italy	6.10	0.310	3.80	N	Papathanassiou et al. (2015); Servizio Geologico (2016)
225	184090U047	20-May-2012	Emilia	Italy	6.10	0.270	4.20	N	Papathanassiou et al. (2015); Servizio Geologico (2016)
226	184090U048	20-May-2012	Emilia	Italy	6.10	0.270	3.70	N	Papathanassiou et al. (2015); Servizio Geologico (2016)
227	184090U049	20-May-2012	Emilia	Italy	6.10	0.270	3.25	N	Papathanassiou et al. (2015); Servizio Geologico (2016)
228	184090U050	20-May-2012	Emilia	Italy	6.10	0.270	3.20	N	Papathanassiou et al. (2015); Servizio Geologico (2016)
229	184090U051	20-May-2012	Emilia	Italy	6.10	0.250	2.50	N	Papathanassiou et al. (2015); Servizio Geologico (2016)

230	184090U052	20-May-2012	Emilia	Italy	6.10	0.250	2.50	N	Papathanassiou et al. (2015); Servizio Geologico (2016)
231	184090U053	20-May-2012	Emilia	Italy	6.10	0.190	4.90	N	Papathanassiou et al. (2015); Servizio Geologico (2016)
232	184090U054	20-May-2012	Emilia	Italy	6.10	0.190	4.90	N	Papathanassiou et al. (2015); Servizio Geologico (2016)
233	184090U055	20-May-2012	Emilia	Italy	6.10	0.230	3.40	N	Papathanassiou et al. (2015); Servizio Geologico (2016)
234	185130B501	20-May-2012	Emilia	Italy	6.10	0.590	3.00	Y	Papathanassiou et al. (2015); Servizio Geologico (2016)
235	185130B502	20-May-2012	Emilia	Italy	6.10	0.600	3.00	Y	Papathanassiou et al. (2015); Servizio Geologico (2016)
236	185130B503	20-May-2012	Emilia	Italy	6.10	0.590	3.00	Y	Papathanassiou et al. (2015); Servizio Geologico (2016)
237	185130B504	20-May-2012	Emilia	Italy	6.10	0.590	3.00	Y	Papathanassiou et al. (2015); Servizio Geologico (2016)
238	185130U006	20-May-2012	Emilia	Italy	6.10	0.730	3.00	N	Papathanassiou et al. (2015); Servizio Geologico (2016)
239	185130U022	20-May-2012	Emilia	Italy	6.10	0.580	1.80	N	Papathanassiou et al. (2015); Servizio Geologico (2016)
240	185130U505	20-May-2012	Emilia	Italy	6.10	0.600	5.00	Y	Papathanassiou et al. (2015); Servizio Geologico (2016)
241	185130U506	20-May-2012	Emilia	Italy	6.10	0.600	4.84	Y	Papathanassiou et al. (2015); Servizio Geologico (2016)
242	185130U507	20-May-2012	Emilia	Italy	6.10	0.600	5.16	Y	Papathanassiou et al. (2015); Servizio Geologico (2016)
243	185130U508	20-May-2012	Emilia	Italy	6.10	0.590	4.22	Y	Papathanassiou et al. (2015); Servizio Geologico (2016)
244	185130U509	20-May-2012	Emilia	Italy	6.10	0.590	2.37	N	Papathanassiou et al. (2015); Servizio Geologico (2016)
245	185130U510	20-May-2012	Emilia	Italy	6.10	0.590	5.23	N	Papathanassiou et al. (2015); Servizio Geologico (2016)
246	185130U511	20-May-2012	Emilia	Italy	6.10	0.590	4.65	N	Papathanassiou et al. (2015); Servizio Geologico (2016)
247	185130U512	20-May-2012	Emilia	Italy	6.10	0.580	4.40	Y	Papathanassiou et al. (2015); Servizio Geologico (2016)

248	185130U513	20-May-2012	Emilia	Italy	6.10	0.580	4.18	Y	Papathanassiou et al. (2015); Servizio Geologico (2016)
249	185130U514	20-May-2012	Emilia	Italy	6.10	0.580	4.55	Y	Papathanassiou et al. (2015); Servizio Geologico (2016)
250	185140B001	20-May-2012	Emilia	Italy	6.10	0.540	2.00	N	Papathanassiou et al. (2015); Servizio Geologico (2016)
251	185140U002	20-May-2012	Emilia	Italy	6.10	0.530	2.30	N	Papathanassiou et al. (2015); Servizio Geologico (2016)
252	185140U003	20-May-2012	Emilia	Italy	6.10	0.540	3.60	N	Papathanassiou et al. (2015); Servizio Geologico (2016)
253	185140U004	20-May-2012	Emilia	Italy	6.10	0.540	3.30	N	Papathanassiou et al. (2015); Servizio Geologico (2016)
254	185140U005	20-May-2012	Emilia	Italy	6.10	0.560	4.90	N	Papathanassiou et al. (2015); Servizio Geologico (2016)
255	203010U001	20-May-2012	Emilia	Italy	6.10	0.650	4.00	Y	Papathanassiou et al. (2015); Servizio Geologico (2016)
256	203010U002	20-May-2012	Emilia	Italy	6.10	0.650	4.90	Y	Papathanassiou et al. (2015); Servizio Geologico (2016)
257	203010U005	20-May-2012	Emilia	Italy	6.10	0.660	2.40	Y	Papathanassiou et al. (2015); Servizio Geologico (2016)
258	203010U006	20-May-2012	Emilia	Italy	6.10	0.650	2.40	Y	Papathanassiou et al. (2015); Servizio Geologico (2016)
259	203010U509	20-May-2012	Emilia	Italy	6.10	0.720	1.90	N	Papathanassiou et al. (2015); Servizio Geologico (2016)
260	203020U095	20-May-2012	Emilia	Italy	6.10	0.480	4.50	Y	Papathanassiou et al. (2015); Servizio Geologico (2016)
261	203020U096	20-May-2012	Emilia	Italy	6.10	0.480	1.60	Y	Papathanassiou et al. (2015); Servizio Geologico (2016)
262	203020U097	20-May-2012	Emilia	Italy	6.10	0.500	2.05	N	Papathanassiou et al. (2015); Servizio Geologico (2016)
263	203020U098	20-May-2012	Emilia	Italy	6.10	0.500	1.90	N	Papathanassiou et al. (2015); Servizio Geologico (2016)
264	203020U099	20-May-2012	Emilia	Italy	6.10	0.510	1.80	N	Papathanassiou et al. (2015); Servizio Geologico (2016)
265	CPTU1	20-May-2012	Emilia	Italy	6.10	0.310	1.40	Y	Papathanassiou et al. (2015); Servizio Geologico (2016); Facciorusso et al. (2015)

Dataset (Table 8.3) References

- Abdel-Haq, A., and Hryciw, R. D. (1998). "Ground settlement in Simi Valley following the Northridge earthquake." *Journal of Geotechnical and Geoenvironmental*, 124(1): 80-89.
- Andrus, R.D. (1986). "Subsurface investigations on a liquefaction induced lateral spread Thousand Springs Valley, Idaho: liquefaction recurrence and a case history in gravel." M.S. Thesis, Dept. of Civil Engineering, Brigham Young University, Provo, Utah.
- Andrus, R. D. and Youd, T. L. (1987). "Subsurface Investigation of a Liquefaction-Induced Lateral Spread Thousand Springs Valley, Idaho." Misc. paper GL-87-8, U.S. Army Corps of Engineers.
- Arulanandan, K., Yogachandran, C., Meegoda, N. J., Ying, L., and Zhauji, S. (1986). "Comparison of the SPT, CPT, SV and electrical methods of evaluating earthquake induced liquefaction susceptibility in Ying Kou City during the Haicheng Earthquake." Use of in situ tests in geotechnical engineering." *Geotech. Spec. Publ.*, 6, 389–415.
- Batilas, A., Pelekis, P., Vlachakis, V., and Athanasopoulos, G. (2014). "Soil Liquefaction/Nonliquefaction in the Achaia-Ilia (Greece) 2008 Earthquake: Field Evidence, Site Characterization and Ground Motion Assessment." *International Journal of Geoengineering Case histories*, 2(4): 270-287.
- Bennett, M. J., McLaughlin, P. V., Sarmiento, J. S., and Youd, T. L. (1984). "Geotechnical investigation of liquefaction sites, Imperial Valley, California." U.S. Geological Survey, Open-File Report 84-252, 103 pp.
- Bennett, M. J., Ponti, D. J., Tinsley, J. C., III, Holzer, T. L., and Conaway, C. H. (1998). Subsurface geotechnical investigations near sites of ground deformations caused by the January 17, 1994, Northridge, California, earthquake. U.S. Geological Survey, Open-file report 98-373, 148 pp.
- Bennett, M. J., and Tinsley, J. C., III (1995). "Geotechnical data from surface and subsurface samples outside of and within liquefactionrelated ground failures caused by the October 17, 1989, Loma Prieta earthquake, Santa Cruz and Monterey Counties, California." U.S. Geological Survey Open-File Rep. 95-663, U.S. Geological Survey.
- Boulanger, R. W., Idriss, I. M., and Mejia, L. H. (1995). "Investigation and evaluation of liquefaction related ground displacements at Moss Landing during the 1989 Loma Prieta earthquake." Report No. UCD/CGM-95/02, Center for Geotechnical Modeling, Department of Civil & Environmental Engineering, University of California, Davis, 231 pp., May.
- Boulanger, R. W., Mejia, L. H., and Idriss, I. M. (1997). "Liquefaction at Moss Landing during Loma Prieta earthquake." *Journal of Geotechnical and Geoenvironmental Engineering*, 123(5): 453–67.

- Boulanger, R. W. and Idriss, I. M. (2014). "CPT and SPT based liquefaction triggering procedures." Report No. UCD/CGM-14/01, Center for Geotechnical Modeling, Department of Civil and Environmental Engineering, University of California, Davis, CA, 134 pp.
- CESMD (2016). "U.S. structural and ground response data." Center for Engineering Strong Motion Data; <http://www.strongmotioncenter.org/>
- Cetin, K. O., Seed, R. B., Moss, R. E. S., Der Kiureghian, A. K., Tokimatsu, K., Harder, L. F., and Kayen, R. E. (2000). "Field Performance Case Histories for SPT-Based Evaluation of Soil Liquefaction Triggering Hazard." Geotechnical Engineering Research Report No. UCB/GT-2000/09, Geotechnical Engineering, Department of Civil Engineering, University of California at Berkeley.
- Christensen, S. A. (1995). "Liquefaction of Cohesionless Soils in the March 2, 1987 Edgecumbe Earthquake, Bay of Plenty, New Zealand, and Other Earthquakes." Masters of Engineering Thesis, Department of Civil Engineering, University of Canterbury, Christchurch, New Zealand.
- Cox, B. R., Boulanger, R. W., Tokimatsu, K., Wood, C., Abe, A., Ashford, S., Donahue, J., Ishihara, K., Kayen, R., Katsumata, K., Kishida, T., Kokusho, T., Mason, B., Moss, R., Stewart, J., Tohyama, K., and Zekkos, D. (2013). "Liquefaction at strong motion stations and in Urayasu City during the 2011 Tohoku-Oki earthquake." *Earthquake Spectra*, 29(S1): S55-S80.
- Diaz-Rodriguez, J. A. (1984). "Liquefaction in the Mexicali Valley During the Earthquake of June 9, 1980." Eighth World Conference on Earthquake Engineering EERI, San Francisco, 223-230.
- Diaz-Rodriguez, J. A., and Armijo-Palacio, G. (1991). "Liquefaction potential of fine cohesionless soils using the CPT." *Soils and Foundations*, 31(3): 111-119.
- Facciorusso, J., Madiari, C., and Vannucchi, G. (2015). "CPT-Based Liquefaction Case History from the 2012 Emilia Earthquake in Italy." *Journal of Geotechnical and Geoenvironmental Engineering*, 141(12): 05015002.
- Farrar, J. A. (1990). "Study of In Situ Testing for Evaluation of Liquefaction Resistance." R-90-06, U.S. Department of the Interior, Bureau of Reclamation, Research and Laboratory Services Division, Geotechnical Services Branch, Denver Office.
- Holzer, T.L and Youd, T.L. (2007). "Liquefaction, Ground Oscillation, and Soil Deformation at the Wildlife Array." *Bulletin of the Seismological Society of America*, 97(3): 961–976.
- Holzer, T. L., Bennett, M. J., Ponti, D. J., and Tinsley, J. C., III (1999). "Liquefaction and soil failure during 1994 Northridge earthquake." *Journal of Geotechnical and Geoenvironmental Engineering*, 125(6): 438-452.
- Ishihara, K., and Koga, Y. (1981). "Case studies of liquefaction in the 1964 Niigata earthquake." *Soils and Foundations*, 21(3): 35-52.
- Kayen, R. E., Mitchell, J. K., Seed, R. B., and Nishio, S. (1998). "Soil liquefaction in the east bay during

- the earthquake." The Loma Prieta, California, Earthquake of October 17, 1989 – Liquefaction. Thomas L. Holzer, editor, U.S. Geological Survey Professional Paper 1551-B, B61-B86.
- Lee, D.H., Ku, C.S., and Juang, C.H. (2000), "Preliminary investigation of soil liquefaction in the 1999 Chi-Chi, Taiwan, earthquake," *Proceedings, International Workshop on Annual Commemoration of Chi-Chi Earthquake, Vol. III – Geotechnical Aspect*, C.H. Loh and W.I. Liao, eds., National Center for Research on Earthquake Engineering, Taipei, Taiwan, pp. 140-151.
- Mitchell, J. K., Lodge, A. L., Coutinho, R. Q., Kayen, R. E., Seed, R. B., Nishio, S., and Stokoe, K. H., II (1994). "Insitu test results from four Loma Prieta earthquake liquefaction sites: SPT, CPT, DMT and shear wave velocity." Report No. UCB/EERC-94/04. Earthquake Engineering Research Center, University of California at Berkeley.
- Moss, R. E. S., Seed, R. B., Kayen, R. E., Stewart, J. P., Youd, T. L., and Tokimatsu, K. (2003). "Field case histories for CPT-based in situ liquefaction potential evaluation." *Geoengineering Research Rep. UCB/GE-2003/04*.
- Moss, R. E. S., Collins, B. D., and Whang, D. H. (2005). "Retesting of liquefaction/nonliquefaction case histories in the imperial valley." *Earthquake Spectra*, 21(1): 179–196.
- Moss, R. E. S., Kayen, R. E., Tong, L.-Y., Liu, S.-Y., Cai, G.-J., and Wu, J. (2009). "Re-investigation of liquefaction and nonliquefaction case histories from the 1976 Tangshan earthquake." Rep. No. 209/102, Pacific Earthquake Engineering Research (PEER) Center, Berkeley, CA.
- Moss, R. E. S., Kayen, R. E., Tong, L.-Y., Liu, S.-Y., Cai, G.-J., and Wu, J. (2011). "Retesting of liquefaction and nonliquefaction case histories from the 1976 Tangshan earthquake." *Journal of Geotechnical and Geoenvironmental Engineering*, 137(4): 334-343.
- Papathanassiou, G., Mantovani, A., Tarabusi, G., Rapti, D., and Caputo, R. (2015). "Assessment of liquefaction potential for two liquefaction prone areas considering the May 20, 2012 Emilia (Italy) earthquake." *Engineering Geology*, 189:1-16.
- Pass, D. G. (1994). "Soil characterization of the deep accelerometer site at Treasure Island, San Francisco, California." MS thesis in Civil Engineering, University of New Hampshire.
- PEER (2000a). "Documenting Incidents of Ground Failure Resulting from the Aug. 17, 1999, Kocaeli, Turkey Earthquake." <http://peer.berkeley.edu/publications/turkey/adapazari/>
- PEER (2000b). "Documentation of Soil Conditions at Liquefaction Sites from 1999 Chi-Chi, Taiwan Earthquake." http://peer.berkeley.edu/lifelines/research_projects/3A02/
- Seed, H. B., Tokimatsu, K., Harder, L. F. Jr., and Chung, R. (1984). "The influence of SPT procedures in soil liquefaction resistance evaluations." Report No. UCB/EERC-84/15. Earthquake Engineering Research Center, University of California, Berkeley.

- Servizio Geologico (2016). "Database of the Emilia-Romagna Region: Geological, Seismic, and Soil Survey." <http://ambiente.regione.emilia-romagna.it/geologia/cartografia/webgis-banchedati/> (Italian).
- Shengcong, F., and Tatsuoka, F. (1984). "Soil liquefaction during Haicheng and Tangshan earthquake in China; A review." *Soils and Foundations*, 24(4): 11-29.
- Shibata, T., and Teparaska, W. (1988). "Evaluation of Liquefaction Potential of Soils Using Cone Penetration Testing." *Soils and Foundations*, 28(2): 49-60.
- Suzuki, Y., Tokimatsu, K., Moss, R. E. S., Seed, R. B., and Kayen, R. E. (2003). "CPT-based liquefaction case histories from the 1995 Hyogoken-Nambu (Kobe) earthquake, Japan." Geotechnical Engineering Research Report No. UCB/GE-2003/03.
- Toprak, S., and Holzer, T. L. (2003). "Liquefaction potential index: Field assessment." *Journal of Geotechnical and Geoenvironmental Engineering*, 129(4): 315-322.
- Turner, B., Brandenberg, S., and Stewart, J. (2016). "Case Study of Parallel Bridges Affected by Liquefaction and Lateral Spreading." *Journal of Geotechnical and Geoenvironmental Engineering*, 142(7): 05016001.
- Youd, T. L., and Carter, B. L. (2005). "Influence of soil softening and liquefaction on spectral acceleration." *Journal of Geotechnical and Geoenvironmental Engineering*, 131(7): 811-825.
- Youd, T. L., DeDen, D. W., Bray, J. D., Sancio, R., Cetin, K. O., and Gerber, T. M. (2009). "Zero displacement lateral spreads, 1999 Kocaeli, Turkey, earthquake." *Journal of Geotechnical and Geoenvironmental Engineering*, 135(1): 46-61.

Chapter 9: Conclusions

The 2010-2011 Canterbury, New Zealand, Earthquake Sequence (CES) resulted in a liquefaction dataset of unprecedented size and quality, presenting a truly unique opportunity to assess and improve the efficacy of liquefaction-analytics in the field. Towards this end, this study developed and analyzed a database of 10,000 high-quality liquefaction case histories resulting from the CES and other global earthquakes. The objectives of these analyses were varied, but underlying each was the desire to more accurately assess liquefaction hazard for civil infrastructure (i.e., to predict both the occurrence and damage-potential of soil liquefaction). Major contributions from this work include, but are not limited to: (1) the Liquefaction Potential Index (LPI), the state-of-practice framework for assessing liquefaction hazard, was shown to produce erroneous predictions for a significant percentage of the assessed case histories; (2) the cause of poor predictions was rigorously investigated and specific shortcomings of the LPI framework were identified; (3) based on the limitations identified, and using insights from historical data, a revised liquefaction hazard framework was developed; and (4) the revised framework was shown to assess liquefaction hazard more efficiently relative to both LPI and a competing alternative framework newly proposed in the literature. The chapters of this dissertation consisted of a series of paper manuscripts that combined to make the contributions outlined above. In the following, Chapters 2 through 8 are each succinctly summarized.

In Chapter 2, the performance of LPI for predicting the occurrence and severity of surficial liquefaction manifestation was evaluated using approximately 2,350 liquefaction case histories resulting from the CES, wherein the Robertson and Wride (1998) liquefaction triggering procedure is used within the LPI framework. These case histories were developed from cone penetration test soundings performed in the 18 months following the 4 September M_w 7.1 Darfield earthquake. This study thus represents a preliminary investigation of the performance of liquefaction hazard assessment in Christchurch. While the assessed dataset is small relative to that developed at the conclusion of this dissertation (Chapter 8), it contains significantly more case histories than had been collected from all previous earthquakes combined. As such, this initial evaluation provided unprecedented insights into liquefaction hazard assessment. Of greatest interest, it was shown that while LPI is generally effective, hazard assessments were highly erroneous for large portions of Christchurch.

In Chapter 3, a significantly larger dataset of approximately 7,000 case histories was developed, to include the use of robust, event-specific ground water models. Moreover, three competing liquefaction triggering procedures were evaluated within the LPI framework: Robertson and Wride (1998); Moss et

al. (2006); and Idriss and Boulanger (2008). In practice, there is considerable debate as to which of these procedures should be used to predict liquefaction triggering. Accordingly, the influence of the adopted triggering procedure on the accuracy of derivative LPI hazard assessments was investigated. Moreover, this investigation introduced and utilized the ROC methodology, which provides a standardized and objective assessment of diagnostic-model performance. Consistent with Chapter 2, it was shown that LPI performs poorly at a significant percentage of locations assessed, regardless of which triggering procedure is used within the LPI framework.

In Chapter 4, “finer-content effects” on liquefaction hazard were investigated. A major conclusion of Chapters 2 and 3 is that LPI hazard assessments were significantly less efficient (i.e., inaccurate) at sites where soils with high fines-content are present. Accordingly, several possible explanations were investigated in Chapter 4. Through these analyses, it is hypothesized that non-liquefiable, high fines-content soils are likely to inhibit liquefaction manifestation by affecting pore pressure development and redistribution, resulting in over-predictions of hazard. It was thus recognized that liquefaction hazard frameworks should consider not only the behavior of liquefiable soils, but also the influence of non-liquefiable soils that “cap” the soil profile or are interbedded among liquefiable deposits.

In Chapter 5, a new liquefaction hazard framework, termed LPI_{ISH} , was derived from the H_1 - H_2 chart proposed by Ishihara (1985). The proposed framework considered the influence of the non-liquefied capping layer on the manifestation of liquefaction, which while shown to be significant, is not accounted for by LPI. LPI_{ISH} was evaluated using select liquefaction case histories and found to be consonant with observed surface effects, demonstrating improvement over LPI in mitigating false-positive predictions.

Coinciding with the development of LPI_{ISH} , an alternative to LPI was also proposed by a group of practitioners and academics from New Zealand and the United States. The proposed Liquefaction Severity Number (LSN) considers the influence of post-liquefaction volumetric strain potential (ϵ_v) on liquefaction hazard. LSN thus recognizes that soils of different density have different consequences once liquefaction is triggered. However, many different techniques exist for estimating ϵ_v , each of which could lead to different computed LSN values, and by corollary, different assessments of liquefaction hazard. Accordingly, Chapter 6 investigated the influence of six techniques for estimating ϵ_v on the accuracy of LSN assessments. It was shown that a control model in which ϵ_v was removed performed best, suggesting that ϵ_v either provides no statistically distinguishable benefits in terms of prediction accuracy, or is accounted for by LSN in such a way that is not optimal.

In Chapter 7, deterministic and probabilistic correlations are developed for predicting (a) soil fines-content; and (b) whether soil is *susceptible* to liquefaction. While each of these predictions is a required input in the LPI, LPI_{ISH}, and LSN hazard frameworks, the use of generic correlations developed from global data could be inaccurate on local scales. The development of Christchurch-specific correlations could thus lead to a better understanding of observed liquefaction phenomena. The findings presented in Chapter 7 represent an extensive case study of CPT-based soil characterization and are particularly pertinent to ongoing research using data from Christchurch. However, the approach used to develop deterministic and probabilistic correlations is not limited to parts of New Zealand, but rather, can be applied worldwide.

In Chapter 8, nearly 10,000 liquefaction case histories, to include 265 cases compiled from 20 global earthquakes, were used to assess and compare the performance of LPI, LPI_{ISH}, and LSN using a methodology considering the consequences, or economies, of misprediction, to which the performance of hazard assessment is intimately linked. It was shown that optimal decision thresholds were inherently tied to underlying economic assumptions, since the threshold that is “optimal” for one project, or one category of land-use, may be inappropriate for others. The decision thresholds proposed in Chapter 8 can be used to inform strategies for assessing and/or mitigating liquefaction hazards. Additionally LPI_{ISH} was the most efficient of the assessed frameworks for both the CES and global case histories.

Ultimately, significant room for improvement remains with respect to accurate assessment of liquefaction hazard, and the findings presented in this dissertation form the basis for development of a further-improved framework. Moreover, using the ROC methodology, improvements can be measured in a standardized and objective manner moving forward. The following challenges, among others, must be addressed by this future research.

- The influence of non-liquefiable, high fines-content soils on liquefaction hazard must be fully understood, quantified, and incorporated into an improved liquefaction hazard framework. It was shown herein that such soils have a tendency to suppress liquefaction manifestation, resulting in significant over-predictions of hazard, yet this effect is not directly considered by LPI or any other liquefaction hazard framework.
- At present, liquefaction triggering procedures and liquefaction hazard frameworks are developed independently, likely resulting in the omission, double counting, and general obscuration of factors that influence liquefaction response. While the mechanics of liquefaction

manifestation are critical to each, they are not accounted for in a consistent manner. Liquefaction triggering procedures are developed almost exclusively from observations of liquefaction manifestation at the ground surface. The developers of these procedures, each using their own judgment, tie the observed manifestation (or lack thereof) to the response of a single “critical” layer within the soil profile. In doing so, these developers implicitly use in reverse an undocumented liquefaction hazard framework that describes the relationship between liquefaction triggering and liquefaction manifestation. A second, independent group of researchers uses the output from the proposed liquefaction triggering procedures to predict liquefaction manifestations at the ground surface. In doing so, this latter group is explicitly proposing a liquefaction hazard framework that describes the relationship between liquefaction triggering and liquefaction manifestation. Importantly, because liquefaction triggering models and liquefaction hazard frameworks have traditionally been developed independently, the factors influencing liquefaction manifestation have very likely not been accounted for in a consistent manner. In the future, liquefaction triggering procedures and liquefaction hazard frameworks should be developed in harmony within an internally consistent framework.